



# THE UNIVERSITY *of* EDINBURGH

This thesis has been submitted in fulfilment of the requirements for a postgraduate degree (e.g. PhD, MPhil, DClinPsychol) at the University of Edinburgh. Please note the following terms and conditions of use:

This work is protected by copyright and other intellectual property rights, which are retained by the thesis author, unless otherwise stated.

A copy can be downloaded for personal non-commercial research or study, without prior permission or charge.

This thesis cannot be reproduced or quoted extensively from without first obtaining permission in writing from the author.

The content must not be changed in any way or sold commercially in any format or medium without the formal permission of the author.

When referring to this work, full bibliographic details including the author, title, awarding institution and date of the thesis must be given.

THE UNIVERSITY OF EDINBURGH

SCHOOL OF ENGINEERING

**The Effect of Rib Cage Deformity in  
Primary Thoracic Idiopathic Scoliosis  
on Pulmonary Function, Airway  
Morphology and Lung Volumes**

*James A. Farrell*

This dissertation is submitted for the degree of

*Doctor of Philosophy*

30th September 2019



# Abstract

Although scoliosis is defined as a Cobb angle of  $10^\circ$  or more as measured in the coronal plane, the combined three-dimensional distortions to both the spine and rib cage in scoliosis are best conceptualised as a thoracic deformity. There is much interest in the relationship between scoliosis and pulmonary function due to the increased morbidity of respiratory failure and mortality of those with untreated progressive scoliosis. Establishing the mechanisms of pulmonary function impairment in scoliosis is important in identifying patients with compromised lung function or those who will benefit from surgical intervention.

In this work, the relationship between thoracic deformity in patients with right-sided, Lenke type 1 or 2, adolescent idiopathic scoliosis (AIS) and pulmonary function impairment is investigated. From radiographic and computer tomographic imaging, measurements of the thoracic deformity were found to be superior predictors of pulmonary function in AIS than conventional Cobb angles. A statistical shape model was constructed from biplanar radiographs to identify modes of variation in the thoracic configuration. Thoracic features such as the extent of the rib hump, narrowed convex hemithoracic width and spinal intrusion were found to be factors contributing to lung function impairment.

Morphological analysis of the tracheobronchial tree demonstrated the presence of right-sided airway narrowing. In particular, patients with hypokyphosis demonstrated significant narrowing of the bronchus intermedius and its bifurcation as a result of extrinsic compression by the vertebral column. Right-sided airway obstruction was found to correspond to the presence of atelectasis and air-trapping in the right middle and lower lobe. Post-operative analysis demonstrated that restoration of natural kyphosis in patients with hypokyphosis and scoliosis resulted in improved lung function post-operatively. Although reduction in lung function in patients with scoliosis is multifactorial, variance in the sagittal thoracic profile plays a more important role in impairing lung function than is generally appreciated.



# Lay Summary

Although scoliosis is measured in terms of the misalignment of the spine as viewed from the front, it is also accompanied by significant distortions to the rib cage. There is much interest in the relationship between scoliosis and lung function due to the increased incidence of respiratory failure and death in those with untreated scoliosis. Establishing the mechanisms of lung function impairment in scoliosis is important in identifying patients most at risk of reduced lung function or those who will benefit from scoliosis surgery.

In this work, the relationship between the distortions of the chest shape in patients with thoracic scoliosis and lung function is investigated. From medical x-ray images, measurements of the chest deformity were found to be better predictors of lung function in scoliosis than measurement focusing solely on the curvature of the spine. A statistical model describing variations in the shape of the chest and spine was constructed to identify features which explained lung function impairment. The features found to contribute to lung function impairment included the size of the rib hump, narrowing of the right-half of the chest and forward protrusion of the spine into the chest.

Measurements of the dimensions of the airway tree showed that airways on the right side were narrowed in scoliosis. Patients with flatter backs demonstrated more airway narrowing as a result of the spine intruding into the chest. The presence of airway narrowing was found to correspond to the presence of lung collapse and trapped air in the right lung. Comparing lung function before and after surgery showed that restoring natural curvature in patients with flat backs and scoliosis resulted in improved lung function after operation. Although there are many factors behind lung function impairment in patients with scoliosis, the profile of the spine as viewed from the side plays a more important role in reducing lung function than is generally appreciated.



# Acknowledgements

I would like to thank my supervisors, Dr. Prashant Valluri and Mr. Enrique Garrido FRCS (Tr & Orth), for their guidance, support and for making this project possible. Martin Connell, from the Clinical Research Imaging Centre (CRIC), University of Edinburgh, provided input on airway segmentation and measurement for which I am grateful. I would also like to thank the Engineering and Physical Sciences Research Council and K2M Inc. for funding this project. Finally, thank you to my family for their continued love and support.





# Contents

<b>Abstract</b>	<b>iii</b>
<b>Lay Summary</b>	<b>v</b>
<b>Acknowledgements</b>	<b>vii</b>
<b>List of Figures</b>	<b>xi</b>
<b>List of Tables</b>	<b>xv</b>
<b>1 Introduction</b>	<b>1</b>
1.1 Background . . . . .	1
1.1.1 Definition of adolescence idiopathic scoliosis (AIS) . . . . .	1
1.1.2 Measurement of AIS deformity . . . . .	1
1.1.3 Classification schemes for AIS . . . . .	2
1.1.4 Pulmonary Function Testing in Scoliosis . . . . .	5
1.2 Motivation . . . . .	5
1.3 Aims and objectives . . . . .	6
1.4 Thesis structure . . . . .	7
<b>I Radiographic Studies</b>	<b>9</b>
<b>2 Radiographic Indices</b>	<b>11</b>
2.1 Summary . . . . .	11
2.2 Introduction . . . . .	11
2.3 Literature Review . . . . .	12
2.4 Materials & Methods . . . . .	14
2.4.1 Subject Characteristics . . . . .	14
2.4.2 Lung Function . . . . .	14
2.4.3 Spinal and Thoracic Parameters . . . . .	14
2.4.4 Statistical Methods . . . . .	15
2.5 Results . . . . .	15
2.5.1 Pre-operative analysis . . . . .	16
2.5.2 Effect of scoliosis surgery . . . . .	17
2.5.3 Multivariate Step-wise Regression Models . . . . .	18
2.6 Discussion . . . . .	19
2.7 Conclusion . . . . .	21

<b>3</b>	<b>Statistical Shape Model</b>	<b>39</b>
3.1	Summary . . . . .	39
3.2	Introduction . . . . .	39
3.3	Literature Review . . . . .	40
3.4	Theory . . . . .	40
3.4.1	Generalised Procrustes Analysis . . . . .	40
3.4.2	Principle Component Analysis . . . . .	42
3.5	Materials & Methods . . . . .	43
3.5.1	Subject Characteristics . . . . .	43
3.5.2	Landmark Acquisition . . . . .	43
3.5.3	Shape Model . . . . .	44
3.5.4	Statistical Methods . . . . .	44
3.6	Results . . . . .	44
3.7	Discussion . . . . .	48
3.8	Conclusion . . . . .	49
<b>II</b>	<b>Computerised Tomography Studies</b>	<b>63</b>
<b>4</b>	<b>Thoracic Deformity Parameters</b>	<b>65</b>
4.1	Summary . . . . .	65
4.2	Introduction . . . . .	65
4.3	Literature Review . . . . .	66
4.4	Materials & Methods . . . . .	67
4.4.1	Subject Characteristics . . . . .	67
4.4.2	Lung Function . . . . .	68
4.4.3	Spinal and Thoracic Parameters . . . . .	68
4.4.4	Statistical Methods . . . . .	68
4.5	Results . . . . .	71
4.5.1	Sagittal thoracic modifier . . . . .	71
4.5.2	Correlational analysis . . . . .	71
4.5.3	Principle component analysis . . . . .	72
4.5.4	Post-operative changes . . . . .	72
4.5.5	Predictive Models . . . . .	72
4.6	Discussion . . . . .	73
4.7	Conclusion . . . . .	83
<b>5</b>	<b>Airway Narrowing in Scoliosis</b>	<b>85</b>
5.1	Summary . . . . .	85
5.2	Introduction . . . . .	85
5.3	Literature Review . . . . .	86
5.4	Materials & Methods . . . . .	87
5.4.1	Subjects . . . . .	87
5.4.2	Anatomical Variables . . . . .	88
5.4.3	Lung Function Data . . . . .	89
5.4.4	Statistics . . . . .	89
5.5	Results . . . . .	89
5.5.1	Standing and supine Cobb angles . . . . .	89

5.5.2	Airway-Spine Proximity . . . . .	89
5.5.3	Lumen area . . . . .	93
5.5.4	Bifurcation Angles and Airway Trajectories . . . . .	93
5.5.5	Post-operative Changes . . . . .	97
5.6	Discussion . . . . .	97
5.7	Conclusion . . . . .	101
<b>6</b>	<b>Lung Volumes and Attenuation</b>	<b>103</b>
6.1	Summary . . . . .	103
6.2	Introduction . . . . .	103
6.3	Literature Review . . . . .	104
6.4	Materials & Methods . . . . .	106
6.4.1	Subjects . . . . .	106
6.4.2	Image Segmentation . . . . .	106
6.4.3	Lung Volume Parameters . . . . .	108
6.4.4	Spine and Thoracic Deformity Parameters . . . . .	108
6.4.5	Lung Function Data . . . . .	108
6.4.6	Statistics . . . . .	109
6.5	Results . . . . .	109
6.5.1	Correlational Analysis . . . . .	115
6.5.2	Multivariate Step-wise Regression . . . . .	115
6.6	Discussion . . . . .	116
6.7	Conclusion . . . . .	119
<b>7</b>	<b>Conclusions &amp; Future Work</b>	<b>121</b>
7.1	Future work . . . . .	122
	<b>References</b>	<b>123</b>



# List of Figures

1.1	Diagram showing the measurement of Cobb angles in the coronal and sagittal plane . . . . .	2
1.2	King classification for adolescent idiopathic scoliosis . . . . .	3
1.3	Lenke criteria for adolescent idiopathic scoliosis. . . . .	4
1.4	Thoracic deformity associated with scoliosis. . . . .	6
2.1	Diagrams of thoracic deformity parameters measured on coronal radiographs for (a) rib-vertebra angle difference (RVAD), (b) inverse of the apical vertebral body-rib ratio ( $AVBRr^{-1}$ ) and (c) space available for lung (SAFL) and lung height-width ratio (LHW $r$ ). Descriptions of the measurements can be found in Table 2.1 . . . . .	23
2.2	Diagrams of thoracic deformity parameters measured on sagittal radiographs for (a) kyphosis-lordosis index (KLi), (b) rib hump index (RHi) and (c) spinal intrusion ratio (SIr). Definitions of the parameters can be found in Table 2.1 . . . . .	24
2.3	Correlation plots of $FEV_1$ with (a) inverse apical vertebral body-rib ratio ( $AVBRr^{-1}$ ) and (b) spinal intrusion ratio (SIr). . . . .	27
2.4	Correlation plots of $FEV_1/FVC$ with (a) T5-T12 thoracic kyphosis (TK) and (b) kyphosis-lordosis index (KLi). . . . .	28
2.5	Box-and-whisker plots of main thoracic Cobb and T5-T12 thoracic kyphosis results pre- and post-operation . . . . .	33
2.6	Box-and-whisker plots of $FEV_1$ , FVC and $FEV_1/FVC$ results pre- and post-operation . . . . .	34
2.7	Examples of patients with (a) high and (b) low inverse apical vertebral body-rib ratio $AVBRr^{-1}$ . $AVBRr^{-1}$ captures the narrowing of the convex hemithorax and is related to rib hump magnitude and rib asymmetry. . . . .	35
2.8	Examples of patients with (a) low and (b) high spinal intrusion ratio (SIr). SIr captures both the narrowing of the sternovertebral distance, spinal intrusion into the thoracic cavity and the extend of the convex rib hump. . . . .	36
3.1	An example of dimensionality reduction using principle component analysis (PCA) . . . . .	43
3.2	An example of the landmarks collected from the coronal and sagittal radiographs for the statistical shape model. . . . .	45
3.3	Superimposed landmarks of the statistical shape model in the (a) coronal and (b) sagittal plane following generalised Procrustes analysis (GPA) . . . . .	46

3.4	A plot of cumulative variance explained against the number of principle components included in the statistical shape model. . . . .	47
3.5	Shape variation of the first principal deformation mode ( $PC_1$ ) with (a) -3; (b) 0 (mean shape); and (c) +3 standard deviations of the shape deformation. Coronal and sagittal views are shown on the top and bottom rows respectively. . . . .	52
3.6	Shape variation of the second principal deformation mode ( $PC_2$ ) with (a) -3; (b) 0 (mean shape); and (c) +3 standard deviations of the shape deformation. Coronal and sagittal views are shown on the top and bottom rows respectively. . . . .	53
3.7	Shape variation of the third principal deformation mode ( $PC_3$ ) with (a) -3; (b) 0 (mean shape); and (c) +3 standard deviations of the shape deformation. Coronal and sagittal views are shown on the top and bottom rows respectively. . . . .	54
3.8	Shape variation of the fourth principal deformation mode ( $PC_4$ ) with (a) -3; (b) 0 (mean shape); and (c) +3 standard deviations of the shape deformation. Coronal and sagittal views are shown on the top and bottom rows respectively. . . . .	55
3.9	Shape variation of the fifth principal deformation mode ( $PC_5$ ) with (a) -3; (b) 0 (mean shape); and (c) +3 standard deviations of the shape deformation. Coronal and sagittal views are shown on the top and bottom rows respectively. . . . .	56
3.10	Shape variation of the sixth principal deformation mode ( $PC_6$ ) with (a) -3; (b) 0 (mean shape); and (c) +3 standard deviations of the shape deformation. Coronal and sagittal views are shown on the top and bottom rows respectively. . . . .	57
3.11	Shape variation of the sixth principal deformation mode ( $PC_7$ ) with (a) -3; (b) 0 (mean shape); and (c) +3 standard deviations of the shape deformation. Coronal and sagittal views are shown on the top and bottom rows respectively. . . . .	58
3.12	Shape variation of the sixth principal deformation mode ( $PC_8$ ) with (a) -3; (b) 0 (mean shape); and (c) +3 standard deviations of the shape deformation. Coronal and sagittal views are shown on the top and bottom rows respectively. . . . .	59
3.13	Shape variation of the sixth principal deformation mode ( $PC_9$ ) with (a) -3; (b) 0 (mean shape); and (c) +3 standard deviations of the shape deformation. Coronal and sagittal views are shown on the top and bottom rows respectively. . . . .	60
4.1	Diagrams showing the definition of landmarks and thoracic deformity parameters . . . . .	70
4.2	Examples of patients with high principle component z-scores . . . . .	76
4.3	Correlation coefficients of CT deformity parameters measured from T3 to T12 with lung function and radiographic Cobb angles . . . . .	78
5.1	Reconstructed spinal column and airway from CT segmentation . . . . .	90
5.2	Segmented airway model with regions of interest . . . . .	91

5.3	Normalised airway–spine minimum distances for representative subjects from (a) controls, (b) hypokyphosis (–), (c) normokyphosis (N) and (d) hyperkyphosis (+). Regions of red represent close proximity whilst green regions represent increased distance between spine and airway. The top row displays the coronal view anterior to the subject and the bottom row displays the sagittal views right of the subject. . . . .	94
5.4	Box-and-whisker plot of normalised lumen area for each group . . . . .	95
5.5	Pre- and post-scoliosis surgery comparison of spine-airway proximity in a hypokyphotic subject . . . . .	99
5.6	Subject with scoliosis and hypokyphosis showing extrinsic compression of the bronchus intermedius . . . . .	102
6.1	A case report from van Ooji et al. (2002) showing extrinsic bronchial compression and a destroyed convex lung . . . . .	106
6.2	Methodology for the segmentation and measurement of lung volumes. . . . .	107
6.3	Correlations between the spinal penetration index, right-left lung volume ratio, right lung airway cross-sectional area index, right lung non-aerated volume and $FEV_1/FVC$ . . . . .	113
6.4	Pre- and post-operative comparison of non-aerated volume . . . . .	114
6.5	Examples of air trapping in the right lung. . . . .	115
6.6	An example of a patient with simultaneous air-trapping and atelectasis. . . . .	116
6.7	Progression of airway obstruction in scoliosis. . . . .	118





# List of Tables

2.1	Radiographic-based thoracic deformity parameters and their definitions. Diagrams of the measurements can be found in Figures 2.1 and 2.2 . . .	22
2.2	Summary of all pre-operative patient characteristics, spirometry results and radiographic deformity parameters ( $n = 136$ ). . . . .	25
2.3	Pearson correlation coefficients between radiographic Cobb angles, deformity parameters and lung function ( $n = 136$ ). . . . .	26
2.4	Pearson correlation coefficients between deformity parameters ( $n = 136$ ). . . . .	29
2.5	Pre- and post-operative comparison of radiographic and pulmonary function measurements segregated by main thoracic curve severity . . . . .	29
2.6	Pre- and post-operative comparison of radiographic deformity parameters segregated by main thoracic curve severity . . . . .	30
2.7	Pre- and post-operative comparison of radiographic and pulmonary function measurements segregated by the Lenke sagittal thoracic modifier . . . . .	31
2.8	Pre- and post-operative comparison of radiographic deformity parameters segregated by the Lenke sagittal thoracic modifier . . . . .	32
2.9	Multivariate step-wise regression results for the prediction of pre-operative ( $n = 136$ ) and post-operative changes ( $n = 72$ ) in lung function using coronal and sagittal Cobb angles. . . . .	37
2.10	Multivariate step-wise regression results for the prediction of pre-operative ( $n = 136$ ) and post-operative changes ( $n = 72$ ) in lung function using radiographic Cobb angles and thoracic deformity parameters. . . . .	38
3.1	Pearson correlation coefficients between pre-operative radiographic Cobb angles, deformity parameters , lung function and the first nine principle components from the statistical shape model ( $n = 136$ ). . . . .	50
3.2	Qualitative descriptions of the first 9 principle components of the statistical shape model . . . . .	51
3.3	Multivariate step-wise regression results for the prediction of pre-operative ( $n = 136$ ) and post-operative changes ( $n = 72$ ) in lung function using principle component scores from statistical shape model. . . . .	61
4.1	CT-based thoracic deformity parameters and their definitions. Landmark definitions can be found in Figure 4.1 . . . . .	69
4.2	Summary of pre-operative lung function, radiographic and CT-measured deformity parameters . . . . .	74

4.3	Variance explained by principle component analysis and Pearson correlation coefficients between CT deformity principle component scores, lung function, Cobb angles and individual CT deformity parameters ( $n = 49$ ).	75
4.4	Pre- and post-operative comparison of radiographic and pulmonary function test measurements . . . . .	79
4.5	Multivariate regression results for the prediction of pre-operative ( $n = 49$ ) and post-operative changes ( $n = 40$ ) in lung function using radiographic parameters. . . . .	80
4.6	Multivariate regression results for the prediction of pre-operative ( $n = 49$ ) and post-operative changes ( $n = 40$ ) in lung function using CT thoracic deformity parameters. . . . .	81
4.7	Pre- and post-operative comparison of apical CT-based deformity parameters ( $n = 9$ ) . . . . .	84
5.1	Summary of pre-operative lung function, radiographic and CT-measured deformity parameters . . . . .	92
5.2	Pearson correlations between normalised airway lumen area, CT measured Cobb angles, deformity parameters and lung function . . . . .	96
5.3	Pre-post-operative comparison of deformity parameters, lung function and normalised airway lumen areas. . . . .	98
6.1	Summary of pulmonary function test results, radiographic and deformity parameters and lung volume parameters. . . . .	109
6.2	Pearson correlation coefficients between lung volume parameters, radiographic and CT deformity parameters, lung function and airway lumen cross sectional areas ( $n = 48$ ). . . . .	110
6.3	Multivariate stepwise regression results for the prediction of pre-operative ( $n = 48$ ) and post-operative changes ( $n = 41$ ) in lung function using CT thoracic deformity, airway and lung volume parameters. . . . .	111

# Chapter 1

## Introduction

### 1.1 Background

#### 1.1.1 Definition of adolescence idiopathic scoliosis (AIS)

In health, the spine is normally straight in the coronal plane whilst in the sagittal plane, the thoracic spine average approximately  $30^\circ$  of kyphosis (ranging from  $10^\circ$  to  $50^\circ$  as measured from T5 to T12) and the lumbar spine has a lordosis of approximately  $55^\circ$  to  $60^\circ$  (range  $30^\circ$  to  $80^\circ$  when measured from T12 to S1) [5, 6]. Scoliosis is defined as a  $10^\circ$  or greater curvature in the spine as measured by the Cobb method in the coronal plane [7, 8]. Although scoliosis has conventionally been regarded as a frontal plane curvature, the deformity is in fact three-dimensional where vertebral rotation occurs alongside displacement from the midline with variable expression in the sagittal plane [9, 10].

The etiology of scoliosis is classified generally as idiopathic, neuromuscular, syndrome related and congenital [11]. Idiopathic scoliosis, the most prevalent form constituting approximately 85% of cases, is defined as a lateral curvature of the spine where no etiology can be established [12]. Idiopathic scoliosis is then further divided according to the age at which the scoliosis is diagnosed. The age classifications are infantile (ages less than 3 years), juvenile (ages greater than 3 and less than 10 years), adolescent (ages between 10 and 18 years) and adult (those older than 18 years) as proposed by the Scoliosis Research Society (SRS) [12]. Thus, adolescence idiopathic scoliosis (AIS) is the presence of spinal curvature greater than  $10^\circ$  Cobb angle in patients first diagnosed between ages of 10 and 18 years in the absence of associated congenital or neurologic abnormalities. The overall prevalence of AIS has been estimated to be between 0.47% and 5.2% in the current literature [13].

#### 1.1.2 Measurement of AIS deformity

The extent of coronal misalignment due to scoliosis is measured using the Cobb method which was recommended by the Terminology Committee of the SRS (Figure 1.1) [8]. The terminal vertebrae of the curve are located on a standing anterior-posterior long spine radiograph. The terminal vertebrae of the curve are defined as the cranial and caudal vertebrae within the curve that are most tilted from the horizontal axis. The Cobb angle is defined as the degree of tilt between the cranial and caudal vertebrae as measured by outlining the superior and inferior endplates of the cranial and caudal

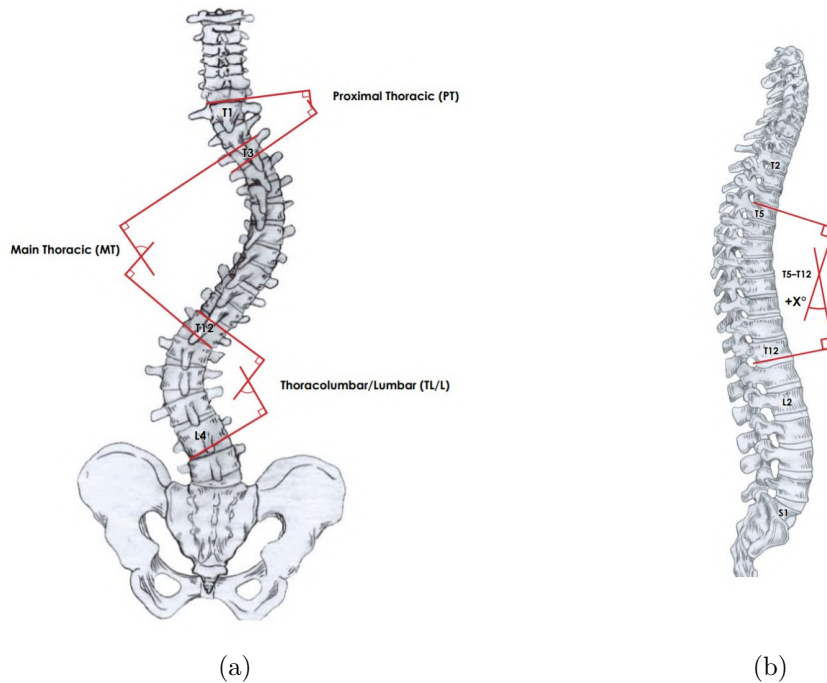


Figure 1.1: Diagram showing the measurement of Cobb angles in the coronal and sagittal plane. (a) Cobb angle measurements of the proximal thoracic (PT), main thoracic (MT) and thoracolumbar/lumbar (TL/L) curves. Intersecting lines are constructed perpendicular to the superior end plate of the superior end vertebra and the inferior end plate of the inferior end vertebra. The angle subtended by the perpendiculars is the Cobb angle for the selected curve. (b) Measurement of T5 to T12 thoracic kyphosis (TK) in the sagittal plane [1]. Figure adapted from [2].

vertebrae respectively. Lines perpendicular to the end plates are then constructed and the angle formed at the intersection of the perpendicular lines defines the Cobb angle of the curve.

The apex of a scoliosis curve is defined as the most laterally deviated and most horizontal vertebra or disk. A single vertebra can often be defined as the apex but if a pair of vertebrae are equally laterally displaced, the apical disk between the vertebrae is used to define the level of the apex.

The sagittal profile is quantified by the Cobb angle between the superior end plate of the proximal and inferior endplate of the distal vertebrae on standing long spine lateral radiographs. Although thoracic kyphosis begins at T1, the endplate of this vertebra is difficult to identify on lateral radiographs due to the surrounding bone structure. Thus T5 is used as the proximal thoracic vertebra and T12 is used as the distal [14].

### 1.1.3 Classification schemes for AIS

There are several classification schemes in the literature which describe the curve patterns of AIS curves [15, 4, 10]. The schemes factor in the magnitude of the curvature, the location and other factors, such as curve rigidity or the sagittal profile. This categorization of different curve pattern allows more effective communication between treating physicians, enabling treatment recommendations and the evaluation or comparison of

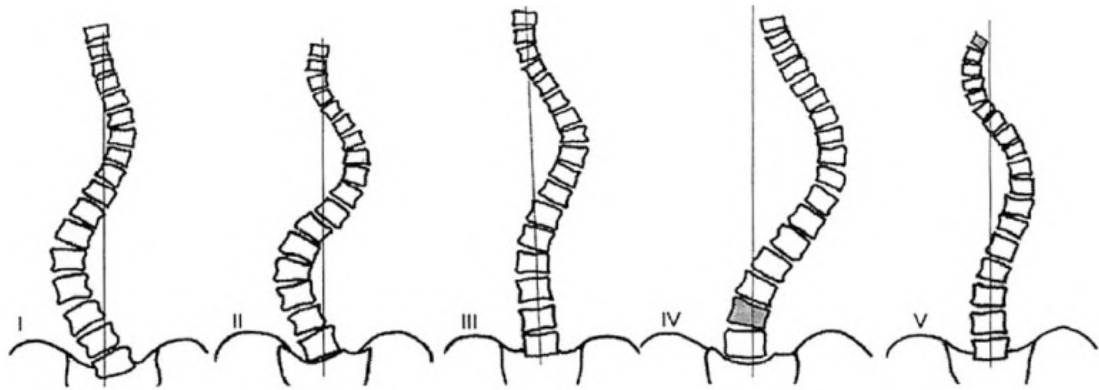


Figure 1.2: King classification for adolescent idiopathic scoliosis. Figure adapted from [3]

different treatment methods.

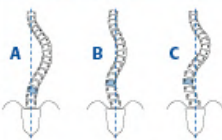
**King Classification** King et al. presented a classification scheme in 1983 to describe thoracic AIS [15]. For over 20 years, the King classification system was the primary scheme used to classify thoracic AIS and evaluation treatment outcomes. In the scheme, a total of five curve types were described embedded in a treatment algorithm which allowed surgeons to determine the appropriate vertebral levels for fusion (Figure 1.2) [16]. King type I curves are S-shaped curves where both the thoracic and lumbar curves crossed the midline. Both the thoracic and lumbar curves are structural and the lumbar curve is typically more severe or less flexible than the thoracic. King type II curves are also S-shaped curves but the thoracic curve is larger or less flexible than the lumbar curve. King type III curves are single thoracic curves without any structural lumbar curve. King type IV curves are long, extended thoracic curves where L5 is positioned over the sacrum but L4 is tilted towards the thoracic curve. King type V are double thoracic curves with T1 tilted into the convexity of the upper curve. The King system, however, has several limitations. Firstly, the system is not comprehensive as only thoracic curves were classified and as a consequence thoracolumbar, lumbar, double and triple major curves were not included. In addition, the patients in the case series of King et al. received Harrington rod instrumentation which focused on correcting only the coronal deformity. Thus the classification scheme fails to recognize the three-dimensional nature of the scoliosis by omitting measurements in the sagittal and axial plane [1]. Finally, fair to poor interobserver and intraobserver validity, reliability and reproducibility has been reported in studies assessing the King classification system [17, 18].

**Lenke Classification** As a result of the limitations of the King classification system, Lenke et al. formulated a new classification system for the operative treatment of AIS [10, 4]. The Lenke classification system was designed to include all curve types; incorporate sagittal plane alignment into the criteria; be treatment based by allowing selective fusion where appropriate; be objective by specifying the criteria to differentiate individual curve types; have good-to-excellent interobserver and intraobserver reliability; and be clinically practical [1].

The Lenke classification system for AIS				
Curve type	Proximal Thoracic	Main Thoracic	Thoracolumbar/Lumbar	Description
1	Nonstructural	Structural*	Nonstructural	Main Thoracic
2	Structural <sup>x</sup>	Structural*	Nonstructural	Double Thoracic
3	Nonstructural	Structural*	Structural <sup>x</sup>	Double Major
4	Structural <sup>x</sup>	Structural <sup>§</sup>	Structural <sup>§</sup>	Triple Major
5	Nonstructural	Nonstructural	Structural*	Thoracolumbar/Lumbar (TL/L)
6	Nonstructural	Structural <sup>x</sup>	Structural*	Thoracolumbar/Lumbar-Main Thoracic (TL/L-MT)

\*Major curve: largest Cobb measurement, always structural; <sup>x</sup>Minor curve: remaining structural curves; <sup>§</sup>Type 4 – MT or TL/L can be the major curve

Structural Criteria (Minor curves)		Location of Apex (SRS Definition)	
Proximal Thoracic	<ul style="list-style-type: none"> <li>Side Bending Cobb <math>\geq 25^\circ</math></li> <li>T2-T5 Kyphosis <math>\geq +20^\circ</math></li> </ul>	Curve	Apex
Main Thoracic	<ul style="list-style-type: none"> <li>Side Bending Cobb <math>\geq 25^\circ</math></li> <li>T10-L2 Kyphosis <math>\geq +20^\circ</math></li> </ul>	Thoracic	T2 to T11-12 Disc
Thoracolumbar/Lumbar	<ul style="list-style-type: none"> <li>Side Bending Cobb <math>\geq 25^\circ</math></li> <li>T10-L2 Kyphosis <math>\geq +20^\circ</math></li> </ul>	Thoracolumbar	T12-L1
		Lumbar	L1-2 Disc to L4

Modifiers			Thoracic Sagittal Profile T5-T12	
Lumbar Spine Modifier	Center Sacral Vertical Line to Lumbar Apex		Modifier	Cobb Angle
A	Between pedicles		- (Hypo)	$< 10^\circ$
B	Touches apical body (ies)		N (Normal)	$10^\circ - 40^\circ$
C	Completely medial		+ (Hyper)	$> 40^\circ$


Curve Type (1-6) + Lumbar Spine Modifier (A, B, C) + Thoracic Sagittal Modifier (-, N, +) = Curve Classification (e.g. 1B+): 

Figure 1.3: Lenke criteria for adolescent idiopathic scoliosis. Figure adapted from AO Foundation based on [4]

There are three elements to the Lenke classification system which consists of the curve type, a lumbar spine modifier and a sagittal thoracic modifier. Each element is determined independently and combined to create a classification triad. The system requires four radiographs: standing anterior-posterior and lateral radiographs along with supine left and right sided bending radiographs.

The spinal column is divided into three regions: a proximal thoracic (PT) curve with an apex at T3, T4 or T5; a main thoracic (MT) with an apex between T6 and T11/T12 disc; and a thoracolumbar/lumbar (TL/L) curve with an apex between T12 and L1 for thoracolumbar curves or between L1/L2 disk and L4 for lumbar curves. The Cobb angle is measured for each region and curves are categorized as major or minor with the largest curve being designated a major curve. The smaller minor curves are the classified as either structural or nonstructural by evaluating the rigidity of the curves and sagittal alignment. Structural curves demonstrate coronal plane rigidity of  $25^\circ$  on side-bending radiographs and/or a kyphosis of  $20^\circ$  on sagittal radiographs. Regional kyphosis is measured for PT curves between T2 and T5; MT from T10 to L2 and TL/L curves from T10 to L2. The identified major and minor structural curves then define the curve type based on Figure 1.3.

A lumbar spine modifier is added to quantify the lumbar coronal plane deformity. It is measured via the center sacral line (CSL) drawn vertically from the midpoint of S1 through the lumbar apical vertebra. If the CSL passes between the pedicles of the apical lumbar vertebra, a lumbar modifier A is assigned. If the CSL falls between the

medial edge of the concave pedicle and the lateral vertebral body, lumbar modifier B is assigned. If the CSL does not touch the lateral edge of the apical lumbar vertebra, lumbar modifier C is assigned [4, 10].

Similarly, a thoracic sagittal modifier is added to the classification to quantify the sagittal deformity. The sagittal modifier is based on the T5 to T12 thoracic kyphosis. For thoracic curves less than  $10^\circ$  a ‘-’ is given to signify hypokyphosis; thoracic kyphosis greater than  $40^\circ$  are designated a ‘+’ modifier to signify hyperkyphosis; and a thoracic kyphosis of between  $10^\circ$  and  $40^\circ$  inclusive is given an ‘N’ modifier to signify normokyphosis [4, 10].

#### 1.1.4 Pulmonary Function Testing in Scoliosis

Spirometry is a basic pulmonary function test that measures the amount of air that is expired or inspired; the three basic measurements are volume, time and flow [19]. Forced vital capacity (FVC) is the maximal tidal excursion from total lung capacity to the residual volume. When the full expiratory maneuver is performed with maximal effort, the volume of air expired in the first second reflects the maximal ventilatory capacity of the lung. This forced expiration in 1 second ( $FEV_1$ ) and FVC are widely used metrics of lung function [20]. In addition, the ratio between  $FEV_1$  and FVC ( $FEV_1/FVC$ ) is often used as a metric of airway resistance as  $FEV_1$  will decrease due to reduced airflow when airway resistance is increased [20]. The measured lung function metrics are usually expressed as a percentage of normal references values which factor in the age, sex and stature (height) of the patient [21, 22]. Standing height is reduced in scoliosis due to curvature of the spine and thus arm-span is used to predict height in the absence of scoliosis [23]. Patients who are selected for scoliosis correction surgery routinely undergo pulmonary function testing prior to surgery with spirometry and lung volume testing [24]. However, patients with mild or moderate curves typically do not undergo pulmonary function testing unless they are symptomatic of respiratory impairment.

## 1.2 Motivation

AIS may lead to severe pulmonary impairment [25, 26, 27], and even death due to cardiorespiratory failure if progressive and left untreated [28], but the contributing factors are poorly understood. Correlational studies analyzing the association between scoliosis and respiratory function have typically found a weak to moderate effect. Newton et al. demonstrated the incidence of moderate or severe pulmonary impairment in moderate thoracic scoliotic curves of less than  $50^\circ$  which contradicted the widely held view that only severe scoliosis results in pulmonary impairment [29]. Although alternate factors such as increased number of vertebrae involved, the cephalad location of the curve and loss of thoracic kyphosis have been found to be associated with impaired lung function [25, 26, 27], studies attempting to predict lung function often produce statistical models with low variance-explained metrics [24, 29].

In addition, due to secondary anatomical interconnections, the spinal deformity affects the thoracic configuration of the chest which may be the primary source of lung function impairment. Thoracic deformity in scoliosis is typically characterise by the formation of a posterior rib hump on the convex side, lateral vertebral translation



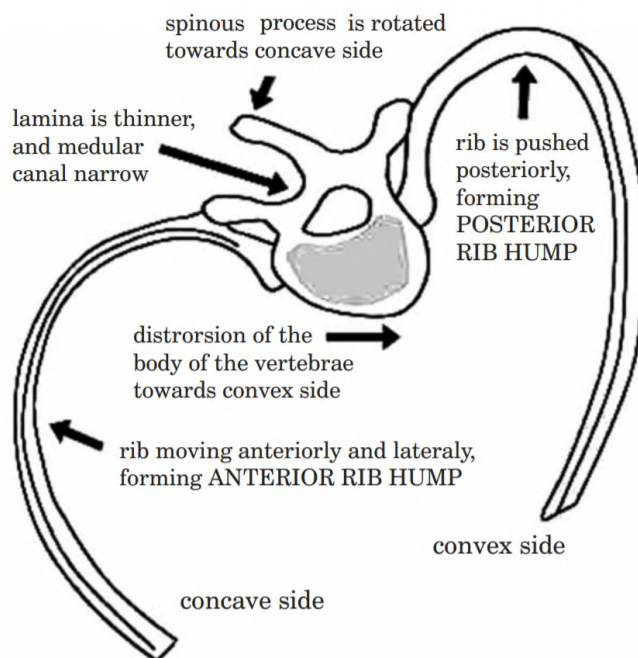


Figure 1.4: Figure showing the thoracic deformity associated with scoliosis. Characteristic features include the posterior rib hump on the convex side, vertebral translation towards the convexity and elevation of the concave ribs.

relative to the chest wall and thoracic rotation via lateral/anterior translation of the concave ribs (Figure 1.4). Investigation into the relationship between the thoracic deformity and lung function may give insight into the mechanisms behind lung function impairment in AIS.

Whilst radiographic imaging is routinely used in the management of scoliosis [7], pulmonary function testing is often limited to patients who are candidates for scoliosis correction surgery, due to curve progression or severity, or those who are already symptomatic of pulmonary impairment. Thus it is plausible that asymptomatic patients with impaired lung function and a moderate thoracic curve would not receive pulmonary function testing until their scoliosis progressed to the extent where they are selected for surgery or until they become symptomatic [29]. Identification of deformity parameters more strongly associated with pulmonary function impairment may allow the identification of patients most at risk of severe pulmonary impairment. From such parameters, the mechanisms associated with the impairment may also be inferred allowing surgeons to correct the deformity with the possibility of improving lung function post-operatively.

### 1.3 Aims and objectives

The purpose of this research was to perform a retrospective imaging study to investigate the effects of scoliosis on respiratory function. Anonymised clinical data, acquired between 2008 and 2019, in the form of radiographic images, computed tomography (CT) images and spirometry results were obtained from the Scottish National Spine

Deformity Service, Royal Hospital for Sick Children, Edinburgh, UK. This project focused specifically on Lenke type I and II curves types as primary thoracic curves have previously been shown to be more associated with respiratory impairment than other curve types [29].

The hypothesis for this research is that measurements from images obtained through routine clinical care are predictive of pulmonary function impairment in AIS. In particular, that measurements which factor in the global thoracic deformity, rather than measurements isolated to the spine, are more successful at predicting respiratory compromise.

The specific objectives of this thesis were to:

- Identify thoracic features or scoliotic phenotypes which are associated with lung function impairment in AIS.
- Examine possible mechanisms in which lung function impairment is exacerbated by the thoracic deformity.
- Identify subgroups most likely to observe lung function improvement postoperatively and benefit from surgical intervention.

## 1.4 Thesis structure

The thesis is split into two parts based on the main imaging modality used in the study; Part I consists of radiographic studies whilst Part II consist of studies which use images from computed tomography (CT). Part I begins with Chapter 2 which assesses the ability of radiographically derived deformity measurements and indices to predict pre-operative lung function and post-operative lung function improvement. Chapter 3 investigates the morphological patterns of the spine and rib cage in the frontal and lateral plane using a statistical shape model. These modes of variation are correlated with lung function to identify thoracic shapes which are predictive of lung function impairment in AIS. In Part II, Chapter 4 uses CT-based thoracic deformity parameters to explain preoperative lung function impairment and postoperative lung function gain. Chapter 5 studies the effect of scoliosis on the tracheobronchial tree to investigate airway narrowing as a potential cause of pulmonary impairment. Chapter 6 investigates variation in lung volume and density to study the role of atelectasis and air-trapping in impairing lung function. Finally, Chapter 7 provides general conclusions and recommendations for future work.



**Part I**

**Radiographic Studies**



## Chapter 2

# Radiographic Indices

### 2.1 Summary

In this chapter, radiographic measurements of thoracic deformity in patients with adolescent idiopathic scoliosis (AIS) were investigated for their utility in predicting pre- and post-operative changes in pulmonary function. The thoracic deformity parameters measured were rib-vertebra angle difference (RVAD), inverse of the apical vertebral body rib ratio (AVBRr<sup>-1</sup>), space available for lung (SAFL), kyphosis-lordosis index (KLi), spinal intrusion ratio (SIr) and rib hump index (RHi). Deformity parameters, Cobb angles of the coronal and sagittal deformity, and pulmonary function was measured in 136 patients with Lenke type 1 or 2 AIS. In 72 of the patients, post-operative radiographs and pulmonary function results were available. Upon multivariate analysis, it was found that deformity parameters were better predictors of pulmonary function in AIS than Cobb angles. Increased spinal intrusion (SIr), reduced convex hemithorax width (AVBRr<sup>-1</sup>), and increased rib hump (RHi) were found to be significant predictors of FEV<sub>1</sub> and FVC reduction. FEV<sub>1</sub>/FVC was found to be best predicted by KLi and RHi. Hypokyphotic patients were found to have lower FEV<sub>1</sub>/FVC ratios implying an obstructive nature to their pulmonary impairment. Whilst hyperkyphotic patients did not significantly improve, hypo- and normokyphotic patients showed improved lung function metrics following scoliosis correction surgery. It is recommended that patients with hypokyphosis and severe respiratory impairment be investigated for possible airway obstruction with operative treatment focussing on the restoration of natural kyphosis.

### 2.2 Introduction

The effect of spinal deformity on pulmonary function in AIS is of particular importance because of the increased morbidity and early mortality due to respiratory failure in untreated progressive scoliosis [28, 30, 31, 32]. Whilst extensive investigation has been conducted into the relationship between pulmonary impairment and spinal deformity [29, 27, 25, 24, 33], research into the role of the associated thoracic deformity in impairing lung function has been limited to a few studies [34, 35, 36]. The objectives of this study are to: (1) investigate whether radiographic measurements of the thoracic morphology have a stronger association with lung function in scoliosis than traditional Cobb angle measurements; (2) identify the thoracic features which are associated with

pulmonary function impairment in scoliosis and infer the mechanisms of impairment; and (3) to determine whether such impairment is reversible with scoliosis correction surgery.

## 2.3 Literature Review

Several radiographic studies have previously demonstrated that scoliosis, as measured on coronal radiographs, influences respiratory function in patients with AIS. In a study of 631 patients with AIS, Newton et al. [29] demonstrated that the incidence of moderate to severe pulmonary impairment increased with increasing coronal deformity. From their study of 41 adults with untreated AIS, Jackson et al. [37] found that FVC was significantly impaired ( $p < 0.008$ ) in patients with scoliosis greater than  $40^\circ$ . This is further supported by a cross-sectional study of 492 AIS patients conducted by Dreimann et al. [27] who found that subjects with FVC less than 50% of predicted had significantly larger scoliosis curves ( $p < 0.001$ ) than those with higher FVC. Kearon et al. [25] had similar findings in their study of 66 patients with AIS. They acknowledged that the coronal deformity contributed to reduced lung function but that it was not an adequate predictor of pulmonary impairment on its own. Upadhyay et al. [34] also found that there was a negative association between curve size and vital capacity.

In the sagittal plane, previous studies have shown mixed effects of thoracic kyphosis on pulmonary function with some studies showing weak or non-significant correlations with expiratory volumes ( $r = 0.15$  to  $0.24$ ) [29, 24, 34] whilst others show a stronger relationship ( $r = 0.30$  to  $0.44$ ) [33, 38]. Newton et al. [29] determined that there was a positive correlation between thoracic kyphosis and spirometry volumes ( $r = 0.157$  to  $0.174$ ) with hypokyphotic ( $< 10^\circ$ ) patients more likely to have pulmonary impairment and hyperkyphotic patients ( $> 40^\circ$ ) having relatively better pulmonary function. Dreimann et al. [27] found that patients with thoracic kyphosis of less than  $10^\circ$  had significantly lower FVC than those with more than  $10^\circ$  ( $p = 0.002$ ). Similarly, Kearon et al. [25] also found that loss of normal thoracic kyphosis significantly contributed to reducing vital capacity ( $p = 0.002$ ). Whilst determining that thoracic kyphosis correlated with static lung volumes such as total lung capacity ( $p = 0.022$ ), functional residual capacity ( $p = 0.036$ ) and residual volume ( $p = 0.046$ ), Upadhyay et al. [34] found that it did not significantly have an effect on spirometry volumes. Although Jackson et al. [37] did not comment on the effects of hypokyphosis, they concluded that thoracic hyperkyphosis greater than  $50^\circ$  was related to decreased FVC.

Despite existing correlational studies between spinal deformity and pulmonary function, studies to date predicting  $FEV_1$  and FVC from radiographic-derived variables have typically yielded models with low percentage of variance explained ( $r^2$ ) with models typically explaining between 5% to 20% of the total variance ( $r^2 = 0.05$  to  $0.2$ ). Predictors incorporated in these statistical models have included scoliosis curve size [24, 29, 27], scoliosis measured on bending [27], thoracic kyphosis [24, 29], number of vertebrae in the thoracic curve [29], 7th cervical vertebra (C7) displacement from central sacral vertical line [29].

The majority of existing radiographic studies have focused on spinal parameters [24, 29, 27, 33] with only a few measuring the associated thoracic deformity. Upadhyay et al. [34] measured elements of the thoracic cage deformity which included the sternovertebral depth, sternovertebral depth normalized by vertebra width and the rib-

vertebral angle difference as measured by Mehta [39]. They found that sternovertebral depth correlated with absolute values of FVC and TLC ( $p = 0.036$  and  $0.029$  respectively) but not with the percent-predicted values; the normalized sternovertebral depth did not correlated with any lung function parameters. Rib-vertebral angle asymmetry correlated with percent-predicted functional residual capacity but not with expiratory volumes. Ilharreborde et al. [38] performed three-dimensional reconstructions of the thorax to measure the spinal penetration index (SPi) [40] – a quantification of the degree of spinal intrusion into the thorax relative to the thoracic space originally measured using computer tomography imaging. They found no correlation between the SPi and FVC or FEV<sub>1</sub> but found that SPi was significantly greater in patients with obstructive symptoms ( $p = 0.01$ ).

Several radiographic thoracic deformity parameters have been proposed in the literature. The apical vertebral body-rib ratio (AVBRr) was proposed by Kuklo et al. [41] to measure the narrowing width of the convex hemithorax as a result of the lateral displacement of the spine. The ratio has been shown to be correlated with the main thoracic angle ( $r = 0.57$ ) and apical vertebral rotation ( $r = 0.49$ ). The use of distances rather than angles recognises a limitation of the Cobb method where two curves of the same angulation at the end-plates may differ in the extent to which they protrude into the hemithorax. Similarly, in the sagittal plane, the kyphosis-lordosis index [42, 43] measures the space available anterior to the spinal column from the T1-T12 midline. Campbell et al. [44] introduced the measurement space available for lung (SAFL) which measures the height of the concave hemithorax relative to the convex hemithorax; this measurement of height asymmetry has typically been used to indicate asymmetric growth in infantile cases. The formation of a rib hump on the convexity is a feature of thoracic scoliosis as the ribs on the convex side are pushed posteriorly. Kuklo et al. [41] measured the distance between the left and right posterior rib prominences at the apex of the rib deformity and showed that the rib prominence correlated significantly with the main thoracic Cobb angle ( $r = 0.65$ ). Grivas et al. [45, 46, 47] proposed the rib index which was defined as the relative distance between the convex and concave ribs measured from the posterior contour of the spinal column.

Kim et al. [48] studied the post-operative pulmonary function change in 139 patients who underwent scoliosis correction using thoracic pedicle screw and thoracic hook instrumentation. They found weak positive correlation between the degree of scoliosis corrected and the post-operative percentage-predicted change in FEV<sub>1</sub> and FVC ( $r = 0.16$  to  $0.26$ ). The authors found no significant difference between the change in FEV<sub>1</sub> or FVC when considering the degree of scoliosis corrected. With regards to the sagittal profile, an average loss of  $8^\circ$  in thoracic kyphosis was observed and there too was no significant difference in the degree of pulmonary function improvement when subjects were segregated based on the direction of kyphosis change. In a 25-year follow-up study in 251 patients who underwent surgical correction of scoliosis, Pehrsson et al. [49] found that percent-predicted vital capacity and FEV<sub>1</sub> were significantly higher than the pre-operative values by 17% and 13% respectively ( $p < 0.001$ ). The patients were found to have increased vital capacity and FEV<sub>1</sub> percent-predicted values by 11% and 6% from 1.4 years after surgery to the 25-year follow-up leading the authors to conclude that patients gradually increase their pulmonary function up to 25 years after treatment.

From this review, it can be seen that although the relationship between coronal Cobb measurements and pulmonary function has been extensively studied, the role of



the sagittal profile in pulmonary function impairment is still unclear. Moreover, the effect of the thoracic deformity, as measured by deformity parameters, has not been widely investigated.

## 2.4 Materials & Methods

### 2.4.1 Subject Characteristics

A retrospective review of the surgeon's imaging database between 2015 and 2019 (Kodak Carestream PACS) at the Scottish National Spine Deformity Service was conducted to identify Lenke type 1 or 2 AIS patients with right-sided, thoracic curves with an apex between the seventh and tenth thoracic vertebrae (T7-T10). Patients who underwent coronal and sagittal radiographic imaging and pulmonary function tests (PFT) were included. Patients with evidence or a history of primary obstructive lung disease were excluded. A total of 136 patients (96 female and 40 male) with a mean age of 15.6 years (standard deviation [SD] = 5.1 years, range = 10.0 to 56.0 years) met the inclusion criteria. Patients underwent scoliosis correction surgery by posterior instrumental fusion using segmental pedicle screws and rods. Out of the 136 patients, 72 patients had post-operative PFTs with a minimum follow-up of 6 months.

### 2.4.2 Lung Function

PFTs were conducted via forced manoeuvres in accordance with the joint American Thoracic Society and European Respiratory Society standards [50]. Forced expiration in 1 second ( $FEV_1$ ) and forced vital capacity (FVC) were measured (Jaeger MasterScreen PFT pro) along with armspan. In calculating lung function predicted values, arm span was used to estimate standing height to correct for scoliotic height loss and age-related or post-operative height gains [23]. Estimated standing height was used along with patient age at the time of testing to determine the predicted values based on reference data by the Global Lung Function Initiative [22].  $FEV_1$ , FVC and  $FEV_1/FVC$  are expressed as a percentage of their respective predicted values (% predicted).

### 2.4.3 Spinal and Thoracic Parameters

Patients underwent coronal and sagittal long-spine plain film radiographic imaging. Using the Cobb method, the main thoracic curve (MT), proximal thoracic curve (PT) and thoracolumbar/lumbar curve (TL/L) were measured on coronal radiographs whilst T5-T12 thoracic kyphosis (TK) was measured in the sagittal plane. In addition, 7 radiographic thoracic deformity parameters were measured (Table 2.1). In the coronal plane, the rib vertebra angle difference (RVAD), as described by Mehta [39], was measured (Figure 2.1a). The inverse of the apical vertebral body-rib ratio ( $AVBRr^{-1}$ ; inverse of the index described by Kuklo et al. ( $AVBRr$ ) [41]) was measured (Figure 2.1b). The index describes the width of the convex hemithorax relative to the concave hemithorax. The space available for lung (SAFL) by Campbell et al. [44] was measured which describes the relative asymmetry in hemithoracic height (Figure 2.1c). To formulate a measurement of thoracic height, the heights measured by SAFL were averaged and normalised by the width of the ribcage to give the lung height-width ratio (LHW<sub>r</sub>). In the sagittal plane, the kyphosis-lordosis index, originally described by Voutsinas and

MacEwen [42, 43], was modified such that the height was taken to be measured between T1 and T12 vertebral body centroids (Figure 2.2a). Although existing measures of the rib hump exist, they are either not normalized [41] or are only suitable to measuring mild/moderate deformities [45] (denominator of zero is possible). In this work, the rib hump index (RHi) is defined as the ratio between the posterior distance of the concave and convex rib hump as measured from the anterior contour of the spinal column subtracted from unity (Figure 2.2b). In the absence of a hump, the index will give a value of zero indicating perfect alignment; in cases with severe rotation, the concave rib contour may be anterior to the vertebral column in which case RHi will have a value greater than unity. The spinal intrusion ratio (SIr), a radiographic approximation of the computed tomographic-based endothoracic hump ratio (EHr) by Ito et al. [51], was also measured on the sagittal radiograph (Figure 2.2). The index measures the degree of spinal intrusion into the thorax relative to the depth of the chest.

#### 2.4.4 Statistical Methods

Pearson correlation coefficients were determined between spirometry results, Cobb angles and deformity parameters for the pre-operative sample. Post-operative comparisons were performed by splitting patients into groups based on the characteristics of their coronal and sagittal profiles. In the coronal plane, patients were split into two groups based on the severity of the MT curve: those with MT less or equal to  $70^\circ$  and those with MT curves greater than  $70^\circ$ . In the sagittal analysis, patients were segregated based on their Lenke sagittal modifier [10]: hypokyphosis ( $-$ ) with  $TK < 10^\circ$ ; normokyphosis (N) with  $10^\circ \leq TK \leq 40^\circ$ ; and hyperkyphosis ( $+$ ) with  $TK > 40^\circ$ . Lung function results and radiographic parameters were compared using the Kruskal-Wallis test and post-hoc Dunn's test to determine whether a significance difference existed between the groups. Pairwise  $t$ -test was conducted between pre- and post-operative results to study the effect of scoliosis correction. The  $p$ -values from Pearson correlations, Kruskal-Wallis tests, Dunn's test and pairwise  $t$ -test were corrected for multiple comparisons ( $q$ -values) using the Benjamini and Hochberg method [52] with  $q$ -value threshold of 0.05 corresponding to a false discover rate of 5%. To determine whether thoracic deformity parameters are better predictors of lung function than radiographic Cobb angles, pre-operative and post-operative change (denoted with  $\Delta$ ) in lung function were regressed against radiographic Cobb angles and radiographic thoracic deformity parameters using step-wise multivariate regression with bi-directional elimination. The Bayesian information criterion (BIC) was employed for model selection with  $k = \ln(n)$  [53]. Models with the best fit are reported with regression coefficients for individual predictors ( $b$ ), their standard errors ( $SE(b)$ ) and standardised coefficients ( $\beta$ ) along with the coefficient of determination adjusted for multiple comparisons ( $r^2$ ) and model standard error (SE). All statistical analysis was implemented using the statistical software R (<http://www.R-project.org>).

## 2.5 Results

A summary of all pre-operative patients characteristics can be found in Table 2.2. Results for the correlational analysis between Cobb angles, lung function and deformity parameters can be found in Tables 2.3 and 2.4. Tables 2.5 and 2.6 show a pre- and

post-operative comparison of Cobb angles, spirometry results and thoracic deformity parameters when patients were segregated by pre-operative MT curve severity. There were 35 patients with an MT of  $70^\circ$  or less and 37 patients with MT greater than  $70^\circ$ . The pre- and post-operative comparison of Cobb angles, spirometry results and thoracic deformity parameters when patients were segregated by pre-operative Lenke sagittal thoracic modifier are shown in Tables 2.7 and 2.8. There were 22 hypokyphotic, 37 normokyphotic and 13 hyperkyphotic patients.

### 2.5.1 Pre-operative analysis

**Cobb Angles and Lung Function** MT was found to be correlated to PT ( $r = 0.35$ ) and TL/L ( $r = 0.35$ ; Table 2.3). Both MT ( $r = -0.52$  and  $-0.54$ ) and PT ( $r = -0.30$ ) were found to correlate negatively with FEV<sub>1</sub> and FVC respectively. There was a weak correlation between TK and MT ( $r = 0.27$ ) as well as TL/L ( $r = 0.35$ ); subjects with MT curves greater than  $70^\circ$  were found to be more kyphotic ( $q = 0.044$ ; Table 2.5). No correlation was found between TK and FEV<sub>1</sub> or FVC but a significant positive correlation was found for FEV<sub>1</sub>/FVC ( $r = 0.35$ ). Hypokyphotic patients were found to have lower FEV<sub>1</sub>/FVC values than both normokyphotic ( $q = 0.044$ ) and hyperkyphotic patients ( $q = 0.031$ ; Table 2.7).

**Rib-vertebra angle difference (RVAD)** RVAD was correlated positively to PT ( $r = 0.30$ ) and MT curves ( $r = 0.52$ ); RVAD was negatively correlated with FEV<sub>1</sub> ( $r = -0.36$ ) and FVC ( $r = -0.35$ ; Table 2.3). RVAD also had significant correlations with other deformity parameters such as AVBRR<sup>-1</sup> ( $r = -0.71$ ), SAFL ( $r = -0.28$ ) and RHi ( $r = 0.38$ ; Table 2.4). Subjects with MT curves greater than  $70^\circ$  were found to have significantly higher rib asymmetry than those with lower MT curves ( $q = 0.004$ ; Table 2.5).

**Inverse apical vertebral body-rib ratio (AVBRR<sup>-1</sup>)** AVBRR<sup>-1</sup> correlated negatively with both MT ( $r = -0.81$ ) and PT curves ( $r = -0.44$ ) whilst positively with FEV<sub>1</sub> ( $r = 0.58$ ) and FVC ( $r = 0.59$ ; Table 2.3). AVBRR<sup>-1</sup> also significantly correlated with SAFL ( $r = 0.35$ ) and RHi ( $r = -0.51$ ; Table 2.4). Subjects with MT curves greater than  $70^\circ$  had significantly reduced convex hemithoracic widths when compared with those with smaller MT curves ( $q < 0.001$ ; Table 2.5). Two examples of patients with high and low AVBRR<sup>-1</sup> are shown in Figure 2.7.

**Space available for lung (SAFL)** SAFL correlated negatively with MT ( $r = -0.50$ ) and TL/L ( $r = -0.44$ ) but positively with PT ( $r = 0.37$ ; Table 2.3). SAFL also correlated weakly with LHWr ( $r = 0.28$ ), KLi ( $r = -0.21$ ) and RHi ( $r = -0.26$ ; Table 2.4). Patients with MT curves greater than  $70^\circ$  showed significantly shorter concave hemithoraxes relative to those with smaller MT curves ( $q = 0.039$ ; Table 2.5).

**Lung height-width ratio (LHWr)** LHWr was found to negatively correlate with MT ( $r = -0.22$ ), TL/L ( $r = -0.35$ ), TK ( $r = -0.42$ ), FEV<sub>1</sub> ( $r = -0.30$ ) and FVC ( $r = -0.27$ ; Table 2.3). LHWr was also found to correlated significantly with KLi ( $r = -0.25$ ) and SIr ( $r = 0.46$ ; Table 2.4). Subjects with MT curves greater than  $70^\circ$  had significantly reduced lung heights when compared with those with smaller MT curves

( $q = 0.21$ ; Table 2.5). Hyperkyphotic patients had significantly shorter lungs relative to both hypokyphotic ( $q < 0.001$ ) and normokyphotic patients ( $q = 0.021$ ; Table 2.8).

**Kyphosis-lordosis index (KLi)** KLi was positively weakly correlated with MT ( $r = 0.26$ ) and TL/L ( $r = 0.26$ ), moderately correlated with FEV<sub>1</sub>/FVC ( $r = 0.40$ ) and strongly correlated with TK ( $r = 0.79$ ; Table 2.3). KLi also showed significant correlations with SIr ( $r = -0.65$ ) and RHi ( $r = 0.41$ ; Table 2.4). Patients with more severe MT curves had higher KLi values ( $q = 0.022$ ; Table 2.5) and KLi was significantly different across all Lenke sagittal modifier groups ( $q < 0.001$ ; Table 2.8).

**Spinal intrusion ratio (SIr)** SIr was positively correlated with PT ( $r = 0.22$ ), negatively correlated with TL/L ( $r = -0.21$ ) and negatively correlated with TK ( $r = -0.60$ ). SIr showed moderate correlations with FEV<sub>1</sub> ( $r = -0.54$ ), FVC ( $r = -0.47$ ) and FEV<sub>1</sub>/FVC ( $r = -0.34$ ; Table 2.3). SIr was found to be significantly different across all Lenke sagittal modifier groups ( $q < 0.02$ ; Table 2.8). Two examples of patients with high and low SIr are shown in Figure 2.8.

**Rib hump index (RHi)** RHi was positively correlated with both MT ( $r = 0.57$ ) and TL/L ( $r = 0.26$ ) as well as TK ( $r = 0.33$ ). RHi also correlated negatively with FEV<sub>1</sub> ( $r = -0.31$ ) and FVC ( $r = -0.32$ ; Table 2.3). Patients with MT curves greater than 70° showed significantly greater rib humps compared to those with smaller MT curves ( $q < 0.001$ ; Table 2.5). Hyperkyphotic patients had significantly larger rib humps relative to both hypokyphotic ( $q = 0.004$ ) and normokyphotic patients ( $q = 0.031$ ; Table 2.8).

### 2.5.2 Effect of scoliosis surgery

**Analysis by coronal profile** MT was corrected from a mean of 60.2° to 29.2° for curves less than 70° whilst those with greater MT were corrected from a mean of 84.4° to 35.6° (Table 2.5). The less severe MT group significantly gained a mean TK of 4.8° from 16.0° to 20.8° whilst the more severe MT group gained a mean TK of 3.6° from 25.5° to 29.0°. No significant difference in the change of lung function or Cobb angles were found between the groups when segregated by MT severity. However, significant post-operative changes in all spirometry metrics were observed for both groups. Less severe MT curves gained 8.7 (% predicted) of FEV<sub>1</sub> from 67.5 (% predicted) to 76.3 (% predicted) whilst more severe curves gained a greater 12.5 (% predicted) from 63.2 (% predicted) to 75.6 (% predicted). FVC was found to increase by a mean of 6.3 (% predicted) from 71.4 (% predicted) to 77.7 (% predicted) in the less severe group whilst the more severe group gained a higher 10.5 (% predicted) from 66.6 (% predicted) to 77.1 (% predicted). FEV<sub>1</sub>/FVC increased by 4.2 (% predicted) in the less severe group from 93.4 (% predicted) to 97.6 (% predicted) whilst the more severe group gained 2.8 (% predicted) from 94.7 (% predicted) to 97.5 (% predicted). The more severe MT group showed a significant degree of correction in RVAD whilst the less severe group did not; there was no significance in RVAD between the groups post-operatively (Table 2.6). AVBRr<sup>-1</sup> showed a significant difference between the groups post-operatively despite the more severe group showing a significantly higher degree of correction. Significant pre-operative differences in SAFL ( $q = 0.04$ ) were resolved post-operatively with the more severe group gaining 15.0% versus the less severe curves of 10.2%. Similarly, the

significant pre-operative difference between groups in LHW<sub>r</sub> ( $q = 0.02$ ) was resolved post-operatively with the more severe group gaining significantly more in LHW<sub>r</sub> ( $q = 0.046$ ). KLi was significantly lower in the less severe group both pre- ( $q = 0.022$ ) and post-operatively ( $q = 0.021$ ). No significant difference in SI<sub>r</sub> was observed between the groups post-operatively. Although both groups showed reductions in RHi, RHi remained higher post-operatively ( $q < 0.001$ ) in the more severe group.

**Analysis by sagittal profile** No significant differences in the change of MT or post-operative MT were observed between the groups (Table 2.7). Hypokyphotic patients were corrected from a mean TK of  $2.1^\circ$  to  $17.5^\circ$  with a significant gain of  $15.5^\circ$ ; normokyphotic patients gained  $3.9^\circ$  from  $21.5^\circ$  to  $25.4^\circ$ ; and hyperkyphotic patients lost  $14.3^\circ$  of TK from  $50.9^\circ$  to  $36.6^\circ$ . Significant differences in TK still existed between all three groups postoperatively ( $q < 0.05$ ). Hypokyphotic and normokyphotic patients observed significant gains in FEV<sub>1</sub>, FVC and FEV<sub>1</sub>/FVC post-operatively ( $q < 0.05$ ). Hypokyphotic patients gained 16.6 (% predicted) in FEV<sub>1</sub> from 57.8 (% predicted) to 74.4 (% predicted) whilst normokyphotic subjects gained 8.9 (% predicted) from 68.4 (% predicted) to 77.3 (% predicted). The gain in FEV<sub>1</sub> in hypokyphotic patients was significantly greater than the gain in hyperkyphotic patients ( $q = 0.029$ ). FVC was increased by 14.0 (% predicted) in hypokyphotic patients from 64.2 (% predicted) to 78.2 (% predicted) whilst normokyphotic patients gained 6.6 (% predicted) from 71.2 (% predicted) to 77.8 (% predicted). FEV<sub>1</sub>/FVC increased by 5.1 (% predicted) to 89.5 (% predicted) in the hypokyphotic group whilst the normokyphotic group gained 3.6 (% predicted) to 99.0 (% predicted). Hyperkyphotic patients did not observe any significant post-operative changes in any of the spirometry metrics. Significant differences in post-operative values and post-operative change for KLi were observed across all three groups ( $q < 0.001$ ; Table 2.8). KLi increased by 5.4% from -2.5% to 2.8% for the hypokyphotic group; whilst the normokyphotic group increased by 2.2% from 4.2% to 6.5%; and the hyperkyphotic group did not change significantly from 13.9% to 12.3% post-operatively. Hypokyphotic patients showed significant reductions in SI<sub>r</sub> post-operatively from 1.19 to 1.01 ( $q = 0.002$ ). SI<sub>r</sub> was significantly different post-operatively across all three groups ( $q < 0.05$ ). All groups showed significant improvements in AVBR<sub>r</sub><sup>-1</sup>, SAFL, RHi post-operatively ( $q < 0.05$ ). Although normokyphotic and hyperkyphotic subjects had significant increases in LHW<sub>r</sub> post-operatively ( $q < 0.01$ ), hypokyphotic subjects did not ( $q = 0.92$ ).

### 2.5.3 Multivariate Step-wise Regression Models

**Cobb Angles** Table 2.9 shows the best regression models for pre-operative and post-operative changes in lung function when using coronal and sagittal Cobb angles as predictors in step-wise regression. Pre-operative FEV<sub>1</sub> was found to be best predicted using MT ( $\beta = -0.609$ ) and TK ( $\beta = 0.341$ ;  $r^2 = 0.365$ ). Pre-operative FVC was also best predicted by MT ( $\beta = -0.6$ ) and TK ( $\beta = 0.231$ ;  $r^2 = 0.329$ ). Pre-operative FEV<sub>1</sub>/FVC was found to be best predicted by TK ( $\beta = 0.350$ ;  $r^2 = 0.116$ ). Post-operative change in FEV<sub>1</sub> was found to be best predicted by  $\Delta$ MT ( $\beta = -0.509$ ) and TK ( $\beta = -0.469$ ;  $r^2 = 0.318$ ). The best predictors of  $\Delta$ FVC were found to be  $\Delta$ MT ( $\beta = -0.533$ ) and TK ( $\beta = -0.463$ ;  $r^2 = 0.254$ ). Post-operative change in FEV<sub>1</sub>/FVC was found to be best predicted by  $\Delta$ TK ( $\beta = 0.319$ ;  $r^2 = 0.089$ ).

**Cobb and Deformity Parameters** Table 2.10 displays the best step-wise regression models for pre-operative and post-operative changes in lung function when Cobb and deformity parameters were used as predictors. Pre-operative FEV<sub>1</sub> was found to be best predicted by SIr ( $\beta = 0.425$ ), AVBRr<sup>-1</sup> ( $\beta = -0.516$ ) and RHi ( $\beta = -0.175$ ;  $r^2 = 0.569$ ). Pre-operative FVC was best predicted by SIr ( $\beta = -0.578$ ), AVBRr<sup>-1</sup> ( $\beta = 0.477$ ) and RHi ( $\beta = -0.175$ ;  $r^2 = 0.512$ ). KLi ( $\beta = 0.482$ ) and RHi ( $\beta = -0.202$ ) were found to be best predictors for pre-operative FEV<sub>1</sub>/FVC ( $r^2 = 0.181$ ).  $\Delta$ FEV<sub>1</sub> was found to be best predicted by SIr ( $\beta = 0.568$ ) and  $\Delta$ AVBRr<sup>-1</sup> ( $\beta = 0.242$ ;  $r^2 = 0.412$ ). SIr ( $\beta = 0.521$ ) and  $\Delta$ AVBRr<sup>-1</sup> ( $\beta = 0.203$ ) were also the best predictors of  $\Delta$ FVC ( $r^2 = 0.331$ ). Post-operative change in FEV<sub>1</sub>/FVC was found to be best predicted by  $\Delta$ KLi ( $\beta = 0.682$ ;  $r^2 = 0.340$ ).

## 2.6 Discussion

The effect of scoliosis on respiratory function has been investigated in numerous studies which have addressed the relationship between radiographic Cobb measurements of spinal deformity and pulmonary function test results [33, 29, 26, 27, 24]. The present study was designed with three objectives in mind: firstly, to test the hypothesis that radiographic measurements of the thoracic morphology have a stronger association with lung function in scoliosis than traditional Cobb angle measurements; secondly, to investigate the thoracic features which are associated with pulmonary function impairment in scoliosis and infer the mechanisms of impairment; and thirdly, to determine whether such impairment is reversible with scoliosis correction surgery.

The correlational analysis was in agreement with prior investigations showing the negative effects of increasing MT curves in impairing FEV<sub>1</sub> and FVC with TL/L showing no effect [33, 29, 25]. In contrast with McPhail et al. [24], who found no correlation between FEV<sub>1</sub>/FVC and spinal parameters, a positive relationship between TK and FEV<sub>1</sub>/FVC was found. The magnitude of the PT curve was shown to correlate negatively with FEV<sub>1</sub> and FVC which agrees with previous correlational studies [26, 54, 33]. However, given the significant correlation between MT and PT, and the absence of PT as a predictor in the multivariate analysis, it is questionable whether such a result merely reflects the effect of the MT curve on pulmonary function.

Thoracic deformity parameters ( $r^2 = 0.18$  to  $0.57$ ) were found to be superior to Cobb angle measurements ( $r^2 = 0.11$  to  $0.37$ ) in predicting pre-operative lung function (Tables 2.9 and 2.10) with the proportion of variance explained substantially higher than prior studies utilizing spinal parameters ( $r^2 = 0.05$  to  $0.20$ ) [24, 29, 27]. Scoliosis, which is quantified by the Cobb angle of the spinal curvature in the coronal plane, often coincides with vertebral rotation in the axial plane [55, 56] and hypokyphosis in the sagittal plane [57]. Although the diagnosis of scoliosis is based on the assessment of the coronal deformity, this curvature results in a complex three-dimensional distortion of both the spinal column and the rib cage. Thus, the simultaneous distortions to the spine and chest wall are best conceptualised as a *thoracic* deformity [58]. Whilst Cobb angles may be a useful metric in quantifying the curvature and malalignment of the spine, they do not fully capture the spatial reductions and asymmetries in the thorax which coincide with the spinal deformity.

The analysis of thoracic features support the association between scoliosis and restrictive lung disease due to reduced thoracic volume [59, 60]. Reduction in the width

of the convex hemithorax ( $AVBRr^{-1}$ ) and spinal intrusion into the thoracic cavity ( $SIr$ ) were found to be associated with reductions in expiratory volume. Ledonio et al. demonstrated that restoration of thoracic volume in severely restrictive AIS patients correlated strongly with post-operative increases in total lung capacity [61]. Posterior displacement and lowering of the convex ribs produces a rib asymmetry which is captured by  $RHi$  and  $RVAD$  which were also negatively associated with expiratory volumes. Such asymmetry in rib morphology has been shown to impede rib cage motion in thoracic scoliosis [62].

However, the results also support the increasing recognition that scoliosis is associated with obstructive lung disease [24, 63]. Flattening of the thoracic spine ( $KLi$ ) and narrowing of thoracic depth ( $SIr$ ) were found to be associated with reductions in  $FEV_1/FVC$  which is a metric of airway conductance. Extrinsic compression of major airways by the vertebral column have previously been reported in patients with hypokyphosis and scoliosis [40, 51]. In a right sided scoliosis, the location of such obstruction has typically been reported to be in the region of the bronchus intermedius [64, 65, 66], resulting in air-trapping, atelectasis and reduction in ventilation of the right middle and lower lobes [67, 68, 51]. As such, the results demonstrate that the nature of pulmonary impairment in AIS may be restrictive, obstructive or mixed depending on the thoracic configuration.

In this investigation, the sample has been limited to the study of Lenke type 1 and 2 curves where the MT curve is major and structural whilst the TL/L curve is non-structural [10]. The focus on this scoliotic subgroup may explain the stronger correlations obtained between Cobb angles and pulmonary function compared to other studies which have not controlled for curve type [24, 29]. The objective of scoliosis surgery is to arrest curve progression, improve surface shape and to maintain, if not improve, pulmonary function [69, 70]. In the normal population, expiratory volumes ( $FEV_1$  and  $FVC$ ) have been shown to peak after the second decade of life with approximately a 5% decline from the peak for every decade thereafter [22]. Given the increased morbidity of respiratory failure and mortality in patients with untreated severe AIS [28, 30, 31, 32], increasing post-operative pulmonary function is a primary surgical objective to ensure long-term quality of life. Surgical correction of scoliosis via a posterior spinal fusion has been shown to improve lung function, not only in the 1-3 years post-operation [71, 48], but up to 20 years following surgery [49]. In this study, the post-operative change in MT ( $\Delta MT$ ) or the increase in width of the convex hemithorax ( $\Delta AVBRr^{-1}$ ) were found to contribute to post-operative gains in  $FEV_1$  and  $FVC$  (Table 2.9 and 2.10). Interestingly, patients with lower TK or high spinal intrusion ( $SIr$ ) gained more than those with more kyphotic sagittal profiles. Changes in  $FEV_1/FVC$  were found to be directly proportion to the post-operative increases in TK or  $KLi$ . The results demonstrate that restoration of natural thoracic kyphosis in hypokyphotic patients can lead to significant gains in lung function post-operation, presumably via the decompression of airways [51, 67] as reflected in improved  $FEV_1/FVC$  values post-operatively. Hyperkyphotic patients did not show any significant gains in lung function post-operatively; it is possible this is due to the volumetric gains as a result of increased thoracic height and convex hemithoracic width being offset by losses due to reductions in thoracic depth. Such differences highlight the different mechanisms involved in pulmonary function impairment in AIS. It is recommended that patients with hypokyphosis and severe respiratory impairment should be investigated for possi-

ble airway obstruction and treatment should focus on restoring natural kyphosis.

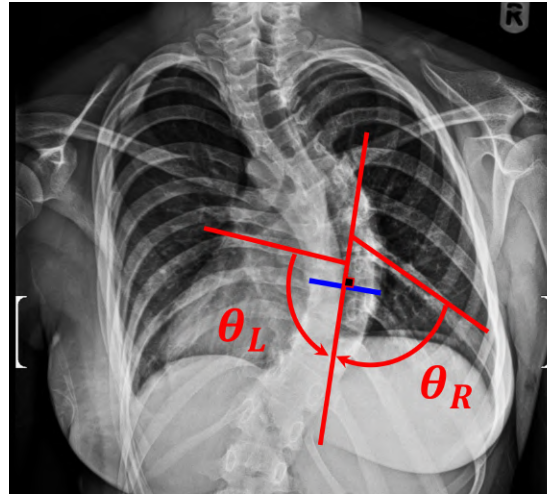
## 2.7 Conclusion

In this investigation, deformity parameters, which captured the global distortions to the rib cage, were found to be more predictive of lung function impairment than conventional Cobb angle measurements. The mechanisms of pulmonary impairment may be restrictive, obstructive or mixed depending on the thoracic configuration. Narrowing of the convex hemithorax, increased rib hump and spinal intrusion were found to reduce expiratory volumes. Increase in airway resistance was found to be associated with hypokyphosis which resolved post-operation. It is recommended that patients with hypokyphosis and severe respiratory impairment be investigated for possible airway obstruction with operative treatment focussing on the restoration of natural kyphosis.

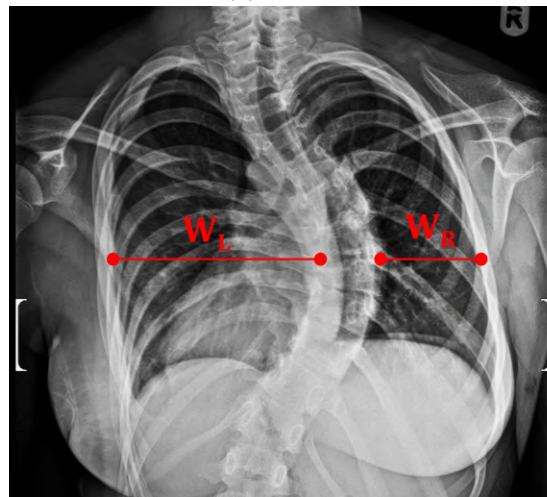
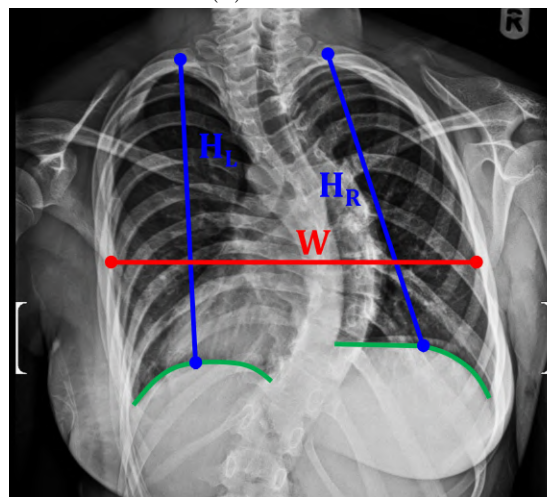


Table 2.1: Radiographic-based thoracic deformity parameters and their definitions. Diagrams of the measurements can be found in Figures 2.1 and 2.2

Parameter	Definition	Formula	Reference
Rib vertebral angle difference (RVAD)	A line is drawn perpendicular to the apical vertebral endplate (blue). Lines are drawn from the mid-neck to the mid head of the corresponding pair of ribs. RVAD is the difference between the concave and convex angle	$\theta_L - \theta_R$	[39]
Inverse apical vertebral body rib ratio (AVBRr <sup>-1</sup> )	A horizontal line is drawn at the apical thoracic vertebrae. The distance between the lateral border of the vertebrae column and the chest on the convex and concave side are measured. AVBRr <sup>-1</sup> is the ratio of the convex side to the concave side	$W_R/W_L$	Modified [41]
Space available for lung (SAFL)	The height of the hemithorax is defined as the distance from the middle of the most cephalad rib down to the center of the hemidiaphragm. SAFL is defined by the ratio between the concave and convex heights, expressed as a percentage	$H_L/H_R \times 100\%$	[44]
Lung height-width ratio (LHW <sub>r</sub> )	The chest width is measured horizontally between the interior surface of the chest walls at the level of the apical vertebrae. Using the averaged height measurements from SAFL, LHW <sub>r</sub> is the width-normalised averaged height of each lung	$(H_R + H_L) / (2W)$	This work
Kyphosis-lordosis index (KLi)	A line is drawn between T1 and T12 vertebral body centroids. At the mid point, a perpendicular line is drawn until the anterior contour of the vertebral column is met	$D_1/H \times 100\%$	Modified [43]
Rib hump index (RHi)	A horizontal line is drawn at the level where the distance between the convex and concave rib contours maximise. The distance between the anterior contour of the vertebral column and the internal contour of the concave ( $D_2$ ) and convex ( $D_3$ ) ribs are measured. The RHi is defined as the ratio between the concave and convex distances subtracted from unity	$1 - D_2/D_3$	This work
Spinal intrusion ratio (Str)	A line is drawn between T1 and T12 vertebral body centroids. At the mid point, a horizontal line is drawn. $D_4$ is distance between the internal sternal surface to the anterior contour of the vertebral column. $D_5$ is the distance from the anterior of the vertebral column contour to the interior contour of the convex ribs.	$D_5/D_4$	Modified [51]

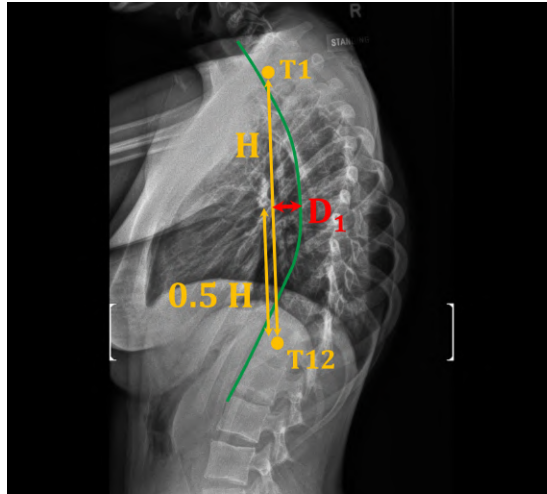


(a) RVAD

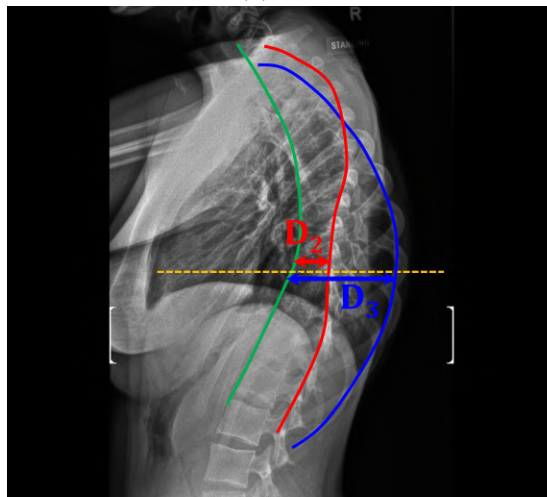
(b)  $AVBRr^{-1}$ 

(c) SAFL and LHWr

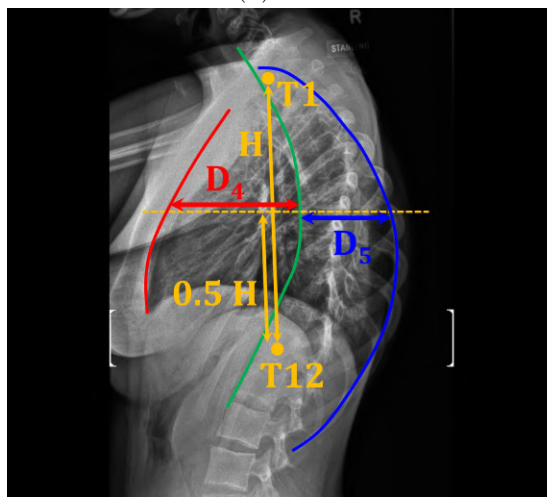
Figure 2.1: Diagrams of thoracic deformity parameters measured on coronal radiographs for (a) rib-vertebra angle difference (RVAD), (b) inverse of the apical vertebral body-rib ratio ( $AVBRr^{-1}$ ) and (c) space available for lung (SAFL) and lung height-width ratio (LHWr). Descriptions of the measurements can be found in Table 2.1



(a) KLi



(b) RH



(c) SIR

Figure 2.2: Diagrams of thoracic deformity parameters measured on sagittal radiographs for (a) kyphosis-lordosis index (KLi), (b) rib hump index (RH) and (c) spinal intrusion ratio (SIR). Definitions of the parameters can be found in Table 2.1

Table 2.2: Summary of all pre-operative patient characteristics, spirometry results and radiographic deformity parameters ( $n = 136$ ).

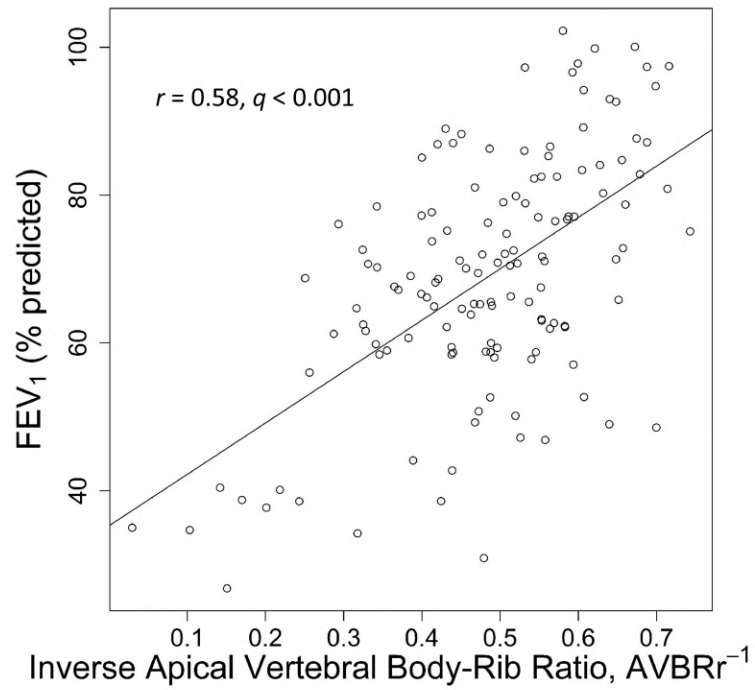
<i>Continuous variables, mean (standard deviation) (range)</i>		
Age at pulmonary function test (years)	15.6	(5.1) (10.0 to 56.0)
Standing Height (cm)	161.9	(10.3) (133.3 to 188.7)
Arm-span (cm)	167.8	(11.9) (125.0 to 190.5)
Weight (kg)	53.3	(13.5) (19.8 to 92.3)
FEV <sub>1</sub> (% predicted)	68.9	(16.3) (26.7 to 102.3)
FVC (% predicted)	72.6	(15.6) (24.7 to 108.8)
FEV <sub>1</sub> /FVC (% predicted)	94.2	(8.3) (68.6 to 111.5)
Proximal thoracic curve, PT (°)	33.8	(12.5) (13.6 to 87.3)
Main thoracic curve, MT (°)	69.9	(15.5) (40.1 to 117.7)
Thoracolumbar/lumbar curve, TL/L (°)	39.4	(13.4) (10.4 to 93.1)
T5-T12 thoracic kyphosis, TK (°)	20.6	(15.9) (-14.0 to 78.5)
Rib vertebrae angle difference, RVAD (°)	22.2	(20.6) (-30.0 to 83.4)
Inverse apical vertebral body-rib ratio, AVBRr <sup>-1</sup> (-)	0.48	(0.14) (0.03 to 0.74)
Space available for lung, SAFL (%)	92.1	(7.7) (60.0 to 119.3)
Lung height-width ratio, LHW <sub>r</sub> (-)	0.85	(0.08) (0.62 to 1.09)
Kyphosis-lordosis index, KLi (%)	4.3	(6.0) (-12.1 to 37.4)
Spinal intrusion ratio, SI <sub>r</sub> (-)	0.87	(0.27) (0.46 to 1.89)
Rib hump index, RHi (-)	0.53	(0.19) (0.11 to 1.21)
<i>Categorical variables, n (%)</i>		
Female	96	(70.6)
FEV <sub>1</sub> < LLN	103	(75.7)
FVC < LLN	96	(70.6)
FEV <sub>1</sub> /FVC < LLN	31	(22.8)

LLN, lower limit of normal; defined as 5th centile of reference population [22].

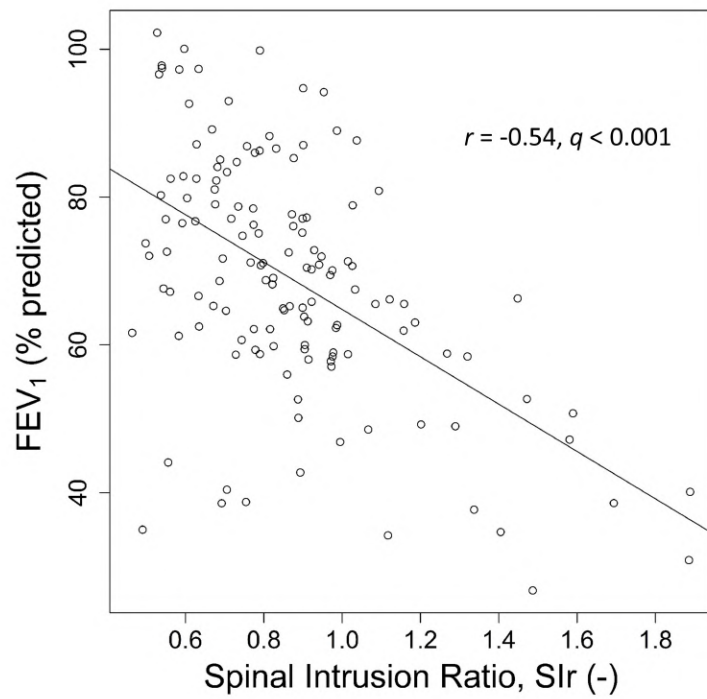
Table 2.3: Pearson correlation coefficients between radiographic Cobb angles, deformity parameters and lung function ( $n = 136$ ).

	PT	MT	TL/L	TK	FEV <sub>1</sub>	FVC	FEV <sub>1</sub> /FVC
PT	-	-	-	-	-0.30 ***	-0.30 ***	-0.06
MT	0.35 ***	-	-	-	-0.52 ***	-0.54 ***	-0.03
TL/L	-0.07	0.55 ***	-	-	-0.11	-0.13	0.05
TK	-0.03	0.27 **	0.35 ***	-	0.18	0.07	0.35 ***
RVAD	0.30 ***	0.52 ***	0.01	0.04	-0.36 ***	-0.35 ***	-0.08
AVBRr <sup>-1</sup>	-0.44 ***	-0.81 ***	-0.16	-0.15	0.58 ***	0.59 ***	0.06
SAFL	0.37 ***	-0.50 ***	-0.44 ***	-0.18	0.13	0.12	0.02
LHW <sup>r</sup>	0.04	-0.22 *	-0.35 ***	-0.42 ***	-0.30 ***	-0.27 **	-0.14
KLi	-0.08	0.26 **	0.26 **	0.79 ***	0.15	0.03	0.4 ***
SIr	0.22 *	0.02	-0.21 *	-0.60 ***	-0.54 ***	-0.47 ***	-0.34 ***
RHI	0.06	0.57 ***	0.26 **	0.33 ***	-0.31 ***	-0.32 ***	0.00

Significant correlation to \*  $q < 0.05$ ; \*\*  $q < 0.01$ ; and \*\*\*  $q < 0.001$ .

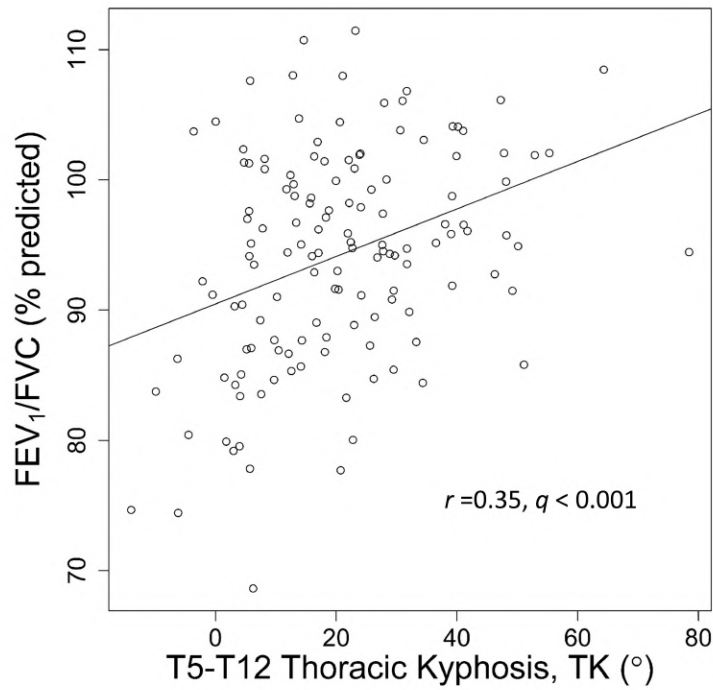


(a)

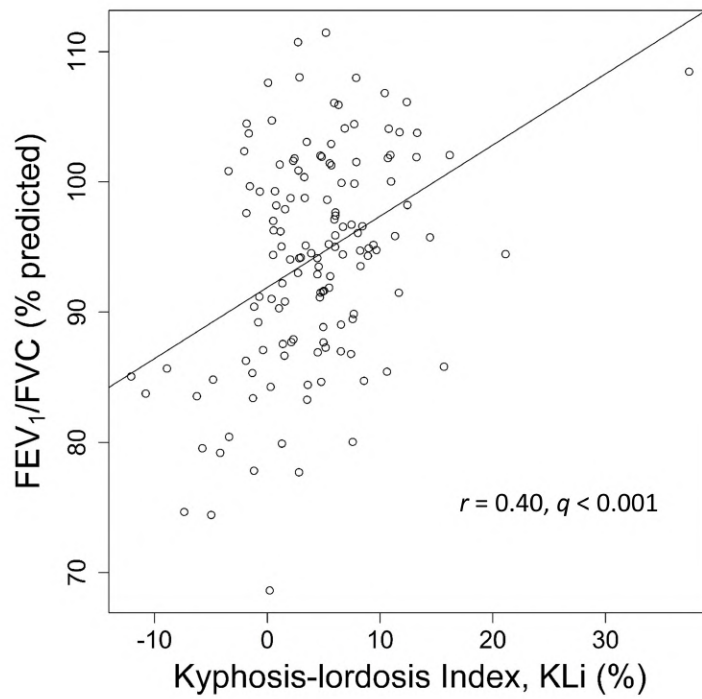


(b)

Figure 2.3: Correlation plots of FEV<sub>1</sub> with (a) inverse apical vertebral body-rib ratio (AVBRr<sup>-1</sup>) and (b) spinal intrusion ratio (SIr).



(a)



(b)

Figure 2.4: Correlation plots of FEV<sub>1</sub>/FVC with (a) T5-T12 thoracic kyphosis (TK) and (b) kyphosis-lordosis index (KLi).

Table 2.4: Pearson correlation coefficients between deformity parameters ( $n = 136$ ).

	RVAD	AVBRr <sup>-1</sup>	SAFL	LHW <sub>r</sub>	KLi	SIr
AVBRr <sup>-1</sup>	-0.71 ***	-	-	-	-	-
SAFL	-0.28 **	0.35 ***	-	-	-	-
LHW <sub>r</sub>	0.09	-0.03	0.28 **	-	-	-
KLi	0.04	-0.16	-0.21 *	-0.25 **	-	-
SIr	0.14	-0.12	0.11	0.46 ***	-0.65 ***	-
RHi	0.38 ***	-0.51 ***	-0.26 **	-0.11	0.41 ***	-0.16

Significant correlation to \*  $q < 0.05$ ; \*\*  $q < 0.01$ ; and \*\*\*  $q < 0.001$ .

Table 2.5: Pre- and post-operative comparison of radiographic and pulmonary function measurements segregated by main thoracic curve severity

	Preoperative Main Thoracic Scoliosis		Kruskal-Wallis $q$ -value
	MT $\leq 70^\circ$ ( $n = 35$ )	MT $> 70^\circ$ ( $n = 37$ )	
MT pre-op ( $^\circ$ )	60.2 (6.9)	84.4 (11.4)	$< 0.001$ †
MT post-op ( $^\circ$ )	29.2 (7.3)	35.6 (12.3)	0.056
Change ( $^\circ$ )	-30.9 (9.4) ***	-48.8 (11.4) ***	$< 0.001$ †
TK pre-op ( $^\circ$ )	16 (16.5)	25.5 (18.8)	0.044 †
TK post-op ( $^\circ$ )	20.8 (8.9)	29 (11.2)	0.005 †
Change ( $^\circ$ )	4.8 (13) *	3.6 (14.2)	0.87
FEV <sub>1</sub> pre-op (% pred.)	67.5 (17)	63.2 (16.1)	0.76
FEV <sub>1</sub> post-op (% pred.)	76.3 (12.2)	75.6 (17.4)	0.89
Change (% pred.)	8.7 (12.1) ***	12.5 (9.1) ***	0.15
FVC pre-op (% pred.)	71.4 (14.7)	66.6 (16.7)	0.72
FVC post-op (% pred.)	77.7 (11.5)	77.1 (17.4)	0.89
Change (% pred.)	6.3 (11.8) **	10.5 (9.4) ***	0.089
FEV <sub>1</sub> /FVC pre-op (% pred.)	93.4 (9.1)	94.7 (8)	0.77
FEV <sub>1</sub> /FVC post-op (% pred.)	97.6 (7.2)	97.5 (6.6)	0.89
Change (% pred.)	4.2 (6.3) ***	2.8 (6.5) *	0.87

Values are mean (standard deviation)

Significant difference between pre- and post-operative values using pairwise  $t$ -test to: \*  $q < 0.05$ ; \*\*  $q < 0.01$ ; and  $q < 0.001$

† Significant difference between MT  $\leq 70^\circ$  and MT  $> 70^\circ$  groups using Krushkal-Wallis to  $q < 0.05$ .



Table 2.6: Pre- and post-operative comparison of radiographic deformity parameters segregated by main thoracic curve severity

	Preoperative Main Thoracic Scoliosis		Kruskal-Wallis <i>q</i> -value
	MT $\leq 70^\circ$ ( <i>n</i> = 35)	MT $> 70^\circ$ ( <i>n</i> = 37)	
RVAD pre-op ( $^\circ$ )	18.2 (18.8)	33.1 (18.5)	0.004 †
RVAD post-op ( $^\circ$ )	15.6 (16.4)	23.2 (17.2)	0.087
Change ( $^\circ$ )	-2.6 (15.3)	-9.8 (19.8) **	0.074
AVBRr <sup>-1</sup> pre-op (-)	0.55 (0.09)	0.37 (0.13)	< 0.001 †
AVBRr <sup>-1</sup> post-op (-)	0.69 (0.09)	0.6 (0.15)	0.008 †
Change (-)	0.15 (0.08) ***	0.22 (0.08) ***	0.003 †
SAFL pre-op (%)	95.1 (7.9)	90.4 (5.5)	0.039 †
SAFL post-op (%)	105.3 (6.2)	105.4 (6.9)	0.87
Change (%)	10.2 (5.4) ***	15 (5.6) ***	0.002 †
LHW <sub>r</sub> pre-op (-)	0.9 (0.08)	0.84 (0.08)	0.021 †
LHW <sub>r</sub> post-op (-)	0.91 (0.08)	0.89 (0.09)	0.53
Change (-)	0.01 (0.07)	0.05 (0.07) ***	0.046 †
KLi pre-op (%)	1.7 (6.6)	6.1 (7.5)	0.022 †
KLi post-op (%)	4.6 (3.3)	8.1 (5.6)	0.021 †
Change (%)	3 (4.9) **	2 (3.9) **	0.53
S <sub>l</sub> r pre-op (-)	1.01 (0.34)	0.86 (0.29)	0.054
S <sub>l</sub> r post-op (-)	0.91 (0.24)	0.8 (0.2)	0.054
Change (-)	-0.1 (0.19) **	-0.06 (0.2)	0.53
RHi pre-op (-)	0.43 (0.14)	0.66 (0.2)	< 0.001 †
RHi post-op (-)	0.27 (0.13)	0.45 (0.21)	< 0.001 †
Change (-)	-0.16 (0.13) ***	-0.21 (0.16) ***	0.25

Values are mean (standard deviation)

Significant difference between pre- and post-operative values using pairwise *t*-test to: \*  $q < 0.05$ ; \*\*  $q < 0.01$ ; and  $q < 0.001$

† Significant difference between MT  $\leq 70^\circ$  and MT  $> 70^\circ$  groups using Kruskal-Wallis to  $q < 0.05$ .

Table 2.7: Pre- and post-operative comparison of radiographic and pulmonary function measurements segregated by the Lenke sagittal thoracic modifier

	Preoperative Lenke Sagittal Thoracic Modifier				Kruskal-Wallis <i>q</i> -value
	Hypokyphosis (-) ( <i>n</i> = 22)	Normokyphosis (N) ( <i>n</i> = 37)	Hyperkyphosis (+) ( <i>n</i> = 13)		
MT pre-op (°)	69.1 (15.5)	70.9 (13.1)	83.6 (17.4)		0.069
MT post-op (°)	31.9 (9.7)	30.8 (8.8)	38.3 (14.9)		0.32
Change (°)	-37.1 (14.3) ***	-40.1 (13.2) ***	-45.3 (13.8) ***		0.21
TK pre-op (°)	2.1 (6.5)	21.5 (7.4)	50.9 (10.5)		< 0.001 † † *
TK post-op (°)	17.6 (6.1) ***	25.4 (8.4)	36.6 (13.4)		< 0.001 † † *
Change (°)	15.5 (7.5) ***	3.9 (9.5) *	-14.3 (10.7) ***		< 0.001 † † *
FEV <sub>1</sub> pre-op (% pred.)	57.8 (17.1)	68.4 (14.5)	69 (18.5)		0.093
FEV <sub>1</sub> post-op (% pred.)	74.4 (12.8)	77.3 (13.0)	74.5 (22.7)		0.54
Change (°)	16.6 (12.7) ***	8.9 (8.2) ***	5.5 (9.7)		0.029 †
FVC pre-op (% pred.)	64.2 (17.0)	71.2 (13.9)	70.4 (18.6)		0.29
FVC post-op (% pred.)	78.2 (12.9)	77.8 (13.7)	74.8 (20.5)		0.79
Change (°)	14.0 (12.3) ***	6.6 (9.1) ***	4.4 (9.6)		0.093
FEV <sub>1</sub> /FVC pre-op (% pred.)	89.5 (9.5)	95.4 (7.6)	97.8 (6.2)		0.044 † †
FEV <sub>1</sub> /FVC post-op (% pred.)	94.6 (5.5)	99.0 (7.2)	98.4 (7.0)		0.093
Change (°)	5.1 (6.7) **	3.6 (5.8) ***	0.5 (7.1)		0.31

Values are mean (standard deviation)

Significant difference between pre- and post-operative values using pairwise *t*-test to: \*  $q < 0.05$ ; \*\*  $q < 0.01$ ; and  $q < 0.001$

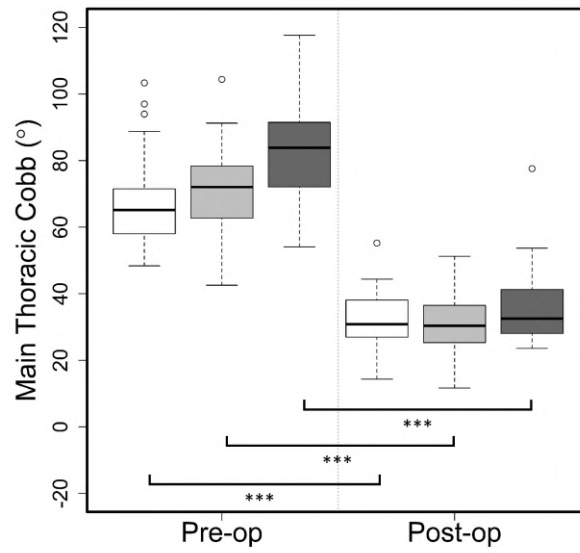
Significant difference using post-hoc Dunn's test between: † hypokyphosis (-) and normokyphosis (N); † hypokyphosis (-) and hyperkyphosis (+); \* normokyphosis (N) and hyperkyphosis (+) groups to  $q < 0.05$ .

Table 2.8: Pre- and post-operative comparison of radiographic deformity parameters segregated by the Lenke sagittal thoracic modifier

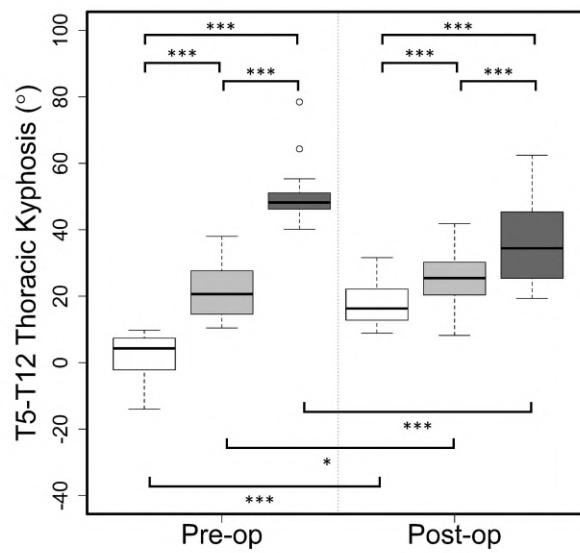
	Preoperative Lenke Sagittal Thoracic Modifier				Kruskal-Wallis <i>q</i> -value
	Hypokyphosis (-) ( <i>n</i> = 22)	Normokyphosis (N) ( <i>n</i> = 37)	Hyperkyphosis (+) ( <i>n</i> = 13)		
RVAD pre-op (°)	28.2 (21.2)	22.2 (19.8)	32.1 (17.3)	0.27	
RVAD post-op (°)	21.8 (13.8)	17 (19.1)	23 (16.6)	0.54	
Change (°)	-6.4 (19.6)	-5.2 (14.4) *	-9.2 (24.6)	0.67	
AVBRr <sup>-1</sup> pre-op (-)	0.46 (0.1)	0.48 (0.14)	0.39 (0.16)	0.23	
AVBRr <sup>-1</sup> post-op (-)	0.65 (0.1)	0.67 (0.13)	0.55 (0.17)	0.074	
Change (-)	0.2 (0.09) ***	0.18 (0.09) ***	0.16 (0.08) ***	0.68	
SAFL pre-op (%)	92.4 (6.5)	93.3 (7.7)	91.4 (6.8)	0.87	
SAFL post-op (%)	102.9 (4.8)	106.2 (5.6)	106.8 (10.1)	0.27	
Change (%)	10.6 (6) ***	12.9 (4.9) ***	15.4 (7.6) ***	0.31	
LHWTr pre-op (-)	0.91 (0.08)	0.87 (0.08)	0.8 (0.06)	0.002 †*	
LHWTr post-op (-)	0.92 (0.1)	0.9 (0.08)	0.88 (0.07)	0.36	
Change (-)	0.01 (0.08)	0.03 (0.06) **	0.07 (0.08) **	0.079	
KLi pre-op (%)	-2.5 (4.3)	4.2 (3.5)	13.9 (8.3)	< 0.001 † † *	
KLi post-op (%)	2.8 (2.5)	6.5 (2.7)	12.3 (6.8)	< 0.001 † † *	
Change (%)	5.4 (3.7) ***	2.2 (3.3) ***	-1.6 (5)	< 0.001 † † *	
SLr pre-op (-)	1.19 (0.39)	0.88 (0.19)	0.66 (0.16)	< 0.001 † † *	
SLr post-op (-)	1.01 (0.27)	0.83 (0.16)	0.67 (0.13)	0.001 † † *	
Change (-)	-0.18 (0.22) **	-0.05 (0.16)	0.01 (0.14)	0.067	
RHi pre-op (-)	0.47 (0.17)	0.53 (0.18)	0.74 (0.25)	0.011 † *	
RHi post-op (-)	0.26 (0.13)	0.35 (0.13)	0.58 (0.29)	0.001 † † *	
Change (-)	-0.21 (0.13) ***	-0.18 (0.14) ***	-0.16 (0.2) *	0.78	

Values are mean (standard deviation). Significant difference between pre- and post-operative values using pairwise *t*-test to: \* *q* < 0.05; \*\* *q* < 0.01; and *q* < 0.001

Significant difference using post-hoc Dunn's test between: † hypokyphosis (-) and normokyphosis (N); † † hypokyphosis (-) and hyperkyphosis (+); \* normokyphosis (N) and hyperkyphosis (+) groups to *q* < 0.05.



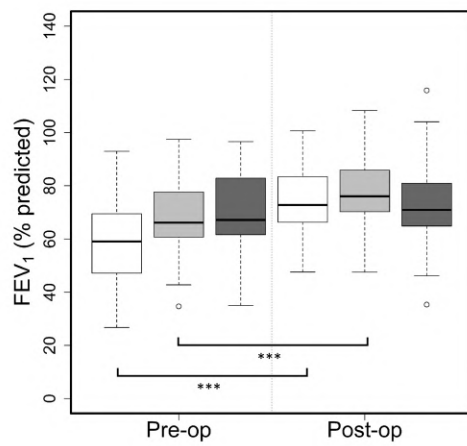
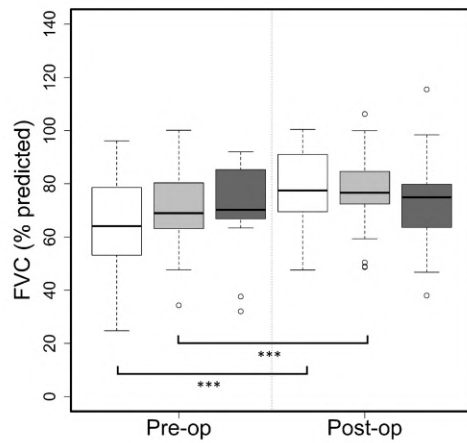
(a) Main thoracic Cobb (MT)



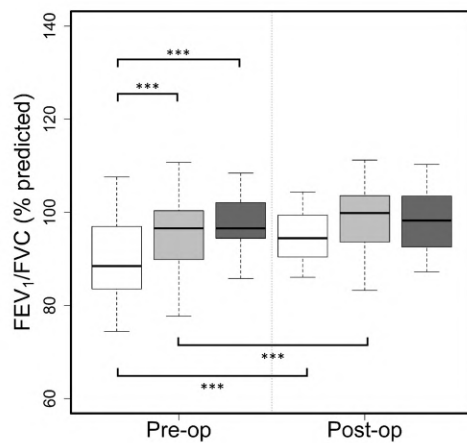
(b) T5-T12 thoracic kyphosis (TK)

□ Hypokyphosis (-)    ■ Normokyphosis (N)    ■ Hyperkyphosis (+)

Figure 2.5: Box-and-whisker plots of (a) main thoracic Cobb (MT) and (b) T5-T12 thoracic kyphosis (TK) results pre- and post-operation segregated by the Lenke sagittal modifier. Significant difference between groups to:  $*q < 0.05$ ;  $**q < 0.01$ ;  $***q < 0.001$

(a) FEV<sub>1</sub>

(b) FVC

(c) FEV<sub>1</sub>/FVC

□ Hypokyphosis (-)    ■ Normokyphosis (N)    ■ Hyperkyphosis (+)

Figure 2.6: Box-and-whisker plots of (a) FEV<sub>1</sub>, (b) FVC and (c) FEV<sub>1</sub>/FVC results pre- and post-operation segregated by the Lenke sagittal modifier. Significant difference between groups to: \* $q < 0.05$ ; \*\* $q < 0.01$ ; \*\*\* $q < 0.001$

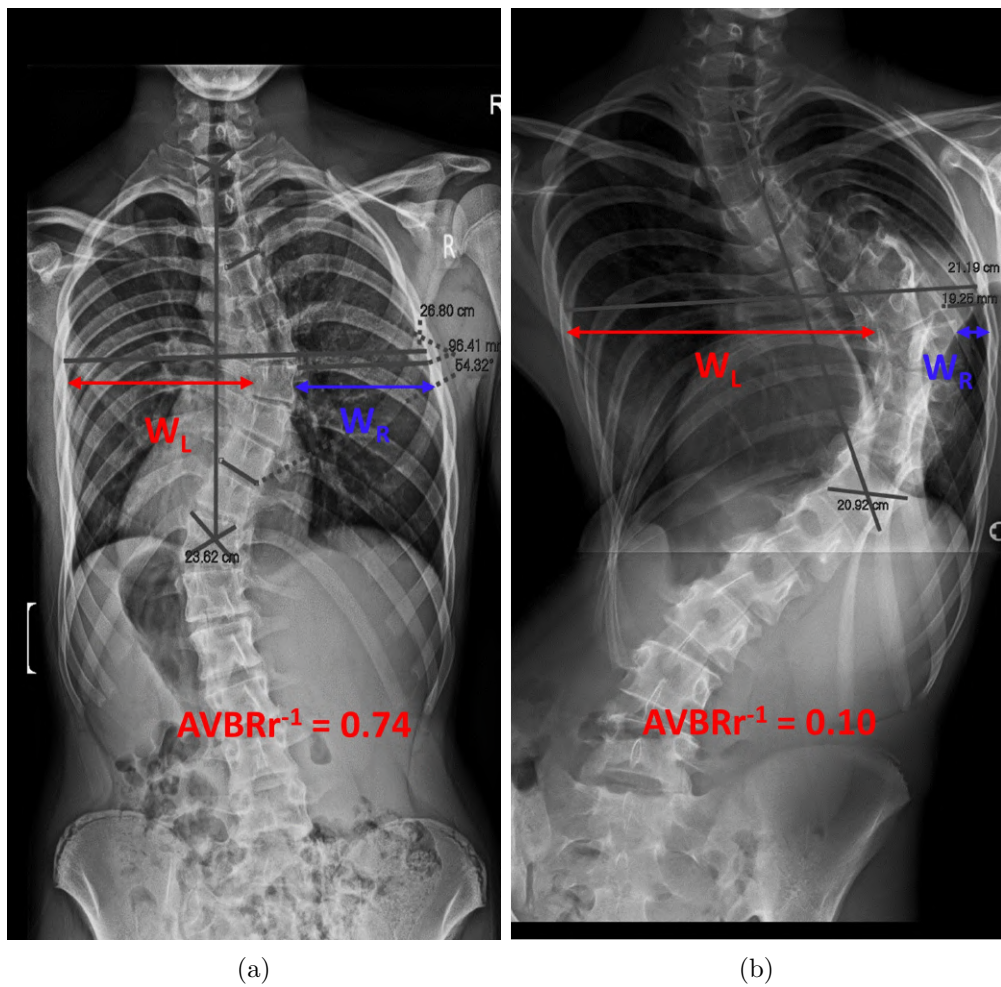
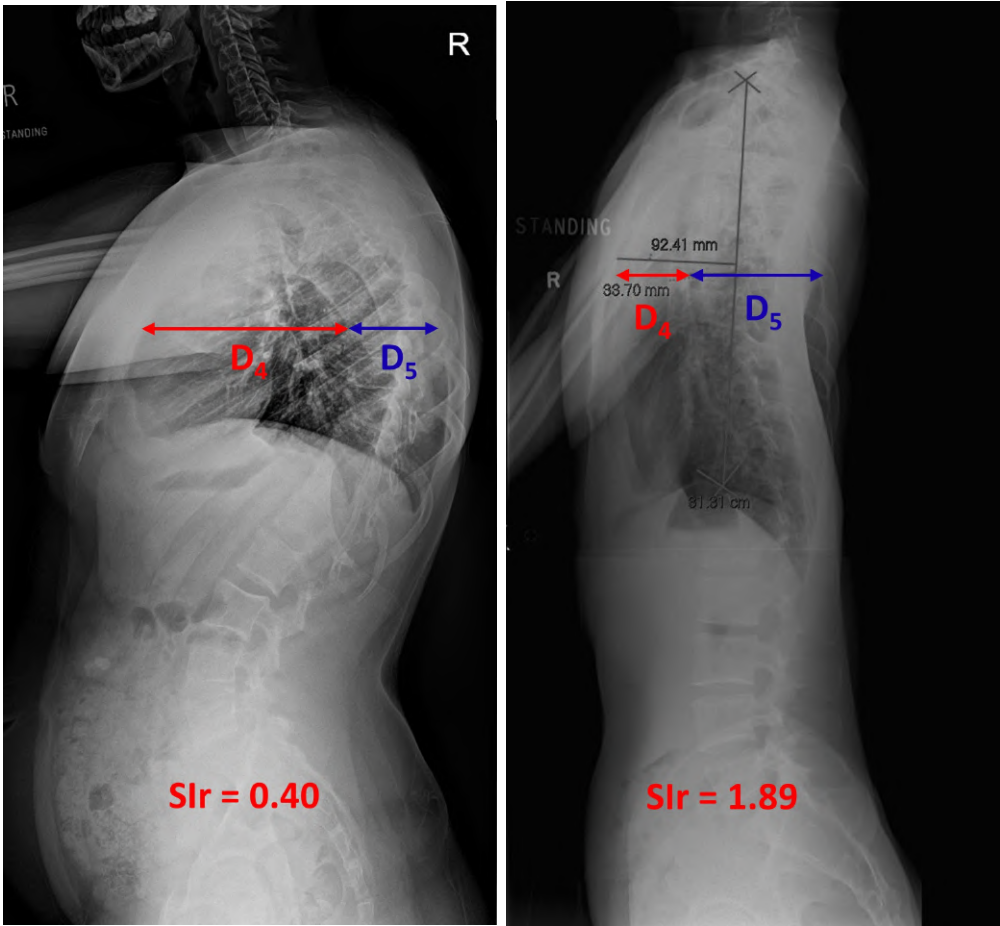


Figure 2.7: Examples of patients with (a) high and (b) low inverse apical vertebral body-rib ratio  $AVBRr^{-1}$ .  $AVBRr^{-1}$  captures the narrowing of the convex hemithorax and is related to rib hump magnitude and rib asymmetry.



(a)

(b)

Figure 2.8: Examples of patients with (a) low and (b) high spinal intrusion ratio (SIr). SIr captures both the narrowing of the sternovertebral distance, spinal intrusion into the thoracic cavity and the extend of the convex rib hump.

Table 2.9: Multivariate step-wise regression results for the prediction of pre-operative ( $n = 136$ ) and post-operative changes ( $n = 72$ ) in lung function using coronal and sagittal Cobb angles.

FEV <sub>1</sub>	Intercept	MT	TK	Model statistics
$b$	106.266	-0.637	0.350	$r^2 = 0.365$
SE( $b$ )	5.138	0.074	0.073	SE = 12.96
$\beta$	-	-0.609	0.341	-
$p$	< 0.001	< 0.001	< 0.001	-
FVC	Intercept	MT	TK	Model statistics
$b$	110.046	-0.603	0.228	$r^2 = 0.329$
SE( $b$ )	5.069	0.073	0.072	12.787
$\beta$	-	-0.600	0.231	-
$p$	< 0.001	< 0.001	0.002	-
FEV <sub>1</sub> /FVC	Intercept	TK	-	Model statistics
$b$	90.474	0.182	-	$r^2 = 0.116$
SE( $b$ )	1.094	0.042	-	SE = 7.76
$\beta$	-	0.350	-	-
$p$	< 0.001	< 0.001	-	-
$\Delta$ FEV <sub>1</sub>	Intercept	$\Delta$ MT	TK	Model statistics
$b$	4.787	-0.299	-0.295	$r^2 = 0.318$
SE( $b$ )	3.326	0.077	0.058	SE = 8.86
$\beta$	-	-0.509	-0.469	-
$p$	0.155	< 0.001	< 0.001	-
$\Delta$ FVC	Intercept	$\Delta$ MT	TK	Model statistics
$b$	1.171	-0.309	-0.244	$r^2 = 0.254$
SE( $b$ )	3.493	0.081	0.061	SE = 9.34
$\beta$	-	-0.533	-0.463	-
$p$	0.738	< 0.001	< 0.001	-
$\Delta$ FEV <sub>1</sub> /FVC	Intercept	$\Delta$ TK	-	Model statistics
$b$	2.872	0.151	-	$r^2 = 0.089$
SE( $b$ )	0.755	0.054	-	SE = 6.12
$\beta$	-	0.319	-	-
$p$	< 0.001	0.006	-	-



Table 2.10: Multivariate step-wise regression results for the prediction of pre-operative ( $n = 136$ ) and post-operative changes ( $n = 72$ ) in lung function using radiographic Cobb angles and thoracic deformity parameters.

FEV <sub>1</sub>	Intercept	SIr	AVBRr <sup>-1</sup>	RHi	Model statistics
$b$	78.714	-30.586	51.110	-14.987	$r^2 = 0.569$
SE( $b$ )	7.680	3.498	8.158	5.823	SE = 10.687
$\beta$	-	-0.516	0.425	-0.175	-
$p$	< 0.001	< 0.001	< 0.001	0.011	-
FVC	Intercept	SIr	AVBRr <sup>-1</sup>	RHi	Model statistics
$b$	75.080	-24.669	52.981	-12.629	$r^2 = 0.512$
SE( $b$ )	7.839	4.606	7.225	0.211	SE = 10.673
$\beta$	-	-0.578	0.477	-0.180	-
$p$	< 0.001	< 0.001	< 0.001	0.001	-
FEV <sub>1</sub> /FVC	Intercept	KLi	RHi	-	Model statistics
$b$	96.029	0.660	-8.739	-	$r^2 = 0.181$
SE( $b$ )	1.918	0.117	3.705	-	SE = 7.474
$\beta$	-	0.482	-0.202	-	-
$p$	< 0.001	< 0.001	0.020	-	-
$\Delta$ FEV <sub>1</sub>	Intercept	SIr	$\Delta$ AVBRr <sup>-1</sup>	-	Model statistics
$b$	-12.526	18.935	29.772	-	$r^2 = 0.412$
SE( $b$ )	3.397	3.084	11.388	-	SE = 8.232
$\beta$	-	0.568	0.242	-	-
$p$	< 0.001	< 0.001	0.011	-	-
$\Delta$ FVC	Intercept	SIr	$\Delta$ AVBRr <sup>-1</sup>	-	Model statistics
$b$	-12.456	17.446	25.119	-	$r^2 = 0.331$
SE( $b$ )	3.637	3.302	12.195	-	SE = 8.815
$\beta$	-	0.521	0.203	-	-
$p$	0.001	< 0.001	0.043	-	-
$\Delta$ FEV <sub>1</sub> /FVC	Intercept	$\Delta$ KLi	-	-	Model statistics
$b$	1.349	0.859	-	-	$r^2 = 0.466$
SE( $b$ )	0.707	0.140	-	-	SE = 5.306
$\beta$	-	0.682	-	-	-
$p$	0.0606	< 0.001	-	-	-

## Chapter 3

# Statistical Shape Model

### 3.1 Summary

In this chapter, a statistical shape model constructed from biplanar radiographs is created to quantify the morphological variations in the rib cage and spine and to identify thoracic features which contribute to lung function impairment in adolescent idiopathic scoliosis (AIS). In the coronal plane, the shape model consisted of the vertices of the thoracic and lumbar vertebral bodies, as well as contours of the ribs, clavicals and the hemidiaphragms. In the sagittal plane, the posterior portion of the sternal wall, diaphragm, posterior convex and concave rib contours and the outline of the vertebral column were included. General Procrustes analysis was used to standardise the landmarks whilst principle components analysis determined the major modes of variation. Principle component scores were correlated with lung function, Cobb angles and deformity parameters and included in multivariate regression to predict pre-operative and post-operative change in lung function. The shape model demonstrated that increasing thoracic scoliosis, flattening of the sagittal profile and increased rib hump correspond to reduction in pulmonary function. Sagittal flattening of the thoracic spine is shown increase airway resistance as measured by  $FEV_1/FVC$ . Patients with severe scoliosis, hypokyphosis and large rib humps demonstrate greater increases in post-operative lung function. It was concluded that statistical shape models are a useful morphometric tool which can provide a quantitative and objective description of the thoracic deformity in AIS.

### 3.2 Introduction

Statistical shape models have been extensively used in medical image analysis and are a key tool for studying morphological variations in disease [72, 73, 74, 75]. In general, statistical shape models are parametric models which represent the deformations which best reflect the variation within the data training set [76]. In the context of scoliosis, statistical shape models have been used to automate measurements of spinal deformity [77], identify modes of variation in spinal morphology in scoliosis [78, 79] and study the geometric effects of scoliosis treatment on the spine [80]. The objectives of this study are to demonstrate the use of statistical shape models in quantifying variations in thoracic morphology in AIS and to identifying the modes of variation which contribute to lung function impairment.

### 3.3 Literature Review

Using Riemannian geometry, Boisvert et al. [78] constructed an articulated model of the spine in pre-operative scoliosis patients with mixed curve types. The models were constructed through the identification of 6 landmarks on each vertebrae. A three dimensional articulated model was constructed by quantifying the relative translation and rotation from one vertebrae to the next. From their analysis, they determined that the first mode of deformation was associated with patients' growth, the second was the progression of a double thoraco-lumbar curve and the third was variation in the thoracic curvature. Using similar methods, Boisvert et al. [79] quantified the effect of Boston bracing and Cotrel-Dubousset instrumentation on spinal morphology. Statistical shape models have also been utilized to provide fast three-dimensional reconstructions of the spine [81] and automated measurement of the Cobb angle from radiographs [77]. Alternative uses of statistical shape models in the thorax have been to quantify thoracic morphology to clinical features or to study variations in anatomical dimensions for implant design. Hollenbeck et al. [82] constructed a three-dimensional statistical shape model of the lumbar spine in a cohort of 52 normal subjects; their model found that major modes of variation corresponded to changes in lumbar lordosis and disc height. Shi et al. [83] constructed a statistical human rib cage geometry model to study the effects of age, sex, stature and body mass on the morphology of the rib cage. In the current literature, no statistical shape models have been constructed to describe or quantify the thoracic deformity in AIS and its association with lung function impairment.

## 3.4 Theory

### 3.4.1 Generalised Procrustes Analysis

Generalised Procrustes analysis (GPA) is method used in shape analysis to standardise a set of coordinates by factoring out the effects of position, rotation and scale to superimpose them onto a reference shape. By removing the effects of translation, rotation and scale, the remaining variance between each sample and the reference is due to variance in shape. The following paragraphs describe the operations used in GPA.

**Translation** Suppose we have  $k$  two-dimensional landmarks arranged in the form  $\mathbf{X} = ((x_1, y_1), (x_2, y_2), \dots, (x_k, y_k))$ . The centroid of these points,  $(\bar{x}, \bar{y})$  is defined as the mean of all the landmarks in each dimension:

$$\begin{aligned}\bar{x} &= \frac{1}{k} (x_1 + x_2 + \dots + x_k) \\ \bar{y} &= \frac{1}{k} (y_1 + y_2 + \dots + y_k)\end{aligned}\tag{3.1}$$

The landmarks can then be centred at the origin by subtracting the coordinates of its centroid from the corresponding coordinates:

$$\mathbf{X}_t = \begin{bmatrix} (x_1 - \bar{x}), & (y_1 - \bar{y}) \\ (x_2 - \bar{x}), & (y_2 - \bar{y}) \\ \vdots & \vdots \\ (x_k - \bar{x}), & (y_k - \bar{y}) \end{bmatrix}\tag{3.2}$$

This can be performed on each set of landmarks. By centring each set of landmarks at the origin, variation due to difference in position are removed.

**Scaling** To apply uniform scaling, the centroid size,  $s$ , is calculated as the square root of the summed squared distances of each landmark from the centroid:

$$s = \sqrt{\frac{1}{k} [(x_1 - \bar{x})^2 + (y_1 - \bar{y})^2 + \dots + (x_k - \bar{x})^2 + (y_k - \bar{y})^2]} \quad (3.3)$$

The landmarks are then scaled by  $s$  to give a centred and scaled landmark matrix,  $\mathbf{X}_s$ , which has a centroid size of unity:

$$\mathbf{X}_s = \begin{bmatrix} (x_1 - \bar{x})/s, & (y_1 - \bar{y})/s \\ (x_2 - \bar{x})/s, & (y_2 - \bar{y})/s \\ \vdots & \vdots \\ (x_k - \bar{x})/s, & (y_k - \bar{y})/s \end{bmatrix} \quad (3.4)$$

**Rotation** To remove the effects of rotation, let us suppose we have a scaled and centred landmark matrix  $\mathbf{X}_s = ((x_1, y_1), \dots)$  and a reference matrix  $\mathbf{Y}_s = ((w_1, z_1), \dots)$ . Rotating the landmarks in  $\mathbf{X}_s$  around the origin by an angle of  $\theta$  will give the rotated landmarks  $\mathbf{X}_r = ((u_1, v_1), \dots)$ :

$$\mathbf{X}_r = \begin{bmatrix} u_1, & v_1 \\ \vdots & \vdots \\ u_k, & v_k \end{bmatrix} = \begin{bmatrix} x_1 \cos \theta - y_1 \sin \theta, & x_1 \sin \theta + y_1 \cos \theta \\ \vdots & \vdots \\ x_k \cos \theta - y_k \sin \theta, & x_k \sin \theta + y_k \cos \theta \end{bmatrix} \quad (3.5)$$

An objective function which describes the error between rotated and reference landmarks can be defined as:

$$f = \sum_{i=1}^k [(u_i - w_i)^2 + (v_i - z_i)^2] \quad (3.6)$$

Taking the derivative of (3.6) with respect to  $\theta$  and setting it to zero will minimise the distance between rotated landmarks and the reference landmarks. This can be rearranged for  $\theta$ :

$$\theta = \tan^{-1} \left( \frac{\sum_{i=1}^k (x_i z_i - y_i w_i)}{\sum_{i=1}^k (x_i w_i + y_i z_i)} \right) \quad (3.7)$$

**Algorithm** In general, the steps of GPA can be described in the following algorithm adapted from Zelditch et al.'s *Geometric Morphometrics for Biologists* [84]:

1. Center each observation to the origin using Equation 3.2.
2. Scale each observation to give a centroid size of 1 using Equation 3.4.
3. Define a reference shape:
  - (a) If a reference shape is available, proceed to step 2.
  - (b) If no reference shape is available, arbitrarily select one amongst the observations.

4. For each instance, rotate the observation using Equation 3.7.
5. If an arbitrary reference was selected in Step 3, calculate the average shape by taking the mean of all landmarks.
6. Define the average shape as the new reference shape and repeat Steps 1 to 5 until the mean shape does not change.

### 3.4.2 Principle Component Analysis

Principal component analysis (PCA) is a technique which uses orthogonal transformations to determine major axes of a variation within the data. Some of these axes explain a larger proportion of the data than others. This is a useful feature, as a complex dataset can be approximated by a few parameters corresponding to the major axes which explain the majority of the variance - this process is labelled dimensionality reduction. The following procedure has been adapted from Coote's *Model-Based Methods in Analysis of Biomedical Images* [72]:

1. Suppose we have a set of vectors  $\{\mathbf{x}_i\}$ , containing observations of variable  $i$  (these can be the  $x$ ,  $y$  or  $z$  coordinates of a particular landmark). The mean of the data is first computed,

$$\bar{\mathbf{x}} = \frac{1}{n} \sum_{i=1}^s \mathbf{x}_i \quad (3.8)$$

2. The covariance matrix  $\mathbf{S}$  is then calculated by,

$$\mathbf{S} = \frac{1}{n-1} \sum_{i=1}^s (\mathbf{x}_i - \bar{\mathbf{x}})(\mathbf{x}_i - \bar{\mathbf{x}}) \quad (3.9)$$

3. The eigenvectors,  $\mathbf{p}_i$ , and corresponding eigenvalues,  $\lambda_i$ , of  $\mathbf{S}$  are calculated and the eigenvalues sorted in ascending order ( $\lambda_i \geq \lambda_{i+1}$ ).
4. Each eigenvalue gives the variance of the data about the mean in the direction of the corresponding eigenvector. The total variance of the data,  $V_T$  can be computed by  $V_T = \sum_t \lambda_i$
5. The first  $t$  largest eigenvalues are selected such that

$$\sum_{i=1}^t \lambda_i \geq f_v V_T \quad (3.10)$$

where  $f_v$  defines the proportion of the total variation one wishes to explain.

The eigenvectors, or *principle components*, are a weighted linear combination of the original variables. A simple example of the reduction of two-dimensional data using PCA is shown in Figure 3.1. A two-dimensional data set is shown with the mean of the data,  $\bar{\mathbf{x}}$ , and the two non-correlated principle components ( $\mathbf{p}_1$  and  $\mathbf{p}_2$ ). Since the majority of the data varies along the first principle component,  $\mathbf{p}_1$ , the second component can be dropped if  $\lambda_2 < f_v V_T$  and the data expressed in terms of the distance along  $\mathbf{p}_1$  from the center. Hence the data point  $\mathbf{x}$  shown in Figure 3.1 (b) can be approximated as point  $\mathbf{x}'$  with the distance  $PC_1$  which is called the *principle component score*.

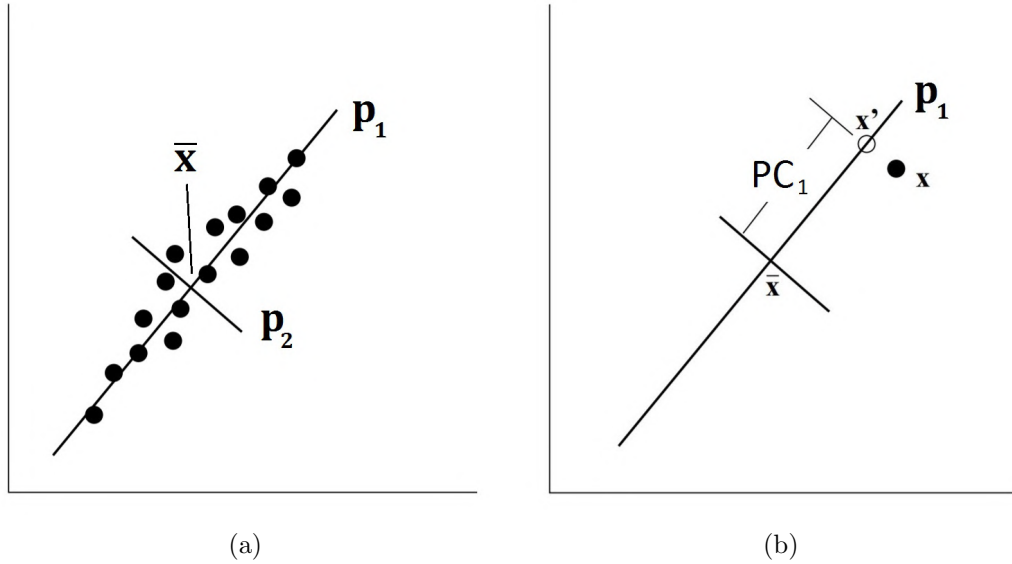


Figure 3.1: An example of dimensionality reduction using principle component analysis (PCA). (a) shows two-dimensional data, the mean of the data  $\bar{\mathbf{x}}$  and the two non-correlated principle components ( $\mathbf{p}_1$  and  $\mathbf{p}_2$ ). Since the majority of the data varies along the first principle component,  $\mathbf{p}_1$ , the second component can be dropped and the data expressed in terms of the distance along  $\mathbf{p}_1$  from the center. This is shown in (b) where the data point  $\mathbf{x}$  can be approximated as point  $\mathbf{x}'$  with the parameter  $PC_1$  which is the *principle component score* of the first principle component. Adapted from [72]

## 3.5 Materials & Methods

### 3.5.1 Subject Characteristics

The same subjects in the analysis conducted in Chapter 2 were used in this study. Pulmonary function tests included measurements of forced expiratory volume in 1 second ( $FEV_1$ ), forced vital capacity (FVC) and the  $FEV_1/FVC$  ratio which are expressed as a percentage of predicted values (% predicted) using reference data [22]. The Cobb angles of the main thoracic (MT), proximal thoracic (PT), thoracolumbar/lumbar (TL/L) curve and T5-T12 thoracic kyphosis (TK) were measured. The thoracic deformity parameters (definitions to be found in Chapter 2) measured were: rib-vertebra angle difference (RVAD) [39], inverse of the apical vertebral body-rib ratio ( $AVBRr^{-1}$ ) [41], space available for lung (SAFL) [44], lung height-width ratio (LHW $r$ ), kyphosis-lordosis index (KLi), endotheracic hump ratio (EH $r$ ) and rib hump index (RH $i$ ).

### 3.5.2 Landmark Acquisition

Coronal and sagittal radiographs were imported into Mimics v18.0 (Materialise N.V., Leuven, Belgium) as JPEG images and landmarks placed using points and spline curves. Figure 3.2 shows an example of the landmarks collected from the coronal and sagittal radiographs. In the coronal plane (Figure 3.2a), four points were placed at the vertex of each vertebrae in the thoracic and lumbar spine (red points). A cubic B-spline was

used to trace out the centreline of the ribs (red), clavicles (green) and the superior outline of the hemidiaphragm (blue) in each hemithorax. In the sagittal plane (Figure 3.2b)), splines were used to draw the anterior and posterior outline of the vertebral body column (red) from the superior endplate of the first thoracic vertebrae (T1) to the inferior endplate of the fifth lumbar vertebrae (L5). The outline of the diaphragm (green) was traced and the interior outline of the convex and concave rib contours were drawn inferiorly from the first ribs until they met with the diaphragm curve (blue). Similarly, the contour of the anterior chest was drawn along the interior side of the manubrium and sternum (orange) until they intersected the diaphragm curve. The landmark data was exported from Mimics and saved as text files.

### 3.5.3 Shape Model

The statistical shape model was constructed in the software R (<http://www.R-project.org>) using a combination of GPA and PCA principles. First, the coronal and sagittal landmarks were imported into R and the spline equations refitted. Pseudo landmarks were generated from each spline by placing points at equidistance along the curve; 10 and 20 pseudo landmarks were placed for each spline in the coronal and sagittal plane respectively. GPA was then performed on the coronal and sagittal datasets independently using a validated R package ‘geomorph’ [85]. The superimposed landmarks from geomorph are shown in Figure 3.3. PCA was performed using the `prcomp()` function in R to determine principle components and principle component scores. The principle component scores of the first  $k$  principle components which explained up to 70% ( $f_v = 0.7$ ) of the total variance were then selected for further analysis.

### 3.5.4 Statistical Methods

To allow better interpretability of the principle components, Pearson correlations were performed between principle component scores and deformity parameters and Cobb angles as well as pulmonary function. The  $p$ -values from Pearson correlations were corrected for multiple comparisons ( $q$ -values) using the Benjamini and Hochberg method [52] with  $q$ -value threshold of 0.05 corresponding to a false discover rate of 5%. To determine which modes of deformity were associated with lung function impairment, pre-operative and post-operative change in lung function metrics were regressed against principle component scores using step-wise multivariate regression with bi-directional elimination. The Bayesian information criterion (BIC) was employed for model selection with  $k = \ln(n)$  [53]. Models with the best fit are reported with regression coefficients for individual predictors ( $b$ ), their standard errors ( $SE(b)$ ) and standardised coefficients ( $\beta$ ) along with the coefficient of determination adjusted for multiple comparisons ( $r^2$ ) and model standard error (SE). All statistical analysis was implemented using the statistical software R.

## 3.6 Results

From the PCA results, it was found that 9 principle components were sufficient to explain 75.4% of the total variance in shape (Figure 3.4). Table 3.1 shows the Pearson correlation coefficient between principle component scores of the statistical shape model, pulmonary function metrics, Cobb angles and thoracic deformity parameters.

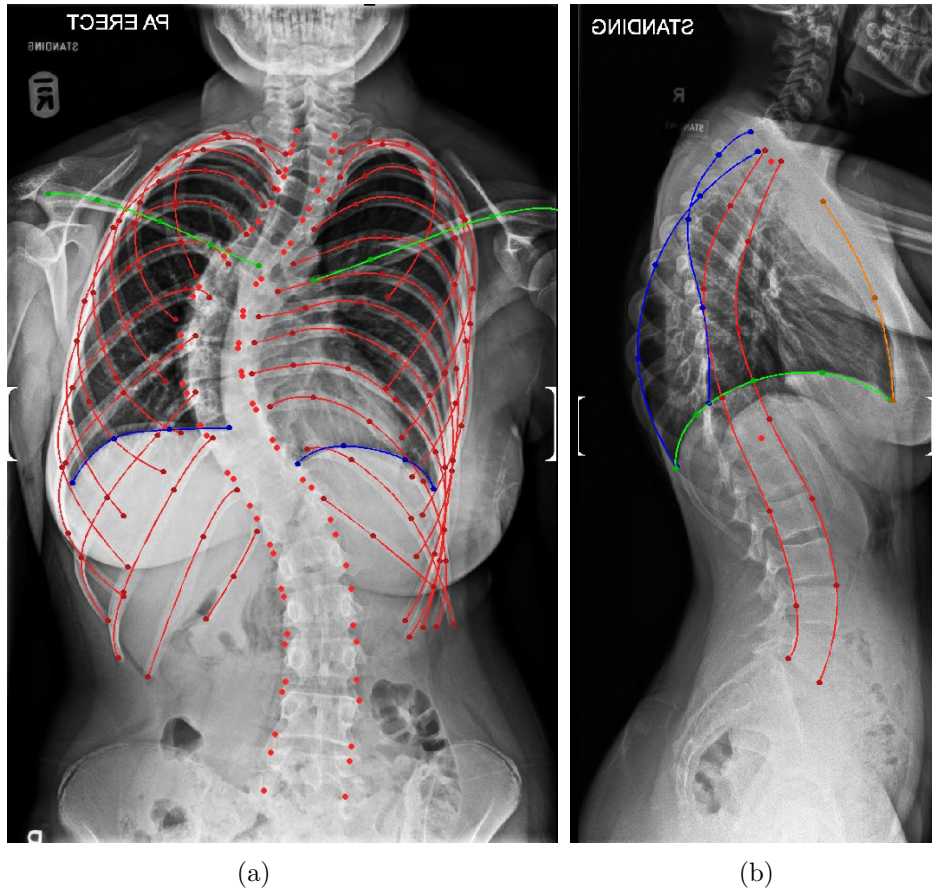
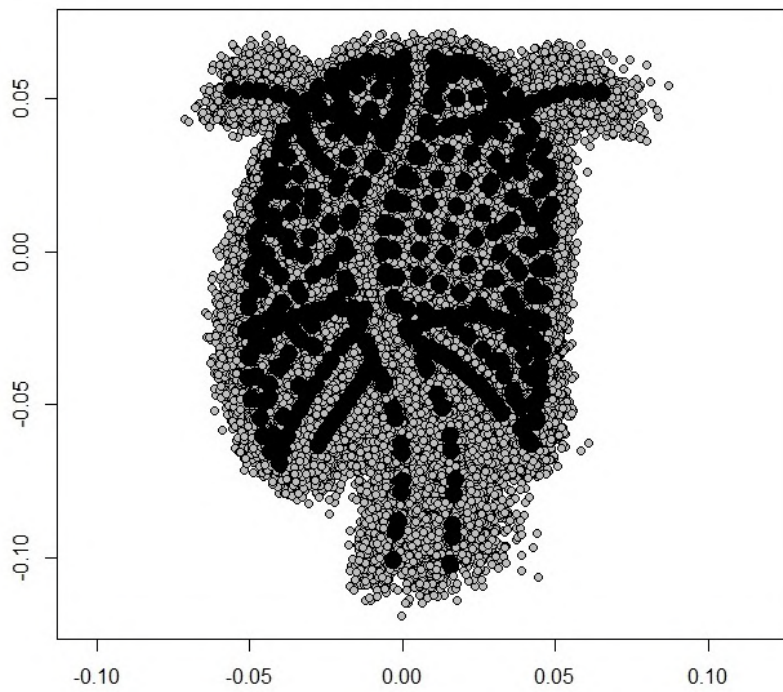
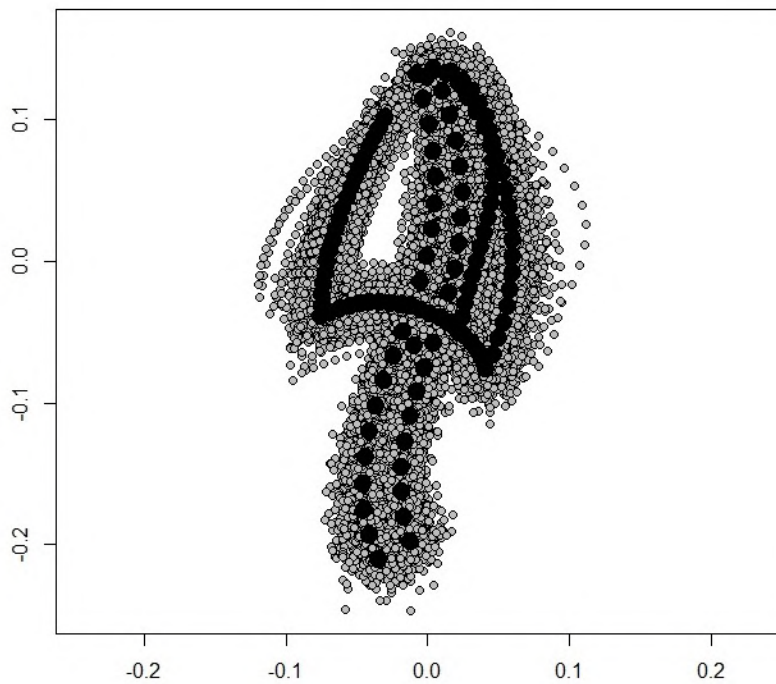


Figure 3.2: An example of the landmarks collected from the coronal and sagittal radiographs for the statistical shape model. In the coronal plane (a), four points were placed at the vertex of each vertebrae in the thoracic and lumbar spine (red points). A spline curve was used to trace out the centreline of the ribs (red), clavicles (green) and the superior outline of the hemidiaphragm (blue) in each hemithorax. In the sagittal plane (b), splines were used to draw the anterior and posterior outline of the vertebral body column (red) from the superior endplate of the first thoracic vertebrae (T1) to the inferior endplate of the fifth lumbar vertebrae (L5). The outline of the diaphragm (green) was traced and the interior outline of the convex and concave rib contours were drawn inferiorly from the first ribs until they met with the diaphragm curve (blue). The contour of the anterior chest was drawn along the interior side of the manubrium and sternum (orange) until they intersected the diaphragm curve.





(a)



(b)

Figure 3.3: Superimposed landmarks of the statistical shape model in the (a) coronal and (b) sagittal plane following generalised Procrustes analysis (GPA). The mean landmarks are shown in large black circles whilst individual observations are shown in small grey points.

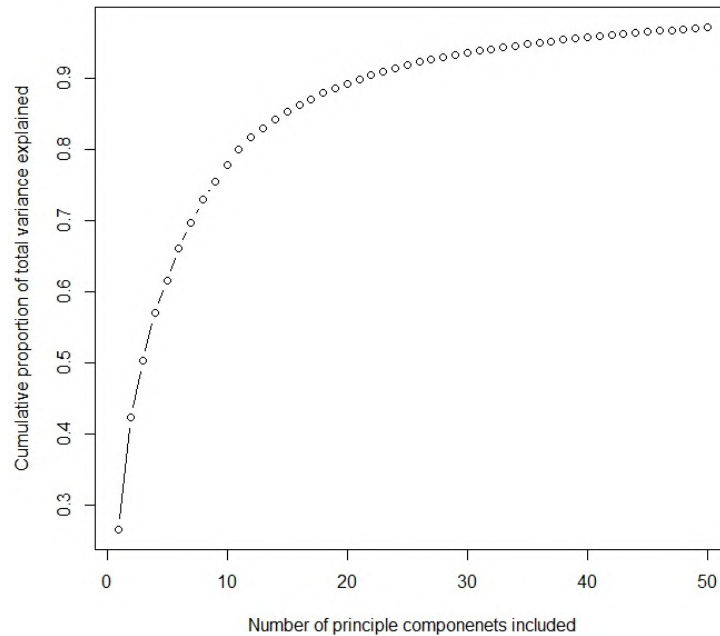


Figure 3.4: A plot of cumulative variance explained against the number of principle components included in the statistical shape model. It was found that 9 principle components were sufficient to explained up to 75.4% of the total variance.

Table 3.2 provides qualitative descriptions of the first nine principle component shape variations whilst Figures 3.5 to 3.13 display the shape deformation of the first nine principle components rendered for -3, 0 (mean shape) and +3 standard deviations of the deformation.

The MT curve was associated with PC<sub>1</sub>, PC<sub>2</sub> and PC<sub>5</sub> modes of variation ( $r = -0.78, 0.32$  and  $0.33$  respectively). The PT curve was associated with increasing scores of PC<sub>4</sub>, PC<sub>5</sub> and PC<sub>6</sub> ( $r = -0.78, 0.32$  and  $0.33$  respectively), whilst TL/L curve corresponded to low scores in PC<sub>1</sub> ( $r = -0.39$ ) and high scores in PC<sub>2</sub> ( $r = 0.43$ ). TK correlated positively with PC<sub>2</sub>, PC<sub>3</sub>, PC<sub>4</sub> scores ( $r = 0.59, 0.32$  and  $0.43$  respectively) and negatively with PC<sub>6</sub> scores ( $r = -0.27$ ).

When considering the thoracic deformity parameters, SAFL correlated positively with PC<sub>1</sub> but negatively with PC<sub>2</sub> ( $r = 0.56$  and  $-0.37$ ). PC<sub>2</sub> and PC<sub>6</sub> were both negatively associated with LHW<sub>r</sub> ( $r = -0.69$  and  $-0.28$ ). KLi was moderately correlated with increasing PC<sub>3</sub> and PC<sub>4</sub> scores and decreasing PC<sub>6</sub> scores ( $r = 0.51, 0.41$  and  $-0.50$ ); it was also weakly correlated with decreasing PC<sub>1</sub> scores ( $r = -0.26$ ). EH<sub>r</sub> was negatively associated with PC<sub>2</sub> and PC<sub>3</sub> scores ( $r = -0.62$  and  $-0.3$ ). Increasing RH<sub>i</sub> was reflected in lower PC<sub>1</sub> scores ( $r = -0.61$  and  $-0.48$ ) and higher PC<sub>2</sub> and PC<sub>5</sub> score ( $r = 0.35$  and  $0.39$ ).

FEV<sub>1</sub> was associated with increasing PC<sub>1</sub>, PC<sub>3</sub> and decreasing PC<sub>5</sub> scores ( $r = 0.50, 0.26$  and  $-0.29$ ) whilst FVC corresponded positively with PC<sub>1</sub> scores and negatively with PC<sub>5</sub> scores ( $r = 0.51$  and  $-0.30$ ). FEV<sub>1</sub>/FVC did not correlate with any of the principle

component scores based on univariate analysis.

Multivariate regression results are shown in Table 3.3. The first three principle components were found to significantly predict FEV<sub>1</sub> ( $\beta = 0.54, 0.23$  and  $0.28$ ;  $r^2 = 0.447$ ) and FVC respectively ( $\beta = 0.55, 0.20, 0.23$ ;  $r^2 = 0.349$ ). Principle components 2 to 4 were significant predictors of FEV<sub>1</sub>/FVC ( $\beta = 0.16, 0.18, 0.17$ ;  $r^2 = 0.069$ ). Post-operatively, lower scores in pre-operative PC<sub>1</sub>, PC<sub>2</sub> and PC<sub>3</sub> score were found to result in greater gains in FEV<sub>1</sub> ( $\beta = -0.36, -0.33$  and  $-0.29$ ) and FVC ( $\beta = -0.35, -0.29$  and  $-0.36$ ). Post-operative change in FEV<sub>1</sub>/FVC was best predicted by the change in PC<sub>2</sub> ( $\beta = 0.29$ ) and pre-operative PC<sub>6</sub> scores ( $\beta = 0.26$ ).

### 3.7 Discussion

Previous studies have used statistical shape models in order to analyse spine morphology in scoliosis progression and the effect of scoliosis treatment [80, 79, 78]. In this study, a statistical shape model of the rib cage and spine was created in order to quantify the modes of variation in thoracic morphology which corresponded to pulmonary function impairment in AIS.

From visual inspection of the principle modes of deformation, it is clear that the principle components reflect variations in thoracic shape seen clinically. The first principle component describes the formation of a main thoracic curve with increased lateral deviation of the curve apex from the central sacral midline. Shortening of the spine is seen as a result of the scoliosis along with the formation of a rib hump, a typical thoracic feature of scoliosis [86]. The second mode of deformation captures loss of thoracic depth which accompanies reductions in thoracic kyphosis resulting in a flat sagittal profile. The third mode of variation reflects changes in the anterior-posterior position of the spine at the level of the diaphragm, possibly due to variations in lumbar lordosis or pelvic tilt, as well as rib hump formation.

The multivariate analysis demonstrated that the first three principle components are predictive of pre-operative FEV<sub>1</sub> and FVC supporting previous studies showing an association between increasing MT curve, loss of TK and increasing rib hump in pulmonary function impairment in AIS [25, 29, 33]. The second to fourth principle components, which all show substantial variations in the sagittal thoracic profile, were shown to be predictive of pre-operative FEV<sub>1</sub>/FVC. This supports prior studies demonstrating the association between scoliosis and obstructive lung disease [63, 24] with extrinsic compression of airways by spinal intrusion reported as a causative factor [40, 51]. As the first three principle components were also predictive of post-operative change in FEV<sub>1</sub> and FVC, the regression analysis suggest that those with severe MT curves, flat sagittal profiles and severe rib humps have most to gain from operative intervention. Interestingly post-operative FEV<sub>1</sub>/FVC change was best predicted by increases in the second principle component score ( $\Delta PC_2$ ) and pre-operative score of sixth mode of variation which is associated with a flat thoracic profile. Previous reports have demonstrated increased pulmonary function and decompression of airways upon restoration of natural kyphosis in hypokyphotic patients with scoliosis [51, 67].

There are several limitation to this study. Firstly, the selection of landmarks and spline control points were placed manually and subject to interobserver error. Secondly, the effect of curve type or the number of control points per spline was not studied in terms of accuracy. Thirdly, the biplanar shape model does not truly capture the three-

dimensional deformity but rather the correlations between shapes in the sagittal and coronal plane. These limitations should be addressed in future investigations.

Overall, statistical shape models are underutilized in the study of AIS, especially considering the routine use of radiographic imaging in both management and treatment. It is estimated that patients with scoliosis receive up to 22 radiographs over a 3 year treatment period, 3.7 radiographs per year for observational treatment, 5.7 per year for bracing treatment and 12.2 per year for those receiving surgical treatment [87, 88, 89]. In contrast to the high availability of imaging data, AIS is still analyzed using classification systems which are subject to high inter- and intraobserver errors. In a comparative study of the King and Lenke classification systems, Richards et al. [90] determined that the Lenke classification system for AIS was less reliable than previously reported. The authors found that the intraobserver and interobserver reliability in the Lenke system was 65.0% and 55.5% respectively whilst the King system was 83.5% and 68.0% respectively. Active shape models, other the other hand, which automatically or semi-automatically identify landmarks have been shown to have high inter- and extraobserver reliability [77]. Statistical shape models have the potential to provide a quantitative and objective description of scoliosis deformity which warrants further investigation in future studies.

### 3.8 Conclusion

Statistical shape models are a useful morphometric tool in analyzing variations in rib cage and spine morphology in AIS. The shape model demonstrated that increasing thoracic scoliosis, flattening of the sagittal profile and increased rib hump correspond to reduction in pulmonary function. Sagittal flattening of the thoracic spine is shown to increase airway resistance as measured by  $FEV_1/FVC$ . Patients with severe scoliosis, hypokyphosis and large rib humps demonstrate greater increases in post-operative lung function. Statistical shape models can provide a quantitative and objective description of the thoracic deformity and should be investigated for further use cases.

Table 3.1: Pearson correlation coefficients between pre-operative radiographic Cobb angles, deformity parameters, lung function and the first nine principle components from the statistical shape model ( $n = 136$ ).

	PC <sub>1</sub>	PC <sub>2</sub>	PC <sub>3</sub>	PC <sub>4</sub>	PC <sub>5</sub>	PC <sub>6</sub>	PC <sub>7</sub>	PC <sub>8</sub>	PC <sub>9</sub>
FEV <sub>1</sub>	0.50 ***	0.20	0.26 *	-0.06	-0.29 *	0.19	-0.05	-0.20	-0.22
FVC	0.51 ***	0.16	0.20	-0.12	-0.3 **	0.22	-0.05	-0.19	-0.22
FEV <sub>1</sub> /FVC	0.05	0.17	0.18	0.17	-0.02	-0.06	-0.02	-0.07	-0.08
PT	-0.10	-0.12	0.06	0.43 ***	0.44 ***	0.38 ***	0.25	-0.03	0.03
MT	-0.78 ***	0.32 **	-0.20	0.17	0.33 **	-0.15	0.00	0.11	-0.03
TL/L	-0.39 ***	0.43 ***	0.08	-0.14	-0.24	-0.19	0.06	0.01	-0.05
TK	-0.22	0.59 ***	0.32 **	0.43 ***	-0.18	-0.27 *	-0.21	-0.10	-0.16
RVAD	-0.47 ***	0.07	-0.28 *	0.23	0.51 ***	-0.04	-0.07	0.04	0.04
AVBRr <sup>-1</sup>	0.71 ***	-0.15	0.22	-0.31 **	-0.59 ***	0.06	0.09	-0.22	-0.03
SAFL	0.56 ***	-0.37 ***	0.20	0.20	0.06	0.22	0.24	-0.05	0.04
LHWr	0.07	-0.69 ***	-0.15	-0.01	0.16	-0.28 *	0.12	0.25	0.20
KLi	-0.26 *	0.51 ***	0.24	0.41 ***	0.01	-0.50 ***	-0.02	-0.20	-0.18
EHR	-0.02	-0.62 ***	-0.3 **	-0.05	0.06	0.05	0.18	0.24	0.23
RHi	-0.61 ***	0.35 ***	-0.18	0.15	0.39 ***	-0.48 ***	0.08	0.03	0.04

Significant correlation to \*  $q < 0.05$ ; \*\*  $q < 0.01$ ; and \*\*\*  $q < 0.001$ .

Table 3.2: Qualitative descriptions of the first 9 principle components of the statistical shape model

---

PC <sub>1</sub>	Decreasing main thoracic and thoracolumbar curve; increase in convex hemithoracic width; increase in concave hemithoracic height; reduced rib hump asymmetry; elevation of diaphragm relative to spine.
PC <sub>2</sub>	Increasing main thoracic curve and thoracolumbar curve; increasing thoracic kyphosis and lumbar lordosis; widening of the chest depth and shortening of lung height. Elevation of the diaphragm relative to spine; increasing rib hump asymmetry.
PC <sub>3</sub>	Reduced main thoracic curve and lateral displacement. The spine occupies an increasingly posterior position in the thorax with increasing thoracic kyphosis. Reduction of rib hump prominence.
PC <sub>4</sub>	Increasing proximal curvature and tilt towards convexity. Lowering of apical height. Increased kyphosis of the thoracic spine. Increased in rib hump with inversion of rib prominence superiorly.
PC <sub>5</sub>	Increasing number of vertebrae in main curve. Reduction of thoracolumbar/lumbar curve. Reduction of convex hemithoracic width. Increasing rib hump.
PC <sub>6</sub>	Formation of proximal thoracic scoliosis curve. Inversion of rib prominence with formation of concave rib hump superiorly. Loss of thoracic kyphosis and lumbar lordosis.
PC <sub>7</sub>	Reduction in the anterior position of the diaphragm relative to the posterior position.
PC <sub>8</sub>	Reduction of size of concave rib prominence.
PC <sub>9</sub>	Increasing length of the twelfth rib

---

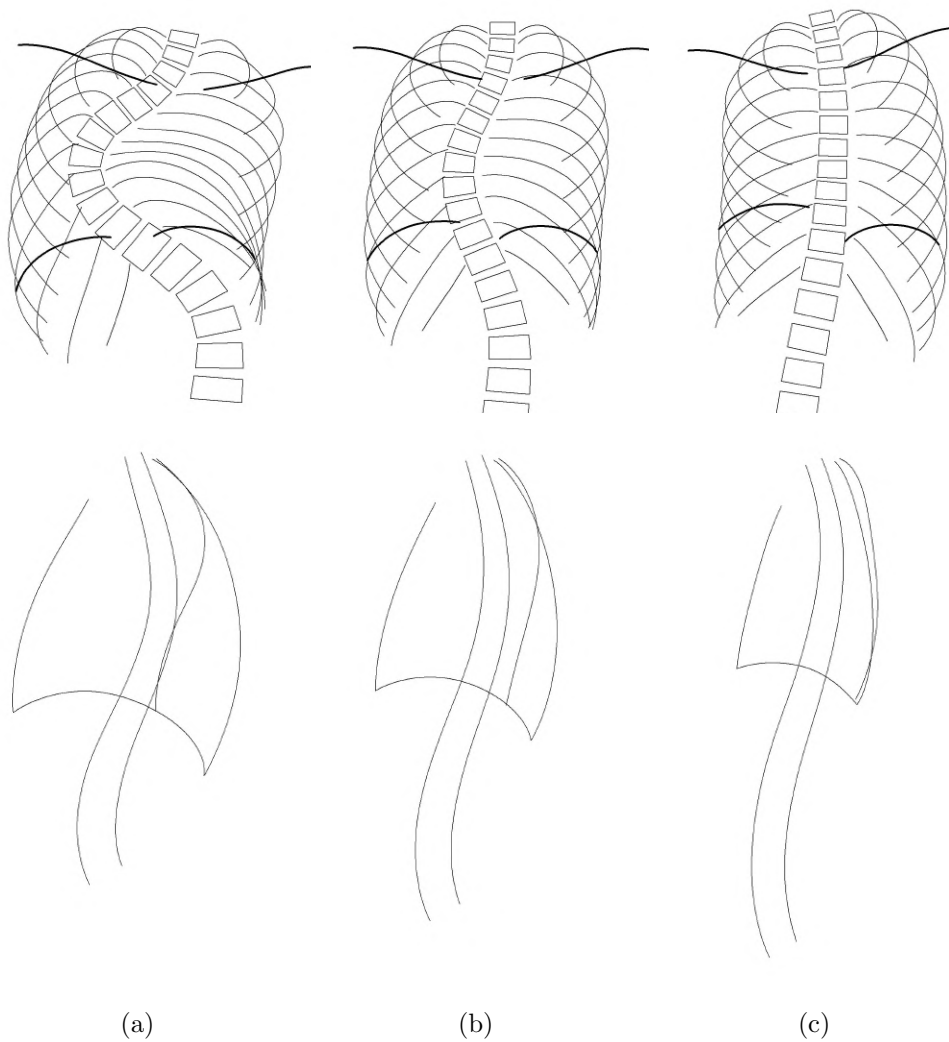


Figure 3.5: Shape variation of the first principal deformation mode (PC<sub>1</sub>) with (a) -3; (b) 0 (mean shape); and (c) +3 standard deviations of the shape deformation. Coronal and sagittal views are shown on the top and bottom rows respectively.

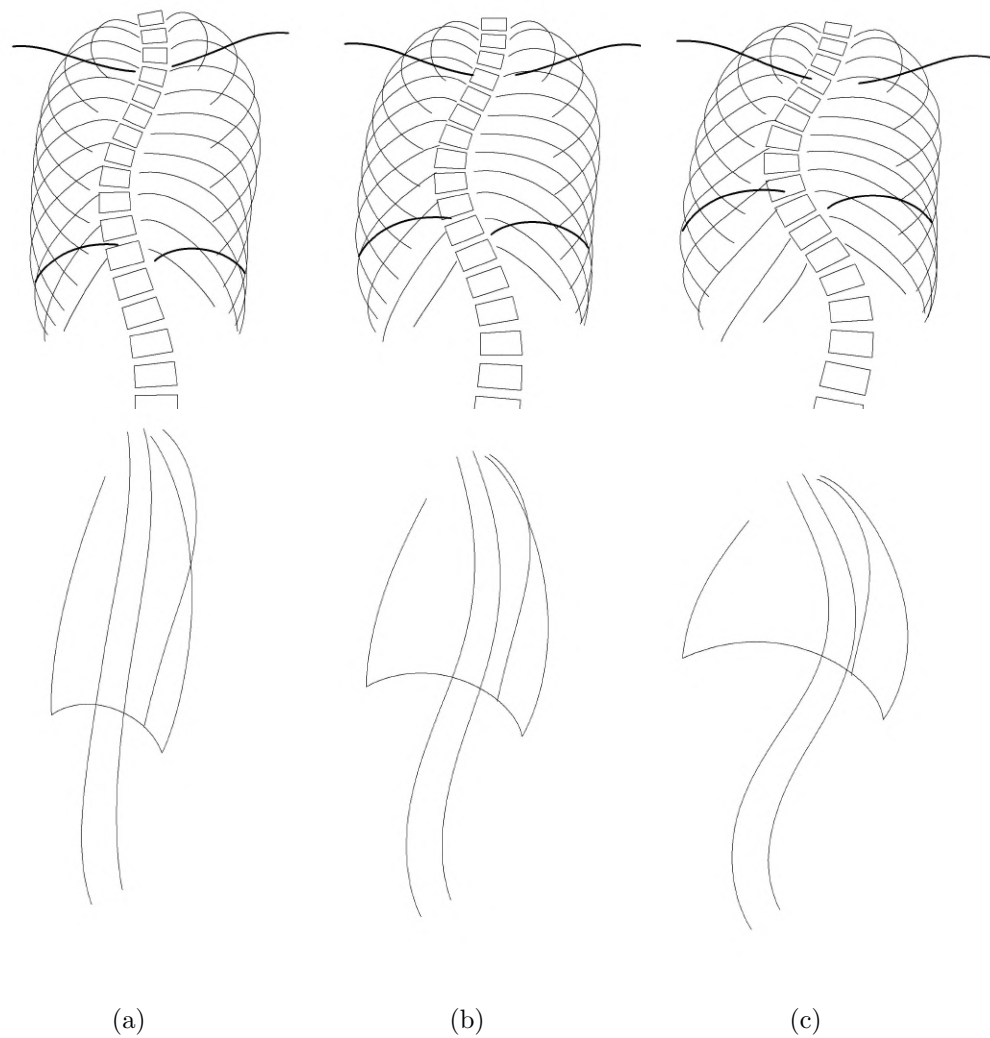


Figure 3.6: Shape variation of the second principal deformation mode ( $PC_2$ ) with (a) -3; (b) 0 (mean shape); and (c) +3 standard deviations of the shape deformation. Coronal and sagittal views are shown on the top and bottom rows respectively.



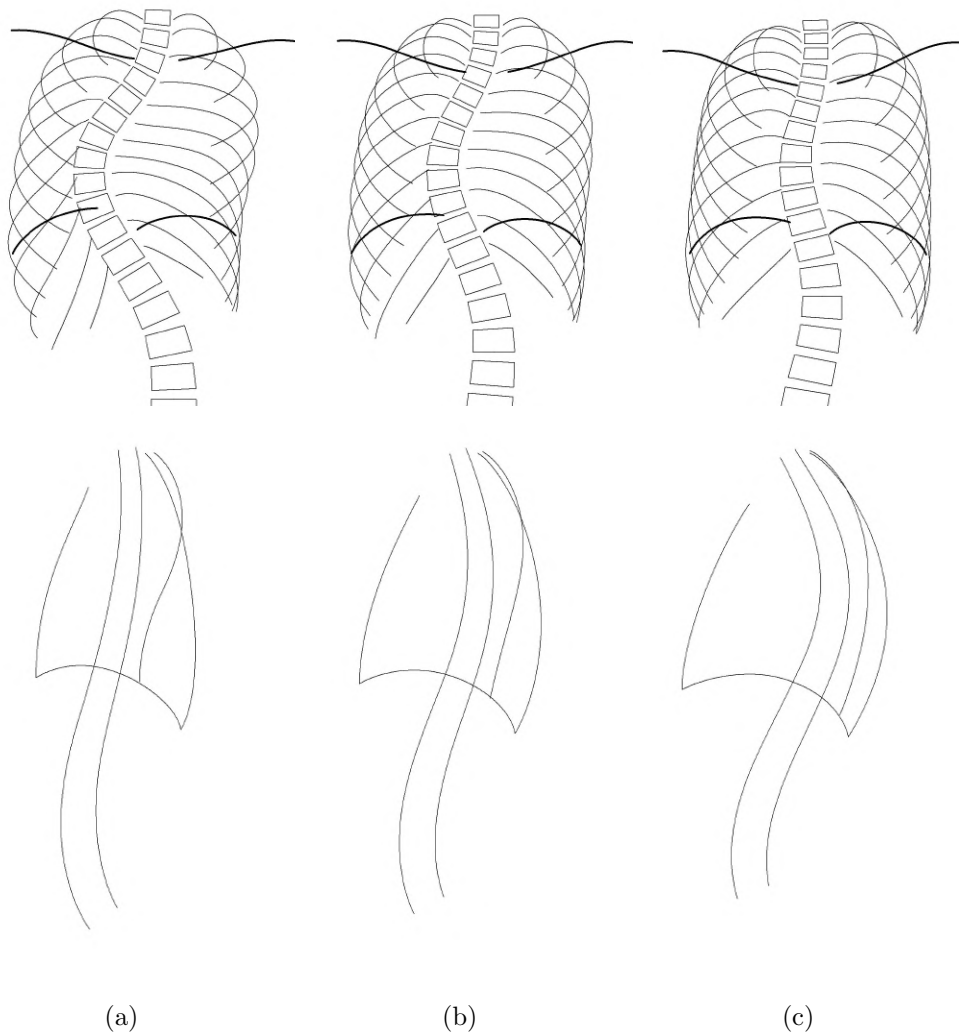


Figure 3.7: Shape variation of the third principal deformation mode ( $PC_3$ ) with (a) -3; (b) 0 (mean shape); and (c) +3 standard deviations of the shape deformation. Coronal and sagittal views are shown on the top and bottom rows respectively.

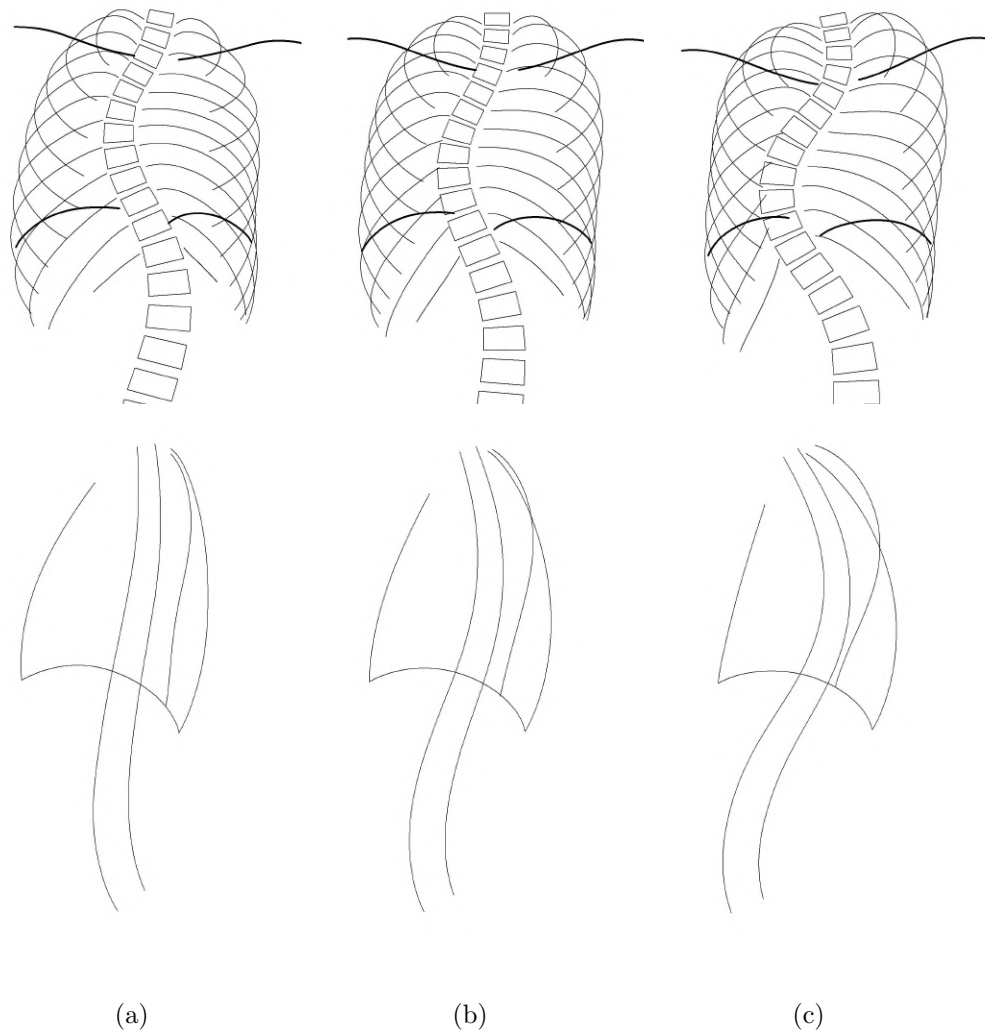


Figure 3.8: Shape variation of the fourth principal deformation mode ( $PC_4$ ) with (a) -3; (b) 0 (mean shape); and (c) +3 standard deviations of the shape deformation. Coronal and sagittal views are shown on the top and bottom rows respectively.

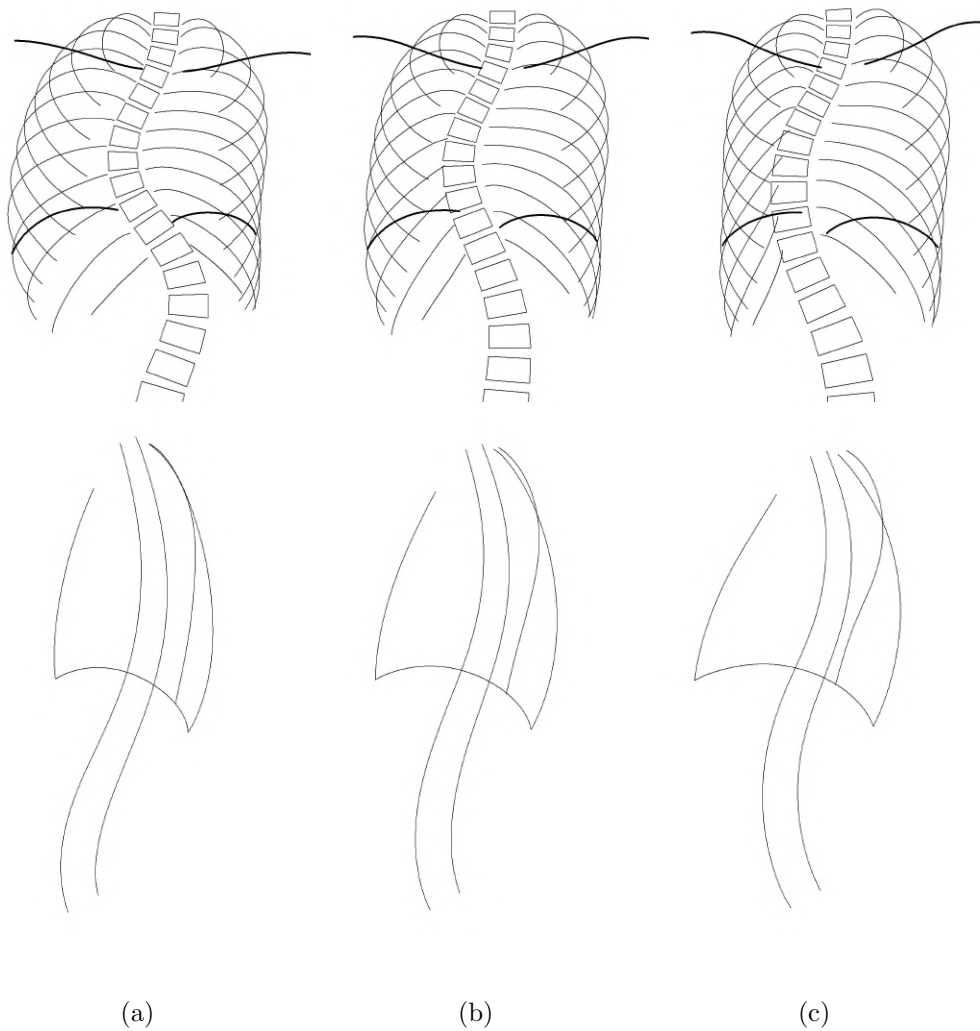


Figure 3.9: Shape variation of the fifth principal deformation mode (PC<sub>5</sub>) with (a) -3; (b) 0 (mean shape); and (c) +3 standard deviations of the shape deformation. Coronal and sagittal views are shown on the top and bottom rows respectively.

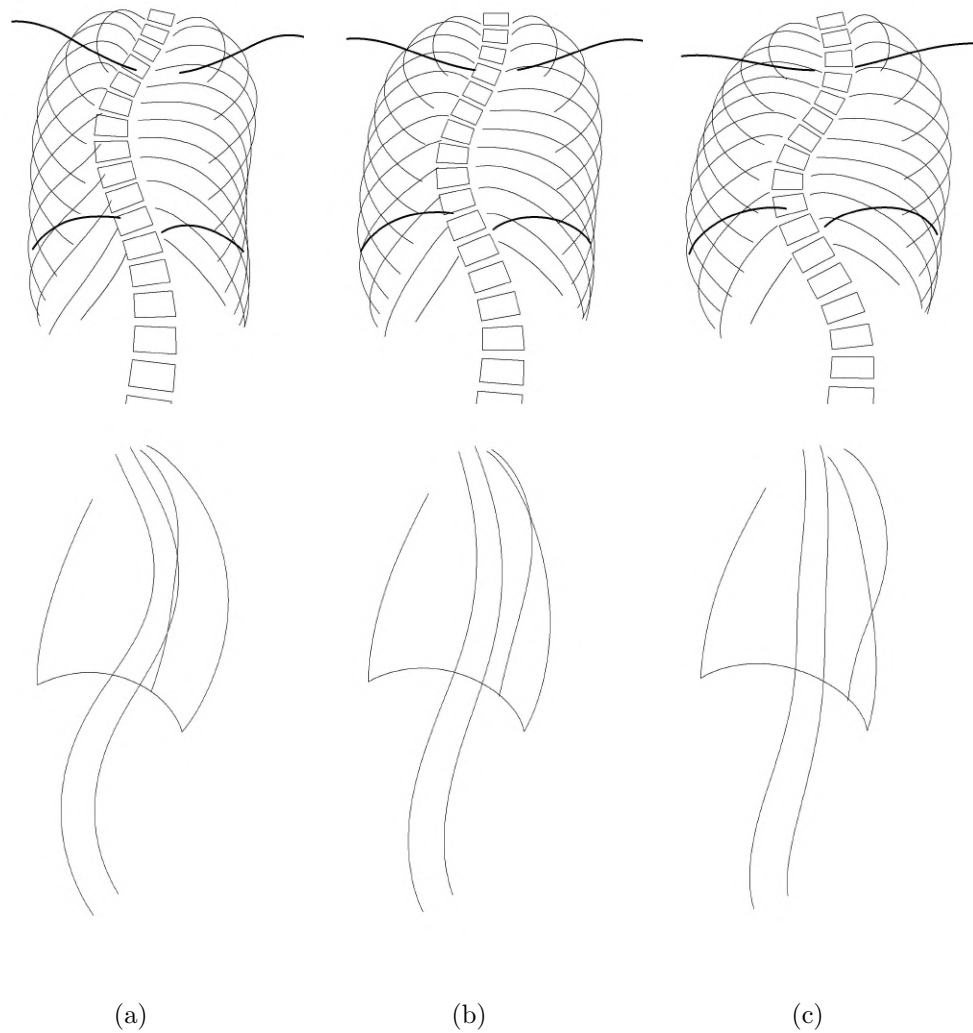


Figure 3.10: Shape variation of the sixth principal deformation mode ( $PC_6$ ) with (a) -3; (b) 0 (mean shape); and (c) +3 standard deviations of the shape deformation. Coronal and sagittal views are shown on the top and bottom rows respectively.

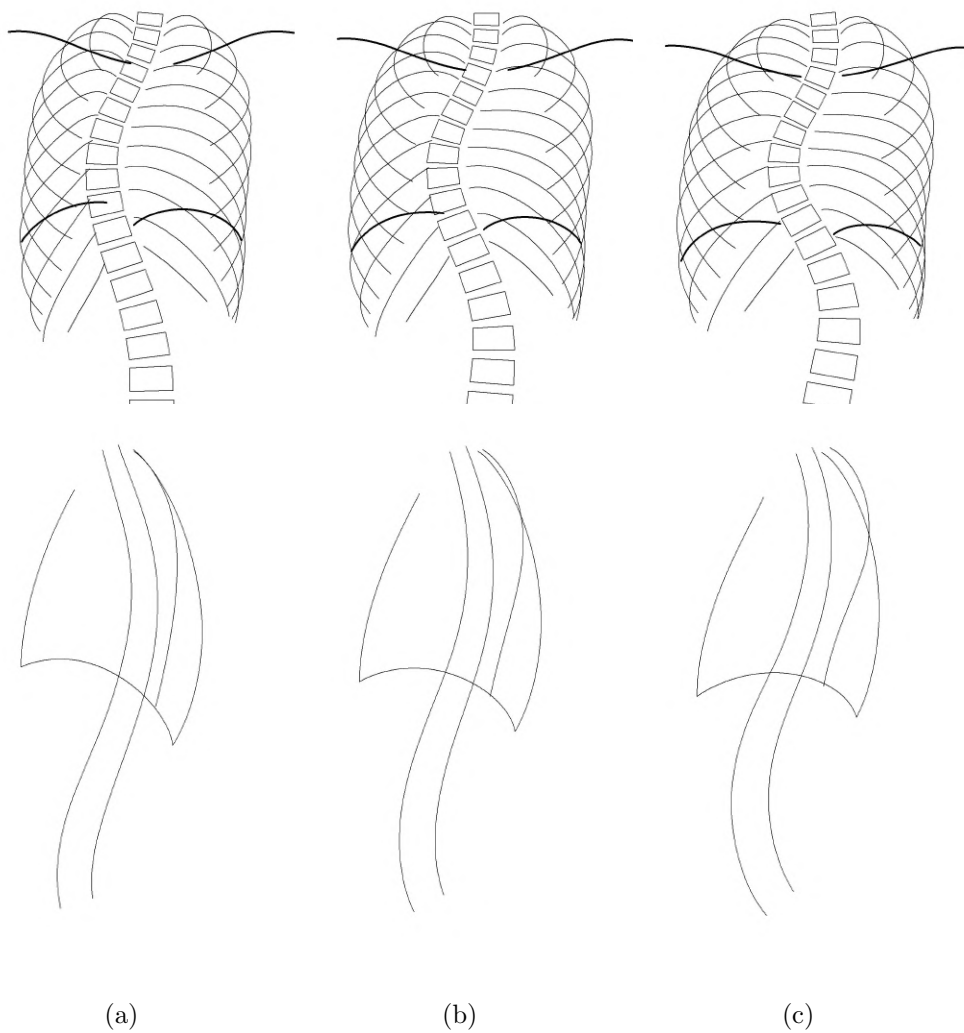


Figure 3.11: Shape variation of the sixth principal deformation mode (PC<sub>7</sub>) with (a) -3; (b) 0 (mean shape); and (c) +3 standard deviations of the shape deformation. Coronal and sagittal views are shown on the top and bottom rows respectively.

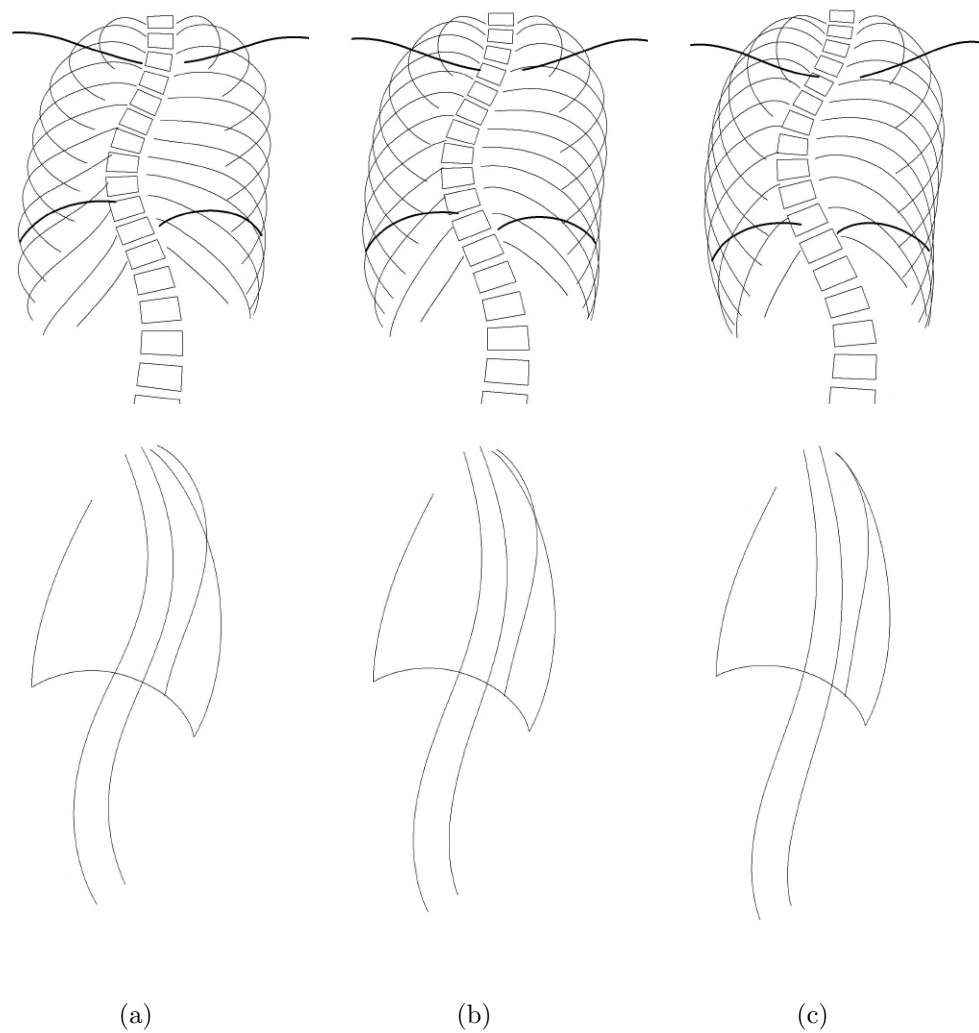


Figure 3.12: Shape variation of the sixth principal deformation mode ( $PC_8$ ) with (a) -3; (b) 0 (mean shape); and (c) +3 standard deviations of the shape deformation. Coronal and sagittal views are shown on the top and bottom rows respectively.

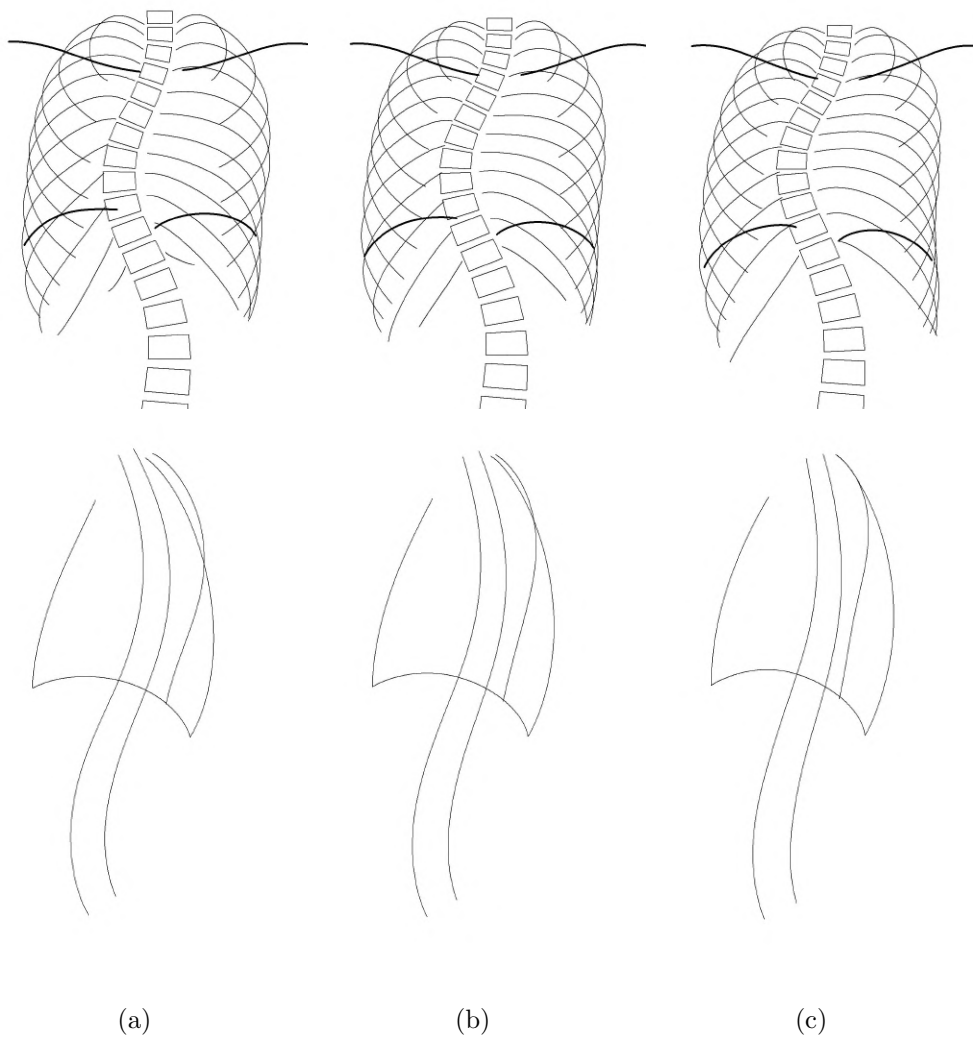


Figure 3.13: Shape variation of the sixth principal deformation mode (PC<sub>9</sub>) with (a) -3; (b) 0 (mean shape); and (c) +3 standard deviations of the shape deformation. Coronal and sagittal views are shown on the top and bottom rows respectively.

Table 3.3: Multivariate step-wise regression results for the prediction of pre-operative ( $n = 136$ ) and post-operative changes ( $n = 72$ ) in lung function using principle component scores from statistical shape model.

FEV <sub>1</sub>	Intercept	PC <sub>1</sub>	PC <sub>2</sub>	PC <sub>3</sub>	Model statistics
$b$	77.406	11.908	3.502	4.580	$r^2 = 0.447$
SE( $b$ )	1.386	1.416	0.976	1.054	SE = 12.103
$\beta$	-	0.543	0.231	0.279	-
$p$	< 0.001	< 0.001	< 0.001	< 0.001	-
FVC	Intercept	PC <sub>1</sub>	PC <sub>2</sub>	PC <sub>3</sub>	Model statistics
$b$	80.633	11.573	2.840	3.553	$r^2 = 0.349$
SE( $b$ )	1.370	1.400	0.966	1.043	SE = 12.600
$\beta$	-	0.550	0.195	0.226	-
$p$	< 0.001	< 0.001	0.004	0.001	-
FEV <sub>1</sub> /FVC	Intercept	PC <sub>2</sub>	PC <sub>3</sub>	PC <sub>4</sub>	Model statistics
$b$	94.621	1.249	1.505	1.249	$r^2 = 0.069$
SE( $b$ )	0.699	0.639	0.692	0.625	SE = 7.968
$\beta$	-	0.163	0.181	0.166	-
$p$	< 0.001	0.048	0.031	0.048	-
$\Delta$ FEV <sub>1</sub>	Intercept	PC <sub>1</sub>	PC <sub>2</sub>	PC <sub>3</sub>	Model statistics
$b$	6.233	-3.481	-3.435	-4.364	$r^2 = 0.270$
SE( $b$ )	1.593	1.004	1.070	1.527	SE = 9.171
$\beta$	-	-0.355	-0.329	-0.294	-
$p$	< 0.001	0.001	0.002	0.006	-
$\Delta$ FVC	Intercept	PC <sub>1</sub>	PC <sub>2</sub>	PC <sub>3</sub>	Model statistics
$b$	3.432	-5.217	-2.817	-3.793	$r^2 = 0.269$
SE( $b$ )	1.588	1.523	1.001	1.067	SE = 9.210
$\beta$	-	-0.350	-0.286	-0.362	-
$p$	0.034	0.001	0.006	0.001	-
$\Delta$ FEV <sub>1</sub> /FVC	Intercept	$\Delta$ PC <sub>2</sub>	PC <sub>6</sub>	-	Model statistics
$b$	3.149	2.013	1.609	-	$r^2 = 0.158$
SE( $b$ )	0.711	0.773	0.693	-	SE = 5.885
$\beta$	-	0.290	0.258	-	-
$p$	< 0.001	0.011	0.023	-	-





Part II

**Computerised Tomography  
Studies**



## Chapter 4

# Thoracic Deformity Parameters

### 4.1 Summary

In this chapter, 13 computer tomography (CT)-based thoracic deformity parameters described in the literature are analysed for their utility in predicting pre-operative impairment and post-operative improvements of lung function in adolescent idiopathic scoliosis (AIS). Principle component analysis found that over 90% of the variance amongst the 13 deformity parameters measured at the apex could be explained by 4 principle components. This suggests high covariance between thoracic deformity features and the spinal deformity. The 4 modes of variations were qualitatively identified as the evolution of lordoscoliosis, kyp hosciosis, convex-concave rib asymmetry and sternal misalignment respectively. Measures of spinal intrusion (spinal penetration index, endothoracic hump ratio) and the size of the rib hump (rib hump index, thoracic rotation, angle of trunk rotation) featured as significant predictors upon multivariate and univariate correlations. Multivariate regression showed that CT-based deformity parameters ( $r^2 = 0.45$  to  $0.57$ ) were superior to conventional radiographic Cobb angle measurements ( $r^2 = 0.22$  to  $0.33$ ) in predicting pre-operative expiratory volumes and post-operative volume gains. The analysis reveals that patients with lordoscoliosis have more impaired lung function than their normo- and hyperkyphotic counter parts; the differential, however, can be reduced if natural kyphosis is restored post-operatively. Thoracic deformity parameters are useful indices that can provide additional understanding of the mechanisms by which scoliosis impairs respiratory function.

### 4.2 Introduction

Moderate to severe pulmonary impairment is present in 20% of preoperative patients with a thoracic idiopathic scoliosis with a coronal curve of  $50-70^\circ$  and in 41% of curves measuring  $71-80^\circ$  [29]. Obstructive lung disease is present in 39% of preoperative patients with idiopathic scoliosis [24]. Pulmonary impairment is most severely affected in Lenke 4, 2 and 1 patterns [29]. However radiographic variables including Cobb angle, number of vertebral segments included in the scoliosis, flexibility, rib vertebral angle differences have shown mild correlation with pulmonary function testing [29, 24, 26, 34]. The weak correlation of current deformity parameters obtained from plain standing radiographs demonstrates the need to develop deformity parameters which capture the structural changes of the entire chest wall. Deformity parameters which show a stronger

relationship with lung function are necessary to allow the assessment of young or uncompliant patients with scoliosis, measure the effect of different treatment methods and to enhance the understanding of the pathophysiology of lung function impairment in scoliosis. The aim of this study was to examine the relationship of CT based thoracic deformity parameters and lung function in AIS.

### 4.3 Literature Review

Aaro and Dahlborn [86] were among the first to propose the use of CT for measuring spinal and rib cage deformity in scoliosis. They proposed a rib hump index (RHi) to quantify the extent of the rib hump; the kyphosis-lordosis index to quantify the sagittal diameter of the thorax; and vertebral/thoracic rotation to quantify the rotational character of the deformity. In a subsequent study [55] consisting of 25 to 39 thoracic AIS curves, they established correlations between scoliosis Cobb angles, rotation angles and the size of the rib hump.

In a retrospective study consisting of predominately Lenke 1 type curves ( $n = 110$  pre-operative and 70 post-operative), Mao et al. [91] described the sternum-rib ratio as a measure of midline displacement; and the angle of trunk rotation to quantify the size of the rib hump. Both indices were moderately correlated to the Cobb angle ( $r = 0.5$ ) and both were shown to improve post-operatively ( $p < 0.001$ ).

Campbell et al. [44] described the features of thoracic insufficiency syndrome in congenital scoliosis, within which the concept of a ‘windswept thorax’ was introduced. The windswept thorax is characterised by thoracic rotation and narrowing of the convex rib hump; the posterior hemithoracic symmetry ratio was proposed as a quantitative measure of this feature.

Pectus excavatum is a thoracic deformity where the anterior section of the chest is depressed into the thoracic cavity reducing the sternovertebral distance and lung volume. The Haller index [92] and chest flatness index [93] have been used to quantify the sagittal narrowing of the chest whilst the hemithoracic depth asymmetry index [93] has been used to describe the resulting left-right asymmetry in pectus excavatum. As pectus excavatum has been shown to be associated with AIS, application of these indices can also be found within the scoliosis literature [94, 95].

In 2014, Harris et al. conducted a review of the literature and compiled the above indices, amongst others, into the first comprehensive summary of CT-based thoracic deformity parameters [58]. The review classified the parameters into eight groups based on the deformity features they described: anterior chest angulation, area enclosed by rib cage, coronal asymmetry, hemithorax depth asymmetry, hemithorax width asymmetry, posterior rib asymmetry, sagittal depth, and sternum deviation.

Not included in the review were measures of spinal intrusion which were proposed by Dubousset et al. [40] and later adapted by Ito et al. [51]. Dubousset et al. introduced the concept of an endothoracic hump in a case series of 18 patients with mixed scoliosis etiology and extrinsic airway compression. They proposed the spinal penetration index (SPi) to quantify the protrusion of vertebral column into the thorax. The SPi is an area ratio of the space occupied by the spine to that of the thoracic cavity. Illharreborde et al. [38] estimated the SPi using 3D reconstructions from biplanar radiographs and correlated it to pulmonary function tests in 80 AIS patients. No correlation was found between pulmonary function test and the radiographically reconstructed SPi but SPi

was significantly greater in patients with obstructive syndrome ( $p = 0.01$ ). Ito et al., in a case series of 6 patients with airflow obstruction and mixed etiology, proposed the endothoracic hump ratio (EHr) which simplifies the SPi by using distance instead of area measurements. They reported mean post-operative improvement of 18.2% in vital capacity from 45.5% to 63.7% of predicted values when the mean EHR was reduced from 1.34 to 1.12.

One of the earliest studies to correlate pulmonary function with chest deformity in scoliosis was by Aaro and Ohlund [36]. In their study of 33 patients, they found that static and dynamic lung volumes were negatively correlated with the coronal Cobb angle and to a lesser extent rotation. They found that KLi was positively correlated to lung volumes, FEV<sub>1</sub> and FVC. They concluded that out of the radiographic and CT-based deformity parameters, the coronal Cobb angle was the best predictor of lung volume compromise. They recommended that operative treatment should target the lateral displacement of the spine while maintaining a normal sagittal thoracic curve.

Takahashi et al. [35] is the only study to date which has systematically correlated pre-operative CT-measured deformity parameters with lung function. In their study, they measured axial vertebral rotation, a modified rib hump index and the kyphosis-lordosis index in 109 AIS patients with a mixture of curve types (predominantly King type II and III; double curve and thoracic curve respectively). Forced vital capacity was found to correlated negatively with axial rotation ( $r = -0.33$ ) and positively with KLi ( $r = 0.33$ ) but their modified RHi did not correlate.

Akazawa et al. [54] conducted a follow-up study (mean of 35.3 years) analysing the effects of RA<sub>sag</sub>, RHi and PHSr in a sample consisting of 18 AIS patients who underwent spinal fusion with Harrington instrumentation. Forced vital capacity was found to have strong negative correlations with RA<sub>sag</sub> ( $r = -0.80$ ), RHi ( $r = -0.82$ ), PHSr ( $r = -0.7$ ) and the proximal thoracic curve ( $r = -0.72$ ).

Delorme et al. [96] studied the effects of Cotrel-Dubousset instrumentation on rib orientations by reconstructing the rib cage from from bi-planar radiographs. Their results showed that trunk rotation in the axial plane reduced by 3° and that concave ribs were lowered by 5° at the apical level in the frontal plane.

From this review, it can be seen that although a large number of indices have been proposed to quantify specific thoracic features, there is still a paucity of information on the interactions between spinal deformity, shape of the thoracic cage, pulmonary function and post-operative changes.

## 4.4 Materials & Methods

### 4.4.1 Subject Characteristics

A retrospective review of the surgeon's imaging database between 2015 and 2019 (Kodak Carestream PACS) at the Scottish National Spine Deformity Service was conducted to identify severe Lenke type 1 or 2 AIS patients with right-sided, thoracic curves with an apex between the seventh and tenth thoracic vertebrae (T7-T10). Patients who underwent pre-operative planning CT imaging and pulmonary function tests (PFT) were included. Patients with evidence or a history of primary obstructive lung disease were excluded. A total of 49 patients (36 female and 13 male, all Caucasian) with a mean age of 16.8 years (standard deviation [SD] = 7.8 years, range = 10.0 to 39.8 years)

met the inclusion criteria. Patients underwent scoliosis correction surgery by posterior instrumental fusion using segmental pedicle screws and rods. Out of the 49 patients, 40 patients had post-operative PFTs at 1-year follow-up.

#### 4.4.2 Lung Function

PFTs were conducted via forced manoeuvres in accordance with the joint American Thoracic Society and European Respiratory Society standards [50]. Forced expiration in 1 second ( $FEV_1$ ) and forced vital capacity (FVC) were measured (Jaeger Master-Screen PFT pro) along with armspan. In calculating lung function predicted values, arm span was used to estimate standing height to correct for scoliotic height loss and age-related or post-operative height gains [23]. Estimated standing height was used along with patient age at the time of testing to determine the predicted values based on reference data by the Global Lung Function Initiative [22].  $FEV_1$ , FVC and  $FEV_1/FVC$  are expressed as a percentage of their respective predicted values (% predicted).

#### 4.4.3 Spinal and Thoracic Parameters

Patients underwent a multidetector CT (64-MDCT Siemens Somatom Scanner) at 0.6 mm collimation, 1 mm slice thickness and 0.7 mm reconstruction increments. The main thoracic curve (MT) and T5-T12 thoracic kyphosis (TK) were measured on coronal and sagittal radiographs using the Cobb method. Following a search in the existing literature for CT-based thoracic deformity parameters, the following indices were measured at each vertebral level from T3-T12: spinal penetration index (SPi), endothoracic hump ratio (EHR), kyphosis-lordosis index (KLi), Haller index, chest flatness index (CFi), hemithoracic depth asymmetry index (HDAi), posterior hemithoracic symmetry ratio (PHSr), rib hump index (RHi), vertebral rotation ( $RA_{sag}$ ), thoracic rotation ( $RA_{ML}$ ), angle of trunk rotation ( $RA_{TR}$ ) and sternum-rib ratio (SRr). Vertebral translation, as described by Easwar et al. [56], was normalised by the transverse width of the thorax to give the vertebral translation ratio (VTr). Table 4.1 provides a summary of the parameter definitions and Figure 4.1 illustrates the landmarks used to calculate the deformity parameters. Landmarks were placed using Mimics v18.0 (Materialised N.V., Leuven, Belgium). For SPi, the area measurement tool in Mimics was used to measure the area of spinal intrusion ( $A_1$ ) and the thoracic area ( $A_2$ ).

#### 4.4.4 Statistical Methods

Deformity parameters measured from T3 to T12 were correlated with radiographic Cobb angles and lung function. Patients were segregated based on their Lenke sagittal modifier and differences between groups were established by applying the Kruskal-Wallis test followed by post-hoc Dunn's test. Pairwise  $t$ -test was conducted between pre- and post-operative results to study the effect of scoliosis correction. To determine the inter-relationships between deformity parameters, principle component analysis was applied to standardised deformity parameters measured at the apical level. The principle component scores were expressed as  $z$ -scores and correlated to deformity parameters, lung function and radiographic Cobb angles. The  $p$ -values from Pearson correlations, Kruskal-Wallis tests, Dunn's test and pairwise  $t$ -test were corrected for

Table 4.1: CT-based thoracic deformity parameters and their definitions. Landmark definitions can be found in Figure 4.1

Parameter	Definition	Landmarks	Ref.
Endothoracic hump ratio (EHR)	A line is draw through the posterior-most points of the hemithoraxes. A second and third line, parallel to the first, are drawn through the anterior point of the vertebral body and the inner surface of the sternum respectively. The perpendicular distances between the first and second line are divided by the distance between the second and third line.	$D_1/D_2$	[51]
Spinal penetration index (SPI)	The area occupied by the spine and enclosed by a line drawn from the most posterior point of each hemithorax divided by the thoracic area	$A_1/A_2$	[40]
Kyphosis-lordosis index (KLI)	Ratio of sagittal diameter to the transverse diameter of the thorax	$AG_y/JC_x$	[86]
Chest flatness index (CFI)	Ratio of twice the transverse diameter and the sum of both anterior-posterior hemithorax diameters	$\frac{2(JC_x)}{(HK_y + EB_y)}$	[93]
Haller index	Chest width measured along the frontal plane divided by the sternovertebral distance along the sagittal plane	$JC_x/AF_y$	[92]
Posterior hemithoracic symmetry ratio (PHSR)	A line intersecting the anterior point of each rib head is drawn. The distance from the spine at each rib head to the inner border of the hemithorax is measured. A ratio is derived by dividing the concave distance by the convex distance.	LM/PN	[44]
Rib hump index (RHi)	Anterior-posterior distance between the most posterior point of each hemithorax divided by the transverse distance between the anterior-most point of the foramen and the posterior-most point of the convex hemithorax	$HE_y/HG_x$	[35]
Vertebral rotation ( $RA_{sag}$ )	Angle between the sagittal plane and the vertebral body bisection line	$\tan^{-1}(GQ_x/GQ_y)$	[44]
Thoracic rotation ( $RA_{ML}$ )	Angle between the line which passes through the anterior most point of the vertebral body along the vertebral bisection line and the vertebral body bisection line	$\tan^{-1}\left(\frac{GQ_x}{GQ_y}\right) + \tan^{-1}\left(\frac{GA_x}{GA_y}\right)$	[44]
Angle of trunk rotation ( $RA_{TR}$ )	Maximum angle formed between the frontal plane and the rib deformity	$\tan^{-1}(HE_y/HE_x)$	[91]
Vertebral translation ratio (VTr)	Lateral distance between sternum and the center of the vertebral foreman normalised by the width of the thorax	$RA_x/JC_x$	[56]
Hemithoracic depth asymmetry index (HDAI)	Ratio of the maximum anterior-posterior hemithorax diameters subtracted from unity	$1 - BE_y/KH_y$	[93]
Sternum-rib ratio ( $SRr$ )	Convex-concave ratio of lateral distance from edge of chest to midpoint of sternum.	$JA_x/AC_x$	[91]

Distances are represented by pairs of landmarks and subscripts denote the axis along which they should be measured.



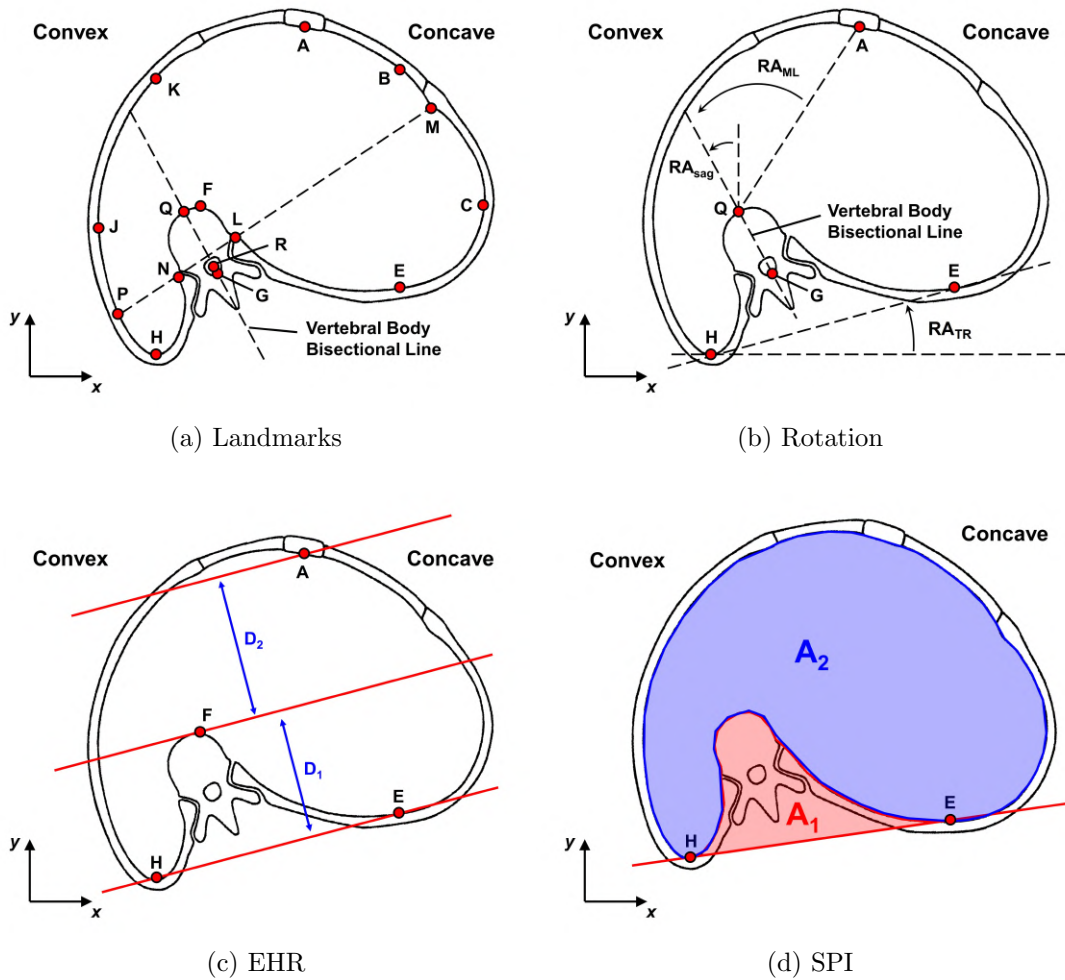


Figure 4.1: (a) Landmarks used in determining CT thoracic deformity parameters as defined in Table 4.1. Definition of anatomical landmarks are: A, center of internal sternal surface; B (K), interior surface of concave (convex) hemithorax directly anterior to E (H); C (J), lateral-most point on the internal surface of the concave (convex) hemithorax; E (H), posterior-most point on the internal surface of the concave (convex) hemithorax; F, anterior-most point on the vertebral body; G, posterior-most point of the vertebral foramen; L (N), most anterior point of the concave (convex) rib head; M (P), point on interior surface of concave (convex) hemithorax which passes through a line drawn through points N and L; Q, anterior point of the vertebral body on the vertebral bisecting line; R, centroid of the vertebral foramen. (b) Schematic showing rotation measurements: vertebral rotation ( $RA_{\text{sag}}$ ); thoracic rotation ( $RA_{\text{ML}}$ ); and angle of trunk rotation ( $RA_{\text{TR}}$ ). The distance and area measurements for the endotheracic hump ratio (EHR) and spinal penetration index (SPI) are shown in (c) and (d) respectively.

multiple comparisons ( $q$ -values) using the Benjamini and Hochberg method [52] with  $q$ -value threshold of 0.05 corresponding to a false discover rate of 5%.

To determine whether deformity parameters are better predictors of lung function than radiographic Cobb angles, pre-operative and post-operative change in lung function were regressed against radiographic Cobb angles and CT-based deformity parameters measured at each vertebral level. Only models with a maximum of 3 predictors were considered for practical reasons. To prevent over-fitting, 10 x 10-fold cross-validation was performed for variable selection and models with the lowest cross-validated root-mean-squared error (RMSE) were reported. Regression coefficients for individual predictors ( $b$ ), their standard errors ( $SE(b)$ ) and standardised coefficients ( $\beta$ ) along with the cross-validated coefficient of determination ( $r^2$ ) and RMSE are reported. All statistical analysis was implemented using the statistical software R (<http://www.R-project.org>).

## 4.5 Results

### 4.5.1 Sagittal thoracic modifier

Table 4.2 shows the pre-operative lung function, radiographic and CT-measured deformity parameter results segregated by the Lenke sagittal thoracic modifier. Age and the size of MT did not significantly differ between the groups although the hypokyphotic group had 5° and 10° smaller curves than the normo- and hyperkyphotic groups respectively. Hypokyphotic patients had significantly lower FEV<sub>1</sub> and FEV<sub>1</sub>/FVC than both normokyphotic and hyperkyphotic patients ( $q = 0.03$  and  $0.02$  respectively); and FVC was significantly lower in hypokyphotic patients than hyperkyphotic patients ( $q = 0.04$ ). Hypokyphotic patients had significant chest flattening, loss of thoracic depth and higher spinal intrusion (EHr, SPi, KLi, CFi and Haller index) when compared with normo- and hyperkyphotic patients. Conversely, PHSr was less severe in hypokyphosis than normo- and hyperkyphosis. There were no significant differences between the groups in other pre-operative CT deformity parameters such as the size of the rib hump or rotation.

### 4.5.2 Correlational analysis

MT did not correlate with TK ( $r = 0.17$ ,  $q = 0.28$ ), FEV<sub>1</sub> ( $r = -0.24$ ,  $q = 0.14$ ), FVC ( $r = -0.3$ ,  $q = 0.07$ ) or FEV<sub>1</sub>/FVC ( $r = 0.14$ ,  $q = 0.32$ ); however, TK significantly correlated with FEV<sub>1</sub>, FVC and FEV<sub>1</sub>/FVC ( $r = 0.48$ ,  $0.34$  and  $0.46$  respectively,  $q < 0.03$ ). Figure 4.3 displays the Pearson correlation coefficients between lung function, radiographic Cobb angles and CT deformity parameters measured from T3 to T12. FEV<sub>1</sub> was found to be significantly correlated to SPi (T4 to T12,  $r = -0.46$  to  $-0.63$ ), EHR (T5 to T12,  $r = -0.41$  to  $-0.61$ ), RA<sub>ML</sub> (T6 to T10,  $r = -0.36$  to  $0.56$ ), RHi (T7 to T12,  $r = -0.37$  to  $-0.51$ ), RA<sub>TR</sub> (T8 to T12,  $r = -0.31$  to  $-0.49$ ), RA<sub>sag</sub> (T8 and T9,  $r = -0.43$  and  $-0.33$  respectively) and the Haller index (T6 and T7,  $r = -0.37$ ). FVC significantly correlated with SPi (T4 to T12,  $r = -0.36$  to  $-0.59$ ), EHR (T6 to T12,  $r = -0.41$  to  $-0.58$ ), RA<sub>ML</sub> (T6 to T10,  $r = -0.41$  to  $-0.57$ ), RHi (T7 to T12,  $r = -0.38$  to  $-0.55$ ), RA<sub>TR</sub> (T8 to T12,  $r = -0.39$  to  $-0.53$ ) and RA<sub>sag</sub> (T7 to T9,  $r = -0.36$  to  $-0.47$ ). FEV<sub>1</sub>/FVC only correlated with PHSr measured at T9 ( $r = 0.42$ ,  $q = 0.01$ ). MT significantly correlated with RHi (T8 to T12,  $r = 0.43$  to  $0.72$ ), RA<sub>ML</sub> (T7 to T12,  $r = 0.43$  to  $0.68$ ), VTr (T7 to T12,  $r = 0.42$  to  $0.68$ ), RA<sub>sag</sub> (T8 to T12,  $r = 0.36$

to 0.68),  $RA_{TR}$  (T8 to T12,  $r = 0.36$  to 0.68),  $PHSr$  (T9 to T12,  $r = 0.49$  to 0.60),  $SPi$  (T11 and T12,  $r = 0.41$  and 0.51 respectively) and  $SRr$  at T12 ( $r = 0.42$ ). TK significantly correlated with  $EHR$  (T5 to T12,  $r = -0.39$  to  $-0.62$ ),  $KLi$  (T5 to T12,  $r = 0.36$  to 0.60),  $SPi$  (T4 to T11,  $r = -0.38$  to  $-0.57$ ), Haller index (T5 to T12,  $r = -0.36$  to  $-0.57$ ),  $CFi$  (T6 to T12,  $r = -0.38$  to  $-0.47$ ) and  $PHSr$  (T8 and T9,  $r = 0.37$  and 0.33 respectively).

### 4.5.3 Principle component analysis

Principle component analysis performed on CT deformity parameters measured at the apical level showed that 4 principle components were sufficient to explain 90.3% of the variation. Table 4.3 shows the proportion of variance explained by each principle component and the correlation between the principle component z-scores, lung function, Cobb angles and individual CT deformity parameters.  $PC_1$  explained 35.7% of the total variance and was associated with increasing scoliosis, loss of kyphosis, spinal intrusion, thoracic rotation and rib hump formation;  $PC_1$  scores correlated negatively with  $FEV_1$  and FVC.  $PC_2$  explained 32.6% of total variance and describes increasing scoliosis and kyphosis, hemithoracic width asymmetry and rib hump formation;  $PC_2$  scores correlated positively with  $FEV_1/FVC$ .  $PC_3$  explained 16.8% of total variance and is related with vertebral translation, lateral deviation of the sternum and chest asymmetry.  $PC_4$  explains only 5.2% of total variance and describes additional lateral deviation of the sternum. Examples of patients with high scores in some of the principle components can be found in Figure 4.2.

### 4.5.4 Post-operative changes

Table 4.4 shows the post-operative changes in Cobb angles and lung function. Approximately 50° of scoliosis was corrected across all three groups with no significant difference in the degree of scoliosis corrected or post-operative MT between the groups. Patients with hypokyphosis gained 15.3° in TK, patients with normokyphosis patients gained 4.9° whilst hyperkyphosis patients lost 15.1°.  $FEV_1$ , FVC and  $FEV_1/FVC$  increased by 19.6%, 17.3% and 5.6% respectively in hypokyphotic patients whilst normokyphotic patients gained 12.9% and 11.2% in  $FEV_1$  and FVC respectively. No significant change in lung function test results were observed in the hyperkyphotic group. A summary of post-operative changes in deformity parameters can be found in Table 4.7. Spinal intrusion decreased post-operatively with  $EHR$  and  $SPi$  decreasing by 9.6% and 3.4% respectively. Sternovertebral depth ( $KLi$  and Haller index) did not change significantly but chest flatness was reduced with  $CFi$  decreasing from 2.09 to 1.88. No significant changes in chest asymmetry were observed based on measures of  $HDAi$ ,  $PHSr$  and  $SRr$ . The size of the rib hump was halved with  $RHi$  decreasing from 91% to 44% and  $RA_{TR}$  decreasing from 16.1° to 8.6°. Although vertebral translation and thoracic rotation ( $RA_{ML}$ ) were reduced, no significant changes in axial vertebral rotation ( $RA_{sag}$ ) were observed.

### 4.5.5 Predictive Models

Multivariate regression models from 10 x 10-fold cross validation using radiographic and CT-based predictors are shown in Table 4.5 and 4.6 respectively. Pre-operative

FEV<sub>1</sub>, FVC and post-operative changes in FEV<sub>1</sub> and FVC were better predicted using CT-based measurements which had between 0.14 to 0.29 higher  $r^2$  values than models based on radiographic measurements. The radiographic model showed that for every 10° increase in MT and TK, FEV<sub>1</sub> would change by -4.1% and 4.1% respectively ( $r^2 = 0.303$ ); whilst FVC would change by -4.5% and 3.1% respectively ( $r^2 = 0.215$ ). For CT models, FEV<sub>1</sub> was best predicted using SPi, RA<sub>TR</sub> and HDAi ( $r^2 = 0.568$ ) whilst FVC was best predicted with SPi, RHi and HDAi measured at T8 ( $r^2 = 0.508$ ). Poor fits were observed for FEV<sub>1</sub>/FVC with the best radiographic model based on TK ( $r^2 = 0.197$ ) and the CT model based on SPi measured at T9 ( $r^2 = 0.068$ ). For the radiographic model, post-operative changes in FEV<sub>1</sub> and FVC were best predicted with pre-operative TK ( $r^2 = 0.330$  and  $0.228$  respectively) whilst changes in FEV<sub>1</sub>/FVC were best predicted with post-operative changes in TK ( $r^2 = 0.167$ ). For the CT-based models, post-operative changes in FEV<sub>1</sub> and FVC were best predicted with pre-operative EHr and PHSr measured at T8 ( $r^2 = 0.474$  and  $0.452$  respectively) whilst changes in FEV<sub>1</sub>/FVC were best predicted with PHSr measured at T9 ( $r^2 = 0.119$ ).

## 4.6 Discussion

Distortions to the thoracic cage have distinct patterns which follow the profile of the scoliotic spine. The correlational analysis supports previous studies showing the relationship between scoliosis, axial thoracic rotation and rib hump formation with regards to the coronal deformity and the association between kyphosis, thoracic sagittal flattening and spinal intrusion [55, 38, 35]. However, the lack of correlation between scoliosis and kyphosis suggests that the coronal and sagittal deformities are independent. Geyer and Le Merrer [97, 40] recognised the variable expression of thoracic sagittal depth in scoliosis. They differentiated between thoraxes where reductions in hemithoracic width on the convexity were compensated for by increased thoracic depth and those where thoracic volume losses were exacerbated via sagittal flattening. The principle component analysis provides a quantitative description of these variations and identified two non-correlated modalities (PC<sub>1</sub> and PC<sub>2</sub>) which describe the effects of lordoscoliosis and kyphoscoliosis on the chest wall deformity. Additional modes of variation describe the hemithoracic asymmetry, a concept which has typically been discussed within the pectus excavatum literature [94, 93]. Lateral displacement of the sternum towards the concavity and lowering of the convex ribs produces additional narrowing of the convex hemithorax resulting in asymmetry of the hemithoracic width and depth.

Lung function was found to be most impaired in hypokyphotic patients and expiratory volumes correlated negatively with the lordoscoliosis principle component (PC<sub>1</sub>). Lung function impairment in lordoscoliosis was recognised early on by Winter et al. who described severe respiratory compromise in patients with thoracic lordosis and scoliosis [98]. Loss of lung volume due to sagittal flattening of the thorax aggravates existing restrictive lung disease caused by the scoliosis. In addition to loss of thoracic volume, extrinsic compression of airways is likely to contribute to lung function impairment in lordoscoliosis. The SPi and EHr are deformity parameters which were proposed in the context of airway obstruction in scoliosis and showed strong correlations with FEV<sub>1</sub> and FVC. Their high correlation with PC<sub>1</sub> and presence as an explanatory variable in the multivariate regressions suggests that spinal intrusion resulting in extrinsic compression of airways plays a causative role in lung function impairment in lordosco-

Table 4.2: Summary of pre-operative lung function, radiographic and CT-measured deformity parameters

	Lenke Sagittal Thoracic Modifier				Kruskal-Wallis q-value
	Hypokyphosis (-) (n = 18)	Normokyphosis (N) (n = 21)	Hyperkyphosis (+) (n = 10)		
Age at PFT (years)	18.16 (7.56)	14.4 (1.74)	19.35 (13.69)	0.67	
FEV <sub>1</sub> (% predicted)	50.69 (14.25)	63.53 (12.03)	69.39 (15.14)	0.008 *†	
FVC (% predicted)	57.84 (15.49)	66.86 (13.31)	71.42 (15.05)	0.046 †	
FEV <sub>1</sub> /FVC (% predicted)	87.56 (9.5)	94.71 (5.7)	96.7 (6.22)	0.015 *†	
Main thoracic scoliosis (°)	70.96 (11.97)	75.89 (9.56)	81.47 (15.69)	0.133	
T5-T12 kyphosis (°)	1.92 (6.32)	22.86 (8.5)	51.5 (10.14)	< 0.001 *†*	
Endothoracic hump ratio (%)	52.82 (9.83)	44.71 (9.84)	40.37 (7.63)	0.004 *†	
Spinal penetration index (%)	17.52 (4.59)	13.89 (3.3)	11.68 (2.62)	0.002 *†	
Kyphosis-lordosis index (%)	40.03 (7.23)	47.7 (6.42)	52.3 (8.38)	0.002 *†	
Chest flatness index (-)	2.03 (0.19)	1.85 (0.2)	1.79 (0.18)	0.011 *†	
Haller index (-)	3.49 (0.75)	2.74 (0.44)	2.48 (0.73)	0.002 *†	
PHSr (-)	2.28 (0.66)	2.84 (0.66)	3.36 (1.06)	0.004 *†	
Rib hump index (%)	61.24 (34.81)	55.45 (33.92)	71.19 (51.99)	0.856	
Axial vertebral rotation (°)	20.41 (8.02)	21.38 (5.22)	25.22 (11.73)	0.856	
Thoracic rotation (°)	58.02 (15.66)	56.92 (10.46)	59.45 (17.29)	0.856	
Angle of trunk rotation (°)	12.39 (5.19)	11.42 (4.97)	14.31 (10.26)	0.856	
Vertebral translation ratio (%)	19.24 (6.43)	21.89 (6.4)	23.44 (8.07)	0.133	
HDAi (%)	-1.74 (8.8)	-2.26 (6.21)	-2.44 (14.41)	0.901	
Sternum-rib ratio (-)	1.24 (0.1)	1.32 (0.17)	1.3 (0.2)	0.454	

Values are mean (standard deviation)

Significant difference using post-hoc Dunn's test between: \*hypokyphosis (-) and normokyphosis (N); †hypokyphosis (-) and hyperkyphosis (+); \*normokyphosis (N) and hyperkyphosis (+) groups to  $q < 0.05$ .

Abbreviations: PFT, pulmonary function test; FEV<sub>1</sub>, forced expiratory volume in 1 second; FVC, forced vital capacity; PHSr, posterior hemithoracic symmetry ratio; HDAi, hemithoracic depth asymmetry index.

Table 4.3: Variance explained by principle component analysis and Pearson correlation coefficients between CT deformity principle component scores, lung function, Cobb angles and individual CT deformity parameters ( $n = 49$ ).

	PC <sub>1</sub>	PC <sub>2</sub>	PC <sub>3</sub>	PC <sub>4</sub>
Variance explained	35.7 %	32.6 %	16.8 %	5.2 %
Cumulative variance explained	35.7 %	68.3 %	85.1 %	90.3 %
FEV <sub>1</sub>	-0.64 ***	-0.01	0.03	0.09
FVC	-0.62 ***	-0.12	0.03	0.09
FEV <sub>1</sub> /FVC	-0.12	0.34 *	0.01	-0.01
Main thoracic scoliosis	0.48 **	0.69 ***	0.04	-0.09
T5-T12 kyphosis	-0.42 **	0.49 ***	0.07	0.01
Endothoracic hump ratio	0.88 ***	-0.35 *	0.04	-0.12
Spinal penetration index	0.82 ***	-0.35 *	-0.01	-0.24
Kyphosis-lordosis index	-0.61 ***	0.76 ***	-0.11	-0.09
Chest flatness index	0.59 ***	-0.63 ***	0.22	0.18
Haller index	0.57 ***	-0.78 ***	0.08	-0.03
PHSr	0.19	0.75 ***	0.44 **	-0.27
Rib hump index	0.71 ***	0.55 ***	-0.32	-0.01
Vertebral rotation	0.56 ***	0.65 ***	-0.25	-0.04
Thoracic rotation	0.81 ***	0.43 **	0.21	-0.09
Angle of trunk rotation	0.61 ***	0.55 ***	-0.47 **	0.12
Vertebral translation	0.44 **	0.57 ***	0.67 ***	0.01
HDAi	0.33 *	0.19	-0.79 ***	0.35 *
Sternum-rib ratio	0.19	0.38 *	0.66 ***	0.59 ***

Abbreviations: FEV<sub>1</sub>, forced expiratory volume in 1 second; FVC, forced vital capacity; PHSr, posterior hemithoracic symmetry ratio; HDAi, hemithoracic depth asymmetry index.

\*  $q < 0.05$ ; \*\*  $q < 0.01$ ; \*\*\*  $q < 0.001$

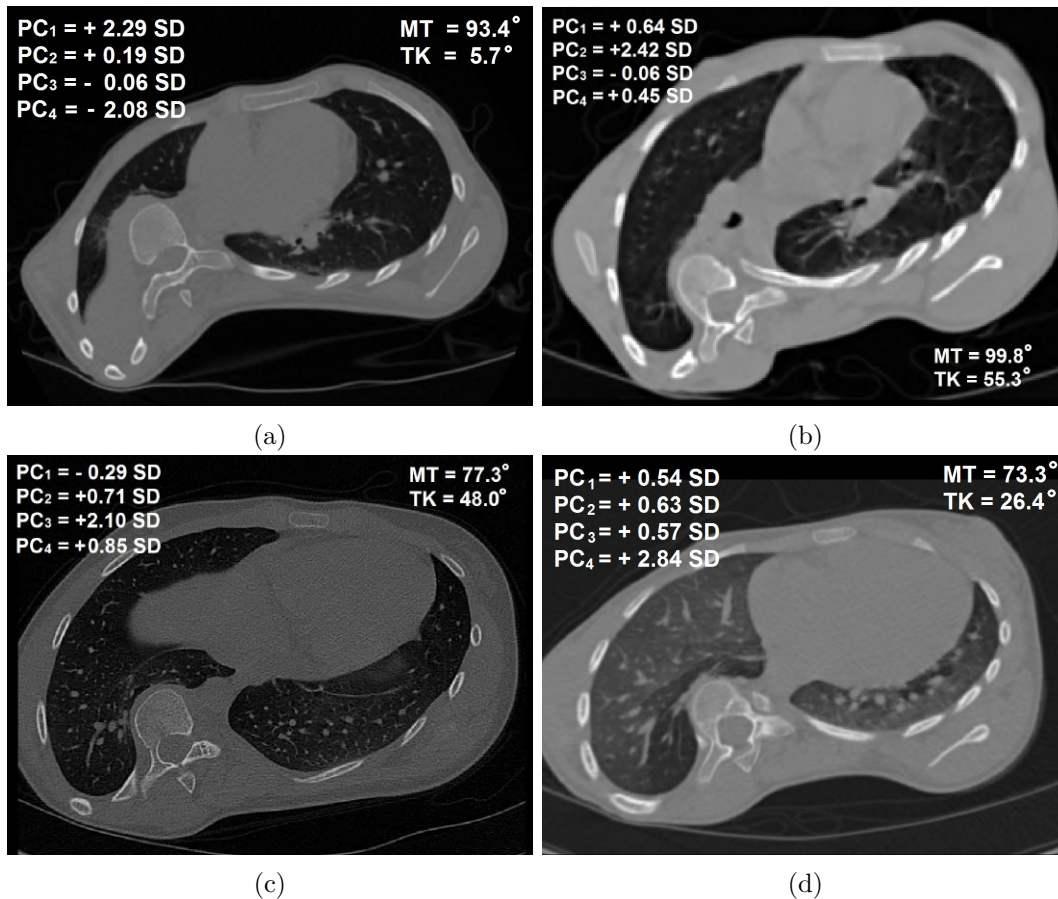
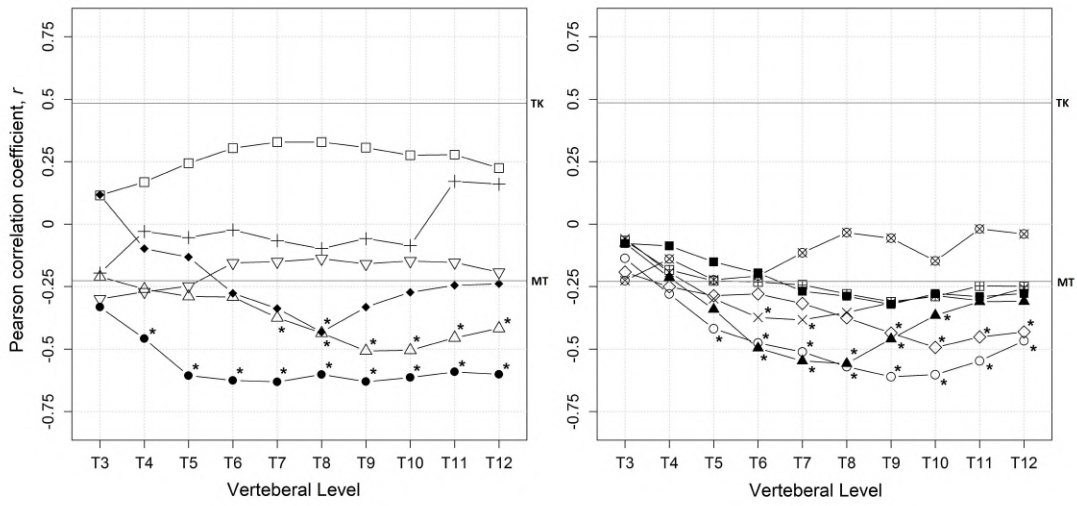
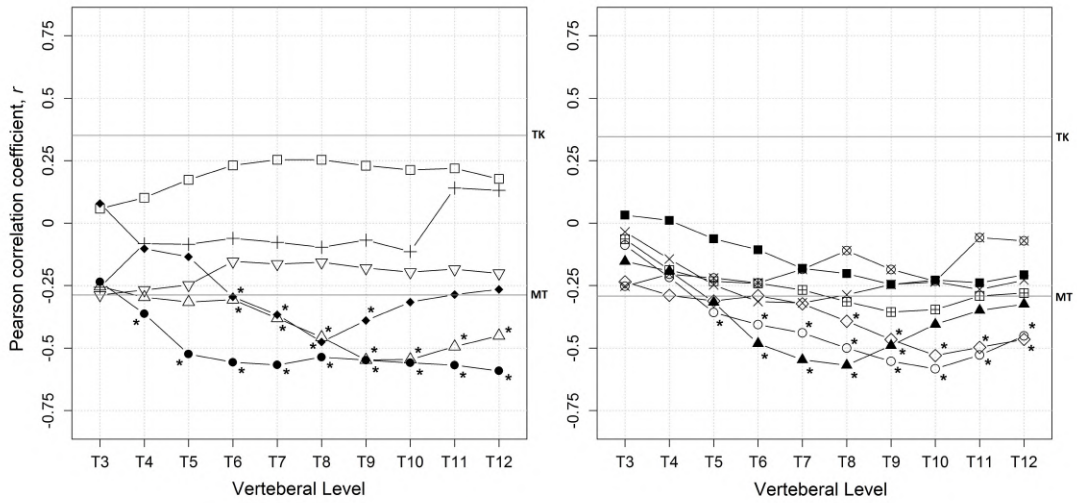


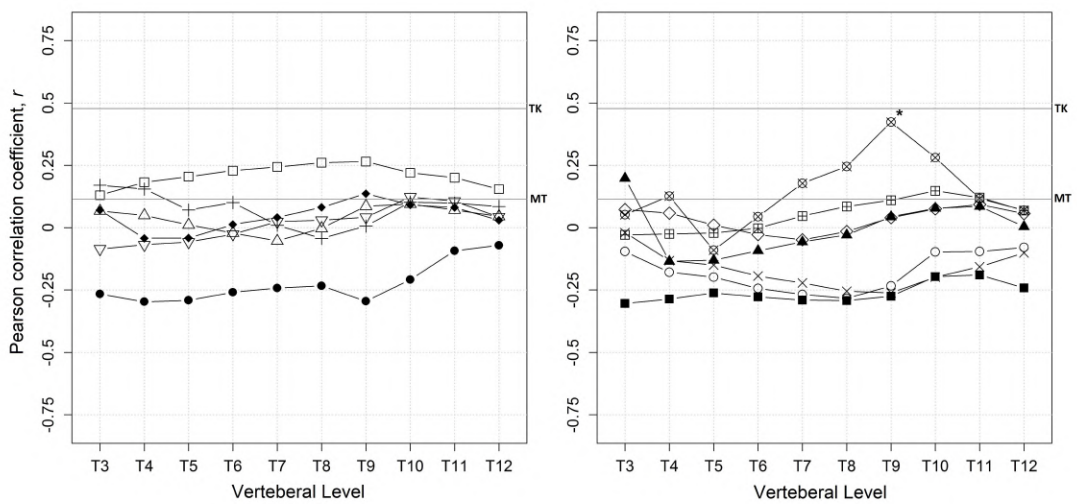
Figure 4.2: Examples of patients with high principle component z-scores for the (a) first (PC<sub>1</sub>), (b) second (PC<sub>2</sub>), (c) third (PC<sub>3</sub>) and (d) fourth (PC<sub>4</sub>) principle components. Increased PC<sub>1</sub> resembles the evolution of lordoscoliosis characterised by increase spinal intrusion, thoracic rotation and sagittal flattening. PC<sub>2</sub> represents a kyphoscoliosis component which manifests in the form of increased thoracic depth, vertebral rotation and hemithoracic width asymmetry. PC<sub>3</sub> signifies lateral shearing of the thorax categorised by increased lateral distance between the spine and sternum. PC<sub>4</sub> describes the degree of sternal misalignment from the midline.



(a) FEV<sub>1</sub> (% pred.)

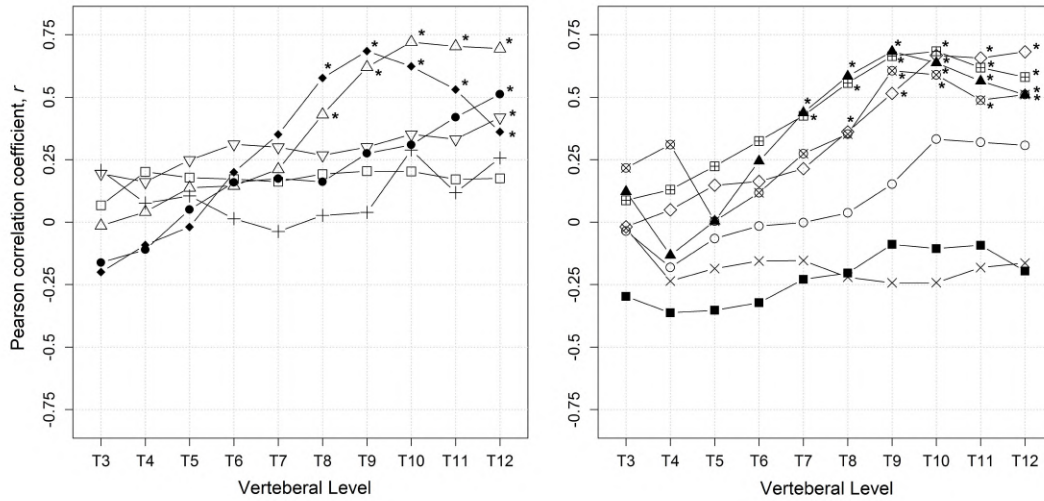


(b) FVC (% pred.)

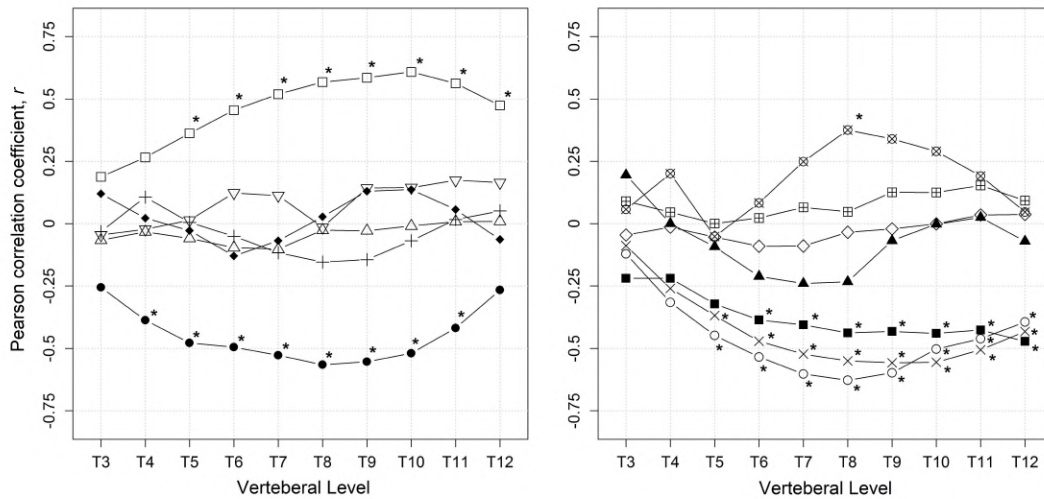


(c) FEV<sub>1</sub>/FVC (% pred.)





(d) Main thoracic Cobb (MT)



(e) T5-T12 kyphosis (TK)



Figure 4.3: Correlation coefficients of CT deformity parameters measured from T3 to T12 with (a) FEV<sub>1</sub>, (b) FVC, (c) FEV<sub>1</sub>, (d) main thoracic Cobb (MT) and (e) T5-T12 thoracic kyphosis (TK) ( $n = 49$ ). Abbreviations: KLi, kyphosis-lordosis index; EHR, endothoracic hump ratio; RA<sub>sag</sub>, axial vertebral rotation; VTr, vertebral translation ratio; RA<sub>TR</sub>, angle of trunk rotation; HDai, hemithoracic depth asymmetry index; SRr, sternum rib ratio; RA<sub>ML</sub>, thoracic rotation; SPi, spinal penetration index; RHi, rib hump index; PHSr, posterior hemithoracic symmetry ratio; Haller, Haller index; CFi, chest flatness index.

Table 4.4: Pre- and post-operative comparison of radiographic and pulmonary function test measurements

	Lenke Sagittal Thoracic Modifier			Kruskal-Wallis $q$ -value
	Hypokyphosis (-) ( $n = 15$ )	Normokyphosis (N) ( $n = 16$ )	Hyperkyphosis (+) ( $n = 9$ )	
MT pre-op (°)	70.1 (12.8)	75.9 (10.2)	80.4 (16.3)	0.096
MT post-op (°)	23.2 (13.4)	25.7 (9.1)	31.9 (8.1)	0.132
Change (°)	-46.9 (13.4)***	-50.2 (10.1)***	-48.5 (16.9)***	0.482
TK pre-op (°)	1.3 (6.8)	22.5 (8.4)	52.0 (10.6)	< 0.001 ††*
TK post-op (°)	16.6 (5.8)	27.3 (7.9)	36.9 (14.9)	< 0.001 ††
Change (°)	15.3 (8.4)***	4.9 (8.7)*	-15.1 (12.9)**	< 0.001 ††*
FEV <sub>1</sub> pre-op (% pred.)	51.5 (15.3)	62.4 (11.8)	69.0 (16.0)	0.017 †
FEV <sub>1</sub> post-op (% pred.)	71.1 (11.4)	75.3 (13.7)	74.3 (19.6)	0.575
Change (% pred.)	19.6 (12.4)***	12.9 (7.1)***	5.3 (9.8)	0.015 †
FVC pre-op (% pred.)	58.9 (16.6)	65.0 (13.6)	71.8 (15.9)	0.063
FVC post-op (% pred.)	76.2 (13.0)	76.3 (14.7)	75.9 (18.6)	0.978
Change (% pred.)	17.3 (13.0)***	11.2 (8.7)***	4.1 (10.0)	0.111
FEV <sub>1</sub> /FVC pre-op (% pred.)	87.4 (10.3)	95.7 (5.8)	95.7 (5.6)	0.026 †
FEV <sub>1</sub> /FVC post-op (% pred.)	93.1 (5.3)	98.2 (5.2)	97.2 (7.0)	0.06
Change (% pred.)	5.6 (6.6)**	2.4 (5.8)	1.6 (5.4)	0.22

Values are mean (standard deviation) Significant difference between pre- and post-operative values using pairwise  $t$ -test to: \*  $q < 0.05$ ; \*\*  $q < 0.01$ ; and  $q < 0.001$

Significant difference using post-hoc Dunn's test between: † hypokyphosis (-) and normokyphosis (N); ‡ hypokyphosis (-) and hyperkyphosis (+); \* normokyphosis (N) and hyperkyphosis (+) groups to  $q < 0.05$ .

Abbreviations: MT, main thoracic scoliosis curve; TK, T5-T12 kyphosis; FEV<sub>1</sub>, forced expiratory volume in 1 second; FVC, forced vital capacity.

Table 4.5: Multivariate regression results for the prediction of pre-operative ( $n = 49$ ) and post-operative changes ( $n = 40$ ) in lung function using radiographic parameters.

FEV <sub>1</sub>	Intercept	MT	TK	Model Statistics
$b$	82.19	-0.409	0.408	$r^2 = 0.303$
SE( $b$ )	11.40	0.152	0.094	SE = 12.7
$p$	< 0.001	0.010	< 0.001	-
$\beta$	-	-0.329	0.328	-
FVC	Intercept	MT	TK	Model Statistics
$b$	92.06	-0.453	0.310	$r^2 = 0.215$
SE( $b$ )	12.07	0.161	0.099	SE = 13.4
$p$	< 0.001	0.007	0.003	-
$\beta$	-	-0.366	0.250	-
FEV <sub>1</sub> /FVC	Intercept	TK	-	Model Statistics
$b$	88.47	0.191	-	$r^2 = 0.197$
SE( $b$ )	1.54	0.054	-	SE = 7.4
$p$	< 0.001	0.001	-	-
$\beta$	-	0.463	-	-
$\Delta$ FEV <sub>1</sub>	Intercept	TK	-	Model Statistics
$b$	20.77	-0.317	-	$r^2 = 0.330$
SE( $b$ )	2.05	0.070	-	SE = 9.1
$p$	< 0.001	< 0.001	-	-
$\beta$	-	-0.589	-	-
$\Delta$ FVC	Intercept	TK	-	Model Statistics
$b$	18.15	-0.281	-	$r^2 = 0.228$
SE( $b$ )	2.31	0.078	-	SE = 10.3
$p$	< 0.001	0.001	-	-
$\beta$	-	-0.497	-	-
$\Delta$ (FEV <sub>1</sub> /FVC)	Intercept	$\Delta$ TK	-	Model Statistics
$b$	2.77	0.181	-	$r^2 = 0.167$
SE( $b$ )	0.93	0.062	-	SE = 5.7
$p$	0.005	0.005	-	-
$\beta$	-	0.426	-	-

Abbreviations: MT, main thoracic scoliosis curve; TK, T5-T12 kyphosis; FEV<sub>1</sub>, forced expiratory volume in 1 second; FVC, forced vital capacity;  $r^2$ , coefficient of determination adjusted for multiple regressors; SE, standard error;  $b$  and  $\beta$ , unstandardised and standardised regression coefficients respectively.

Table 4.6: Multivariate regression results for the prediction of pre-operative ( $n = 49$ ) and post-operative changes ( $n = 40$ ) in lung function using CT thoracic deformity parameters.

FEV <sub>1</sub>	Intercept	SPi <sub>T8</sub>	RA <sub>TR,T8</sub>	HDAi <sub>T8</sub>	Model Statistics
$b$	107.15	-1.894	-1.605	0.497	$r^2 = 0.568$
SE( $b$ )	6.16	0.285	0.326	0.192	SE = 10.0
$p$	< 0.001	< 0.001	< 0.001	0.013	-
$\beta$	-	-0.632	-0.535	0.166	-
FVC	Intercept	SPi <sub>T8</sub>	RHi <sub>T8</sub>	HDAi <sub>T8</sub>	Model Statistics
$b$	105.29	-1.524	-0.333	0.436	$r^2 = 0.508$
SE( $b$ )	6.039	0.304	0.069	0.191	SE = 10.6
$p$	< 0.001	< 0.001	< 0.001	0.027	-
$\beta$	-	-0.510	-0.111	0.146	-
FEV <sub>1</sub> /FVC	Intercept	SPi <sub>T9</sub>	-	-	Model Statistics
$b$	101.23	-0.571	-	-	$r^2 = 0.068$
SE( $b$ )	4.28	0.270	-	-	SE = 7.9
$p$	< 0.001	0.04	-	-	-
$\beta$	-	-0.295	-	-	-
$\Delta$ FEV <sub>1</sub>	Intercept	EHr <sub>T8</sub>	PHSr <sub>T8</sub>	-	Model Statistics
$b$	-40.88	0.970	3.866	-	$r^2 = 0.474$
SE( $b$ )	10.33	0.158	1.877	-	SE = 8.1
$p$	< 0.001	< 0.001	0.046	-	-
$\beta$	-	0.775	0.260	-	-
$\Delta$ FVC	Intercept	EHr <sub>T8</sub>	PHSr <sub>T8</sub>	-	Model Statistics
$b$	-47.29	1.000	5.120	-	$r^2 = 0.452$
SE( $b$ )	11.06	0.170	2.008	-	SE = 8.6
$p$	< 0.001	< 0.001	0.015	-	-
$\beta$	-	0.762	0.064	-	-
$\Delta$ (FEV <sub>1</sub> /FVC)	Intercept	PHSr <sub>T9</sub>	-	-	Model Statistics
$b$	11.51	-3.114	-	-	$r^2 = 0.119$
SE( $b$ )	3.29	1.230	-	-	SE = 5.9
$p$	< 0.001	0.016	-	-	-
$\beta$	-	-0.376	-	-	-

Abbreviations: SPi, spinal penetration index; RA<sub>TR</sub>, angle of trunk rotation; HDAI, hemithoracic depth asymmetry index; RHi, rib hump index; PHSr, posterior hemithoracic symmetry ratio; EHR, endothoracic hump ratio; FEV<sub>1</sub>, forced expiratory volume in 1 second; FVC, forced vital capacity;  $r^2$ , coefficient of determination adjusted for multiple regressors; SE, standard error;  $b$  and  $\beta$ , unstandardised and standardised regression coefficients respectively. Subscripts denote vertebral level at which parameters are measured.

liosis. The kyphoscoliosis component is not significantly related to expiration volumes but the positive correlation between  $PC_2$  and  $FEV_1/FVC$  suggests that kyphoscoliosis results in less airway resistance relative to lordoscoliosis. These results suggest that both restrictive and obstructive lung disease play a role in lung function impairment in scoliosis and is dependent on the sagittal profile of the spine and thorax.

Despite having the most impaired lung function pre-operatively, hypokyphotic subjects gained the most lung function post-operatively such that their lung function was no different from normo- or hyperkyphotic patients. The post-operative results showed simultaneous correction of the coronal deformity and restoration of kyphosis which may have contributed to the improvement. Previous studies on the relationship between lung function and scoliosis correction tend not to segregate patients based on the sagittal profile. Demura et al. [99] ( $n = 154$ ) reported no change in  $FEV_1$  or FVC when correcting mean MT from  $20.4^\circ$  to  $17.6^\circ$  and TK from  $20.4^\circ$  to  $17.6^\circ$ . Kim et al [48] also reported no change in  $FEV_1$  or FVC when using thoracic pedicle screws ( $n = 53$ ); MT was corrected from  $62^\circ$  to  $17^\circ$  and TK decreased from  $24^\circ$  to  $15^\circ$ . Posterior approaches to scoliosis correction utilising pedicle screws have been known to generally decrease kyphosis [100, 101]. The pre-post comparison suggests that although lordoscoliotic subjects have diminished preoperative respiratory function relative to their normo- and hyperkyphotic counterparts, differences in respiratory function between sagittal profiles are resolved when natural kyphosis is restored postoperatively. de Jonge et al. [102] showed that the Cotrel-Dubouset technique could increase kyphosis by  $12^\circ$  in thoracic hypokyphosis, however only 55% were corrected back into the normal range of  $20^\circ$  to  $40^\circ$ . Suk et al. [103] demonstrated segmental pedicle screw fixation was more effective at restoring kyphosis in hypokyphosis patients than multiple-hook fixation with mean increases in kyphosis of  $19.2^\circ$  versus  $10.0^\circ$ . Targeting kyphosis restoration should be made in patients with hypokyphosis and severe scoliosis if post-operative improvements in respiratory function are to be achieved.

Although CT-based deformity parameters have a stronger relationship with lung function than radiographic Cobb angles, additional CT imaging may pose unnecessary radiation risk. Hoffman estimated that women with scoliosis undergoing multiple radiographic studies are already 82% more likely to be diagnosed with breast cancer than normal [104]; it is estimated that 22 radiographic examinations are already performed over the course of scoliosis management [87]. To reduce radiation dosage of CT imaging, modifications to thorax CT imaging has recently reduced radiation exposure to between 0.1 and 0.6 mSV without affecting image quality or clinical evaluation [105]. However, despite such advances in CT protocol, these dosages remain 2-3 times greater than traditional radiographs. With correlations between deformity parameters and lung function maximising at the apical level, focusing the region of interest to the level of the apical vertebrae may reduce radiation dose.

Alternatives to CT imaging which alleviate radiation exposure include magnetic resonance imaging (MRI) and newer biplanar radiographic imaging methods such as EOS (EOS Imaging, Paris France). Magnetic resonance imaging (MRI) has typically been used for preoperative planning and to investigate spinal cord abnormalities [106]. It allows the assessment of the whole spine and thorax without additional radiation exposure and has been shown to reveal 47% of bony anomalies omitted in radiographs in congenital spinal deformities [107]. EOS acquires biplanar radiographs of the whole body which can be combined to reconstruct the bony structures. It has been in clinical

use since 2000 and has reduced radiation exposure by approximately 6 times over conventional radiography. As a result of recent technical advances, a microdose protocol has been developed further reducing the radiation dose to patients [108]. Thoracic deformity parameters have already been derived from three-dimensional reconstructions of the thoracic cage using EOS imaging [38]. These modalities offer alternative methods with which thoracic deformity parameters can be measured with reduced radiation risk.

Both PFT results and Cobb angle measurements have been known to be position dependent. Previous studies have demonstrated differences in measurements across upright, prone and supine positions for Cobb angle, thoracic kyphosis and apical vertebral rotation [109, 110]. In the supine position, the scoliosis Cobb angle and vertebral rotation tend to be reduced by approximately 20% to 30% while kyphosis is reduced by an average of 8°. Posture dependent lung function changes have been demonstrated in scoliosis [111]. Holden et al. found that lordoscoliosis patients observed improved lung function when adopted a forward-flexed position [112]. Differences in position between CT deformity parameters and PFT results may understate the relationship between chest deformity and lung function. Supine PFTs could be performed in addition to the conventional upright position in order to take into account changes in pulmonary function due to position [113].

## 4.7 Conclusion

CT-based thoracic deformity parameters are better predictors of pulmonary function in AIS than conventional Cobb angle measurements as changes to the thoracic configuration are captured. Measures of spinal intrusion and the size of the rib hump featured as significant factors in impairing lung function. The analysis revealed that patients with lordoscoliosis have more impaired lung function than their normo- and hyperkyphotic counter parts which can be corrected post-operatively if natural kyphosis is restored. Thoracic deformity parameters are useful indices that can provide additional understanding of the mechanisms by which scoliosis impairs respiratory function.

Table 4.7: Pre- and post-operative comparison of apical CT-based deformity parameters ( $n = 9$ )

	Pre-operative	Post-operative	$q$ -value
Endothoracic hump ratio (%)	60.99 (12.92)	51.38 (11.19)	0.002 *
Spinal penetration index (%)	19.96 (5.96)	16.59 (4.33)	0.005 *
Kyphosis-lordosis index (%)	37.29 (8.15)	39.33 (7.41)	0.11
Chest flatness index (-)	2.09 (0.15)	1.88 (0.2)	0.007 *
Haller index (-)	3.79 (0.87)	3.52 (0.78)	0.18
PHSr (-)	2.95 (1.3)	2.37 (1.53)	0.17
Rib hump index (%)	90.71 (53.17)	44.03 (60.31)	0.023 *
Axial vertebral rotation (°)	25.98 (8.41)	19.49 (10.18)	0.13
Thoracic rotation (°)	72.55 (12.3)	53.43 (15.81)	0.002 *
Angle of trunk rotation (°)	16.12 (7.09)	8.59 (9.1)	0.010 *
Vertebral translation ratio (%)	25.43 (9.81)	16.08 (5.18)	0.005 *
HDAi (%)	-1.71 (6.23)	1.2 (16.98)	0.63
Sternum-rib ratio (-)	1.32 (0.22)	1.26 (0.17)	0.46

Values are mean (standard deviation)

\* Significant change between pre-operative and post-operative values using pairwise  $t$ -test to  $q < 0.05$ . Abbreviations: PHSr, posterior hemithoracic symmetry ratio; HDAi, hemithoracic depth asymmetry index.

## Chapter 5

# Airway Narrowing in Scoliosis

This chapter has been adapted from a prior publication [114].

### 5.1 Summary

In this chapter, the effect of scoliosis on the first three generations of the tracheo-bronchial tree is analysed as a contributing factor to lung function impairment. Pre-operative surgical planning computer tomography scans of patients with right-sided thoracic scoliosis were retrospectively analysed and compared with non-scoliotic controls. Three-dimensional models of spine and the airway tree were reconstructed. Based on thoracic sagittal profile, patients were divided into hypokyphosis, normokyphosis and hyperkyphosis groups. Lumen area of bronchi, bifurcation angles and minimum spine-airway distance were measured. Airway lumen areas were compared between controls and scoliosis patients and a correlation analysis was performed between spinal and thoracic deformity, lumen area and lung function. Loss of kyphosis led to proximity between the bronchus intermedius and spine. With decreasing kyphosis in right thoracic scoliosis, the spine intrudes into the thorax producing a rightward deflection of the bronchus intermedius and its branches around the spine causing airway narrowing. Patients with increased airway resistance should be investigated for extrinsic bronchial compression by the scoliosis. Kyphosis restoration is essential to relieve obstruction and improve post-operative lung function.

### 5.2 Introduction

Although restrictive lung defects are the most prevalent pulmonary function abnormalities in scoliosis, obstructive or mixed lung disease with moderate to severe air trapping has been reported in up to 46% of patients undergoing preoperative evaluation for scoliosis surgery [63]. McPhail et al. [24] reported a prevalence of obstructive lung disease in 39% of patients scheduled for operative correction of thoracic scoliosis. Airway obstruction in patients with scoliosis and loss of thoracic kyphosis is probably more common than generally appreciated; early diagnosis allows specific planning of the scoliosis correction to restore lung function and to reduce postoperative complications [115, 67]. There is a paucity of information on the relationship of the thoracic deformity produced by the scoliosis and the effect on the bronchial tree. Extrinsic compression



of the airway by the scoliosis causing loss of lung function may be wrongly attributed to progression of restrictive lung disease. The purpose of this study was to measure the 3D relationship of the spine and airways on CT reconstructions in patients with idiopathic right thoracic scoliosis. Subsequently, scoliosis, kyphosis and spine–airway proximity were correlated with airway narrowing and lung function to determine their relationships.

### 5.3 Literature Review

Several studies have associated the presence of bronchial obstruction with scoliosis. Al-kattan et al. [116] reported the presence of bronchial obstruction in three patients with congenital kyphoscoliosis and lung function impairment. Upon bronchoscopic examination, obstructed airways took on a slit-like appearance at the site of obstruction. The location of the obstruction was found to be the right bronchus intermedius, right middle lobe bronchus and left main bronchus in each of the cases. Stent placement resulted in immediate improvements in both respiratory function and symptoms. The spinal deformity of these patients was not described. Qiabi [65] presented a case of a 52-year-old female with obstruction of the right bronchus intermedius who had previously undergone surgical treatment for scoliosis at the age of 12. Despite the obstruction, pulmonary function tests and volume-flow loops were normal. She was treated with a metallic stent which resulted in re-expansion of the airway. There was no significant change in the post-stenting pulmonary function tests. ter Wee et al. [117] presented a 38-year-old male with severe lordoscoliosis who demonstrated compression of the right lower lobar bronchus and atelectasis in the right lower lobe. Alotaibi et al. [64] described a 13-year-old male with severe scoliosis who had previous spinal surgery. The pulmonary function test revealed a scooped flow-volume curve with a fixed moderate-to-severe obstruction pattern and evidence of air trapping. Bronchoscopy demonstrated a compression of the right lower and middle lobes with slit-like appearance.

Ventilation-perfusion scans have been used to assess the severity of airway obstruction in scoliosis and to demonstrate the effectiveness of surgical intervention. Bartlett et al. [67] described two cases of right-sided lordoscoliosis with obstruction of right sided airways. The first case was a 4-year-old female with a thoracic scoliosis of  $56^\circ$  and T5-T9 lordosis of  $34^\circ$ . Ventilation-perfusion studies showed that right lung perfusion was 27% of cardiac output. The lordoscoliosis was corrected via posterior spinal surgery with growing rod insertion and pedicle hooks and screws. Post-operative results showed coronal Cobb angle of  $20^\circ$  and thoracic lordosis of  $5^\circ$  whilst right lung ventilation and perfusion improved to 45% and 44% respectively. The second case was a 15-year-old female with thoracic scoliosis of  $75^\circ$  and a T5-T12 lordosis of  $26^\circ$ . CT of the chest revealed obstruction of the right main bronchus which was wrapped around the lordotic spine. The right lung contributed to 26% of total ventilation whilst right sided perfusion was 24% of cardiac output. Following scoliosis correction via posterior spinal fusion, coronal Cobb was reduced to  $21^\circ$  and thoracic kyphosis increased to  $21^\circ$ . Forced vital capacity improved from 28% to 54% predicted after surgery. Fujii et al. [68] described an 18-year-old male with severe scoliosis of  $91^\circ$  and hypokyphosis of  $6^\circ$  with obstruction of the right main bronchus. Ventilation-perfusion scans revealed decreased distribution to the right lung with 23% and 17% in the prone and supine position respectively. The patient underwent posterior correction surgery with pedicle

screws and a vertebral column resection was performed at T9 to decompress the right main bronchus.

Thoracic deformity parameters have been proposed to quantify features which contribute to extrinsic airway compression. Dubosset et al. [40] presented a case series of scoliosis patients with mixed etiologies and extrinsic airway compression. They introduced the concept of the endothoracic hump, the internal protrusion of the vertebral column into the thoracic cavity, as a key feature contributing to airway compression. To quantify the endothoracic hump on CT images, they proposed the spinal penetration index (SPI) which is a ratio of the area occupied by the intruding spine relative to the area of the thoracic cavity. Ito et al. [51] in a similar case series proposed the endothoracic hump ratio (EHR) which simplifies the SPI by using distance instead of area measurements. They reported post-operative improvements in lung function when EHR and SPI were reduced.

Distortions to the thoracic bone structure have been shown to change the internal configuration of the thorax leading to airway compromise. Andrews et al. [118] studied 2 cases of airway compression caused by spine and chest bone abnormalities (scoliosis, pectus excavatum and chest flatness). Donnelly and Bisset [119] reviewed radiographic and magnetic resonance images of six patients with mixed spine and thoracic deformities (pectus excavatum, scoliosis, thoracic asymmetry and abnormal ribs) and airway obstruction. Three patients had compression of the trachea whilst the remaining three had compression of the left main bronchus. Tatekawa et al. [120] reported the case of a 15-year-old female with tracheobronchomalacia and hypoxemia due to severe scoliosis. Upon radiological evaluation, they found that the cervical trachea was wedged between the innominate artery and the deformed spine as a result of the anteroposterior narrowing of the thorax.

Although many case reports on airway obstruction in scoliosis exist in the literature, no systematic study has been conducted into quantifying the degree of obstruction, identifying which airways are affected or analysing the relationship between lung function and airway narrowing in scoliosis.

## 5.4 Materials & Methods

### 5.4.1 Subjects

After institutional review board approval, a retrospective review of the surgeon's imaging database (Kodak Carestream PACS) was conducted to identify patients with idiopathic adolescent scoliosis with right-sided, thoracic curves and apical vertebra between the seventh and tenth thoracic vertebrae (T7-T10). Patients who underwent computed tomography (CT) scans for pre-operative planning with pulmonary function tests (PFTs) were included in the study. A total of 49 patients (36 female and 13 male) with an average age of 16.8 years (standard deviation [SD] = 7.8 years, range of 10.0 to 39.8 years) met the inclusion criteria. Of the 49 patients included, 36 had post-operative PFTs of which 9 also had post-operative CT scans. Patients were stratified into three groups based on their Lenke sagittal thoracic modifier. Group '-' included patients with hypokyphosis (T5-T12 kyphosis  $< 10^\circ$ ), Group 'N' included patients with normokyphosis ( $10^\circ$  to  $40^\circ$  inclusive) and Group '+' consisted of hyperkyphosis patients ( $> 40^\circ$ ). Fifteen non-scoliotic controls were obtained from normal oncology staging CT

examinations. Patients underwent a multidetector CT (64-MDCT Siemens Somatom Scanner) at 0.6 mm collimation, 1 mm slice thickness and 0.7 mm reconstruction increments. Control CT scans were obtained as part of routine clinical care and scoliotic CT scans as part of preoperative planning.

#### 5.4.2 Anatomical Variables

**Image Segmentation** CT scans were imported into Mimics v18.0 (Materialise N.V., Leuven, Belgium) in DICOM format. The spinal column from vertebrae T1 to T12 was isolated via Hounsfield thresholding (above 225 HU) and the masks of individual vertebrae manually segmented. The airways were segmented via a previously validated semiautomatic region growing method (-1024 to -750 HU) as part of the Pulmonary Module in Mimics [121]. Missing airways or leakages into the parenchyma were manually removed. Three-dimensional models were created by wrapping and smoothing the masks in 3-matic v10.0 (Materialise N.V., Leuven, Belgium).

**CT Deformity Parameters** A plane of best fit was constructed for the superior and inferior endplates of each vertebrae (Figure 5.1a) and the normal vector calculated. For a given pair of vertebrae, the coronal and sagittal Cobb angles were determined by calculating the angle between the superior and inferior vectors projected onto the coronal and sagittal planes respectively. The main thoracic Cobb angle (MT) was defined as the maximum coronal Cobb angle and the thoracic kyphosis (TK) Cobb angle was measured between vertebrae T5 and T12. The SPI [40] and rib hump index (RHI) [86] were also measured at the apical level (see Figure 4.1 and Table 4.1 for landmark definitions).

**Airway Parameters** A skeleton centreline was generated from the three-dimensional airway model (Figure 5.1b). Airway segments were truncated along a surface perpendicular to the centreline and the volume and length were documented for each airway segment. The average lumen area was calculated by dividing the lumen volume by the segment length. Airway trajectories were calculated from proximal and distal bifurcation points of each airway. The bifurcation angles between daughter branches were determined via the rearrangement of the dot product from the vectors of the daughter branches. Airway trajectories were also measured relative to the axial, coronal and sagittal planes.

**Region of Interest** The following airways were studied and shown in Figure 5.2: trachea, right main bronchus (RMB), right upper lobe bronchus (RUL), bronchus intermedius (BI), middle lobe bronchus (RB4+5), right lower lobe superior segmental bronchus (RB6), right lower lobe bronchus (RLL7), left main bronchus (LMB), left upper lobe bronchus (LUL), left apicoposterior and anterior segmental bronchus (LB1+2+3), left lingula bronchus (LB4+5), superior segment of the left lower lobe (LB6) and left lower lobe bronchus (LLB).

**Spine-Airway Distance** The distance from the surface of the airway lumen to the spine was computed for the whole airway tree and the minimum airway-spine distance and the corresponding vertebra was documented for each airway segment.

**Normalisation** Intersubject variability was accounted for by normalising airway lumen areas with the trachea lumen area measured at the T2 level. The spine-airway distance was normalised by the T1-T12 spine length which was determined by summing the distance between vertebrae centroids from T1 to T12. The mean trachea lumen area was  $148 \pm 48 \text{ mm}^2$  and  $162 \pm 49 \text{ mm}^2$  for control and scoliotic subjects respectively. The mean T1-T12 spine length was  $235 \pm 31 \text{ mm}$  and  $243 \pm 26 \text{ mm}$  for control and scoliotic subjects respectively.

### 5.4.3 Lung Function Data

PFTs were conducted via forced manoeuvres in accordance with the joint American Thoracic Society and European Respiratory Society standards [50]. Forced expiration in 1 second ( $\text{FEV}_1$ ) and forced vital capacity (FVC) were measured (Jaeger Master-Screen PFT pro) along with armspan. In calculating lung function predicted values, arm span was used to estimate standing height to correct for scoliotic height loss and age-related or post-operative height gains [23]. Estimated standing height was used along with patient age at time of testing to determine the predicted values based on reference data by the Global Lung Function Initiative [22].  $\text{FEV}_1$ , FVC and  $\text{FEV}_1/\text{FVC}$  are expressed as a percentage of their respective predicted values (% predicted).

### 5.4.4 Statistics

The nonparametric one-way ANOVA by ranks (Kruskal-Wallis) test followed by post hoc pairwise multiple comparisons Dunn test were performed to determine whether airway and deformity characteristics differed between groups. Pearson correlations coefficients were determined between airway, spinal and PFT variables. To study the effect of scoliosis correction on airway morphology, pairwise  $t$ -test was conducted between pre- and post-operative results. The  $p$ -values from Pearson correlations, Kruskal-Wallis tests, Dunn's post-hoc test and pairwise  $t$ -test were corrected for multiple comparisons ( $q$ -values) using the method proposed by Benjamini and Hochberg [52] with a threshold of 0.05 corresponding to a false discover rate of 5%. All statistical analysis was generated using the software R (<http://www.R-project.org>).

## 5.5 Results

### 5.5.1 Standing and supine Cobb angles

Supine CT measured MT and TK gave Pearson correlation coefficients of 0.75 and 0.81 respectively when compared to their radiographic standing equivalents ( $q < 0.001$ ). Scoliosis was reduced by  $12.9^\circ$ ,  $12.0^\circ$  and  $9.28^\circ$  from standing to supine whilst kyphosis decreased by  $1.4^\circ$ ,  $7.9^\circ$  and  $22.3^\circ$  for hypokyphosis, normokyphosis and hyperkyphosis groups respectively.

### 5.5.2 Airway-Spine Proximity

Figure 5.3 shows the minimum airway-spine distance throughout the airway tree for representative subjects from each group. Both hypokyphosis and normokyphosis subjects showed increased airway-spine proximity for RMB, RUL, BI, RB4+5, RB6 and

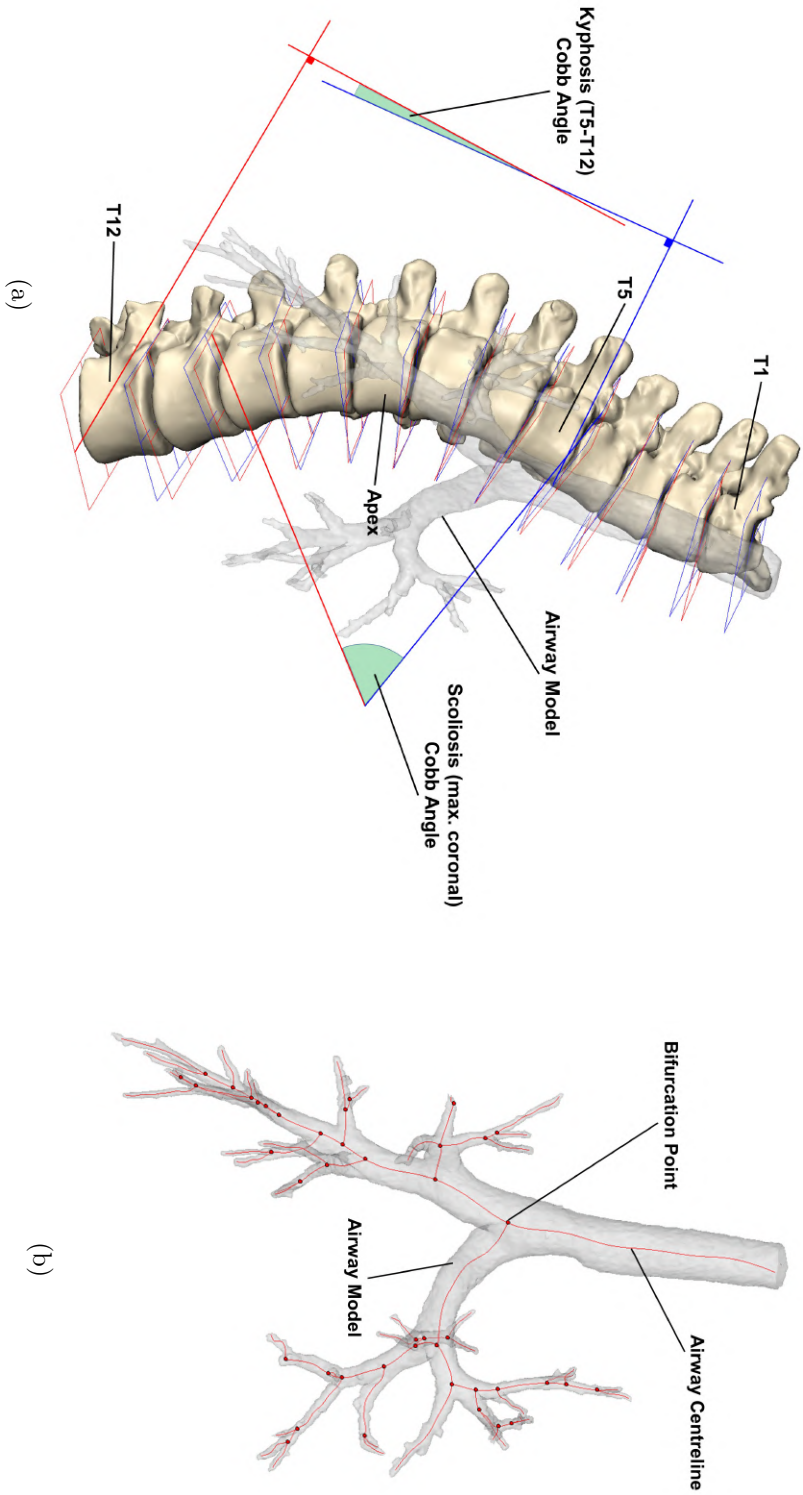


Figure 5.1: Reconstructions from CT segmentation. (a) Reconstructed spinal column from CT segmentation. Planes of best fit were fitted onto the superior (blue) and inferior (red) endplates. The coronal and sagittal Cobb angles were computed from the normal vectors of the endplate planes. (b) Reconstructed airway lumen with centerline and bifurcation points. Bifurcation points were used to estimate the trajectory of each airway segment.

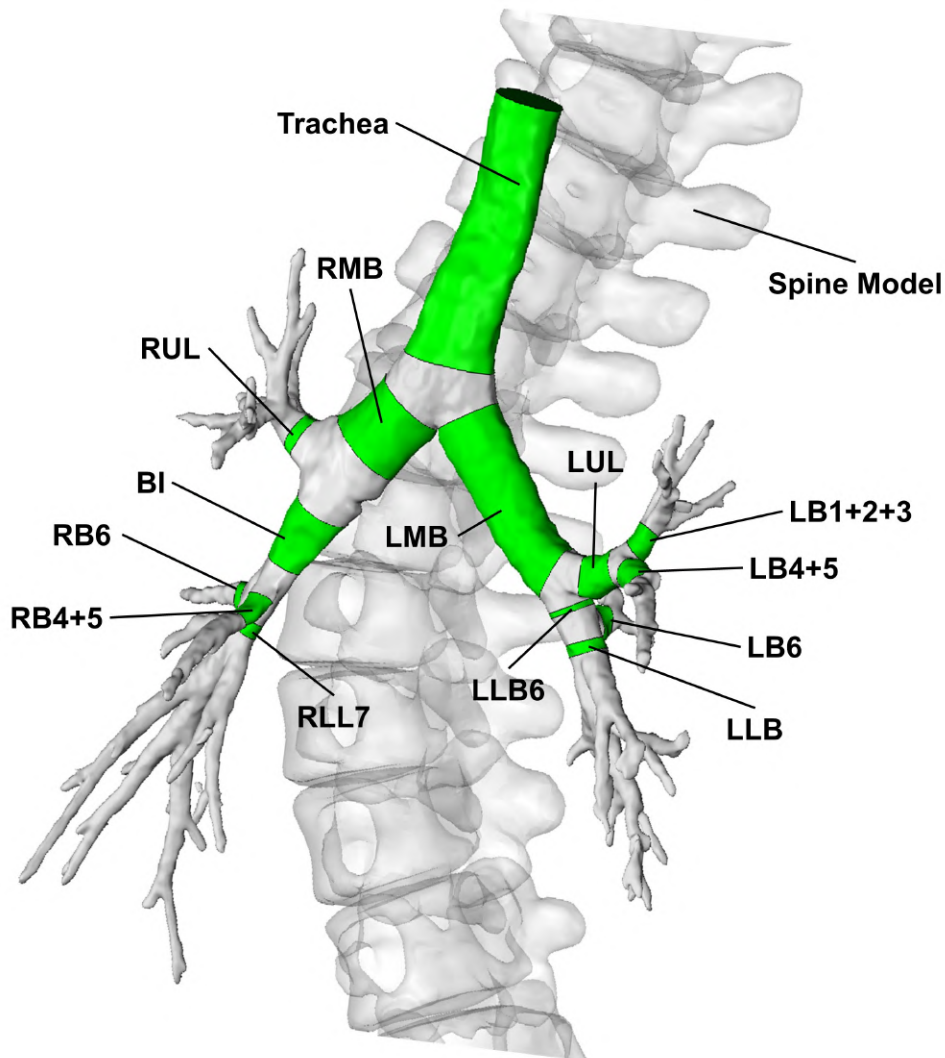


Figure 5.2: Segmented airway model with regions of interest highlighted in green. Abbreviations: RMB, right main bronchus; RUL, right upper lobe bronchus; BI, bronchus intermedius; RB4+5, right middle lobe bronchus; RLL, right lower lobe bronchus; RB6, right superior segmental bronchus; RLL7, right lower lobe bronchus; LMB, left main bronchus; LUL, left upper lobe bronchus; LB1+2+3, left apicoposterior and anterior segmental bronchus; LB4+5, left lingula bronchus; LB6, superior segment of the left lower lobe; LLB, left lower lobe bronchus.

Table 5.1: Summary of pre-operative lung function, radiographic and CT-measured deformity parameters

	Controls ( <i>n</i> = 18)	Hypokyphosis (-) ( <i>n</i> = 18)	Normokyphosis (N) ( <i>n</i> = 21)	Hyperkyphosis (+) ( <i>n</i> = 10)	Kruskal-Wallis <i>q</i> -value
Age at PFT (years)	16.45 (4.77)	18.16 (7.56)	14.4 (1.74)	19.35 (13.69)	0.478
Radiographic MT (°)	-	70.96 (11.97)	75.89 (9.56)	81.47 (15.69)	0.088
CT measured MT (°)	5.35 (4.37)	57.85 (14.77)	63.86 (9.45)	72.2 (15.13)	< 0.001 **◇
Radiographic TK (°)	-	1.92 (6.32)	22.86 (8.5)	51.5 (10.14)	< 0.001 †‡⊕
CT measured TK (°)	20.38 (7.7)	0.51 (13.21)	14.94 (8.3)	28.69 (11.87)	< 0.001 * †‡
Spinal penetration index (%)	7.44 (1.02)	17.52 (4.59)	13.89 (3.3)	11.68 (2.62)	< 0.001 **◇†
Rib hump index (%)	1.31 (8.3)	61.24 (34.81)	55.45 (33.92)	71.19 (51.99)	< 0.001 **◇
FEV <sub>1</sub> (% predicted)	-	50.69 (14.25)	63.53 (12.03)	69.39 (15.14)	0.005 †‡
FVC (% predicted)	-	57.84 (15.49)	66.86 (13.31)	71.42 (15.05)	0.03
FEV <sub>1</sub> /FVC (% predicted)	-	87.56 (9.5)	94.71 (5.7)	96.7 (6.22)	0.01 †‡

Significant difference using post-hoc Dunn's test between: \* controls and hypokyphosis (-); \* controls and normokyphosis (N); ◇ controls and hyperkyphosis (+); † hypokyphosis (-) and normokyphosis (N); ‡ hypokyphosis (-) and hyperkyphosis (+); ⊕ normokyphosis (N) and hyperkyphosis (+) groups to  $q < 0.05$ .  
 Abbreviations: PFT, pulmonary function test; MT, main thoracic curve; TK, T5-T12 thoracic kyphosis; FEV<sub>1</sub>, forced expiratory volume in 1 second; FVC, forced vital capacity.

RLL7 when compared to controls ( $q < 0.05$ ). Reduced spine-airway distance occurs in the region of the BI and its bifurcation which is more pronounced in the hypokyphotic subjects. A mean reduction of 87%, 62% and 4% in distance was observed for BI in hypokyphotic, normokyphotic and hyperkyphotic groups respectively. When comparing the airway and spine landmarks, it was found that airway bifurcation points in scoliotic patients were  $0.65 \pm 0.45$  vertebral bodies lower than in controls. In patients with scoliosis the bifurcation of RMB, BI and RLL were at the level of vertebral bodies T6, T7 and T7/8 disk respectively. Airway lumen area was positively correlated with airway-spine distance for RMB, BI, RB4+5, RB6 and RLL7 ( $r = 0.46, 0.62, 0.51, 0.64, 0.65$  respectively;  $q < 0.05$ ).

### 5.5.3 Lumen area

Normalised lumen areas are displayed in Figure 5.4. The majority of differences appeared in right sided airways with high reductions in airways surrounding the BI trifurcation while left sided airways were not significantly affected other than LMB in the hypokyphosis group. The lumen of BI was reduced by 45% and 23% in hypokyphosis and normokyphosis relative to the control group whilst hyperkyphotic subjects did not appear to be significantly affected. Significant reductions in RMB, RB4+5, RLL7 were also observed when comparing hypokyphotic and normokyphotic patients with controls. RB6 was reduced by approximately 40-60% across all scoliotic groups ( $q < 0.005$ ).

Pearson correlations between lumen area, deformity parameters and lung function are shown in Table 5.2. SPI showed the strong relationships with airway narrowing and correlated negatively with right-sided airways and LMB ( $r = -0.32$  to  $-0.63$ ). TK significantly correlated positively with right-sided and the trachea ( $r = 0.25$  to  $0.53$ ). MT correlated negatively with right-sided airways (in particular RB6 and RLL) and LMB. RHI correlated negatively with right-sided airways ( $r = -0.29$  to  $-0.56$ ) other than RB4+5.

Lumen area of the trachea and right-sided airways were found to correlate positively with FEV<sub>1</sub> and FVC (% predicted,  $r = 0.27$  to  $0.66$ ) with RMB and airways surrounding the BI bifurcation showing the strongest relationships. FEV<sub>1</sub>/FVC correlated positively with lumen areas of the trachea, RMB, RUL, BI, RB6, RLL7 and LUL ( $r = 0.3$  to  $0.43$ ).

### 5.5.4 Bifurcation Angles and Airway Trajectories

Bifurcation angles were found to be significantly reduced between the daughter branches of BI (namely RB4+5, RB6 and RLL7) for hypokyphotic and normokyphotic subjects. Narrowing of BI, RB6 and RLL7 correlated with the narrowing of trifurcation angles of the BI ( $r = 0.55$  to  $0.68$ ,  $q < 0.001$ ). Differences in airway trajectories were present with RB6 being rotated towards the right in the axial plane by  $22^\circ \pm 13^\circ$  in scoliotic subjects ( $q = 0.03$ ). In the coronal plane, significant differences were measured in BI ( $q < 0.001$ ) and RLL7 ( $q < 0.001$ ) between groups. BI was more horizontal in the coronal plane by  $14^\circ$ ,  $10^\circ$  and  $8^\circ$  in hypokyphosis, normokyphosis and hyperkyphosis respectively from a control average of  $156^\circ \pm 4^\circ$ . As BI, RLL7 was elevated by a mean of  $16.6^\circ \pm 4^\circ$  in scoliotic subjects when compared to the control mean of  $148^\circ \pm 8^\circ$ . In the sagittal plane, RB4+5 was angled inferior by  $27^\circ$ ,  $10^\circ$  and  $9^\circ$  from the control mean of  $119^\circ \pm 6^\circ$  in hypokyphosis, normokyphosis and hyperkyphosis respectively ( $q = 0.01$ ).



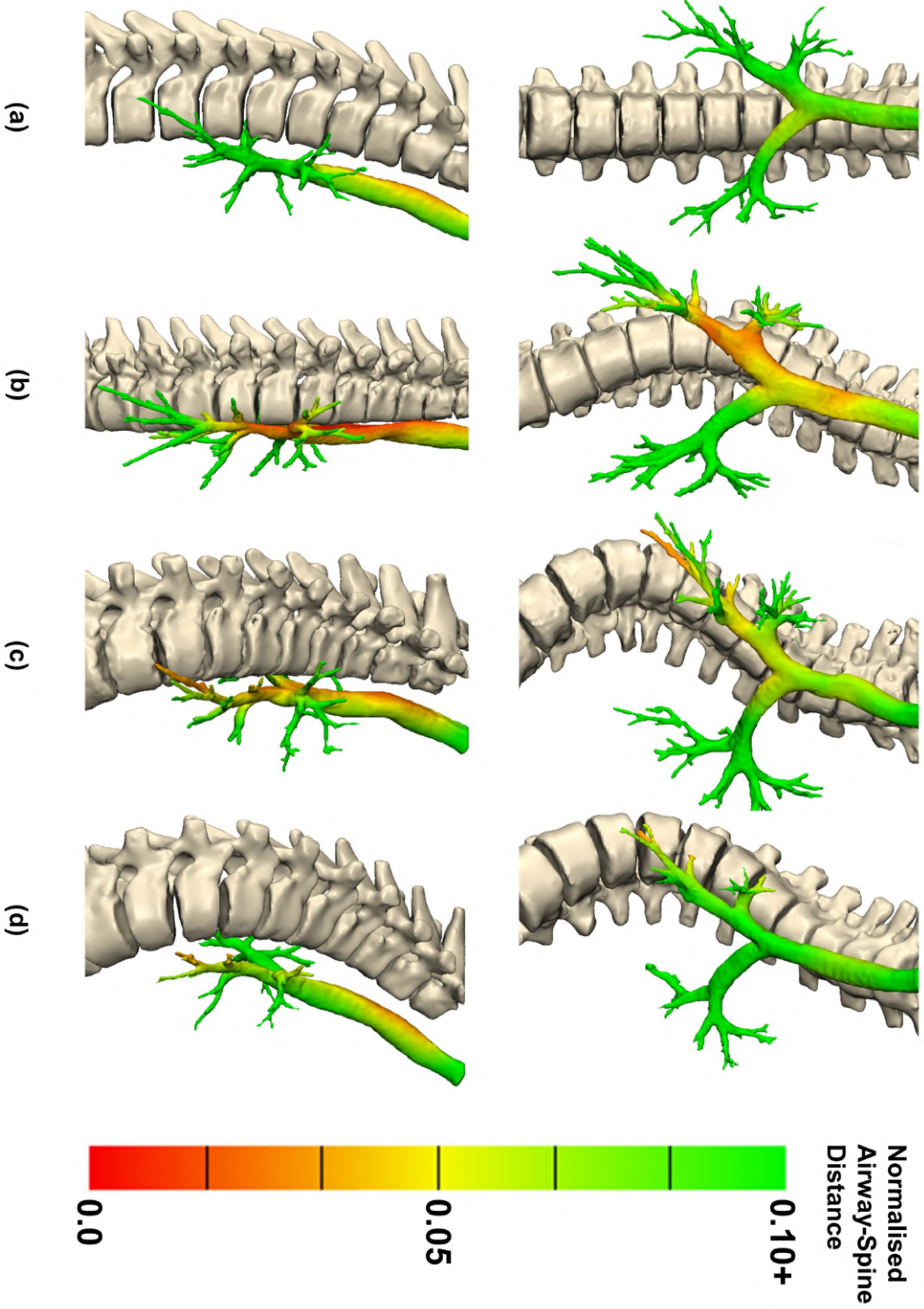


Figure 5.3: Normalised airway-spine minimum distances for representative subjects from (a) controls, (b) hypokyphosis (−), (c) normokyphosis (N) and (d) hyperkyphosis (+). Regions of red represent close proximity whilst green regions represent increased distance between spine and airway. The top row displays the coronal view anterior to the subject and the bottom row displays the sagittal view right of the subject.

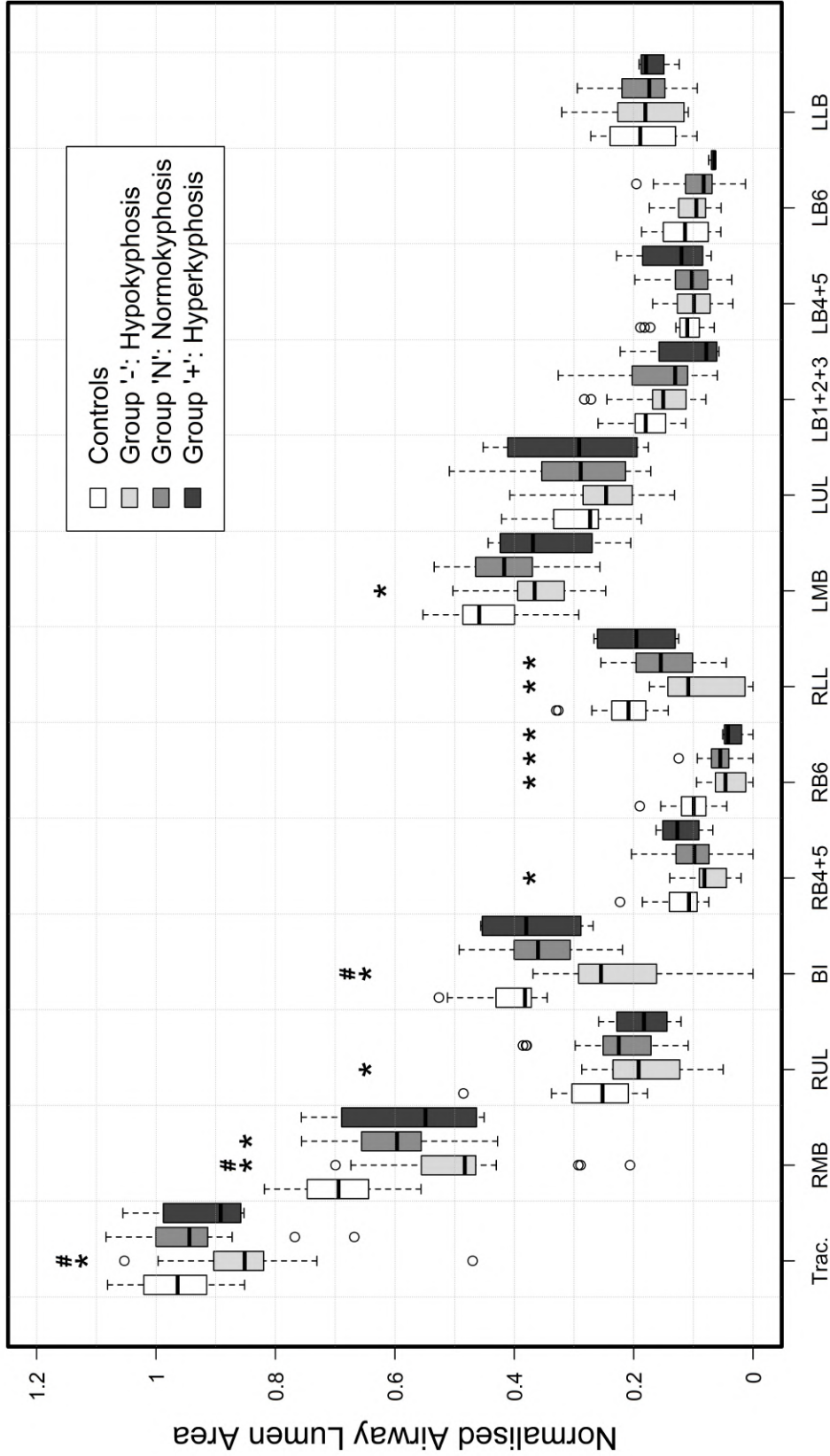


Figure 5.4: Box-and-whisker plot of normalised lumen area for each group. Boxes delineate the first and third quartiles with the median shown as a black bar. Whiskers show the minimum and maximum of the normal range. Outliers are defined as 1.5 times the interquartile range and are plotted as points. Airway lumen areas are expressed as a fraction of the Trachea lumen area measured at the T2 level. \* Significantly different when compared with Controls to  $q < 0.05$ . # Significantly different when compared with Group ‘N’ to  $q < 0.05$ .

Table 5.2: Pearson correlations between normalised airway lumen area, CT measured Cobb angles, deformity parameters and lung function

Airway	MT	TK	SPI	RHI	FEV <sub>1</sub>	FVC	FEV <sub>1</sub> /FVC
Trachea	-0.16	0.40 *	-0.43 *	-0.12	0.34 *	0.28 *	0.36 *
RMB	-0.44 *	0.38 *	-0.57 *	-0.40 *	0.61 *	0.56 *	0.43 *
RUL	-0.33 *	0.26 *	-0.37 *	-0.34 *	0.40 *	0.36 *	0.37 *
BI	-0.29 *	0.53 *	-0.63 *	-0.29 *	0.60 *	0.55 *	0.42 *
RB4+5	-0.28 *	0.32 *	-0.33 *	-0.14	0.38 *	0.36 *	0.24
RB6	-0.65 *	0.25 *	-0.51 *	-0.56 *	0.63 *	0.60 *	0.31 *
RLL7	-0.56 *	0.47 *	-0.64 *	-0.55 *	0.66 *	0.62 *	0.39 *
LMB	-0.26 *	0.18	-0.32 *	-0.18	0.30 *	0.27 *	0.20
LUL	-0.07	0.22	-0.10	-0.08	0.15	0.09	0.30 *
LB1+2+3	-0.07	-0.11	0.09	0.04	0.10	0.08	0.18
LB4+5	-0.08	0.24	-0.19	-0.11	0.18	0.13	0.26
LB6	-0.22	-0.06	-0.05	-0.21	0.19	0.19	0.10
LLB	-0.08	0.07	0.06	-0.01	0.04	-0.01	0.26

\* Significant Pearson correlation to  $q < 0.05$ . Airway lumen are expressed as a fraction of the trachea lumen area measured at the T2 level. Lung function data are expressed as a percentage of their predicted values.

Abbreviations: MT, main thoracic curve; TK, T5-T12 thoracic kyphosis; SPI, spinal penetarion index; RHI, rib hump index; FEV<sub>1</sub>, forced expiratory volume in 1 second; FVC, forced vital capacity. Refer to Figure 5.2 for definition of airway segments.

### 5.5.5 Post-operative Changes

The 9 patients with post-operative data consisted of 7 hypokyphosis, 1 normokyphosis and 1 hyperkyphosis. Table 5.3 shows the changes in deformity parameters, lung function and airway areas as a result of surgery. Radiographic MT was corrected from  $79.1^\circ$  to  $25.1^\circ$  ( $q < 0.001$ ) and TK increased from  $10.2^\circ$  to  $20.3^\circ$  ( $q = 0.09$ ). Mean SPI was reduced from 20.0% to 16.6% ( $q = 0.005$ ) whilst RHI decreased from 90.7% to 44.0% ( $q = 0.03$ ). Expiratory volumes increased with FEV<sub>1</sub> increasing from 40.8% to 67.8% ( $q = 0.001$ ) and FVC increasing from 44.5% to 72.1% of predicted values ( $q < 0.001$ ). Changes in the FEV<sub>1</sub>/FVC ratio were not significant (92.7% to 94.2% predicted,  $q = 0.53$ ). Post-operative increases in lumen area were observed for RMB, RML, RB6 and RLL ( $q < 0.05$ ).

## 5.6 Discussion

The results demonstrate that close proximity between spine and airway results in significant airway narrowing. Distal to the RMB, loss of kyphosis was a strong predictor of airway stenosis. The BI was reduced by 45% and 23% in hypokyphosis and normokyphosis respectively but not significantly affected in hyperkyphosis. Patients with hypokyphosis had on average a 42%, 62% and 66% reduction of normalised airway lumen area in RB4+5, RB6 and RLL7 respectively. Interestingly, RB6 was significantly narrowed in all scoliotic groups when compared to controls. This is likely to be due to the posterior trajectory of RB6 whose position coincides with the laterally displaced spine. Previous reports have shown that bronchial compression occurs on the convex side of a right thoracic scoliosis causing ventilation defects in the middle and/or right lower lobe. Slit-like anteroposterior compression of the BI has been described on bronchoscopy [67, 116, 51].

The trajectory of the BI and RLL7 showed a more horizontal trajectory with decreasing kyphosis. It can be hypothesised that the anterior protrusion of the spine produces a rightward deflection of the trajectory of BI and RLL7. Furthermore, the right hemithorax is rotated posteriorly wrapping the airway around the spine. Anteriorly, the right pulmonary artery or interlobar artery crosses anterior to the BI and it seems plausible that the vessel has a causative role in the airway impingement (Figure 5.6) [122].

Winter et al. [98] reported decreased vital capacities due to reduced anteroposterior diameters of the chest in patients with hypokyphosis. The results demonstrated that hypokyphosis correlated negatively with FVC, FEV<sub>1</sub> and FEV<sub>1</sub>/FVC. In 1970, Bjure et al. [123] already indicated that airway closure was an aetiological factor of lung function impairment in patients with severe scoliosis. Dubousset et al. [40] reported direct airway compression by the scoliosis. They described the spinal penetration index (SPI) which is a transverse plane measurement obtained by CT to quantify the spinal intrusion into the thorax. High SPI measured with biplanar stereoradiographic reconstruction have shown to correlate with the presence of obstructive lung disease [38]. It is likely that different pathophysiological mechanisms result in the loss of lung function in patients with scoliosis. Disturbed chest mechanics and reduced lung volumes lead to a restrictive lung defect while airway narrowing increases airway resistance, particularly in patients with severe scoliosis and decreased thoracic kyphosis, causing a mixed

Table 5.3: Pre-post-operative comparison of deformity parameters, lung function and normalised airway lumen areas.

	Pre-operative ( $n = 9$ )	Post-operative ( $n = 9$ )	Pairwise $t$ test $q$ -value
Age	18.37 (7.08)	20.84 (6.74)	0.001 *
Radiographic MT (°)	79.1 (18.41)	25.14 (12.71)	< 0.001 *
CT measured MT (°)	70.57 (17.99)	34.27 (12.1)	< 0.001 *
Radiographic TK (°)	10.18 (21.38)	20.3 (16.82)	0.037 *
CT measured TK (°)	-0.08 (20.3)	14.36 (12.01)	0.019 *
SPI (%)	19.96 (5.96)	16.59 (4.33)	0.005 *
RHI (%)	90.71 (53.17)	44.03 (60.31)	0.026 *
FEV <sub>1</sub> (% predicted)	40.8 (10.28)	67.77 (16.31)	0.001 *
FVC (% predicted)	44.49 (12.61)	72.14 (20.16)	< 0.001 *
FEV <sub>1</sub> /FVC (% predicted)	92.69 (11.12)	94.28 (5.47)	0.53
Trachea	0.83 (0.08)	0.89 (0.06)	0.263
RMB	0.48 (0.09)	0.55 (0.1)	0.045 *
RUL	0.15 (0.07)	0.21 (0.06)	0.12
BI	0.21 (0.09)	0.29 (0.08)	0.037 *
RB4+5	0.06 (0.03)	0.09 (0.04)	0.040 *
RB6	0.02 (0.02)	0.06 (0.03)	0.040 *
RLL	0.04 (0.05)	0.12 (0.05)	0.045 *
LMB	0.33 (0.08)	0.36 (0.09)	0.11
LUL	0.28 (0.05)	0.27 (0.06)	0.69
LB1+2+3	0.18 (0.08)	0.16 (0.08)	0.42
LB4+5	0.09 (0.03)	0.08 (0.01)	0.17
LB6	0.09 (0.03)	0.08 (0.03)	0.30
LLB	0.16 (0.07)	0.16 (0.07)	0.69

\* Significant difference between pre- and post-operation results using pairwise  $t$  test to  $q < 0.05$ . Airway lumen are expressed as a fraction of the Trachea lumen area measured at the T2 level.

Abbreviations: MT, main thoracic curve; TK, T5-T12 thoracic kyphosis; SPI, spinal penetrarion index; RHI, rib hump index; FEV<sub>1</sub>, forced expiratory volume in 1 second; FVC, forced vital capacity. Refer to Figure 5.2 for definition of airway segments.

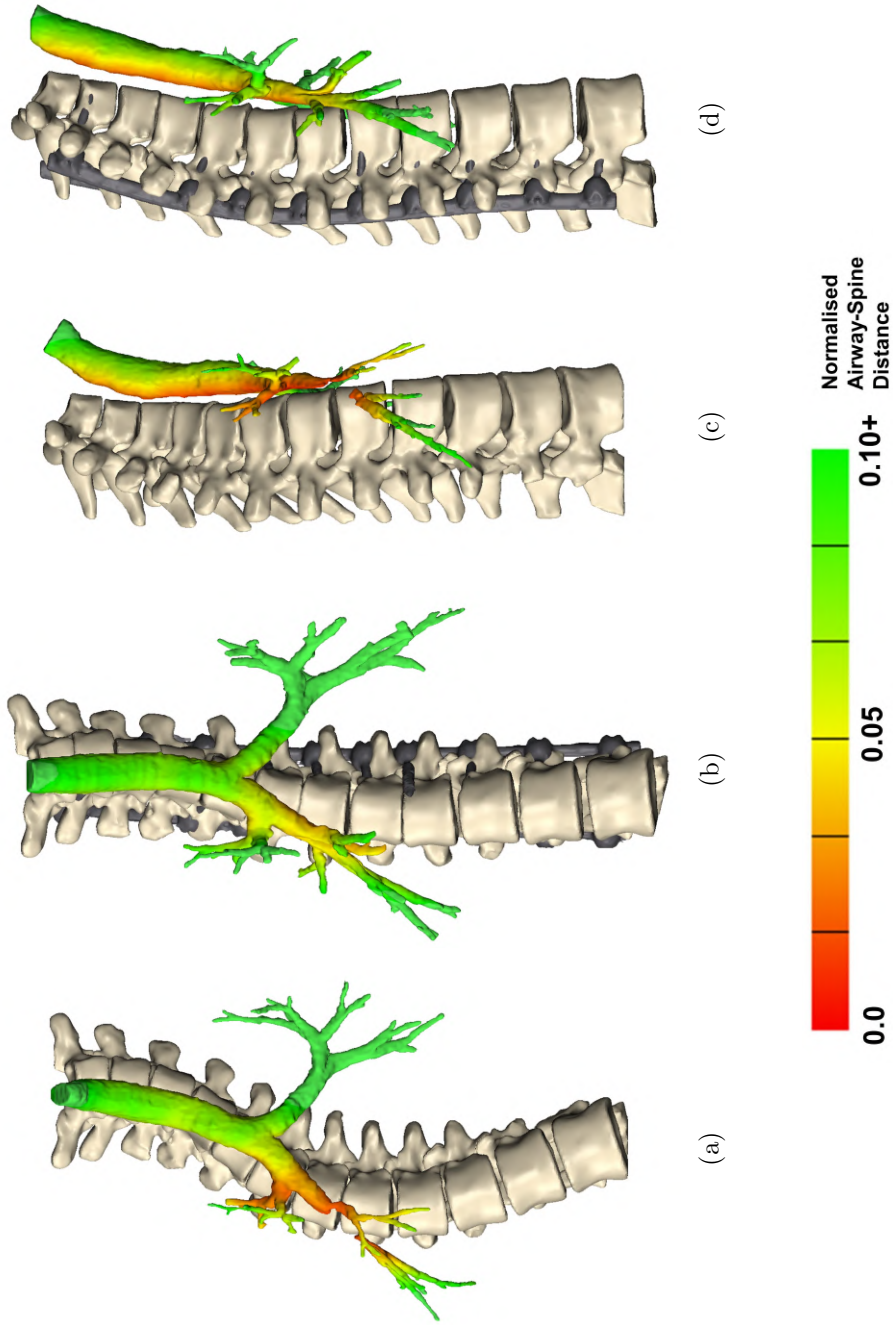


Figure 5.5: Pre- (a,c) and post- (b,d) scoliosis surgery comparison of spine-airway proximity in a hypokyphotic subject. Scoliosis was corrected from 59.1° to 23.5° in the coronal plane (a,b) and T5-T12 kyphosis increased from 6.5° to 14.6° in the sagittal plane (c,d). Close proximity between the spine and the bronchus intermedius (BI) bifurcation can be seen pre-operatively with right lower airways (RLL7 and RB6) being completely obstructed. Resolution of the stenosis is observed post-operatively as spinal intrusion is reduced.

ventilatory defect. Based on the results, spirometric evaluation of patients with scoliosis and reduced thoracic kyphosis is recommended. Patients with reduced  $FEV_1/FVC$  ratios or  $FVC < 65\%$  predicted are likely to suffer significant pulmonary morbidity and should undergo further diagnostic workup [26]. Flow volume patterns are frequently normal in patients with bronchomalacia [51, 124, 65]. Air trapping reflected in an increased ratio of residual lung volume to total lung capacity and increased airway resistance can indicate airway narrowing with expanded pulmonary function testing by body plethysmography [20].

Bronchial obstruction leads to physiological disturbance based on location, degree of narrowing and the history of the stenosis. The morphological analysis has shown that with increased hypokyphosis, airway narrowing begins more proximal at the BI potentially limiting airflow of the right middle lobe and lower lobe which each contribute in health to 9% and 25% of total lung volume respectively [124]. Several mechanisms can exacerbate the stenosis of the airway. Increased intrapleural pressure during expiration narrows the airway increasing resistance and decreasing flow. Bernoulli's principle states that increased velocity through the narrowed airway occurs simultaneously with a decrease in internal airway pressure. The more stenotic the airway and the more forceful the expiration the more likely the airway will obstruct [125]. Early recognition of airway stenosis is important before obstruction becomes chronic, causing atelectasis and recurrent infection with irreversible loss of lung function [115, 117].

Location and characterisation of the narrowing is paramount to plan surgical correction of the scoliosis and decompress the obstructed airway. There is no agreement on the diagnostic workup for extrinsic compression of the airway by scoliosis. Bronchoscopy with forced expiratory manoeuvres is the current 'gold standard' for the diagnosis of bronchomalacia of the trachea and main stem bronchi [126]. Bronchoscopy is performed under sedation and requires the patient to inhale and forcibly exhale when instructed. Due to the invasive nature and risk of complications, it may not be appropriate to perform bronchoscopic examinations in the immediate period prior to scoliosis correction, particularly in patients with impaired respiratory function.

CT scanning allows objective delineation of the location, extent and adjacent relationships of anatomic structures including spine and vasculature causing extrinsic airway compression. CT allows simultaneous evaluation of lung and spine for surgical planning of the scoliosis correction [127]. Low-dose dynamic CT including end-inspiratory and dynamic-expiratory imaging has shown a high level of concordance with bronchoscopy in the diagnosis of tracheobronchomalacia [128]. There is potential for high radiation doses with CT, thus adherence to pediatric guidelines to produce diagnostic images without excessive radiation exposure is mandatory [129]. Dynamic volumetric CT technique has demonstrated the ability to obtain diagnostic images at low radiation dose and much less than previous paired inspiratory and expiratory CT techniques [130].

Ventilation/perfusion scanning is not used routinely in the assessment of patients with scoliosis but can provide a regional functional assessment in patients with significant respiratory symptoms. Use of krypton-81m as a ventilation agent with its ability to assess tidal breathing has been used to assess the posture dependant right bronchial obstruction in patients with scoliosis [111].

In the future, hyperpolarized helium-3 ( $HP\ 3He$ ) magnetic resonance imaging (MRI) may provide accurate airway lumen measurement and dynamic imaging with regional

lung function assessment without the use of ionising radiation [131]. It is likely that these techniques will lead to a better understanding of the pathophysiology of respiratory disease in scoliosis translating to improved care and specific scoliosis correction techniques.

In hypokyphotic subjects, postoperative improvements in lung function coincide with the re-expansion of right-sided airways [67, 68]. Respiratory complications such as hyperinflation and atelectasis have been reported to improve post scoliosis correction [132, 51]. Whilst distal airways may benefit from scoliosis correction and derotation of the spine, insufficient coronal correction may not resolve the obstruction of more proximal airways. Correction techniques which have been shown to successfully target kyphosis restoration should be adopted for patients with severe curves and hypokyphosis to restore airway conductance [102, 133].

There are several limitations to this study. The preoperative CT scans analysed in this study were performed as planning scans prior to correction of the scoliosis via spinal instrumentation and were not controlled with respect to respiratory phase. Thus, end-expiration lumen reductions were not captured. Secondly, the scans were performed on larger deformities with abnormal sagittal profiles and as such represent a more severe sample of patients with idiopathic scoliosis. Idiopathic hyperkyphosis is rare and consequently the sample size is relatively small. Thirdly, the scans were obtained in the supine position changing the coronal and sagittal alignment of the spine. Posture dependant lung function changes have been demonstrated in patients with scoliosis. The supine position further decreases thoracic kyphosis producing additional narrowing of the airways [111, 112].

## 5.7 Conclusion

The morphological analysis of large airways in patients with right idiopathic thoracic scoliosis demonstrated that the loss of thoracic kyphosis causes right-sided airway narrowing. More severe hypokyphosis led to more proximal and severe narrowing in the bronchus intermedius and its surrounding airways.  $FEV_1/FVC$  correlated positively with airway lumen area, implying an obstructive element to lung function impairment in patients with scoliosis and loss of kyphosis. Preoperative diagnosis of extrinsic airway narrowing by the scoliosis is essential to plan scoliosis correction techniques that can adequately decompress the airway. Although decrease in lung function in patients with scoliosis is multifactorial, morphological changes in airways from variance in the sagittal profile play a more important role in impairing lung function than is generally appreciated.



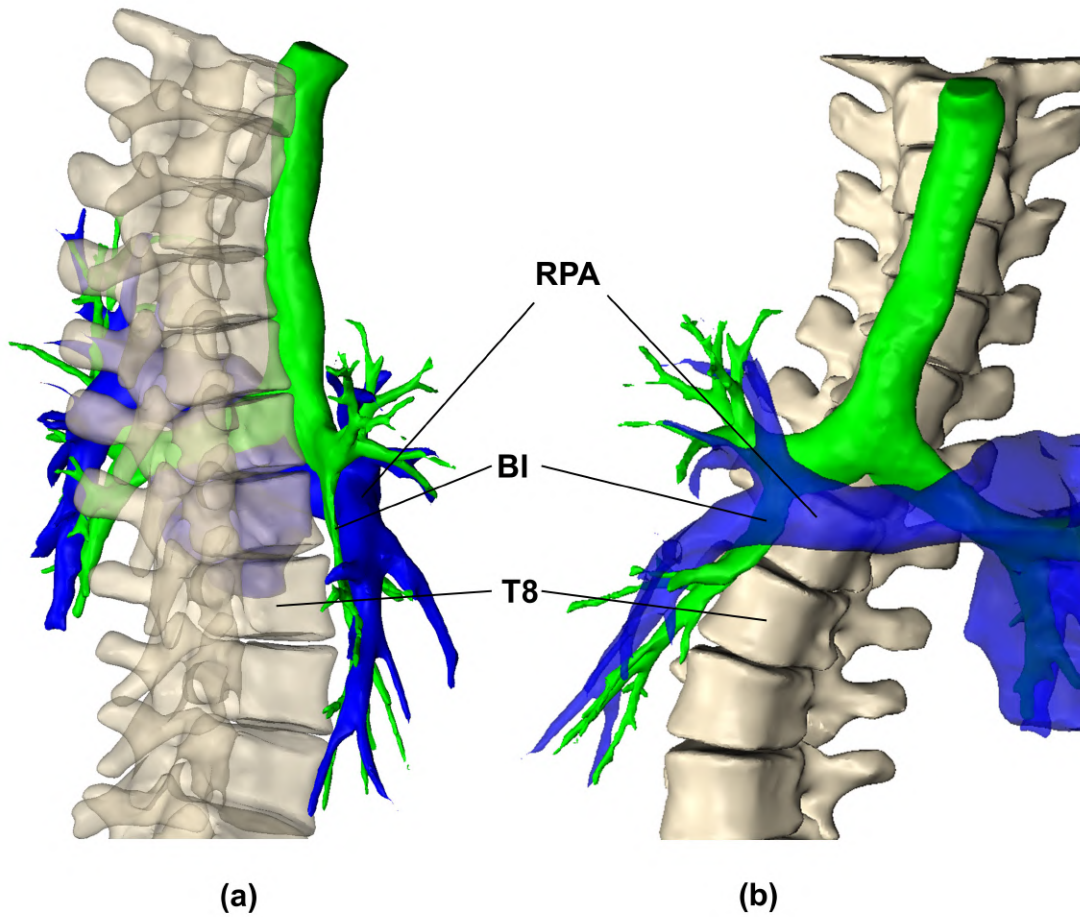


Figure 5.6: Subject with scoliosis ( $MT = 62^\circ$ ) and hypokyphosis ( $TK = 4.6^\circ$ ). Intra-venous contrast allowed the segmentation of the pulmonary arterial structure. Shown are T1–T10 vertebrae (bone), airway lumen (green) and pulmonary artery (blue) displayed from the (a) sagittal and (b) coronal perspectives. The right pulmonary artery (RPA) crosses anteriorly to the bronchus intermedius (BI) impinging the airway against the spinal column.

## Chapter 6

# Lung Volumes and Attenuation

### 6.1 Summary

In this chapter, the relationship between lung volumes, air-trapping, atelectasis, pulmonary function and thoracic deformity are examined in patients with adolescence idiopathic scoliosis (AIS). Segmentations from computed tomography imaging is used to measure airway lumen cross-sectional areas (CSA), lung volume and the proportion of hyper-aerated and non-aerated volume (proxies for air-trapping and atelectasis respectively) within the lung. Lung volumes, right-left lung volume asymmetry, the degree of hyper- and non-aerated volume in each lung were correlated with deformity parameters, lung function and airway narrowing. The right (convex) lung was found to decrease relative to the left (concave) lung with increasing spinal intrusion and rib hump. Right-left lung volume ratio correlated positively with FEV<sub>1</sub>, FVC and right-sided airway CSA. Scoliosis, rib hump formation and spinal intrusion were found to result in right-sided atelectasis; and right-sided air-trapping correlated with spinal intrusion, FEV<sub>1</sub> and FEV<sub>1</sub>/FVC. FEV<sub>1</sub>/FVC, an indicator of airway conductance, was shown to decrease with increased spinal intrusion and increase with atelectasis. Patients with reduced expiratory volumes and hypokyphotic profiles should be investigated for airway obstruction as atelectasis can mask the effects of severe airway obstruction with normal FEV<sub>1</sub>/FVC values. The combination of low expiratory volumes and normal FEV<sub>1</sub>/FVC may be misinterpreted as severe restrictive lung disease. Postoperatively, gains in lung function parameters were found to improve with preoperative spinal intrusion and decrease with preoperative atelectasis. These results suggest that patients with hypokyphosis can expect to regain lung function following decompression of obstructed airways but existing atelectasis may have already caused irreversible damage to the lung structure.

### 6.2 Introduction

Scoliosis has generally been associated with the development of restrictive lung disease [134], however, obstructive lung disease [24], incidence of air-trapping [63, 64] and presence of atelectasis [51, 40, 66, 117] have previously been reported in patients with AIS. Although pulmonary function tests can give an aggregated assessment of lung function, regional pulmonary abnormalities such asymmetrical ventilation, atelectasis and air-trapping are difficult to identify and only confirmed upon additional radiolog-

ical examination. Such regional information is of importance in identifying patients with curve phenotypes at additional risk of pulmonary impairment as well as effective treatment strategies. The objective of this study is to analyse the relationship between thoracic deformity, pulmonary function, lung volumes and lung attenuation.

### 6.3 Literature Review

Computed tomography has been previously used to study the effects of scoliosis on lung volume and lung volume asymmetry. Chun et al. [135] studied convex-concave lung volume asymmetry in 77 AIS patients with predominately thoracic/thoracic-lumbar double curves (68 King type II, 9 King type III). The patients had a mean Cobb angle of  $33.3^\circ$ , kyphosis angle of  $16.0^\circ$  and were free of respiratory symptoms (patients with respiratory symptoms,  $FEV_1/FVC < 80\%$  or  $FEV_1 < 80\%$  predicted were excluded from their sample). They found that right to left lung volume ratio was negatively correlated to kyphosis ( $r = -0.26$ ,  $p = 0.01$ ) and positively correlated to axial rotation ( $r = 0.271$ ,  $p = 0.007$ ). The authors attributed the greater loss of volume on the concave side due to loss of vertical height, a concept illustrated radiographically via the space available for lung ratio [44]. However, in a similar study of 28 individuals with predominately Lenke 1 curves, Adam et al. [60] found that the convex lung decreased more relative to the concave lung with increasing rib hump size. The authors attributed the decrease in the right-left ratio to the spine being rotated into the convex hemithorax impinging the right lung. In their study, no relationship between kyphosis and lung volumes was found.

The presence of air-trapping and pulmonary atelectasis in scoliosis has been described sparsely in the respiratory and spine literature. Alotaibi et al. [64] and Al-Kattan et al. [116] reported the presence of air-trapping in scoliosis as the result of airway narrowing and bronchial torsion. Boyer et al. [63] found that 46% of pre-operative scoliosis patients had moderate to severe gas trapping as measured by plethysmography-functional residual capacity to helium dilution ratio. The presence of atelectasis in scoliosis has been described to manifest on the convex side in patients with high spinal intrusion [51, 40]. Surgical correction of the scoliosis and restoration of thoracic kyphosis has been reported to resolve pre-operative atelectasis through the decompression of airways on the convex side [51, 132, 66]. Ito et al. [51] presented a case series of 6 patients with mixed etiology who showed airflow obstruction as a result of intrusive endothoracic vertebral hump within the thorax. In 4 of the cases, preoperative atelectasis was present in the lower lobe of the convex hemithorax. Postoperatively, the spinal penetration index (SPi) improved from 23% to 16% and lessening of atelectasis was observed in all patients. Lung function improved post-operatively with mean FVC improving from 45.5% to 63.7% predicted. However, despite restoration of thoracic kyphosis and decompression of airways, the authors found no obvious difference between pre- and post-operative  $FEV_1/FVC$  (89.0% and 89.3% predicted respectively). Goussard et al. [66] reported the case of a 17-year-old male with cerebral palsy,  $107^\circ$  scoliosis, narrow chest, obstruction of the bronchus intermedius and collapse of the right middle and lower lobes. Posterior correction with fusion from T2 to the pelvis resulted in the re-expansion of collapsed lobes. Imagama et al. [132] presented a case report of a 7-year-old female with arthrogryposis multiplex congenita who developed a  $65^\circ$  right-sided thoracic scoliosis and a  $13^\circ$  thoracolumbar lordosis. Chest computed

tomography (CT) showed obstruction of right bronchi due to intrathoracic vertebral protrusion resulting in atelectasis of the right lower lobe. The lordoscoliosis was corrected posteriorly and resulted in a reduction of the scoliosis to 14° and a thoracic kyphosis of 9°. Post-operative CT showed resolution of the atelectasis.

Late recognition of the potential for hypokyphotic sagittal profiles to cause chronic bronchial compression, or failure of scoliosis correction to restore natural kyphosis, have been reported to result in recurrent pulmonary infections with irreversible lung destruction [136, 117]. ter Wee et al. [117] described a 38-year-old male with right-sided thoracic lordoscoliosis who presented with intermittent fever and position-dependent cough. Bronchoscopy examination revealed a stenosis of the right lower lobe bronchus which could be passed with a brush resulting in the discharge of purulent sputum upstream. Computed tomographic scanning confirmed extrinsic compression of the right lower lobe bronchus and atelectasis of the right lower lobe. Lung function test reveal reduced lung volumes, with total lung capacity, forced vital capacity and forced expiratory volume in 1 second at 57%, 54% and 44% of predicted values respectively. Due to the presence of atelectasis and intermittent fever over a period of 5-years, it was assumed that the right lower lobe was destroyed and a lobectomy was performed to remove the affected lobe. No reoccurrence of symptoms or pulmonary dysfunction appeared post-operatively. Histological examination of the right lower lobe showed fibrosis and evidence of chronic inflammation. van Ooij et al. [136] presented a case of flat-back syndrome in a 40-year-old female who received scoliosis correction surgery via Harrington instrumentation in 1976. Over a 26-year period post-operation, the patient experienced several episodes of severe dyspnea. Figure 6.1 shows the computed tomography scan 18-years post-operation showing an estimated SPi of 23.1%, bronchial obstruction of the right-sided airways caused by vertebral compression (red arrow) and destruction of the right lower lobe (blue arrow). Lateral spine radiographs showed a flattened thoracic spine with 3° of kyphosis between T5 and L1. Ventilation-perfusion scans showed lack of both perfusion and ventilation of the right lung. Forced vital capacity was reported as 20% of predicted with blood gas analysis showing hypoxia.

Identification of regions within the lung with similar attenuation can often provide information about the level of lung function and cause of impairment. A common classification segregates the lung volume into regions of functional interest based on the attenuation in Hounsfield units (HU): hyper-aerated (<-900 HU), normo-aerated (between -900 and -500 HU), hypo-aerated (-500 to -100 HU) and non-aerated regions (-100 to 100 HU) [137, 138, 139]. The non-aerated volume criteria has been used extensively in the anaesthesia literature to quantify post-operative atelectasis in anaesthetised patients [140, 141, 142]. Common quantification of air-trapping is based on the proportion of voxels in expiratory CT with an attenuation below -856 HU ( $EXP_{-856}$ ) and an expiratory to inspiratory ratio of the mean lung density ( $E/I\text{-ratio}_{MLD}$ ) [143, 144]. Although atelectasis and air-trapping has been reported to manifest in the convex middle and lower lobes in scoliosis patients with hypokyphosis and airway obstruction, no study to date has quantified the proportion of the affected regions or correlated CT-measured atelectasis or air-trapping with thoracic deformity and pulmonary function tests in scoliosis.



Figure 6.1: van Ooji et al. [136] reported a case of extrinsic bronchial compression (red arrow) and destroyed convex lung (blue arrow) 18 years post-operation in a patient with narrowed anterior-posterior chest. Forced vital capacity was 20% of predicted and the convex lung showed no perfusion or ventilation on perfusion scans. Image adapted from [136].

## 6.4 Materials & Methods

### 6.4.1 Subjects

A retrospective review of the surgeon’s imaging database between 2015 and 2019 (Kodak Carestream PACS) at the Scottish National Spine Deformity Service was conducted to identify severe Lenke type 1 or 2 AIS patients with right-sided, thoracic curves with an apex between the seventh and tenth thoracic vertebrae (T7-T10). Patients who underwent pre-operative planning CT imaging and pulmonary function tests (PFT) were included. Patients with evidence or a history of primary obstructive lung disease were excluded. A total of 48 patients (35 female and 13 male, all Caucasian) with a mean age of 16.8 years (standard deviation [SD] = 7.9 years, range = 10.0 to 39.8 years) met the inclusion criteria. Patients underwent scoliosis correction surgery by posterior instrumental fusion using segmental pedicle screws and rods. Out of the 48 patients, 41 patients had post-operative PFTs at 1-year follow-up. Patients underwent a multidetector CT (64-MDCT Siemens Somatom Scanner) at 0.6 mm collimation, 1 mm slice thickness and 0.7 mm reconstruction increments.

### 6.4.2 Image Segmentation

Image segmentation was performed using Mimics v18.0 (Materialise N.V., Leuven, Belgium). CT images were imported into Mimics in DICOM format (Figure 6.2 (a)). Airways were segmented using the in-built airway segmentation algorithm in Mimics. Lungs were segmented via an initial thresholding between -1024 HU and -500 HU (Figure 6.2 (b)). Peripheral atelectatic regions which were not captured were included into

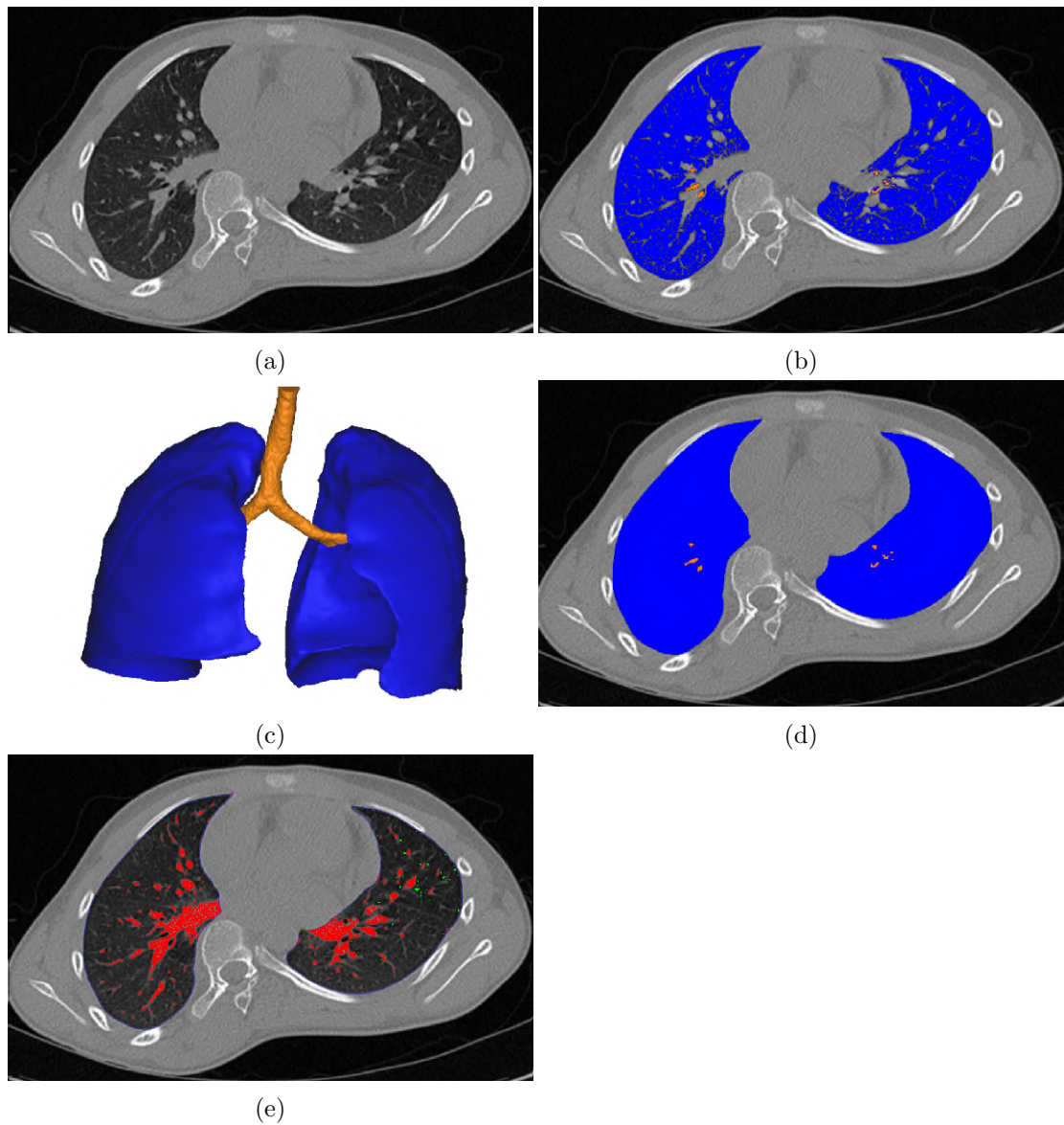


Figure 6.2: Methodology for the segmentation and measurement of lung volumes. (a) The original CT image. (b) Lungs were segmented by by thresholding between -1024 HU and -500 HU; the airway lumens were trimmed off from the mask. (c) Three-dimensional (3D) models which were wrapped and smoothed to fill holes less than 15 mm wide. (d) A new mask following the contour of the 3D model was mapped onto the CT slices. (e) Additional thresholding was applied on the new mask to identify hyper-aerated (-1024 to -900 HU, green) and non-aerated (-100 to 100 HU, red) voxels.

the region of interest by tracing the contour of the rib structures. A smoothed and wrapped three-dimensional (3D) model was created from the masks with holes less than 15 mm wide filled using the wrap and smoothing functions in Mimics (Figure 6.2 (c)). A new mask was generated which conformed to the contours of the 3D model (Figure 6.2 (d)). Voxels of hyper-aerated (-1024 to -900 HU, green) and non-aerated (-100 to 100 HU, red) regions were segregated based on the voxel attenuation (Figure 6.2 (e)).

### 6.4.3 Lung Volume Parameters

The degree of atelectasis and air-trapping in each lung was estimated by dividing the number of non-aerated and hyper-aerated voxels with the total number of voxels within each lung respectively. The proportion of non-aerated volume ( $V_{\text{non,RL}}$  and  $V_{\text{non,LL}}$ ) and hyper-aerated volume ( $V_{\text{hyper,RL}}$  and  $V_{\text{hyper,LL}}$ ) were expressed as a percentage of the volume of the individual right and left lungs respectively. The right-left lung volume ratio ( $V_{\text{RL}}:V_{\text{LL}}$ ) was determined by dividing the number of voxels in the right lung with that of the left lung. Reference values for right ( $V_{\text{RL}}$ ), left ( $V_{\text{LL}}$ ) and total ( $V_{\text{Total}}$ ) lung volumes were calculated for patients under 20 years of age using 50 percentile reference data from Gollogly et al. [145] and expressed as a percentage of the predicted value ( $n = 41$ ). An index of airway cross sectional area was created by summing the lumen areas of the first three generations of airways in the right and left lung ( $CSA_{\text{RL}}$  and  $CSA_{\text{LL}}$ ).  $CSA_{\text{RL}}$  consisted of the cross-sectional areas of the right main bronchus (RMB), right upper lobe bronchus (RUL), bronchus intermedius (BI), middle lobe bronchus (RB4+5), right lower lobe superior segmental bronchus (RB6), right lower lobe bronchus (RLL7).  $CSA_{\text{LL}}$  consisted of the left main bronchus (LMB), left upper lobe bronchus (LUL), left apicoposterior and anterior segmental bronchus (LB1+2+3), left lingula bronchus (LB4+5), superior segment of the left lower lobe (LB6) and left lower lobe bronchus (LLB).  $CSA_{\text{RL}}$  and  $CSA_{\text{LL}}$  were normalised by the trachea cross-sectional area measured at the T2 level.

### 6.4.4 Spine and Thoracic Deformity Parameters

The main thoracic curve (MT) and T5-T12 thoracic kyphosis (TK) were measured on coronal and sagittal radiographs using the Cobb method. The spinal penetration index (SPi) [40], endothoracic hump ratio (EHR) [51] and rib hump index (RHi) [86] were measured at the apical level on axial CT images.

### 6.4.5 Lung Function Data

PFTs were conducted via forced manoeuvres in accordance with the joint American Thoracic Society and European Respiratory Society standards [50]. Forced expiration in 1 second ( $FEV_1$ ) and forced vital capacity (FVC) were measured (Jaeger Master-Screen PFT pro) along with armspan. In calculating lung function predicted values, arm span was used to estimate standing height to correct for scoliotic height loss and age-related or post-operative height gains [23]. Estimated standing height was used along with patient age at the time of testing to determine the predicted values based on reference data by the Global Lung Function Initiative [22].  $FEV_1$ , FVC and  $FEV_1/FVC$  are expressed as a percentage of their respective predicted values (% predicted).

Table 6.1: Summary of pulmonary function test results, radiographic and deformity parameters and lung volume parameters.

Age (years)	16.78 (7.91)	(10.0 to 39.8)
FEV <sub>1</sub> (% pred.)	59.54 (15.02)	(26.74 to 88.99)
FVC (% pred.)	64.02 (14.99)	(24.72 to 91.46)
FEV <sub>1</sub> /FVC (% pred.)	92.44 (8.31)	(74.43 to 107.61)
MT (°)	75.39 (12.33)	(50.7 to 105.4)
TK (°)	20.98 (20.1)	(-13.99 to 78.45)
RHi (%)	60.74 (38.48)	(14.59 to 182.52)
SPi (%)	14.86 (4.3)	(8.17 to 27.46)
EHr (%)	46.94 (10.54)	(29.68 to 83.8)
V <sub>RL</sub> (% pred.) †	69.32 (22.04)	(39.27 to 130.82)
V <sub>LL</sub> (% pred.) †	73.26 (24.18)	(38.76 to 132.88)
V <sub>Total</sub> (% pred.) †	71.04 (22.26)	(38.98 to 131.09)
V <sub>RL</sub> :V <sub>LL</sub> (-)	1.14 (0.21)	(0.68 to 1.88)
V <sub>non,RL</sub> (% RL)	5.16 (3.02)	(1.44 to 18.95)
V <sub>non,LL</sub> (% LL)	4.55 (1.55)	(1.69 to 8.18)
V <sub>hyper,RL</sub> (% RL)	15.68 (10.74)	(0.01 to 39.25)
V <sub>hyper,LL</sub> (% LL)	15.72 (10.36)	(0.05 to 39.41)
CSA <sub>RL</sub> (-)	1.33 (0.34)	(0.54 to 1.92)
CSA <sub>LL</sub> (-)	1.45 (0.29)	(1.00 to 2.25)

Values are mean (standard deviation) (range).

†  $n = 41$  due to age range of reference data (0 to 20 years)

Abbreviations: RL, right lung; LL, left lung; Total, total lung; CSA, airway cross-sectional area.

#### 6.4.6 Statistics

Lung volume parameters were correlated with spine and thoracic deformity parameters, as well as airway CSA and lung function, using the Pearson method. The  $p$ -values from Pearson correlations were corrected for multiple comparisons ( $q$ -values) using the Benjamini and Hochberg method [52] with  $q$ -value threshold of 0.05 corresponding to a false discover rate of 5%. Multivariate step-wise regression was also performed using lung volume, airway CSA and deformity parameters to predict pre-operative lung function and post-operative lung function change. Regression coefficients for individual predictors ( $b$ ), their standard errors ( $SE(b)$ ) and standardised coefficients ( $\beta$ ) along with the adjusted coefficient of determination for multiple comparisons ( $r^2$ ) are reported. All statistical analysis was implemented using the statistical software R (<http://www.R-project.org>).

### 6.5 Results

A summary of pre-operative pulmonary function, deformity parameters, lung and airway parameters can be found in Table 6.1. Mean preoperative MT was 75.4° (50.7° to 105.4°) and mean TK was 21.0° (-14.0° to 78.5°). Percent-predicted volumes were not



Table 6.2: Pearson correlation coefficients between lung volume parameters, radiographic and CT deformity parameters, lung function and airway lumen cross sectional areas ( $n = 48$ ).

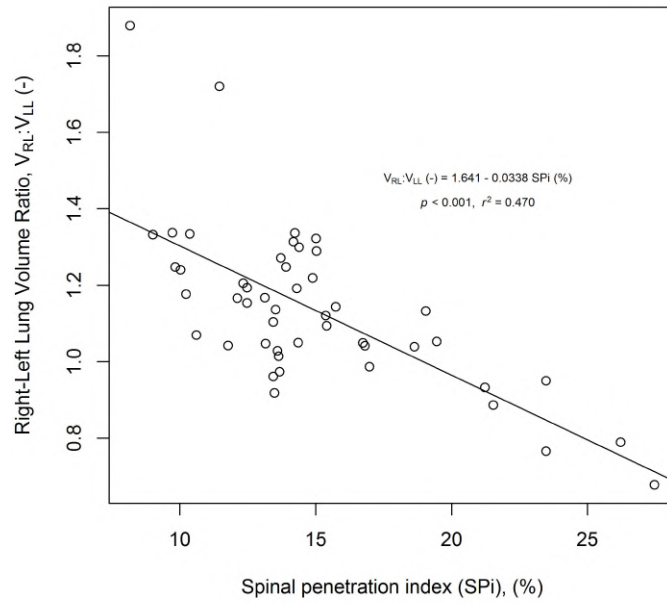
	$V_{RL}^\dagger$ (% pred.)	$V_{LL}^\dagger$ (% pred.)	$V_{Total}^\dagger$ (% pred.)	$V_{RL}:V_{LL}$ (-)	$V_{non,RL}$ (% RL)	$V_{non,LL}$ (% LL)	$V_{hyper,RL}$ (% RL)	$V_{hyper,LL}$ (% LL)
MT	-0.21	0.05	-0.09	-0.20	0.38*	0.07	0.11	0.23
TK	0.00	-0.13	-0.06	0.35	-0.14	0.05	-0.37	-0.23
RHi	-0.21	0.08	-0.08	-0.42*	0.46*	-0.12	0.11	0.22
SPi	-0.21	0.13	-0.05	-0.69***	0.54**	-0.11	0.33	0.36
EHR	-0.06	0.26	0.10	-0.63***	0.46*	-0.22	0.38*	0.28
FEV <sub>1</sub>	0.25	0.02	0.14	0.49**	-0.29	0.25	-0.41*	0.25
FVC	0.29	0.04	0.17	0.45*	-0.34	0.24	-0.29	-0.27
FEV <sub>1</sub> /FVC	-0.08	-0.03	-0.06	0.18	0.24	0.16	-0.40*	-0.26
CSAR	0.18	0.02	0.10	0.42*	-0.13	0.22	-0.20	-0.14
CSAL	-0.07	0.02	-0.02	-0.10	0.28	0.15	-0.15	-0.04

Significant to: \*  $q < 0.05$ , \*\*  $q < 0.01$ , \*\*\*  $q < 0.001$ .<sup>†</sup>  $n = 41$  due to age range of reference data (0 to 20 years).

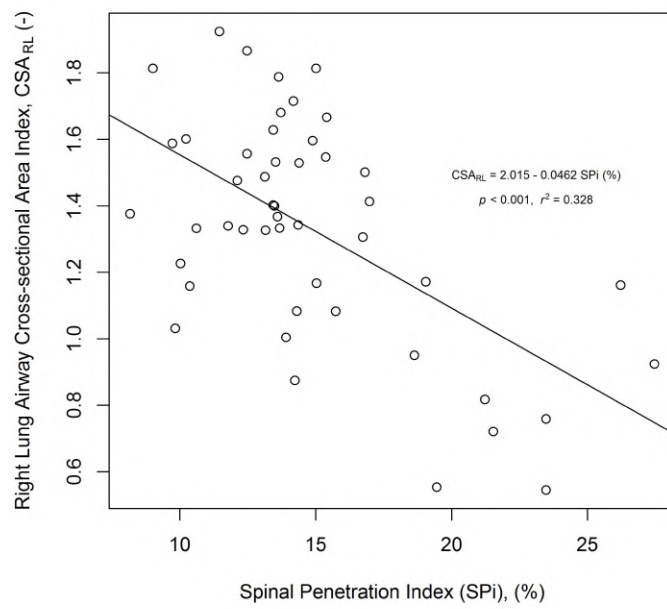
Table 6.3: Multivariate stepwise regression results for the prediction of pre-operative ( $n = 48$ ) and post-operative changes ( $n = 41$ ) in lung function using CT thoracic deformity, airway and lung volume parameters.

FEV <sub>1</sub>	Intercept	RHi	V <sub>hyper,RL</sub>	CSA <sub>RL</sub>	Model Statistics
$b$	48.644	-0.156	-38.602	19.892	$r^2 = 0.569$
SE( $b$ )	7.514	0.039	13.689	4.427	SE = 9.86
$\beta$	-	-0.401	-0.276	0.450	-
$p$	< 0.001	< 0.001	0.007	< 0.001	-
FVC	Intercept	RHi	CSA <sub>RL</sub>	-	Model Statistics
$b$	53.467	-0.196	16.906	-	$r^2 = 0.468$
SE( $b$ )	7.632	0.043	4.833	-	SE = 10.93
$\beta$	7.005	-0.504	0.383	-	-
$p$	< 0.001	< 0.001	0.001	-	-
FEV <sub>1</sub> /FVC	Intercept	V <sub>non,RL</sub>	V <sub>hyper,RL</sub>	CSA <sub>RL</sub>	Model Statistics
$b$	81.427	68.371	-23.980	8.459	$r^2 = 0.267$
SE( $b$ )	5.500	34.978	9.952	3.157	SE = 7.11
$\beta$	-	0.249	-0.310	0.345	-
$p$	< 0.001	0.047	0.020	0.010	-
$\Delta$ FEV <sub>1</sub>	Intercept	SPi	V <sub>non,RL</sub>	-	Model Statistics
$b$	-	1.993	-1.451	-	$r^2 = 0.403$
SE( $b$ )	-	0.370	0.502	-	SE = 8.51
$\beta$	-	0.788	-0.423	-	-
$p$	-	< 0.001	0.006	-	-
$\Delta$ FVC	Intercept	SPi	V <sub>non,RL</sub>	-	Model Statistics
$b$	-	1.877	-1.300	-	$r^2 = 0.321$
SE( $b$ )	-	0.411	0.558	-	SE = 9.46
$\beta$	-	0.712	-0.363	-	-
$p$	-	< 0.001	0.025	-	-
$\Delta$ FEV <sub>1</sub> /FVC	Intercept	SPi	V <sub>non,RL</sub>	-	Model Statistics
$b$	-	0.611	-0.929	-	$r^2 = 0.123$
SE( $b$ )	-	0.269	0.364	-	SE = 6.18
$\beta$	-	0.403	-0.452	-	-
$p$	-	0.029	0.015	-	-

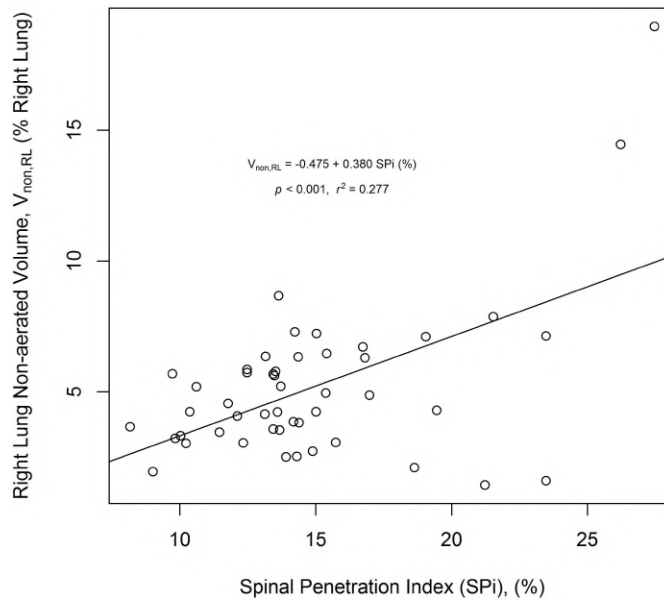
Abbreviations:  $\Delta$ , post-operative change; RHi, rib hump index; SPi, spinal penetration index; RL, right lung; V<sub>hyper</sub>, hyper-aerated volume; V<sub>non</sub>, non-aerated volume; CSA<sub>hyper,RL</sub>, airway cross-sectional area index.



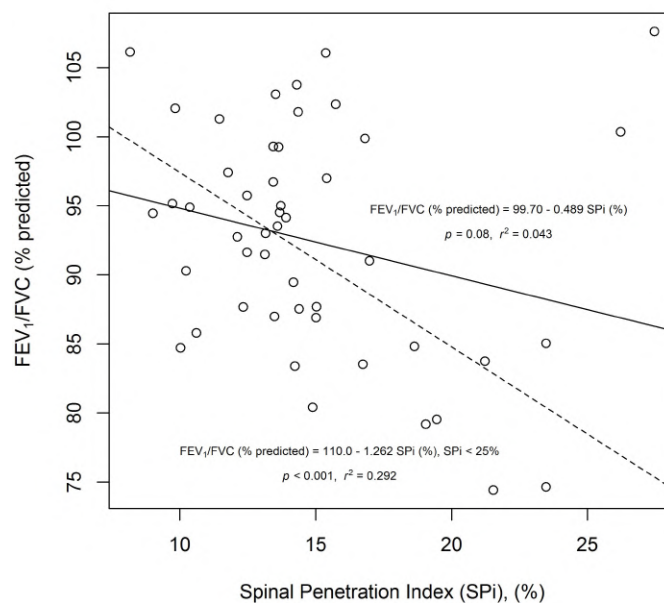
(a)



(b)



(c)



(d)

Figure 6.3: Correlations between the spinal penetration index (SPi), (a) right-left lung volume ratio, (b) right lung airway cross-sectional area index, (c) right lung non-aerated volume and (d) FEV<sub>1</sub>/FVC. As the scoliotic spine intrudes into the convex hemithorax, right-sided airways are obstructed in addition to the restriction. Formation of atelectasis is seen in patients with SPi greater than 25%. Despite having obstructed airways, patients with reduced expiratory volumes, high SPi and atelectasis can exhibit normal FEV<sub>1</sub>/FVC values which may be misinterpreted as purely a restrictive effect.

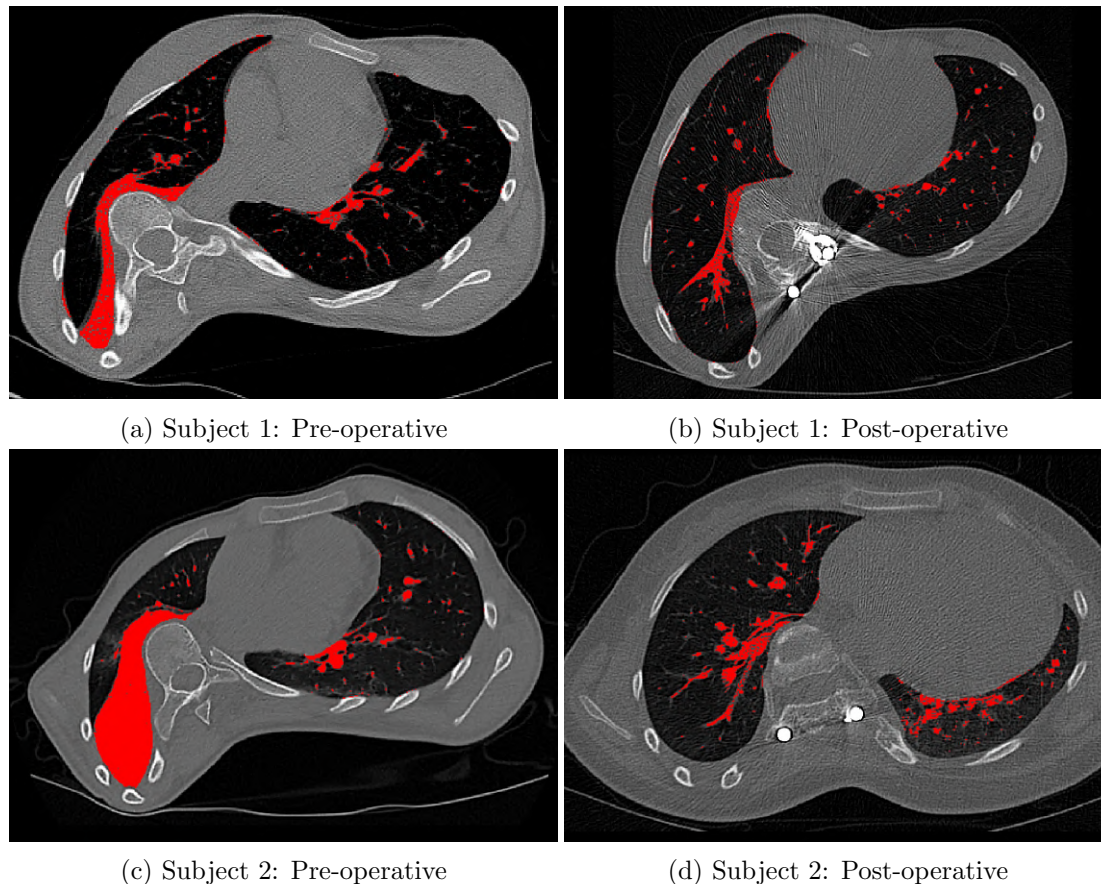


Figure 6.4: Pre- and post-operative comparison of non-aerated volume ( $V_{\text{non}}$ ), shown in red ( $-100 \leq \text{HU} < 100$ ), within the lung in two atelectatic subjects. The first patient is shown in the first row. Scoliosis (MT) was corrected from  $105.4^\circ$  to  $45.6^\circ$ ; T5-T12 thoracic kyphosis (TK) remained unchanged at  $12^\circ$  but the spinal penetration index (SPi) was reduced from 26.2% to 22.2% and the endothoracic hump ratio (EHr) decreased from 83.8% to 68.2%. CT measured lung volume remained unchanged at 90% of predicted but  $V_{\text{non,RL}}$  decreased from 14.5% to 5.6%;  $V_{\text{non,LL}}$  was unchanged at 3.9%. Right-left lung volume ratio ( $V_{\text{RL}}:V_{\text{LL}}$ ) increased from 0.79 to 0.99. FEV<sub>1</sub> and FVC increased from 34.7% to 47.5% and 34.3% to 50.5% of predicted values respectively. However, FEV<sub>1</sub>/FVC decreased from 89.4% to 83.2% of predicted values. In the second row, the second subject showed a reduction in the proportion of  $V_{\text{non,RL}}$  from 19.0% to 5.1%; left-sided NAV remained unchanged at approximately 6%.  $V_{\text{RL}}:V_{\text{LL}}$  increased from 0.68 to 1.54. MT was corrected from  $93.4^\circ$  to  $14.4^\circ$ , TK was restored from  $5.7^\circ$  to  $22.2^\circ$ , SPi was reduced from 27.5% to 20.7% and EHR decreased from 71.5% to 55.1%. Total lung volume decreased slightly from 57.9% to 53.3% of predicted. FEV<sub>1</sub> and FVC both improved from 26.7% to 47.5% and 24.7% to 47.6% of predicted respectively. FEV<sub>1</sub>/FVC decreased from 96.3% to 89.0% of predicted. These examples illustrate that the presence of atelectasis can elevate FEV<sub>1</sub>/FVC values masking the obstruction of main-stem bronchi. Post-operative gains in lung function are not due to increases in total lung volume but due to the re-recruitment of the right lung. Simultaneous scoliosis correction and kyphosis restoration decompresses airways, re-expands right-sided atelectic segments and restores a R:L ratio closer to the normal value of 1.2.

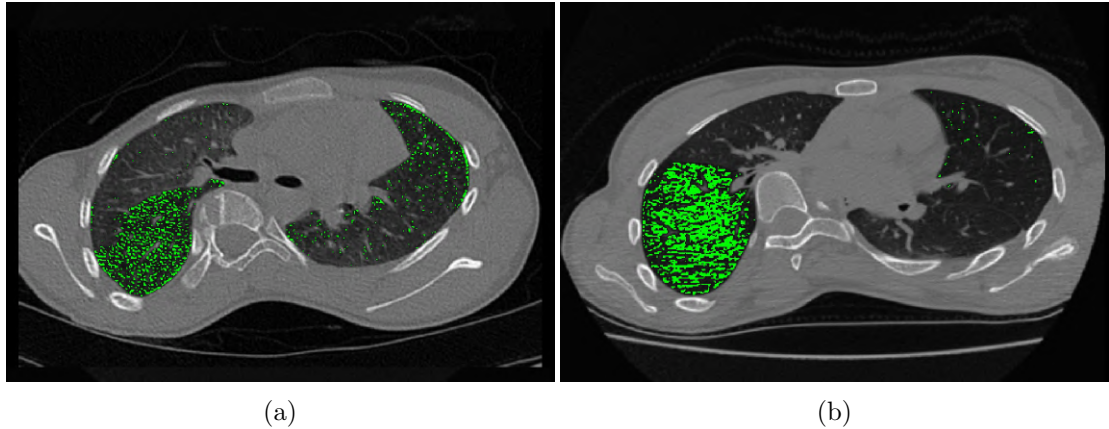


Figure 6.5: Examples of air trapping in the right lung. Regions of green show hyper-aerated volumes ( $V_{\text{hyper}}$ ) with an attenuation of between -1024 and -900 HU. Such regional differences in attenuation are only visible in CT scans taken post-expiration. Intrusion of the spine into the thorax causes secondary bronchomalacia of right-sided airways increasing airway resistance resulting in air-trapping post-expiration. Air-trapping reduces gas exchange within these regions leading to carbon dioxide retention and hypoxia.

calculated for 7 patients whose age exceeded the age limits of the reference data (9 to 20 years) [145]. For the 41 patients with post-operative pulmonary function tests, percent-predicted values in  $FEV_1$  increased from a mean of 59.2% to 73.6%, FVC from 63.8% to 76.3%, and  $FEV_1/FVC$  from 92.3% to 96.1% postoperatively. This was achieved by correcting MT from 74.7° to 26.0° and TK from 20.7° to 25.2°. Figure 6.4 shows two examples of surgical correction and post-operative resolution of atelectasis.

### 6.5.1 Correlational Analysis

Pearson correlation coefficients between lung volume parameters, deformity parameters and lung function are shown in Table 6.2. No significant correlation was found between  $V_{\text{RL}}$ ,  $V_{\text{LL}}$ ,  $V_{\text{Total}}$  and deformity parameters, lung function or airway CSA.  $V_{\text{RL}}:V_{\text{LL}}$  was found to correlate negatively with SPi ( $r = -0.69$ ) and EHr ( $r = -0.63$ ,  $q < 0.001$ ); and positively with  $FEV_1$  ( $r = 0.49$ ,  $q = 0.007$ ), FVC ( $r = 0.45$ ,  $q = 0.02$ ) and  $CSA_{\text{RL}}$  ( $r = 0.42$ ,  $q = 0.03$ ). Right-sided non-aerated volume ( $V_{\text{non,RL}}$ ) correlated positively with MT ( $r = 0.38$ ,  $q = 0.04$ ), RHi ( $r = 0.46$ ,  $q = 0.01$ ), SPi ( $r = 0.54$ ,  $q = 0.002$ ) and EHr ( $r = 0.46$ ,  $q = 0.01$ ). Right-sided hyper-aerated volume ( $V_{\text{hyper,RL}}$ ) correlated positively with EHr ( $r = 0.38$ ) and negatively with both  $FEV_1$  ( $r = -0.41$ ) and  $FEV_1/FVC$  ( $r = -0.4$ ,  $q = 0.04$ ).

### 6.5.2 Multivariate Step-wise Regression

Upon multivariate step wise regression, pre-operative  $FEV_1$  (% pred) was found to be best explained by RHi ( $\beta = -0.40$ ,  $p < 0.001$ ),  $V_{\text{hyper,RL}}$  ( $\beta = -0.28$ ,  $p = 0.007$ ) and  $CSA_{\text{RL}}$  ( $\beta = 0.45$ ,  $p < 0.001$ ;  $r^2 = 0.57$ ). Pre-operative FVC (% pred) was best explained by RHi ( $\beta = -0.50$ ,  $p < 0.001$ ) and  $CSA_{\text{RL}}$  ( $\beta = 0.38$ ,  $p < 0.001$ ;  $r^2 = 0.47$ ). For pre-operative  $FEV_1/FVC$ , SPi ( $\beta = -0.40$ ,  $p < 0.001$ ) and  $V_{\text{non,RL}}$  ( $\beta = -0.40$ ,  $p$

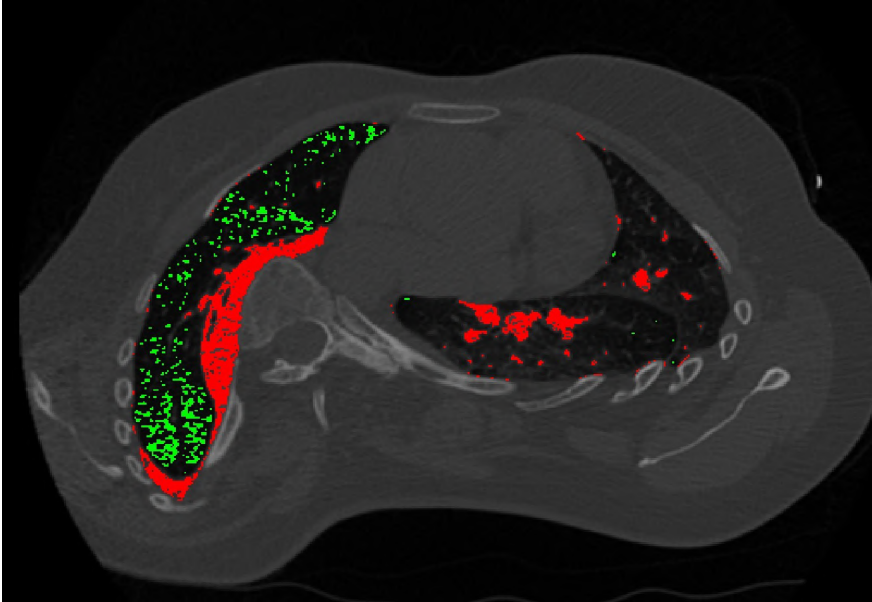


Figure 6.6: An example of a patient with simultaneous air-trapping and atelectasis. Hyper-aerated volumes are shown in green and non-aerated volumes in red. Co-occurrence of air-trapping and atelectasis imply that physiological changes to respiratory function depend on the degree of spinal intrusion as well as the history of the deformity. With progression of scoliosis and hypokyphosis, stenosis of right-sided airways may progress into secondary bronchomalacia resulting in air-trapping and heterogenous ventilation. Prolonged obstruction of these airways further deteriorates lung function as a consequence of retained secretions, atelectasis and chest infection.

$<0.001$ ) were found to be the best predictors ( $r^2 = 0.27$ ). Post-operative changes in  $FEV_1$ , FVC and  $FEV_1/FVC$  were all found to have SPi ( $\beta = 0.79, 0.71$  and  $0.40$  respectively) and  $V_{non,RL}$  ( $\beta = -0.42, -0.36$  and  $-0.45$  respectively) as best predictors ( $r^2 = 0.40, 0.32$  and  $0.12$  respectively).

## 6.6 Discussion

Comparing lung volumes to the reference data, mean percent-predicted values of the right lung (69.3% predicted) were less than the left lung (73.3% predicted), demonstrating that both lungs are impaired by the spinal deformity with the right lung being impaired further. In agreement with Adam et al. [60], the coefficient of variance for  $V_{RL}:V_{LL}$  (18%) was demonstrably lower than those of  $V_{RL}$  and  $V_{LL}$  (32% and 33%) suggesting high variation within the sample not normalised by the reference data. Reference data based solely on age and gender, without consideration for physical scales such as height, may explain the lack of correlation between percent-predicted lung volumes, deformity parameters and lung function. Significant correlations between  $V_{RL}:V_{LL}$  and RHi, SPi, EHr and  $CSA_{RL}$  suggest that rib hump formation and anterior intrusion of the spine into the convex hemithorax results in reduction of right-sided lung volume and airway conductance.

The spinal deformity modifies the thoracic configuration causing impairment in res-

piratory function which are reflected in changes in lung attenuation. Increased  $V_{\text{non,RL}}$  was associated with the progression of scoliosis, rib hump formation and spinal intrusion (Figure 6.2). The formation of atelectasis typically occurred in patients with severe scoliosis and hypokyphosis and took the form of dense strands spanning from the mediastinum towards the posterior part of the right lower lobe following the contour of the ribs. Severe atelectasis presented as a thick band occupying the space directly anterior to the vertebral column spreading across the posterior concavity of the rib hump (Figure 6.4). The presence of  $V_{\text{hyper,RL}}$  correlated positively with EHR and negatively with  $FEV_1$  and  $FEV_1/FVC$ . Air-trapping was typically observed in the lower lobe, occasionally the middle lobe, of the right lung which coincided with extrinsic compression of right sided airways in the region of the bronchus intermedius by a vertebral body (Figure 6.5). Co-occurrence of air-trapping and atelectasis were observed in some patients (Figure 6.6) suggesting a similar root cause. Such a phenomenon implies that the physiological changes to respiratory function depend on the degree of spinal intrusion as well as the history of the deformity. It is plausible that with progression of scoliosis and hypokyphosis, stenosis of right-sided airways may progress into secondary bronchomalacia resulting in air-trapping and heterogenous ventilation. Prolonged obstruction of these airways further deteriorates lung function as a consequence of retained secretions, atelectasis and chest infection which culminates in lung destruction [136] (Figure 6.7). In addition, hyperinflation in the lower lung may be the consequence of physiological space accommodation of nearby collapse/atelectasis or the primary consequence of airway obstruction consequent hyperinflation. In the former the overinflation is functional but in the latter the overinflation is non-functional. It is thus important to identify the cause of hyperinflation as this will determine the amount of functional lung available.

The rib hump produced by scoliosis and sagittal flattening has previously been shown to be associated with reduction in expiratory volumes [36, 27]. Upon multivariate regression,  $FEV_1$  was shown to be best predicted by RHi,  $V_{\text{hyper,RL}}$  and  $CSA_{\text{RL}}$  whilst FVC was best predicted by RHi and  $CSA_{\text{RL}}$ . Rib hump formation is associated with scoliosis and thoracic rotation [55, 146] which reduces the overall height of the thorax and restricts the convex lung leading to loss of lung volume. Hypokyphosis in scoliosis results in the formation of an endothoracic hump which has been shown to extrinsically compress airways, obstructing access to the right lower and middle lobes [40, 51]. Such de-recruitment of right-sided lung volume exacerbates existing restrictive lung disease through heterogenous ventilation between the right and left lungs [67, 111]. The resulting air-trapping and atelectasis is associated with decreased lung compliance and increasing the work of breathing as a result [147].

The  $FEV_1/FVC$  ratio is a common measure of airway conductance and reduced values are a marker of obstructive lung disease [24]. However, the results suggest that care should be taken in ruling out airway obstruction in patients with normal  $FEV_1/FVC$  and high spinal intrusion. Upon multivariate regression,  $FEV_1/FVC$  was shown to decrease with increased spinal intrusion and increase with atelectasis. Given that spinal intrusion is also positively correlated with atelectasis, patients with severely obstructed airways and atelectasis typically exhibit normal  $FEV_1/FVC$  values. Figure 6.3 shows the relationship between SPi,  $FEV_1/FVC$ ,  $CSA_{\text{RL}}$  and  $V_{\text{non,RL}}$ . Initial increases in SPi correspond to reductions in  $FEV_1/FVC$  and  $CSA_{\text{RL}}$  whilst  $V_{\text{non,RL}}$  remains steady. Declining  $FEV_1/FVC$  trend is reversed when SPi exceeding 25% due increasing at-



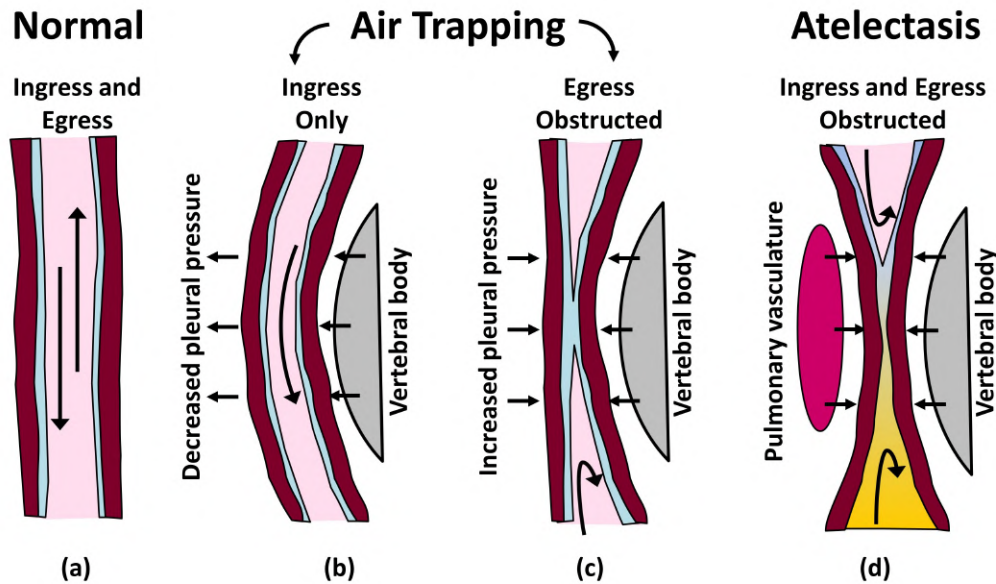


Figure 6.7: Figure showing the progression of airway obstruction in scoliosis. (a) Normal lung function facilitates both the ingress and egress of air into and out of the lungs. With increasing vertebral body intrusion, the airway is narrowed increasing airway resistance. This causes air trapping where the airway lumen is dilated during the inspiratory phase with decreased pleural pressure (b) but obstructed during the expiratory phase (c). Pinching of the airway between the vertebral body and mediastinal structures produced fixed obstruction where both inspiration and expiration are impaired (d); this retains secretions and results in lung collapse and atelectasis.

electasis. McPhail et al. [24] examined the relationship between spinal deformity and obstructive lung disease; segregating their sample by  $FEV_1/FVC$  did not reveal a deformity phenotype which could be associated with airway obstruction in scoliosis. It is plausible that this is because  $FEV_1/FVC$  does not strictly decrease with increased airway obstruction due to the development of atelectasis in cases where obstruction is severe. Chronic obstruction of right-sided airways and derecruitment of the right lobes renders the  $FEV_1/FVC$  metric a measurement of left-sided airway conductance which is typically unaffected by the scoliosis [114]. Reduced expiratory volumes and normal  $FEV_1/FVC$  ratio may be misinterpreted as severe restrictive lung disease in patients with hypokyphotic sagittal profiles.

Postoperatively, lung function improvements were found to be positively associated with pre-operative spinal penetration and negatively with pre-operative atelectasis. Restoration of thoracic kyphosis and decompression of obstructed airways has been shown to improve expiratory volumes post-operation in patients with hypokyphosis and scoliosis [67, 51]. Airway decompression by kyphosis restoration allows recruitment of the middle and lower lobes resulting in greater functional capacity. The negative relationship between post-operative lung function gain and pre-operative atelectasis suggests irreversible lung function loss possibly due to lung destruction. Although the purpose of corrective surgery in severe thoracic scoliosis is to arrest curve progression,

improve surface shape and improve respiratory function [69, 70], restrictive and obstructive lung disease are recognized risk factors for complications following scoliosis surgery [69, 148]. In addition, pulmonary function declines by 50% in the first post-operative week and preoperative atelectasis is a known risk factor for postoperative complications [149]. The use of continuous positive airway pressure and lower fraction of inspired oxygen ( $\text{FiO}_2$ ) during anesthetic induction, intraoperative use of lower  $\text{FiO}_2$ , low tidal volumes, lung recruitment and PEEP ('protective ventilatory strategy') in conjunction with postoperative early mobilization, breathing exercises and continuous positive airway pressure may help in maintaining lung aeration, thereby decreasing hypoxemia and risk of postoperative pneumonia [149, 132].

The investigations in this research have been limited to using spirometry results as a metric of pulmonary function. Although  $\text{FEV}_1$ , FVC and  $\text{FEV}_1/\text{FVC}$  are sufficient metrics of pulmonary function, inclusion of other pulmonary function metrics may give a more comprehensive view of pulmonary impairment [134]. Measurements of static lung volumes such as total lung capacity (TLC), function residual capacity (FRC) may offer better insight into lung volume loss whilst increased residual volume (RV) may reflect the presence of air-trapping. Helium dilution techniques can measure FRC whilst full body plethysmography has the ability to measure both FRC and airway resistance. Boyer et al. has demonstrated the incidence of air-trapping in scoliosis using these techniques; the association between these lung function metrics and thoracic deformity could be investigated further [63].

There are several short-comings to the study which should be acknowledged and addressed in future studies. The present study has been limited to Lenke type I and II curves with a focus on the thoracic curve. It is plausible that other curve types produce variations in lung volume, asymmetry and attenuation. Variations in patient expiratory efforts or ability may affect the respiratory phase at which the CT scans were acquired hence affecting lung attenuation. In particular, the quantification of air-trapping requires good expiratory effort to properly identify regions upstream of high airway resistance. The CT scans were obtained in the supine position changing the coronal and sagittal alignment of the spine. Posture dependant lung function changes have been demonstrated in patients with scoliosis [111, 112].

## 6.7 Conclusion

In conclusion, progression of spinal deformity in patients with AIS leads to reduction in lung volumes and increase in lung volume asymmetry. The reduction of the convex lung relative to the concave lung produces heterogenous ventilation due to reduced lung volumes and increased airway resistance. In the sagittal plane, hypokyphosis results in spinal intrusion of the convex hemithorax causing extrinsic compression of right-sided airways leading to air-trapping and atelectasis of the right and middle lobes.  $\text{FEV}_1/\text{FVC}$ , a conventional indicator of airway conductance, should not be relied on as an indicator of airway obstruction due to possible co-occurrence of atelectasis. Post-operatively, patients with high spinal intrusion observed the greatest percent-predicted increases in lung function due to decompression of airways and resolution of atelectasis. However, presence of pre-operative results in less lung function gain presumably due to irreversible lung destruction.



## Chapter 7

# Conclusions & Future Work

In this work, the deformity of the rib cage was investigated for its effect on pulmonary function, the morphology of tracheobronchial tree and lung volumes in idiopathic adolescent scoliosis (AIS) patients with Lenke type 1 and 2 curve types. The hypothesis for this research was that measurements from images obtained through routine clinical care are predictive of pulmonary function impairment in AIS. In particular, measurements which factor in the global thoracic deformity, rather than measurements of the scoliotic spine, are more likely to be successful at predicting respiratory compromise. The specific objectives of this thesis were to identify thoracic features or scoliotic phenotypes which are associated with lung function impairment in AIS; examine possible mechanisms in which lung function impairment is exacerbated by the thoracic deformity; and to identify subgroups most likely to observe lung function improvement postoperatively and benefit from surgical intervention. Some of the key findings in each chapter are summarized below:

- In Chapter 2, radiographic deformity parameters, which included the morphology of the chest wall, were found to be superior to Cobb angle measurements in predicting preoperative lung function. The endotheracic hump ratio, rib hump index, kyphosis-lordosis index and apical vertebral body-rib ratio were found to be significant predictors of pulmonary function. Spinal intrusion, size of the rib hump and narrowing of the convex hemithorax were found to be predictive factors of  $FEV_1$  and FVC whilst  $FEV_1/FVC$  was found to decrease with the loss of kyphosis and increasing rib hump. Hypokyphotic subjects were found to have reduced  $FEV_1/FVC$  relative to normokyphotic and hyperkyphotic patients which improved post-operatively when natural kyphosis was restored.
- Chapter 3 showed that a statistical shape model could be constructed from the outline of the thorax to analyze variations in thoracic shape in scoliosis. The shape model demonstrated that increasing thoracic scoliosis, flattening of the sagittal profile and increased rib hump correspond to reduction in pulmonary function. Sagittal flattening of the thoracic spine is shown increase airway resistance as measured by  $FEV_1/FVC$ . Patients with severe scoliosis, hypokyphosis and large rib humps demonstrate greater increases in post-operative lung function. It was concluded that statistical shape models are a useful morphometric tool which can provide a quantitative and objective description of the thoracic deformity in AIS.

- In Chapter 4, computed-tomography (CT)-based thoracic deformity parameters were measured and correlated with pulmonary function tests. The spinal penetration index, endothoracic hump ration, thoracic rotation, rib hump index and angle of trunk rotation all featured as significant predictors upon multivariate and univariate regression. The analysis revealed that patients with hypokyphosis have more impaired lung function than normo- and hyper-kyphotic patients. The differential, however, is resolved post-operatively if natural kyphosis is restored.
- Chapter 5 consisted of a morphometric study on airway narrowing in AIS patients. Hypokyphotic patients were found to have significant right-sided airway narrowing in the region of the bronchus intermedius and its bifurcation. Interestingly, the right superior segmental bronchus in the right lower lobe was found to be narrowed across all sagittal profiles. Airway lumen area was found to be positively associated with spirometry results. Post-operative expansion of the airways was found to correspond with lung function improvement.
- Chapter 6 was based on an analysis of lung volumes and lung attenuation. The proportion of non-aerated and hyper-aerated volume within each lung was measured to represent atelectasis and air-trapping respectively. Increased spinal intrusion was found to be associated with reduced convex lung volumes and the presence of atelectasis.  $FEV_1/FVC$ , an indicator of airway conductance, was shown to decrease with increased spinal intrusion and increase with the presence of atelectasis. From these results, it was recommended that patients with reduced expiratory volumes and hypokyphotic profiles be investigated for airway obstruction as atelectasis can mask the effects of severe airway obstruction.

## 7.1 Future work

The investigations in this research have been limited to using spirometry results as a metric of pulmonary function. Although  $FEV_1$ , FVC and  $FEV_1/FVC$  are sufficient metrics of pulmonary function, inclusion of other pulmonary function metrics may give a more comprehensive view of pulmonary impairment [134]. Measurements of static lung volumes such as total lung capacity (TLC), function residual capacity (FRC) may offer better insight into lung volume loss whilst increased residual volume (RV) may reflect the presence of air-trapping. Helium dilution techniques can measure FRC whilst full body plethysmography has the ability to measure both FRC and airway resistance. Boyer et al. has demonstrated the incidence of air-trapping in scoliosis using these techniques; the association between these lung function metrics and thoracic deformity could be investigated further [63].

With the advancement in imaging technology, a greater number of studies are performing three-dimensional reconstructions of the ribcage from biplanar radiographs [38, 150]. At the present, EOS imaging technology is not common in clinical practice due to prohibitive costs. However, as it becomes more prevalent, the CT-based thoracic deformity parameters studied in Chapter 4 could be extended to the reconstructed chests from biplanar radiographs in larger cohorts. The availability of three-dimensional co-ordinates would also allow the two-dimensional statistical shape model in Chapter 3 to be extended to a three-dimensional model thus including rotation in the axial plane.

# References

- [1] J. L. Gum, L. G. Lenke, and B. Shay, “The Lenke Classification System for Adolescent Idiopathic Scoliosis,” in *Spinal Deformities*, R. F. Heary and T. J. Albert, Eds. Stuttgart: Georg Thieme Verlag, 2014, p. 49. [Online]. Available: <http://www.thieme-connect.de/products/ebooks/abstract/10.1055/b-0034-99339>
- [2] M. F. O’Brien, T. R. Kuklo, K. M. Blanke, and L. G. Lenke, Eds., *Radiographic measurement manual - Spinal Deformity Study Group*. Medtronic Sofamor Danek USA, 2004.
- [3] C.-K. Lee, K.-H. Koo, and J.-H. An, “The Classification of Idiopathic Scoliosis,” *Journal of Korean Society of Spine Surgery*, vol. 14, no. 1, p. 57, 2007. [Online]. Available: <https://synapse.koreamed.org/DOIx.php?id=10.4184/jkss.2007.14.1.57>
- [4] L. G. Lenke, R. R. Betz, J. Harms, K. H. Bridwell, D. H. Clements, T. G. Lowe, and K. Blanke, “Adolescent Idiopathic Scoliosis,” *The Journal of Bone and Joint Surgery-American Volume*, vol. 83, no. 8, pp. 1169–1181, aug 2001. [Online]. Available: <https://insights.ovid.com/crossref?an=00004623-200108000-00006>
- [5] M. C. Makhni, J. N. Shillingford, J. L. Laratta, S. J. Hyun, and Y. J. Kim, “Restoration of sagittal balance in spinal deformity surgery,” *Journal of Korean Neurosurgical Society*, vol. 61, no. 2, pp. 167–179, 2018.
- [6] M. BERNHARDT and K. H. BRIDWELL, “Segmental Analysis of the Sagittal Plane Alignment of the Normal Thoracic and Lumbar Spines and Thoracolumbar Junction,” *Spine*, vol. 14, no. 7, pp. 717–721, jul 1989. [Online]. Available: <https://insights.ovid.com/crossref?an=00007632-198907000-00012>
- [7] H. Kim, H. S. Kim, E. S. Moon, C. S. Yoon, T. S. Chung, H. T. Song, J. S. Suh, Y. H. Lee, and S. Kim, “Scoliosis imaging: What Radiologists should know,” *Radiographics*, vol. 30, no. 7, pp. 1823–1842, 2010.
- [8] L. A. Goldstein and T. R. Waugh, “Classification and Terminology of Scoliosis,” *Clinical Orthopaedics and Related Research*, vol. 93, no. 93, pp. 10–22, jun 1973. [Online]. Available: <https://insights.ovid.com/crossref?an=00003086-197306000-00003>
- [9] I. A. F. Stokes, L. C. Bigalow, and M. S. Moreland, “Measurement of Axial Rotation of Vertebrae in Scoliosis,” *Spine*, vol. 11, no. 3, pp. 213–218, apr 1986.

- [Online]. Available: <https://insights.ovid.com/crossref?an=00007632-198604000-00006>
- [10] L. G. Lenke, R. R. Betz, D. Clements, A. Merola, T. Haheer, T. Lowe, P. Newton, K. H. Bridwell, and K. Blanke, "Curve prevalence of a new classification of operative adolescent idiopathic scoliosis: does classification correlate with treatment?" *Spine*, vol. 27, no. 6, pp. 604–11, 2002. [Online]. Available: <http://www.ncbi.nlm.nih.gov/pubmed/11884908>
- [11] J. A. Janicki and B. Alman, "Scoliosis: Review of diagnosis and treatment." *Paediatrics & child health*, vol. 12, no. 9, pp. 771–6, nov 2007. [Online]. Available: <http://www.ncbi.nlm.nih.gov/pubmed/19030463>  
<http://www.pubmedcentral.nih.gov/articlerender.fcgi?artid=PMC2532872>
- [12] T. Lowe, S. H. Berven, F. J. Schwab, and K. H. Bridwell, "The SRS Classification for Adult Spinal Deformity," *Spine*, vol. 31, no. Suppl, pp. S119–S125, sep 2006. [Online]. Available: <https://insights.ovid.com/crossref?an=00007632-200609011-00003>
- [13] M. R. Konieczny, H. Senyurt, and R. Krauspe, "Epidemiology of adolescent idiopathic scoliosis," *Journal of Children's Orthopaedics*, vol. 7, no. 1, pp. 3–9, feb 2013. [Online]. Available: <http://online.boneandjoint.org.uk/doi/10.1007/s11832-012-0457-4>
- [14] D. E. Gelb, L. G. Lenke, K. H. Bridwell, K. Blanke, and K. W. McEnery, "An Analysis of Sagittal Spinal Alignment in 100 Asymptomatic Middle and Older Aged Volunteers," *Spine*, vol. 20, no. 12, pp. 1351–1358, jun 1995. [Online]. Available: <https://insights.ovid.com/crossref?an=00007632-199520120-00005>
- [15] H. A. King, J. H. Moe, D. S. Bradford, and R. B. Winter, "The selection of fusion levels in thoracic idiopathic scoliosis." *The Journal of bone and joint surgery. American volume*, vol. 65, no. 9, pp. 1302–13, dec 1983. [Online]. Available: <http://www.ncbi.nlm.nih.gov/pubmed/6654943>
- [16] J. W. Roach, "Adolescent idiopathic scoliosis." *The Orthopedic clinics of North America*, vol. 30, no. 3, pp. 353–65, vii–viii, jul 1999. [Online]. Available: <http://www.ncbi.nlm.nih.gov/pubmed/10393761>
- [17] R. J. Cummings, E. A. Loveless, J. Campbell, S. Samelson, and J. M. Mazur, "Interobserver Reliability and Intraobserver Reproducibility of the System of King et al. for the Classification of Adolescent Idiopathic Scoliosis\*," *The Journal of Bone & Joint Surgery*, vol. 80, no. 8, pp. 1107–11, aug 1998. [Online]. Available: <https://insights.ovid.com/crossref?an=00004623-199808000-00003>
- [18] L. G. Lenke, R. R. Betz, K. H. Bridwell, D. H. Clements, J. Harms, T. G. Lowe, and H. L. Shufflebarger, "Intraobserver and Interobserver Reliability of the Classification of Thoracic Adolescent Idiopathic Scoliosis," *The Journal of Bone & Joint Surgery*, vol. 80, no. 8, pp. 1097–1106, aug 1998. [Online]. Available: <https://insights.ovid.com/crossref?an=00004623-199808000-00002>

- [19] V. Moore, "Spirometry: step by step," *Breathe*, vol. 8, no. 3, pp. 232–240, mar 2012. [Online]. Available: <http://breathe.ersjournals.com/lookup/doi/10.1183/20734735.0021711>
- [20] J. Cotes, D. Chinn, and M. Miller, *Lung Function: Physiology, Measurement and Application in Medicine*, sixth edit ed. Blackwell Publishing, 2006, vol. 50, no. 3.
- [21] M. Rosenthal, S. H. Bain, D. Cramer, P. Helms, D. Denison, A. Bush, and J. O. Warner, "Lung function in white children aged 4 to 19 years: I–Spirometry." *Thorax*, vol. 48, no. 8, pp. 794–802, aug 1993. [Online]. Available: <http://link.springer.com/10.1007/s00117-009-1877-0> <http://thorax.bmj.com/cgi/doi/10.1136/thx.48.8.794>
- [22] P. H. Quanjer, S. Stanojevic, T. J. Cole, X. Baur, G. L. Hall, B. H. Culver, P. L. Enright, J. L. Hankinson, M. S. Ip, J. Zheng, J. Stocks, and C. Schindler, "Multi-ethnic reference values for spirometry for the 3-95-yr age range: The global lung function 2012 equations," *European Respiratory Journal*, vol. 40, no. 6, pp. 1324–1343, 2012.
- [23] P. H. Quanjer, A. Capderou, M. M. Mazicioglu, A. N. Aggarwal, S. D. Banik, S. Popovic, F. A. Tayie, M. Golshan, M. S. Ip, and M. Zelter, "All-age relationship between arm span and height in different ethnic groups," *European Respiratory Journal*, vol. 44, no. 4, pp. 905–912, 2014.
- [24] G. L. Mcphail, Z. Ehsan, S. A. Howells, R. P. Boesch, M. C. Fenchel, R. Szczesniak, V. Jain, S. Agabegi, P. Sturm, E. Wall, and G. J. Redding, "Obstructive Lung Disease in Children with Idiopathic Scoliosis," *The Journal of Pediatrics*, vol. 166, no. 4, pp. 1018–1021, 2015.
- [25] C. Kearon, G. R. Viviani, A. Kirkley, and K. J. Killian, "Factors determining pulmonary function in adolescent idiopathic thoracic scoliosis." *The American review of respiratory disease*, vol. 148, no. 2, pp. 288–94, aug 1993. [Online]. Available: <http://www.ncbi.nlm.nih.gov/pubmed/8342890>
- [26] C. E. Johnston, B. Stephens Richards, D. J. Sucato, K. H. Bridwell, L. G. Lenke, and M. Erickson, "Correlation of preoperative deformity magnitude and pulmonary function tests in adolescent idiopathic scoliosis," *Spine*, vol. 36, no. 14, pp. 1096–1102, 2011.
- [27] M. Dreimann, M. Hoffmann, K. Kossow, W. Hitzl, O. Meier, and H. Koller, "Scoliosis and chest cage deformity measures predicting impairments in pulmonary function: A cross-sectional study of 492 patients with scoliosis to improve the early identification of patients at risk," *Spine*, vol. 39, no. 24, pp. 2024–2033, 2014.
- [28] M. A. Branthwaite, "Cardiorespiratory consequences of unfused idiopathic scoliosis." *British journal of diseases of the chest*, vol. 80, no. 4, pp. 360–9, oct 1986. [Online]. Available: <http://www.ncbi.nlm.nih.gov/pubmed/3620323>
- [29] P. Newton, F. D. Faro, S. Gollogly, R. R. Betz, L. G. Lenke, and T. G. Lowe, "Results of Preoperative Pulmonary Function Testing of Adolescents with Idiopathic



- Scoliosis,” *The Journal of Bone and Joint Surgery*, vol. 87, no. 9, pp. 1937–1946, 2005.
- [30] K. Pehrsson, B. Bake, S. Larsson, and A. Nachemson, “Lung function in adult idiopathic scoliosis: a 20 year follow up.” *Thorax*, vol. 46, no. 7, pp. 474–478, jul 1991. [Online]. Available: <http://thorax.bmj.com/cgi/doi/10.1136/thx.46.7.474>
- [31] E. H. Bergofsky, “Respiratory failure in disorders of the thoracic cage.” *The American review of respiratory disease*, vol. 119, no. 4, pp. 643–69, apr 1979. [Online]. Available: <http://www.ncbi.nlm.nih.gov/pubmed/375788>
- [32] A. Nachemson, “A long term follow-up study of non-treated scoliosis.” *Acta orthopaedica Scandinavica*, vol. 39, no. 4, pp. 466–76, 1968. [Online]. Available: <http://www.ncbi.nlm.nih.gov/pubmed/5726117>
- [33] B. Yaszay, T. P. Bastrom, C. E. Bartley, S. Parent, and P. O. Newton, “The effects of the three-dimensional deformity of adolescent idiopathic scoliosis on pulmonary function,” *European Spine Journal*, vol. 26, no. 6, pp. 1658–1664, 2017.
- [34] S. S. Upadhyay, A. B. Mullaji, K. D. Luk, and J. C. Leong, “Relation of spinal and thoracic cage deformities and their flexibilities with altered pulmonary functions in adolescent idiopathic scoliosis.” *Spine*, vol. 20, no. 22, pp. 2415–20, 1995. [Online]. Available: <http://www.ncbi.nlm.nih.gov/pubmed/8578392>
- [35] S. Takahashi, N. Suzuki, T. Asazuma, K. Kono, T. Ono, and Y. Toyama, “Factors of thoracic cage deformity that affect pulmonary function in adolescent idiopathic thoracic scoliosis,” *Spine*, vol. 32, no. 1, pp. 106–112, 2007.
- [36] S. Aaro and C. Ohlund, “Scoliosis and pulmonary function,” *Spine*, vol. 9, no. 2, pp. 220–222, 1984.
- [37] R. P. Jackson, E. H. Simons, and D. Stripinis, “Coronal and Sagittal Plane Spinal Deformities Correlating with Back Pain and Pulmonary Function in Adult Idiopathic Scoliosis,” *Spine*, vol. 14, no. 12, pp. 1391–1397, dec 1989. [Online]. Available: <https://insights.ovid.com/crossref?an=00007632-198912000-00018>
- [38] B. Ilharreborde, J. Dubousset, W. Skalli, and K. Mazda, “Spinal penetration index assessment in adolescent idiopathic scoliosis using EOS low-dose biplanar stereoradiography,” *European Spine Journal*, vol. 22, no. 11, pp. 2438–2444, 2013.
- [39] M. H. Mehta, “The Rib-Vertebra Angle in the Early Diagnosis Between Resolving and Progressive Infantile Scoliosis,” *The Journal of Bone and Joint Surgery. British volume*, vol. 54-B, no. 2, pp. 230–243, may 1972. [Online]. Available: <http://online.boneandjoint.org.uk/doi/10.1302/0301-620X.54B2.230>
- [40] J. Dubousset, P. Wicart, V. Pomeroy, A. Barois, and B. Estournet, “Spinal penetration index: New three-dimensional quantified reference for lordoscoliosis and other spinal deformities,” *Journal of Orthopaedic Science*, vol. 8, no. 1, pp. 41–49, 2003.

- [41] T. R. Kuklo, B. K. Potter, and L. G. Lenke, "Vertebral Rotation and Thoracic Torsion in Adolescent Idiopathic Scoliosis," *Journal of Spinal Disorders & Techniques*, vol. 18, no. 2, pp. 139–147, 2005.
- [42] S. A. Voutsinas and G. D. MacEwen, "Sagittal Profiles of the Spine," *Clinical Orthopaedics & Related Research*, vol. 210, pp. 235–242, 1986.
- [43] T. Vrtovec, F. Pernuš, and B. Likar, "A review of methods for quantitative evaluation of spinal curvature," *European Spine Journal*, vol. 18, no. 5, pp. 593–607, may 2009. [Online]. Available: <http://link.springer.com/10.1007/s00586-009-0913-0>
- [44] R. Campbell, M. Smith, T. Mayes, J. Mangos, D. Willey-Courand, N. Kose, R. Pinero, M. Alder, H. Duong, and J. Surber, "The Characteristics of Thoracic Insufficiency Syndrome Congenital Scoliosis," *The Journal of Bone and Joint Surgery*, vol. 85, no. 3, pp. 399–408, 2003.
- [45] T. B. Grivas, S. Dangas, B. D. Polyzois, and P. Samelis, "The Double Rib Contour Sign (DRCS) in lateral spinal radiographs, aetiologic implications for scoliosis," *Studies in Health Technology and Informatics*, vol. 88, pp. 38–43, 2002.
- [46] T. B. Grivas, "Rib index," *Scoliosis*, vol. 9, no. 1, p. 20, dec 2014. [Online]. Available: <https://scoliosisjournal.biomedcentral.com/articles/10.1186/s13013-014-0020-9>
- [47] K. C. Soultanis, K. Tsiavos, T. B. Grivas, N. A. Stavropoulos, V. I. Sakallariou, A. F. Mavrogenis, and P. J. Papagelopoulos, "Reliability study for rib index," *Scoliosis*, vol. 10, no. S1, pp. 4–7, 2015.
- [48] Y. J. Kim, L. G. Lenke, K. H. Bridwell, G. Cheh, J. Whorton, and B. Sides, "Prospective pulmonary function comparison following posterior segmental spinal instrumentation and fusion of adolescent idiopathic scoliosis: Is there a relationship between major thoracic curve correction and pulmonary function test improvement?" *Spine*, vol. 32, no. 24, pp. 2685–2693, 2007.
- [49] K. Pehrsson, A. Danielsson, and A. Nachemson, "Pulmonary function in adolescent idiopathic scoliosis: a 25 year follow up after surgery or start of brace treatment." *Thorax*, vol. 56, no. 5, pp. 388–93, may 2001.
- [50] M. R. Miller, J. Hankinson, V. Brusasco, F. Burgos, R. Casaburi, A. Coates, R. Crapo, P. Enright, C. P. van der Grinten, P. Gustafsson, R. Jensen, D. C. Johnson, N. MacIntyre, R. McKay, D. Navajas, O. F. Pedersen, R. Pellegrino, G. Viegi, and J. Wagner, "Standardisation of spirometry," *European Respiratory Journal*, vol. 26, no. 2, pp. 319–338, 2005.
- [51] K. Ito, N. Kawakami, K. Miyasaka, T. Tsuji, T. Ohara, and A. Nohara, "Scoliosis associated with airflow obstruction due to endothoracic vertebral hump," *Spine*, vol. 37, no. 25, pp. 2094–2098, 2012.
- [52] Y. Benjamini and Y. Hochberg, "Controlling the False Discovery Rate: A Practical and Powerful Approach to Multiple Testing," *Journal of the Royal Statistical Society. Series B (Methodological)*, vol. 57, no. 1, pp. 289–300, 1995.

- [53] Z. Zhang, "Variable selection with stepwise and best subset approaches," *Annals of Translational Medicine*, vol. 4, no. 7, pp. 136–136, apr 2016. [Online]. Available: <http://atm.amegroups.com/article/view/9706/10561>
- [54] T. Akazawa, S. Kuroya, M. Inuma, K. Asano, Y. Torii, T. Umehara, T. Kotani, T. Sakuma, S. Minami, S. Orita, K. Inage, K. Fujimoto, Y. Shiga, G. Inoue, M. Miyagi, W. Saito, S. Ohtori, and H. Niki, "Pulmonary function and thoracic deformities in adolescent idiopathic scoliosis 27 years or longer after spinal fusion with Harrington instrument," *Journal of Orthopaedic Science*, vol. 23, no. 1, pp. 45–50, 2018. [Online]. Available: <https://doi.org/10.1016/j.jos.2017.08.016>
- [55] S. Aaro and M. Dahlborn, "The Longitudinal Axis Rotation of the Apical Vertebra, the Vertebral, Spinal, and Rib Cage Deformity in Idiopathic Scoliosis Studied by Computer Tomography," *Spine*, vol. 6, no. 6, pp. 567–572, 1981.
- [56] T. R. Easwar, J. Y. Hong, J. H. Yang, S. W. Suh, and H. N. Modi, "Does lateral vertebral translation correspond to Cobb angle and relate in the same way to axial vertebral rotation and rib hump index? A radiographic analysis on idiopathic scoliosis," *European Spine Journal*, vol. 20, no. 7, pp. 1095–1105, 2011.
- [57] T. B. Sullivan, F. G. Reighard, E. J. Osborn, K. C. Parvaresh, and P. O. Newton, "Thoracic Idiopathic Scoliosis Severity Is Highly Correlated with 3D Measures of Thoracic Kyphosis," *The Journal of Bone and Joint Surgery*, vol. 99, no. 11, p. e54, jun 2017. [Online]. Available: <http://insights.ovid.com/crossref?an=00004623-201706070-00011>
- [58] J. A. Harris, O. H. Mayer, S. A. Shah, R. M. Campbell, and S. Balasubramanian, "A comprehensive review of thoracic deformity parameters in scoliosis," *European Spine Journal*, vol. 23, no. 12, pp. 2594–2602, 2014.
- [59] Y. Wen, S. Kai, Z. Yong-gang, Z. Guo-quan, and D. Tian-xiang, "Relationship between Lung Volume and Pulmonary Function in Patients With Adolescent Idiopathic Scoliosis," *Clinical Spine Surgery*, vol. 29, no. 8, pp. E396–E400, oct 2016. [Online]. Available: <http://insights.ovid.com/crossref?an=01933606-201610000-00011>
- [60] C. J. Adam, S. C. Cargill, and G. N. Askin, "Computed Tomographic-Based Volumetric Reconstruction of the Pulmonary System in Scoliosis," *Journal of Pediatric Orthopaedics*, vol. 27, no. 6, pp. 677–681, sep 2007. [Online]. Available: <https://insights.ovid.com/crossref?an=01241398-200709000-00015>
- [61] C. G. T. Ledonio, B. E. Rosenstein, C. E. Johnston, W. E. Regelman, D. J. Nuckley, and D. W. Polly, "Pulmonary function tests correlated with thoracic volumes in adolescent idiopathic scoliosis," *Journal of Orthopaedic Research*, vol. 35, no. 1, pp. 175–182, 2017.
- [62] T. Kotani, S. Minami, K. Takahashi, K. Isobe, Y. Nakata, M. Takaso, M. Inoue, T. Maruta, T. Akazawa, T. Ueda, and H. Moriya, "An Analysis of Chest Wall and Diaphragm Motions in Patients With Idiopathic Scoliosis Using Dynamic Breathing MRI," *Spine*, vol. 29, no. 3, pp. 298–302, feb 2004. [Online]. Available: <https://insights.ovid.com/crossref?an=00007632-200402010-00012>

- [63] J. Boyer, N. Amin, R. Taddonio, and a. J. Dozor, "Evidence of airway obstruction in children with idiopathic scoliosis," *Chest*, vol. 109, pp. 1532–1535, 1996.
- [64] S. Alotaibi, J. Harder, and S. Spier, "Bronchial obstruction secondary to idiopathic scoliosis in a child: A case report," *Journal of Medical Case Reports*, vol. 2, pp. 2–5, 2008.
- [65] M. Qiabi, K. Chagnon, A. Beaupré, J. Hercun, and G. Rakovich, "Scoliosis and bronchial obstruction," *Canadian Respiratory Journal*, vol. 22, no. 4, pp. 206–208, 2015.
- [66] P. Goussard, R. Gie, S. Andronikou, and P. R. Fourie, "A correctable cause of lung collapse in an adolescent with severe scoliosis causing compression of the bronchial tree," *Case Reports*, vol. 2013, no. nov15 1, pp. bcr2013 202 017–bcr2 013 202 017, nov 2013. [Online]. Available: <http://casereports.bmj.com/cgi/doi/10.1136/bcr-2013-202017>
- [67] W. Bartlett, E. Garrido, C. Wallis, S. K. Tucker, and H. Noordeen, "Lordoscoliosis and large intrathoracic airway obstruction," *Spine*, vol. 34, no. 1, pp. 59–65, 2009.
- [68] T. Fujii, K. Watanabe, Y. Toyama, and M. Matsumoto, "Pulmonary function recovery demonstrated by ventilation-perfusion scan after posterior vertebral column resection for severe adolescent idiopathic scoliosis: A case report," *Spine*, vol. 39, no. 19, pp. 1190–1194, 2014.
- [69] B. A. Rawlins, R. B. Winter, J. E. Lonstein, F. Denis, P. T. Kubic, W. B. Wheeler, and A. L. Ozolins, "Reconstructive Spine Surgery in Pediatric Patients with Major Loss in Vital Capacity," *Journal of Pediatric Orthopaedics*, vol. 16, no. 3, pp. 284–292, may 1996. [Online]. Available: <http://gateway.ovid.com/ovidweb.cgi?T=JS&PAGE=crossref&AN=00004694-199605000-00002>
- [70] J. Payo, F. S. Perez-Grueso, N. Fernandez-Baillo, and A. Garcia, "Severe restrictive lung disease and vertebral surgery in a pediatric population," *European Spine Journal*, vol. 18, no. 12, pp. 1905–1910, dec 2009. [Online]. Available: <http://link.springer.com/10.1007/s00586-009-1084-8>
- [71] R. Vedantam, L. G. Lenke, K. H. Bridwell, J. Haas, and D. A. Linville, "A Prospective Evaluation of Pulmonary Function in Patients With Adolescent Idiopathic Scoliosis Relative to the Surgical Approach Used for Spinal Arthrodesis," *Spine*, vol. 25, no. 1, pp. 82–90, 2000.
- [72] T. Cootes, "Model-Based Methods in Analysis of Biomedical Images," *Image processing and analysis a practical approach*, pp. 223–248, 2000.
- [73] T. Heimann, B. van Ginneken, M. Styner, Y. Arzhaeva, V. Aurich, C. Bauer, A. Beck, C. Becker, R. Beichel, G. Bekes, F. Bello, G. Binnig, H. Bischof, A. Bornik, P. Cashman, Ying Chi, A. Cordova, B. Dawant, M. Fidrich, J. Furst, D. Furukawa, L. Grenacher, J. Hornegger, D. Kainmuller, R. Kitney, H. Kobatake, H. Lamecker, T. Lange, Jeongjin Lee, B. Lennon, Rui Li, Senhu Li,

- H.-P. Meinzer, G. Nemeth, D. Raicu, A.-M. Rau, E. van Rikxoort, M. Rousson, L. Rusko, K. Saggi, G. Schmidt, D. Seghers, A. Shimizu, P. Slagmolen, E. Sorantin, G. Soza, R. Susomboon, J. Waite, A. Wimmer, and I. Wolf, "Comparison and Evaluation of Methods for Liver Segmentation From CT Datasets," *IEEE Transactions on Medical Imaging*, vol. 28, no. 8, pp. 1251–1265, aug 2009. [Online]. Available: <http://ieeexplore.ieee.org/document/4781564/>
- [74] S. M. Humphries, K. S. Hunter, R. Shandas, R. R. Deterding, and E. M. DeBoer, "Analysis of pediatric airway morphology using statistical shape modeling," *Medical & Biological Engineering & Computing*, vol. 54, no. 6, pp. 899–911, 2016. [Online]. Available: <http://link.springer.com/10.1007/s11517-015-1445-x>
- [75] E. J. Mastej, E. M. DeBoer, S. M. Humphries, M. C. Cook, K. S. Hunter, D. R. Liptzin, J. P. Weinman, and R. R. Deterding, "Lung and airway shape in neuroendocrine cell hyperplasia of infancy," *Pediatric Radiology*, pp. 1–10, 2018.
- [76] M. Lüthi, A. Forster, T. Gerig, and T. Vetter, "Shape Modeling Using Gaussian Process Morphable Models," in *Statistical Shape and Deformation Analysis*, 1st ed. Elsevier, 2017, pp. 165–191. [Online]. Available: <http://dx.doi.org/10.1016/B978-0-12-810493-4.00008-0>  
<https://linkinghub.elsevier.com/retrieve/pii/B9780128104934000080>
- [77] S. Allen, E. Parent, M. Khorasani, D. L. Hill, E. Lou, and J. V. Raso, "Validity and Reliability of Active Shape Models for the Estimation of Cobb Angle in Patients with Adolescent Idiopathic Scoliosis," *Journal of Digital Imaging*, vol. 21, no. 2, pp. 208–218, jun 2008. [Online]. Available: <http://link.springer.com/10.1007/s10278-007-9026-7>
- [78] J. Boisvert, X. Pennec, H. Labelle, F. Chieriet, and N. Ayache, "Principal Spine Shape Deformation Modes Using Riemannian Geometry and Articulated Models," in *Lecture Notes in Computer Science (including subseries Lecture Notes in Artificial Intelligence and Lecture Notes in Bioinformatics)*, 2006, vol. 4069 LNCS, no. July, pp. 346–355. [Online]. Available: [http://link.springer.com/10.1007/11789239\\_36](http://link.springer.com/10.1007/11789239_36)
- [79] J. Boisvert, F. Chieriet, X. Pennec, H. Labelle, and N. Ayache, "Principal Deformations Modes of Articulated Models for the Analysis of 3D Spine Deformities," *ELCVIA Electronic Letters on Computer Vision and Image Analysis*, vol. 7, no. 4, p. 13, dec 2008. [Online]. Available: <http://elcvia.cvc.uab.es/article/view/v7-n4-boisvert-chieriet-pennec-et-al>
- [80] —, "Geometric variability of the scoliotic spine using statistics on articulated shape models," *IEEE Transactions on Medical Imaging*, vol. 27, no. 4, pp. 557–568, 2008.
- [81] D. C. Moura, J. Boisvert, J. G. Barbosa, H. Labelle, and J. M. R. Tavares, "Fast 3D reconstruction of the spine from biplanar radiographs using a deformable articulated model," *Medical Engineering & Physics*, vol. 33, no. 8, pp. 924–933, oct 2011. [Online]. Available: <http://dx.doi.org/10.1016/j.medengphy.2011.03.007>  
<https://linkinghub.elsevier.com/retrieve/pii/S135045331100066X>

- [82] J. F. Hollenbeck, C. M. Cain, J. A. Fattor, P. J. Rullkoetter, and P. J. Laz, “Statistical shape modeling characterizes three-dimensional shape and alignment variability in the lumbar spine,” *Journal of Biomechanics*, vol. 69, pp. 146–155, 2018. [Online]. Available: <https://doi.org/10.1016/j.jbiomech.2018.01.020>
- [83] X. Shi, L. Cao, M. P. Reed, J. D. Rupp, C. N. Hoff, and J. Hu, “A statistical human rib cage geometry model accounting for variations by age, sex, stature and body mass index,” *Journal of Biomechanics*, vol. 47, no. 10, pp. 2277–2285, 2014. [Online]. Available: <http://dx.doi.org/10.1016/j.jbiomech.2014.04.045>
- [84] M. L. Zelditch, D. L. Swiderski, and H. D. Sheets, “Simple Size and Shape Variables,” in *Geometric Morphometrics for Biologists*. Elsevier, 2012, pp. 51–74. [Online]. Available: <https://linkinghub.elsevier.com/retrieve/pii/B9780123869036000010>  
<https://linkinghub.elsevier.com/retrieve/pii/B9780123869036000034>
- [85] D. C. Adams and E. Otárola-Castillo, “geomorph: an R package for the collection and analysis of geometric morphometric shape data,” *Methods in Ecology and Evolution*, vol. 4, no. 4, pp. 393–399, apr 2013. [Online]. Available: <http://doi.wiley.com/10.1111/2041-210X.12035>
- [86] S. Aaro and M. Dahlborn, “Estimation of vertebral rotation and the Spinal and Rib Cage Deformity in Scoliosis by Computer Tomography,” *Spine*, vol. 6, no. 5, pp. 460–467, 1981.
- [87] C. L. Nash, E. C. Gregg, R. H. Brown, and K. Pillai, “Risks of exposure to X-rays in patients undergoing long-term treatment for scoliosis.” *The Journal of bone and joint surgery. American volume*, vol. 61, no. 3, pp. 371–4, apr 1979. [Online]. Available: <http://www.ncbi.nlm.nih.gov/pubmed/429405>
- [88] S.-Y. Ng and J. Bettany-Saltikov, “Imaging in the Diagnosis and Monitoring of Children with Idiopathic Scoliosis,” *The Open Orthopaedics Journal*, vol. 11, no. 1, pp. 1500–1520, 2018.
- [89] S. M. Presciutti, T. Karukanda, and M. Lee, “Management decisions for adolescent idiopathic scoliosis significantly affect patient radiation exposure,” *Spine Journal*, vol. 14, no. 9, pp. 1984–1990, 2014. [Online]. Available: <http://dx.doi.org/10.1016/j.spinee.2013.11.055>
- [90] B. S. Richards, D. J. Sucato, D. E. Konigsberg, and J. A. Ouellet, “Comparison of Reliability Between the Lenke and King Classification Systems for Adolescent Idiopathic Scoliosis Using Radiographs That Were Not Premeasured,” *Spine*, vol. 28, no. 11, pp. 1148–1156, jun 2003. [Online]. Available: <https://insights.ovid.com/crossref?an=00007632-200306010-00012>
- [91] S. H. Mao, Y. Qiu, Z. Z. Zhu, F. Zhu, Z. Liu, and B. Wang, “Clinical evaluation of the anterior chest wall deformity in thoracic adolescent idiopathic scoliosis,” *Spine*, vol. 37, no. 9, pp. E540–E548, 2012.
- [92] J. A. J. Haller, S. S. Kramer, and S. A. Lietman, “Use of CT scans in selection of patients for pectusexcavatum surgery: A preliminary report,” *Journal of Pediatric Surgery*, vol. 22, no. 10, pp. 904–906, 1987.

- [93] A. Kilda, A. Basevicius, V. Barauskas, S. Lukosevicius, and D. Ragaisis, "Radiological assessment of children with pectus excavatum," *The Indian Journal of Pediatrics*, vol. 74, no. 2, pp. 143–147, feb 2007. [Online]. Available: <http://link.springer.com/10.1007/s12098-007-0007-0>
- [94] J. Y. Hong, S. W. Suh, H. J. Park, Y. H. Kim, J. H. Park, and S. Y. Park, "Correlations of adolescent idiopathic scoliosis and pectus excavatum," *Journal of Pediatric Orthopaedics*, vol. 31, no. 8, pp. 870–874, 2011.
- [95] R. Tauchi, N. Kawakami, T. Tsuji, T. Ohara, Y. Suzuki, T. Saito, and A. Nohara, "Evaluation of thoracic factors after scoliosis surgery in patients with both scoliosis and pectus excavatum," *European Spine Journal*, vol. 27, no. 2, pp. 381–387, 2018.
- [96] S. Delorme, P. Violas, J. Dansereau, J. De Guise, C. A. Aubin, and H. Labelle, "Preoperative and early postoperative three-dimensional changes of the rib cage after posterior instrumentation in adolescent idiopathic scoliosis," *European Spine Journal*, vol. 10, no. 2, pp. 101–106, 2001.
- [97] B. Geyer and Y. Le Merrer, "Clinical landmarks, horizontal strains and prognosis in thoracic scoliosis," *Studies in Health Technology and Informatics*, vol. 37, pp. 327–330, 1997.
- [98] R. Winter, W. Lovell, and J. Moe, "Excessive thoracic lordosis and loss of pulmonary function in patients with idiopathic scoliosis," *Journal of Bone and Joint Surgery - American Volume*, vol. 57, no. 7, pp. 972–977, 1975.
- [99] S. Demura, T. P. Bastrom, J. Schlechter, B. Yaszay, and P. O. Newton, "Should postoperative pulmonary function be a criterion that affects upper instrumented vertebra selection in adolescent idiopathic scoliosis surgery?" *Spine*, vol. 38, no. 22, pp. 1920–1926, 2013.
- [100] Y. Kim, L. Lenke, J. Kim, K. Bridwell, S. Cho, G. Cheh, and B. Sides, "Comparative analysis of pedicle screw versus hybrid instrumentation in posterior spinal fusion of adolescent idiopathic scoliosis," *Spine*, vol. 31, no. 3, pp. 291–298, 2006.
- [101] J. E. Lowenstein, H. Matsumoto, M. G. Vitale, M. Weidenbaum, J. A. Gomez, F. Y.-I. Lee, J. E. Hyman, and D. P. Roye, "Coronal and Sagittal Plane Correction in Adolescent Idiopathic Scoliosis," *Spine*, vol. 32, no. 4, pp. 448–452, 2007.
- [102] T. de Jonge, J. Dubousset, and T. Illes, "Sagittal plane correction in idiopathic scoliosis," *Spine*, vol. 27, no. 7, pp. 754–760, 2002.
- [103] S.-I. Suk, W.-J. Kim, J.-H. Kim, and S.-M. Lee, "Restoration of thoracic kyphosis in the hypokyphotic spine: A comparison between multiple-hook and segmental pedicle screw fixation in adolescent idiopathic scoliosis," *Journal of Spinal Disorders*, vol. 12, no. 6, pp. 489–495, 1999.
- [104] D. A. Hoffman, J. E. Lonstein, M. M. Morin, W. Visscher, B. S. H. Harris, and J. D. Boice, "Breast Cancer in Women With Scoliosis Exposed to Multiple Diagnostic X Rays," *JNCI Journal of the National*

- Cancer Institute*, vol. 81, no. 17, pp. 1307–1312, sep 1989. [Online]. Available: [papers://7fb3a579-17eb-4f3e-967a-87b6e77fe28f/Paper/p1749](https://papers://7fb3a579-17eb-4f3e-967a-87b6e77fe28f/Paper/p1749)  
<https://academic.oup.com/jnci/article-lookup/doi/10.1093/jnci/81.17.1307>
- [105] M. K. Kalra, P. Quick, S. Singh, M. Sandborg, and A. Persson, “Whole spine CT for evaluation of scoliosis in children: Feasibility of sub-milliSievert scanning protocol,” *Acta Radiologica*, vol. 54, no. 2, pp. 226–230, mar 2013. [Online]. Available: <http://journals.sagepub.com/doi/10.1258/ar.2012.110625>
- [106] S. Redla, T. Sikdar, and A. Saifuddin, “Magnetic Resonance Imaging of Scoliosis,” *Clinical Radiology*, vol. 56, no. 5, pp. 360–371, may 2001. [Online]. Available: <https://linkinghub.elsevier.com/retrieve/pii/S0009926001906762>
- [107] A. P. Trenga, A. Singla, M. A. Feger, and M. F. Abel, “Patterns of congenital bony spinal deformity and associated neural anomalies on X-ray and magnetic resonance imaging,” *Journal of Children’s Orthopaedics*, vol. 10, no. 4, pp. 343–352, aug 2016. [Online]. Available: <http://online.boneandjoint.org.uk/doi/10.1007/s11832-016-0752-6>
- [108] B. Ilharreborde, E. Ferrero, M. Alison, and K. Mazda, “EOS microdose protocol for the radiological follow-up of adolescent idiopathic scoliosis,” *European Spine Journal*, vol. 25, no. 2, pp. 526–531, 2016.
- [109] R. C. Brink, D. Colo, T. P. C. Schlösser, K. L. Vincken, M. van Stralen, S. C. N. Hui, L. Shi, W. C. W. Chu, J. C. Y. Cheng, and R. M. Castelein, “Upright, prone, and supine spinal morphology and alignment in adolescent idiopathic scoliosis,” *Scoliosis and Spinal Disorders*, vol. 12, no. 1, p. 6, dec 2017. [Online]. Available: <http://scoliosisjournal.biomedcentral.com/articles/10.1186/s13013-017-0111-5>
- [110] M. Yazici, E. R. Acaroglu, A. Alanay, V. Deviren, A. Cila, and A. Surat, “Measurement of vertebral rotation in standing versus supine position in adolescent idiopathic scoliosis,” *Journal of Pediatric Orthopaedics*, vol. 21, no. 2, pp. 252–256, 2001.
- [111] T. D. Barwick, I. Goddard, M. Easty, C. Wallis, and L. Biassoni, “Postural change in ventilation and perfusion secondary to a thoracic scoliosis with complete resolution after surgery,” *British Journal of Radiology*, vol. 82, no. 979, pp. 137–140, 2009.
- [112] W. E. Holden, W. A. Carr, and R. K. Beals, “Position dependence of pulmonary function in a patient with lordoscoliosis,” *European Journal of Respiratory Diseases*, vol. 68, no. 2, pp. 146–150, 1986.
- [113] S. Katz, N. Arish, A. Rokach, Y. Zaltzman, and E. L. Marcus, “The effect of body position on pulmonary function: A systematic review,” *BMC Pulmonary Medicine*, vol. 18, no. 1, pp. 1–16, 2018.
- [114] J. Farrell and E. Garrido, “Effect of idiopathic thoracic scoliosis on the tracheobronchial tree,” *BMJ Open Respiratory Research*, vol. 5, no. 1, p. e000264, mar 2018. [Online]. Available: <http://bmjopenrespres.bmj.com/content/5/1/e000264.abstract>  
<http://bmjopenrespres.bmj.com/lookup/doi/10.1136/bmjresp-2017-000264>



- [115] G. Scuder, D. P. Sanders, R. M. Brustowicz, C. B. Berde, A. Colin, J. Allen, G. B. Healy, and J. E. Hall, "Postoperative Lordoscoliosis Causing Extrinsic Compression of the Right Main Stem Bronchus and Respiratory Insufficiency," *Spine*, vol. 14, no. 1, pp. 110–114, 1989.
- [116] K. Al-Kattan, A. Simonds, K. F. Chung, and D. K. Kaplan, "Kyphoscoliosis and bronchial torsion," *Chest*, vol. 111, no. 4, pp. 1134–1137, 1997.
- [117] P. M. Ter Wee, W. J. Luth, A. C. Van der Schee, and J. Stam, "Scoliosis as cause of pulmonary atelectasis," *European Respiratory Journal*, vol. 4, no. 3, pp. 371–373, 1991.
- [118] T. M. Andrews, C. M. Myer, and S. P. Gray, "Abnormalities of the bony thorax causing tracheobronchial compression," *International Journal of Pediatric Otorhinolaryngology*, vol. 19, no. 2, pp. 139–144, 1990.
- [119] L. F. Donnelly and G. S. Bisset, "Airway compression in children with abnormal thoracic configuration," *Radiology*, vol. 206, no. 2, pp. 323–326, 1998.
- [120] Y. Tatekawa, T. Tojo, H. Kanehiro, and Y. Nakajima, "Multistage approach for tracheobronchomalacia caused by a chest deformity in the setting of severe scoliosis," *Surgery Today*, vol. 37, no. 10, pp. 910–914, 2007.
- [121] P. J. Reynisson, M. Scali, E. Smistad, E. F. Hofstad, H. O. Leira, F. Lindseth, T. A. N. Hernes, T. Amundsen, H. Sorger, and T. Langø, "Airway segmentation and centerline extraction from thoracic CT - Comparison of a new method to state of the art commercialized methods," *PLoS ONE*, vol. 10, no. 12, pp. 1–20, 2015.
- [122] W. Dakkak and A. R. Tonelli, "Compression of adjacent anatomical structures by pulmonary artery dilation," *Postgraduate Medicine*, vol. 128, no. 5, pp. 451–459, 2016. [Online]. Available: <http://dx.doi.org/10.1080/00325481.2016.1157442>
- [123] J. Bjure, G. Grimby, J. Kasalický, M. Lindh, and A. Nachemson, "Respiratory impairment and airway closure in patients with untreated idiopathic scoliosis." *Thorax*, vol. 25, no. 4, pp. 451–456, 1970.
- [124] T. Daimon, K. Fujimoto, K. Tanaka, J. Yamamoto, K. Nishimura, Y. Tanaka, M. Yanagawa, H. Sumikawa, A. Inoue, O. Honda, N. Tomiyama, H. Nakamura, Y. Sugiyama, and T. Johkoh, "Volume of pulmonary lobes and segments in chronic obstructive pulmonary diseases calculated using newly developed three-dimensional software," *Japanese Journal of Radiology*, vol. 27, no. 3, pp. 115–122, 2009.
- [125] Q. Hamid, J. Shannon, and J. Martin, *Physiologic Basis of Respiratory Disease*. Hamilton: BC Decker, 2005.
- [126] K. Carden, P. Boiselle, D. Waltz, and A. Ernst, "Tracheomalacia and Tracheobronchomalacia in Children and Adults: An In-depth Review," *Chest*, vol. 127, no. 3, pp. 984–1005, 2005.

- [127] E. Sorantin, B. Geiger, F. Lindbichler, E. Eber, and G. Schimpl, "CT-based virtual tracheobronchoscopy in children - Comparison with axial CT and multi-planar reconstruction: Preliminary results," *Pediatric Radiology*, vol. 32, no. 1, pp. 8–15, 2002.
- [128] K. S. Lee, M. R. Sun, A. Ernst, D. Feller-Kopman, A. Majid, and P. M. Boiselle, "Comparison of dynamic expiratory CT with bronchoscopy for diagnosing airway malacia: A pilot evaluation," *Chest*, vol. 131, no. 3, pp. 758–764, 2007.
- [129] W. Huda, S. C. Bushong, and W. R. Hendee, "In x-ray computed tomography, technique factors should be selected appropriate to patient size," *Medical Physics*, vol. 28, no. 8, pp. 1543–1545, aug 2001. [Online]. Available: <http://doi.wiley.com/10.1118/1.1415075>  
<http://doi.wiley.com/10.1118/1.1388903>
- [130] J. Z. Y. Tan, M. Crossett, and M. Ditchfield, "Dynamic volumetric computed tomographic assessment of the young paediatric airway: Initial experience of rapid, non-invasive, four-dimensional technique," *Journal of Medical Imaging and Radiation Oncology*, vol. 57, no. 2, pp. 141–148, 2013.
- [131] S. Fain, M. L. Schiebler, D. G. McCormack, and G. Parraga, "Imaging of lung function using hyperpolarized helium-3 magnetic resonance imaging: Review of current and emerging translational methods and applications," *Journal of Magnetic Resonance Imaging*, vol. 32, no. 6, pp. 1398–1408, 2010.
- [132] S. Imagama, N. Kawakami, T. Tsuji, T. Ohara, A. Nohara, Y. Matsubara, T. Kanemura, Y. Katayama, R. Tauchi, and N. Ishiguro, "Improvement of atelectasis after corrective fusion for lordoscoliosis with intrathoracic vertebral protrusion in arthrogryposis multiplex congenita: Efficacy of positive-pressure ventilation test," *Journal of Orthopaedic Science*, vol. 18, no. 5, pp. 856–860, 2013. [Online]. Available: <http://dx.doi.org/10.1007/s00776-012-0216-x>
- [133] J.-L. Clement, E. Chau, C. Kimkpe, and M.-J. Vallade, "Restoration of Thoracic Kyphosis by Posterior Instrumentation in Adolescent Idiopathic Scoliosis," *Spine*, vol. 33, no. 14, pp. 1579–1587, 2008.
- [134] T. Tsiligiannis and T. Grivas, "Pulmonary function in children with idiopathic scoliosis," *Scoliosis*, vol. 7, no. 1, p. 7, dec 2012. [Online]. Available: <https://scoliosisjournal.biomedcentral.com/articles/10.1186/1748-7161-7-7>
- [135] E. M. Chun, S. W. Suh, H. N. Modi, E. Y. Kang, S. J. Hong, and H.-R. Song, "The change in ratio of convex and concave lung volume in adolescent idiopathic scoliosis: a 3D CT scan based cross sectional study of effect of severity of curve on convex and concave lung volumes in 99 cases," *European Spine Journal*, vol. 17, no. 2, pp. 224–229, feb 2008. [Online]. Available: <http://link.springer.com/10.1007/s00586-007-0488-6>
- [136] A. van Ooij, A. van Belle, R. Timmer, and L. van Rhijn, "The Destroyed Lung Syndrome: Report of a Case After Harrington Rod Instrumentation and Fusion for Idiopathic Scoliosis," *Spine*, vol. 27, no. 14, pp. E337–E341, 2002.

- [137] S. R. Vieira, L. Puybasset, J. Richecoeur, Q. Lu, P. Cluzel, P. B. Gusman, P. Coriat, and J. J. Rouby, "A lung computed tomographic assessment of positive end-expiratory pressure-induced lung overdistension," *American Journal of Respiratory and Critical Care Medicine*, vol. 158, no. 5 PART I, pp. 1571–1577, 1998.
- [138] J. Karmrodt, C. Bletz, S. Yuan, M. David, C.-P. Heussel, and K. Markstaller, "Quantification of atelectatic lung volumes in two different porcine models of ARDS †," *British Journal of Anaesthesia*, vol. 97, no. 6, pp. 883–895, dec 2006. [Online]. Available: <http://dx.doi.org/10.1093/bja/ael275> <https://linkinghub.elsevier.com/retrieve/pii/S0007091217353448>
- [139] A. W. Reske, A. Rau, A. P. Reske, M. Koziol, B. Gottwald, M. Alef, J.-C. Ionita, P. M. Spieth, P. Hepp, M. Seiwerts, A. Beda, S. Born, G. Scheuermann, M. B. Amato, and H. Wrigge, "Extrapolation in the analysis of lung aeration by computed tomography: a validation study," *Critical Care*, vol. 15, no. 6, p. R279, 2011. [Online]. Available: <http://ccforum.com/content/15/6/R279> <http://ccforum.biomedcentral.com/articles/10.1186/cc10563>
- [140] A.-S. Eichenberger, S. Proietti, S. Wicky, P. Frascarolo, M. Suter, D. R. Spahn, and L. Magnusson, "Morbid Obesity and Postoperative Pulmonary Atelectasis: An Underestimated Problem," *Anesthesia & Analgesia*, vol. 95, no. 6, pp. 1788–1792, dec 2002. [Online]. Available: <https://insights.ovid.com/crossref?an=00000539-200212000-00060>
- [141] L. Gunnarsson, L. Tokics, H. Lundquist, B. Brismar, A. Strandberg, B. Berg, and G. Hedenstierna, "Chronic obstructive pulmonary disease and anaesthesia: formation of atelectasis and gas exchange impairment." *The European respiratory journal*, vol. 4, no. 9, pp. 1106–16, oct 1991. [Online]. Available: <http://www.ncbi.nlm.nih.gov/pubmed/1756845>
- [142] L. Magnusson and D. Spahn, "New concepts of atelectasis during general anaesthesia," *British Journal of Anaesthesia*, vol. 91, no. 1, pp. 61–72, jul 2003. [Online]. Available: <https://linkinghub.elsevier.com/retrieve/pii/S0007091217374974>
- [143] O. M. Mets, I. Isgum, C. P. Mol, H. A. Gietema, P. Zanen, M. Prokop, and P. A. de Jong, "Variation in quantitative CT air trapping in heavy smokers on repeat CT examinations," *European Radiology*, vol. 22, no. 12, pp. 2710–2717, dec 2012. [Online]. Available: <http://link.springer.com/10.1007/s00330-012-2526-y>
- [144] O. M. Mets, R. A. van Hulst, C. Jacobs, B. van Ginneken, and P. A. de Jong, "Normal Range of Emphysema and Air Trapping on CT in Young Men," *American Journal of Roentgenology*, vol. 199, no. 2, pp. 336–340, aug 2012. [Online]. Available: <http://www.ajronline.org/doi/abs/10.2214/AJR.11.7808>
- [145] S. Gollogly, J. T. Smith, S. K. White, S. Firth, and K. White, "The volume of lung parenchyma as a function of age: A review of 1050 normal CT scans of the chest with three-dimensional volumetric reconstruction of the pulmonary system," *Spine*, vol. 29, no. 18, pp. 2061–2066, 2004.

- [146] R. Nowak, A. Tokarowski, J. Dec, K. Wójcik, and P. Wojciechowski, "Pathomechanics of spinal and rib cage deformity in idiopathic scoliosis," *Chirurgia Narzadow Ruchu I Ortopedia Polska*, vol. 62, no. 3, pp. 211–217, 1997.
- [147] A. C. Koumbourlis, "Scoliosis and the respiratory system," *Paediatric Respiratory Reviews*, vol. 7, no. 2, pp. 152–160, 2006.
- [148] P. R. ANDERSON, M. R. PUNO, S. L. LOVELL, and C. R. SWAYZE, "Postoperative Respiratory Complications in Non-Idiopathic Scoliosis," *Acta Anaesthesiologica Scandinavica*, vol. 29, no. 2, pp. 186–192, feb 1985. [Online]. Available: <http://link.springer.com/10.1007/s00586-009-1084-8> <http://doi.wiley.com/10.1111/j.1399-6576.1985.tb02183.x>
- [149] G. Tusman, S. H. Böhm, D. O. Warner, and J. Sprung, "Atelectasis and perioperative pulmonary complications in high-risk patients," *Current Opinion in Anaesthesiology*, vol. 25, no. 1, pp. 1–10, feb 2012. [Online]. Available: <https://insights.ovid.com/crossref?an=00001503-201202000-00002>
- [150] J. Dubousset, B. Ilharreborde, and J. C. Le Huec, "Use of EOS imaging for the assessment of scoliosis deformities: Application to postoperative 3D quantitative analysis of the trunk," *European Spine Journal*, vol. 23, no. Suppl 4, pp. S397–S405, 2014.